# The role of partial melting on trace element and isotope systematics of granitic melts

*Kumulative Dissertation*

*zur Erlangung des akademischen Grades*

*"doctor rerum naturalium"*

*(Dr. rer. nat.)*

*in der Wissenschaftsdisziplin Geochemie*

**eingereicht an der**

**Mathematisch-Naturwissenschaftlichen Fakultät**

**Institut für Erd- und Umweltwissenschaften**

**der Universität Potsdam**

**von**

**Mathias Johannes Wolf**

**Potsdam, im Januar 2018**

**Datum der Disputation: 16.01.2019**

Supervisor: **Prof. Dr. Rolf L. Romer**
1. Referee *GFZ German Research Centre for Geosciences, Potsdam, Germany*
*University of Potsdam, Institute of Earth and Environmental Science, Germany*

2. Referee **Prof. Dr. Leander Franz**
*Institute of Mineralogy and Petrography, University of Basel, Switzerland*

3. Referee **Prof. Dr. Michel Pichavant**
*CNRS, Earth Science Institute of Orléans, France*

Published online at the
Institutional Repository of the University of Potsdam:
https://doi.org/10.25932/publishup-42370
https://nbn-resolving.org/urn:nbn:de:kobv:517-opus4-423702

**Zusammenfassung**

Sedimentäre Gesteine werden durch zunehmenden Druck und Temperatur zu metamorphen Gesteinen umgewandelt, wobei abhängig von der chemischen Zusammensetzung des Ausgangsgesteines und den Umwandlungsbedingungen unterschiedliche Mineralparagenesen entstehen. Die chemische Zusammensetzung und die Verfügbarkeit von Wasser bestimmen bei welcher Temperatur ein Gestein zu schmelzen beginnt. Da sich die Schmelztemperaturen verschiedener gesteinsbildender Minerale unterscheiden, sind bei einer bestimmten Temperatur und einem bestimmten Druck nicht alle Minerale eines Gesteines in den Schmelzprozess involviert (sog. partielles Aufschmelzen). Die Bedingungen der Schmelzbildung kontrollieren somit die chemische Zusammensetzung der gebildeten Schmelzen. Partielles Aufschmelzen führt daher dazu, dass chemische Elemente in der Kruste neu verteilt werden, da der aufgeschmolzene Teil eines Gesteines als Magma in der Kruste aufsteigt und beim Abkühlen und Auskristallisieren sogenannte Intrusivgesteine (z. B. Granite) bildet.

Intrusionen mit besonders hohen Konzentrationen an bestimmten Metallen (z. B. Sn, W), können zur Bildung von räumlich und genetisch assoziierten Lagerstätten führen. Ob sich aus einer Intrusion eine Lagerstätte bildet, entscheidet sich bereits während der Schmelzbildung im Ausgangsgestein, da die erzbildenden Elemente abhängig von der Schmelztemperatur bevorzugt in die Schmelze oder in den Restit (= nicht mobilisierter Teil) verteilt werden. Sind im Restit Minerale stabil, die bevorzugt erzbildende Elemente einbauen, entstehen Schmelzen die an diesen Elementen verarmt sind und es kommt komplementär zu einer Anreicherung dieser Elemente im Restit. Erfahren derart angereicherte Gesteine eine erneute Schmelzbildung, entstehen Schmelzen mit stark erhöhten Gehalten dieser Erzelemente. Während frühe Schmelzen nur ein sehr geringes Potential haben eine Vererzung auszubilden, haben spätere Schmelzen ein höheres Potential, dass sich aus einer entsprechenden Intrusion eine Erzlagerstätte bildet.

Die Isotopenzusammensetzungen magmatischer Gesteine werden als „Fingerabdruck“ für die Quelle dieser Gesteine verwendet. Dies basiert auf der Annahme, dass die Isotopenzusammensetzung der Quelle an die Schmelze „vererbt“ wird. Die Art der Schmelzreaktion und variable Isotopenzusammensetzungen für verschiedene Minerale können jedoch zu abweichenden Signaturen in der Schmelze und der Quelle führen. Daraus kann die falsche Zuordnung des geochemischen/Isotopen-„Fingerabdruckes“ resultieren.

**Abstract**

Sedimentary rocks are transformed into metamorphic rocks by increasing pressure and temperature. Depending on the chemical composition of the source rock and the metamorphic conditions, different mineral parageneses are formed. The chemical composition and the availability of water control under which conditions a rock starts to melt. Since different rock forming minerals have different melting temperatures, not all minerals in a rock are involved in the melting process (so-called partial melting). Therefore, the conditions of melt formation control the chemical composition of the melt. Partial melting therefore causes chemical elements to be redistributed in the crust, since the molten part of a rock may rise in the crust as magma body and forms so-called intrusive rocks (e.g. granites) during cooling and crystallization.

Intrusions with particularly high concentrations of certain metals (e.g. Sn, W) can lead to the formation of spatially and genetically associated deposits. Whether a deposit is formed from an intrusion is already decided during melt formation in the source rock, since the ore-forming elements are preferably distributed into the melt or into the restite (= non-mobilized part) depending on the melting temperature. If the stable minerals in the restite preferentially incorporate ore-forming elements, the melts will be depleted in these elements and complementary accumulation of these elements in the restite occurs.

Remelting of such enriched restitic rocks leads to significant enrichment of ore elements in the melt. While early melts only have a very limited potential to develop mineralization, later melts have a significantly higher potential to form an ore deposit from a corresponding intrusion.

The isotopic composition of magmatic rocks is commonly used as a “fingerprint” for the source of these rocks. This application is based on the fundamental assumption that the isotopic composition of the melt is identical to its source. The nature of the partial melting reaction and variable isotopic compositions for different minerals may, however, lead to distinct isotopic compositions in the melt and the source. This may lead to incorrect assumptions regarding the source of magmatic rocks.

# Table of Content

# List of Figures

# List of Tables

# Chapter 1: Introduction

**Abstract**

Partial melting is a first order process for the chemical differentiation of the crust (Vielzeuf et al., 1990). Redistribution of chemical elements during melt generation crucially influences the composition of the lower and upper crust and provides a mechanism to concentrate and transport chemical elements that may also be of economic interest. Understanding of the diverse processes and their controlling factors is therefore not only of scientific interest but also of high economic importance to cover the demand for rare metals.

The redistribution of major and trace elements during partial melting represents a central step for the understanding how granite-bound mineralization develops (Hedenquist and Lowenstern, 1994). The partial melt generation and mobilization of ore elements (e.g. Sn, W, Nb, Ta) into the melt depends on the composition of the sedimentary source and melting conditions. Distinct source rocks have different compositions reflecting their deposition and alteration histories. This specific chemical "memory" results in different mineral assemblages and melting reactions for different protolith compositions during prograde metamorphism (Brown and Fyfe, 1970; Thompson, 1982; Vielzeuf and Holloway, 1988). These factors do not only exert an important influence on the distribution of chemical elements during melt generation, they also influence the volume of melt that is produced, extraction of the melt from its source, and its ascent through the crust (Le Breton and Thompson, 1988). On a larger scale, protolith distribution and chemical alteration (weathering), prograde metamorphism with partial melting, melt extraction, and granite emplacement are ultimately depending on a (plate-)tectonic control (Romer and Kroner, 2016). Comprehension of the individual stages and their interaction is crucial in understanding how granite-related mineralization forms, thereby allowing estimation of the mineralization potential of certain areas.

Partial melting also influences the isotope systematics of melt and restite. Radiogenic and stable isotopes of magmatic rocks are commonly used to trace back the source of intrusions or to quantify mixing of magmas from different sources with distinct

isotopic signatures (DePaolo and Wasserburg, 1979; Lesher, 1990; Chappell, 1996). These applications are based on the fundamental requirement that the isotopic signature in the melt reflects that of the bulk source from which it is derived. Different minerals in a protolith may have isotopic compositions of radiogenic isotopes that deviate from their whole rock signature (Ayres and Harris, 1997; Knesel and Davidson, 2002). In particular, old minerals with a distinct parent-to-daughter (P/D) ratio are expected to have a specific radiogenic isotope signature. As the partial melting reaction only involves selective phases in a protolith, the isotopic signature of the melt reflects that of the minerals involved in the melting reaction and, therefore, should be different from the bulk source signature. Similar considerations hold true for stable isotopes.

### 1.1. Partial melting process

Rocks develop distinct mineral assemblages depending on their chemical composition and pressure-temperature conditions that they experience. With increasing temperatures rocks eventually start to melt. Melt generation is not a bulk process affecting the whole system at once, but is a localized process as the melting reactions involve specific phases (Mehnert et al., 1973). In the presence of free water, most rocks start to melt at temperatures around 650 °C (Huang and Wyllie, 1975). Most crustal metasedimentary rocks that reach temperatures high enough for melt generation, however, are assumed to be “dry”, as free fluid phases are expelled due to compaction and decreasing pore space during prograde metamorphism (Bowen and Tuttle, 1950; Tuttle and Bowen, 1958). Therefore, melting under mid crustal conditions is generally accepted to be dominated by dehydration melting reactions (Fig. 1.1; Clemens and Vielzeuf, 1987). In these reactions, water is contributed by OH-group bearing minerals such as muscovite, biotite, and amphibole. At relatively low pressures dehydration melting starts at elevated temperatures (> 700 °C) with the breakdown of muscovite, followed by dehydration melting of biotite (>800 °C) and amphibole melting at temperatures above 900 °C (Wyllie, 1977). The order of dehydration melting reactions as well as the specific temperatures may vary as they strongly depend on mineral assemblage, chemical composition, and pressure. For instance, at elevated pressures, biotite dehydration melting is likely to start at lower temperatures than muscovite melting as the biotite dehydration melting reactions backbends with increasing pressure (Clemens, 1984). The presence of fluxing agents, such as F and B, may further influence the melting

behavior of a specific rock, as these elements generally lower the solidus temperature (Pichavant, 1981; Manning and Pichavant, 1983).

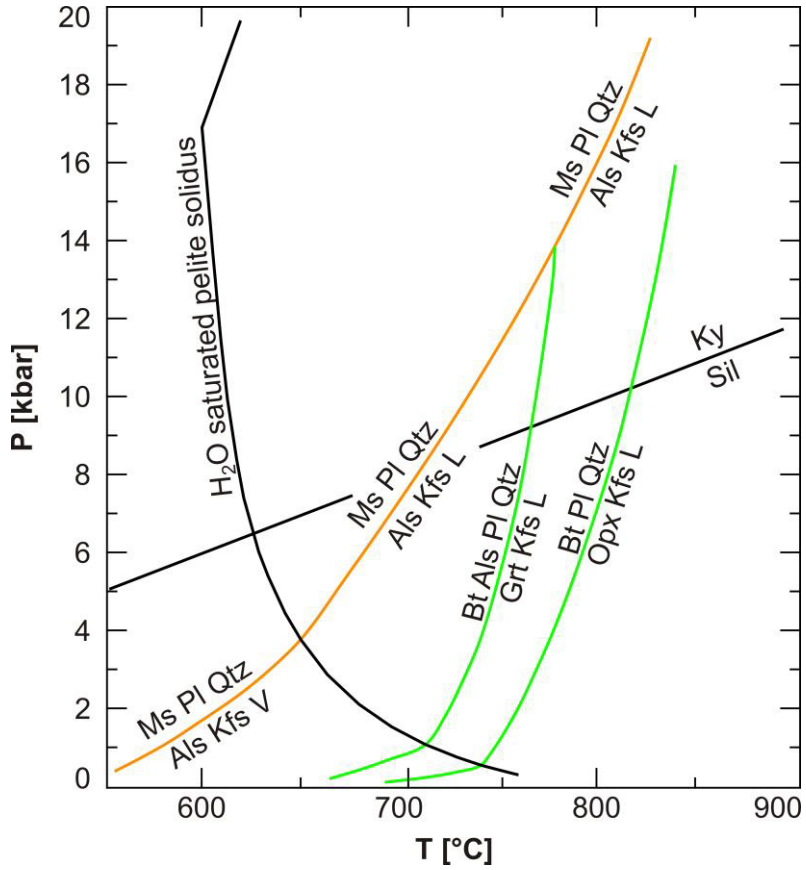


Fig. 1.1. P-T diagram showing vapor-absent melting reactions for pelites. The red line denotes muscovite dehydration melting reaction and the green lines represent biotite-dehydration melting reactions. Modified after Spear (1995). Ms = muscovite, Bt = biotite, Pl = plagioclase, Qtz = quartz, Als = alumosilicate, Grt = garnet, Kfs = K-feldspar, Ky = kyanite, Sil = sillimanite, Opx = orthopyroxene, V = vapor, L = liquid melt

From a chemical point of view, the partial melting reaction and the composition of the involved minerals control which chemical elements are mobilized and available for redistribution. This is especially true for major elements and trace elements that are mainly hosted in rock forming minerals. The concentration of these elements in the melt is therefore buffered by the melting reaction. For trace elements that are mainly hosted in accessory phases (e.g. REE, Zr, U, Th), the solubility of the corresponding accessory phase in the melt determines their availability to partition into the melt. The solubility of accessory phases is mainly controlled by the chemical composition of the melt and temperature (Watson and Harrison, 1983; Rapp and Watson, 1986; Boehnke et al., 2013). Therefore, partial melting at distinct conditions may result in a decoupling of major and trace elements hosted in rock forming minerals and trace elements hosted in accessory phases.

## 1.2. Different models for Sn enrichment

The close relationship of Sn deposits and granitic intrusions has been recognized early on. It has also been recognized that granitic rocks with an elevated oxidation state do not have high Sn concentrations as they have lost Sn to magnetite (Ishihara, 1978). Traditionally, accumulation of Sn in granitic melts has been explained by the incompatible character of (reduced) $Sn^{2+}$ and extreme fractional crystallization (Lehmann, 1990). However, not all reduced, highly evolved granites also develop mineralization. It has therefore been argued that Sn mineralized granites are derived from source rocks that already have anomalously high Sn concentrations (Plimer, 1980). A combination of these two end-member scenarios (source enrichment *vs.* fractional crystallization) may not only explain Sn enrichment in specific granites but also explains their spatial distribution. In the multistage model presented by Romer and Kroner (2014; 2016), chemical alteration of the source rocks, the partial melting relationships, and the tectonic setting control the generation of Sn specific granites. In such a multistage model, each individual stage exerts a critical influence on the potential of a granitic melt to develop Sn mineralization.

One part of the presented work focuses on the controlling factors during source alteration and the behavior of Sn hosting phases during prograde metamorphism up to partial melting conditions. The chemical composition of the source rock influences the mineral assemblage and their modal proportions during prograde metamorphism. The distribution of chemical elements during partial melting as well as the melt volume directly depend on the modal composition of the protolith. Mineral stabilities, their modal proportions, and melt volumes at various pressure and temperature conditions can be calculated by thermodynamic modeling (De Capitani and Petrakakis, 2010). Chemically different protoliths are used in thermodynamic modeling to identify the factors that control the behavior of Sn at partial melting conditions.

The mineralogical control on Sn distribution during partial melting is analyzed in natural samples from different migmatic rocks that formed under different temperature conditions. The chemical compositions of melt and restite domains are used to qualitatively/semiquantitatively understand the role of different minerals and partial melting reactions on the trace element, specifically Sn, budget. Combining these observations with results from thermodynamic modeling for different protolith compositions highlights the critical role of protolith chemistry and partial melting conditions on the potential of Sn mineralization in granitic rocks.

### *1.2.1. The role of protolith chemistry*

The decomposition of minerals during intense weathering of crustal sediments modifies the chemical composition of a protolith as some chemical elements are mobilized and transported away whereas others are relatively enriched. In the light of ore element enrichment and melt generation, two different aspects are important: Sn (and possibly W and Ta) show a residual enrichment, as these elements are adsorbed on clay mineral surfaces during weathering (Rose et al., 1979; Kronberg et al., 1982). Residual enrichment by this process may lead to enhanced concentration of a specific trace element in the sedimentary protolith, which is important for mass balance aspects in relation to protolith and melt volume (see chapter 2). However, in the light of ore element concentrations found in mineralized granites, source enrichment is of subordinate importance (several thousand ppm *vs.* a few tens ppm). The more important consequences of the intense chemical alteration are the loss of Na, Ca, Sr and Pb due to the decomposition of feldspar and the relative enrichment of Al, K, and Rb that are incorporated into secondary minerals and adsorbed on clay mineral surfaces. The chemical composition of a protolith defines the mineral assemblage during prograde metamorphism, which critically influences the melting behavior of a rock and also controls the distribution of trace elements between melt and restite. The distinct composition of the intensely weathered sediments favors high modal amounts of muscovite and biotite during prograde metamorphism. These minerals are essential for partial melting reactions at different conditions, as these phases contribute $H_2O$ in the form of OH-groups during fluid absent melting reactions. Elevated mica contents provide a source for high amounts of water, thereby elevating the fertility of the rock.

### *1.2.2. Tin partitioning between different phases*

Besides their central role in dehydration melting, micas also influence the distribution of trace elements. Among common rock forming minerals, muscovite and biotite represent two important trace element hosts, in particular for Sn, Li, V, Cr, Zn, Rb, Nb, and Cs (Neiva, 1998; Yang and Rivers, 2000). As dehydration melting reactions involve those two phases at distinct pressure and temperature conditions, mica-hosted trace elements are available for redistribution and may be mobilized into the melt during partial melting at different conditions. The breakdown of muscovite during low-temperature melting, for instance, releases Sn. A significant portion of this Sn may be

sequestered in restitic minerals and the generated melt is depleted in Sn. With increasing temperature, the melting reaction changes from muscovite-dehydration melting to biotite-dehydration melting (Petö, 1976; Le Breton and Thompson, 1988). With no other Sn sequestering phase present, Sn released during the breakdown of biotite partitions mainly into the melt. Under closed system conditions, the concentration of Sn in these late melts is not expected to result in significant Sn enrichment as high volumes of melt from low-temperature melting are present resulting in a dilution of Sn. Such melts would require extreme fractional crystallization to develop mineralization grade Sn concentrations (Groves and McCarthy, 1978). If, however, low-temperature melt is extracted from the source, high-temperature melts are not diluted by low-temperature melts, therefore resulting in relatively small melt volumes with high Sn contents. Further accumulation by fractional crystallization is particularly efficient in melts that already start with enhanced Sn concentrations.

### 1.3. Radiogenic and stable isotopes

Chemical differentiation of the earth has led to distinct P/D ratios of radioactive elements in different reservoirs. Therefore, with time, these reservoirs have developed characteristic isotopic signatures. The radiogenic isotope signatures of different reservoirs are widely used to constrain the source of magmatic rocks or to quantify magma mixing processes and the contributions from different melt sources (DePaolo and Wasserburg, 1979; McCulloch and Chappell, 1982). This application assumes complete isotopic equilibration of a melt with its source. However, partial melting may lead to melt batches with distinct radiogenic signatures that deviated from the bulk signature of their source (Hogan and Sinha, 1991; Ayres and Harris, 1997; Harris and Ayres, 1998; Farina and Stevens, 2011; McLeod et al., 2012). This is particularly true for source rocks that are old and, therefore, have variable radiogenic isotope compositions on the mineral scale. The preferred incorporation of specific elements in some minerals results in distinct P/D ratios between different minerals. Over time, these differences result in distinct radiogenic isotope signatures in these minerals. As partial melting is a selective process that involves specific minerals under certain conditions (see chapter partial melting), the radiogenic isotope signature of the melt reflects that of the minerals involved in the melting reaction rather than the bulk source.

The budgets of the various radiogenic isotopes are controlled by different minerals. The whole rock Rb and Sr budget is largely controlled by rock forming

minerals, in metasedimentary rocks mainly by feldspar, muscovite, and biotite. The variable ratios of Rb/Sr in these phases result, over time, in distinct $^{87}Sr/^{86}Sr$ compositions in these phases. Low-temperature dehydration melting mainly involves muscovite and feldspar while biotite is largely unaffected (Clemens, 1984). In contrast, high-temperature melt generation is controlled by biotite dehydration melting (Vielzeuf and Holloway, 1988). Therefore, the isotopic signature of distinct melt batches may vary, if the respective minerals in the protolith are old enough to develop distinct Sr isotopic compositions (Knesel and Davidson, 2002). In contrast, the Sm and Nd budget and Nd isotope systematics of common crustal rocks is controlled by accessory phases that may also have different Sm/Nd (Ayres and Harris, 1997) and, after some time, also higher $^{143}Nd/^{144}Nd$ ratios. As accessory phases do not participate in partial melting reactions, their stability mainly depends on their solubility in the melt (Watson and Harrison, 1983; Rapp and Watson, 1986; Boehnke et al., 2013). The Nd isotopic composition of melt and restite, which originate from sufficiently old protoliths, may therefore be different.

Differences in the Li and B stable isotope compositions of different minerals are controlled by temperature and the distinct coordination of the same chemical element in different phases (Kakihana et al., 1977; Wunder et al., 2005; Marschall and Foster, 2018). As fractionation of stable isotopes is caused by mass differences between different isotopes of the same element, it is expected to be largest during low temperature processes and between phases with different coordination. It is therefore widely established that stable isotope fractionation at elevated, particularly at magmatic temperatures, is insignificant (Trumbull and Slack, 2018). If, however, minerals with distinct stable isotopic signatures are stable up to partial melting conditions, different melt batches might in fact also have distinct stable isotope signatures.

This dissertation consists of five chapters. Chapter 1 and 5 provide a general introduction and a discussion of the results. Chapters 2 – 4 were written as stand-alone manuscripts for publication in scientific journals. Chapter 2 has been published in *Lithos*, the manuscript of chapter 3 is submitted to *Geochimica et Cosmochimica Acta*, and the manuscript of chapter 4 is in preparation to be submitted to a peer-reviewed journal.

Chapter 2: “Tin in granitic melts: The role of melting temperature and protolith composition” by Wolf et al. has been published in *Lithos* in April 2018. Mathias Wolf is first author of this publication. Sampling of different migmatites in the Central Iberian

Zone and writing of the geological context were supported by F. J. López-Moro (University of Salamanca). Laboratory work and analyses of major and trace elements were done by Mathias Wolf under the guidance of technical staff at GFZ. Petrographic sample description and thermodynamic modeling with Theriak/Domino was done by Mathias Wolf with the support of L. Franz (University of Basel). Evaluation and interpretation of the chemical data as well as the discussion were done in close cooperation with R. L. Romer (GFZ Potsdam). Mathias Wolf has written the paper, the co-authors have contributed with discussion and editing the final version.

Chapter 3: "Isotope disequilibrium during partial melting of metasedimentary rocks" by Wolf et al. was submitted to *Geochimica et Cosmochimica Acta* (1.10.2018) and is currently under review. Mathias Wolf is first author of this manuscript. Clean room chemistry was done by Mathias Wolf with the support of B. Hübner (GFZ). TIMS measurement of radiogenic isotopes was done by Mathias Wolf under the supervision of R.L. Romer (GFZ). Stable isotope analyses and data evaluation were done by Mathias Wolf together with J. Glodny (GFZ). Mathias Wolf has written the paper, the co-authors have contributed with discussion and editing the final version.

Chapter 4: "Mobilization and fractionation of Sn, W, Nb, and Ta during partial melting and its impact on rare metal mineralization" by Wolf et al. is a manuscript in an advanced stage that will be submitted to a peer reviewed journal. Mathias Wolf is first author of this manuscript. Trace element analyses by LA-ICP-MS were carried out at "Laboratoire GeoRessources, CNRS" in Nancy by Mathias Wolf under the supervision of J. Mercadier (CNRS). Data reduction and evaluation were done by Mathias Wolf in close collaboration with J. Mercadier. Electron microprobe analyses were carried out by Mathias Wolf with support of the technical staff at GFZ. Interpretation and discussion of the results were done in close collaboration with R. L. Romer (GFZ). Mathias Wolf has written the paper, the co-authors have contributed with discussion and editing the final version.

# Chapter 2: Tin in granitic melts: The role of melting temperature and protolith composition

**Abstract**

Granite bound tin mineralization typically is seen as the result of extreme magmatic fractionation and late exsolution of magmatic fluids. Mineralization, however, also could be obtained at considerably less fractionation if initial melts already had enhanced Sn contents. We present chemical data and results from phase diagram modeling that illustrate the dominant roles of protolith composition, melting conditions, and melt extraction/evolution for the distribution of Sn between melt and restite and, thus, the Sn content of melts. We compare the element partitioning between leucosome and restite of low-temperature and high-temperature migmatites. During low-temperature melting, trace elements partition preferentially into the restite with the possible exception of Sr, Cd, Bi, and Pb, that may be enriched in the melt. In high-temperature melts, Ga, Y, Cd, Sn, REE, Pb, Bi, and U partition preferentially into the melt whereas Sc, V, Cr, Co, Ni, Mo, and Ba stay in the restite. This contrasting behavior is attributed to the stability of trace element sequestering minerals during melt generation. In particular muscovite, biotite, titanite, and rutile act as host phases for Sn and, therefore prevent Sn enrichment in the melt as long as they are stable phases in the restite. As protolith composition controls both the mineral assemblage and modal contents of the various minerals, protolith composition eventually also controls the fertility of a rock during anatexis, restite mineralogy, and partitioning behavior of trace metals. If a particular trace element is sequestered in a phase that is stable during partial melting, the resulting melt is depleted in this element whereas the restite becomes enriched. Melt generation at high temperature may release Sn when Sn-hosts become unstable. If melt has not been lost before the breakdown of Sn-hosts, Sn contents in the melt will increase but never will be high. In contrast, if melt has been lost before the decomposition of Sn-hosts, the small volume of the high-temperature melt will not be diluted by low-temperature, low-Sn melts and, therefore, could have high Sn-contents. The combination of multiple melt extractions and Sn-mobilization at high temperature results in strong Sn enrichment in late, high-temperature melts. Metal enrichment during partial melting becomes particularly

efficient, if the sedimentary protolith had experienced intense chemical alteration as the loss of Na and Ca together with a relative enrichment of K favors muscovite-rich metamorphic mineral assemblages that produce large amounts of melt during muscovite dehydration melting.

## 2.1. Introduction

Partial melting and melt extraction in crustal rocks are first order processes for the differentiation of continental crust (Brown and Rushmer, 2006). Metapelites, metagreywackes, and granites start to melt at temperatures of about 650 °C (Sawyer et al., 2011), producing melts of granitic composition. Melting at such low temperature requires free water (i.e. $H_2O$ fluid-present melting) or network-modifying elements like boron and phosphorus (Chorlton and Martin, 1978; Manning and Pichavant, 1983). Melting of rocks that do not contain free water is controlled by the incongruent breakdown of hydrous minerals such as muscovite, biotite, and amphibole (e.g. Brown and Fyfe, 1970; Huang and Wyllie, 1973; Le Breton and Thompson, 1988). Protolith chemistry controls the mineralogy of the melting rock and, thus, controls melting conditions and amount of melt produced at particular P-T conditions, as well as the partitioning behavior of trace elements between melt and restite (i.e. solid fraction left after partial melting and segregation/extraction of the melt). Zirconium in zircon and REE in monazite or xenotime (Rapp and Watson, 1986), represent examples of trace elements whose budget is dominated by accessory phases. Other trace elements do not form phases of their own and their budget in the bulk rock sample is controlled by rock forming minerals into which they substitute. Thus, the behavior of trace elements during partial melting is controlled either by the stability of rock forming phases or the solubility of trace element sequestering accessory phases in the melt. For example, tin may be sequestered in muscovite, biotite, titanite, magnetite, rutile, and ilmenite (Neves, 1997; Tischendorf et al., 2001; Zack et al., 2002; Klemme et al., 2006; Wang et al., 2013; Zhao and Zhou, 2015). Thus, the behavior of tin during partial melting and its potential to enrich in melts largely depends on the stability of these Sn-sequestering phases. If these phases remain stable during prograde metamorphism and partial melting, Sn eventually becomes enriched in the restite. If melt is extracted after low-temperature melting (~750 °C), high-temperature melting (>800 °C), involving the Sn-carrier phases in the enriched restite, leads to distinct Sn enrichment in these high-temperature melt(s).

The formation of Sn-specific granites and eventually mineralization, which seems to follow the margin of continents (De Wit et al., 1999; Romer and Kroner, 2014), traditionally has been explained with (a) Sn-rich sources (Schuiling, 1967), (b) extreme fractional crystallization (Ishihara, 1978; Štemprok, 1990) followed by hydrothermal processes (Lehmann, 1990), or (c) multiple melt extraction from the same source with restite enrichment (Tischendorf and Förster, 1990). While most explanations favoring extreme fractional crystallization do not involve an enriched source, Romer and Kroner (2014) argued that an enriched protolith requires the melting of a smaller volume and less fractionation to reach the same level of enrichment compared to an unenriched protolith. Several Variscan massifs host major granite-related Sn deposits, most importantly in Cornwall, the Erzgebirge, Iberia, and the French Massif Central (Halliday, 1980; Štemprok, 1995; Förster et al., 1999; Neiva, 2002; López-Moro et al., 2017; Fig. 2.1). Romer and Kroner (2014, 2016) demonstrated that the distribution of Sn mineralization with the Variscides is controlled by the distribution of (i) intensely altered sediments, which represent the Sn-enriched protolith, at continent margins explaining the occurrence of Sn-mineralization in belts and (ii) the tectonically controlled availability of heat sources accounting for partial melting of the source rocks and the transfer of Sn from the protolith to the granitic melt.

Migmatites that formed at different temperatures were analyzed to characterize the trace element partitioning between melt and restite as a function of thermal regime. The analyzed migmatites formed under low- and high-temperature conditions, representing natural examples for muscovite and biotite dehydration melting (Escuder Viruete et al., 1994; Barbero, 1995). The analyzed samples do not have strongly weathered shales as protoliths, but they are used to illustrate the general distribution of Sn during low- and high-temperature partial melting. Equilibrium phase diagram calculations are combined with these findings to characterize the influence of P-T conditions, melt volume and extraction, $fO_2$, and protolith bulk rock chemistry on trace element distribution based on mineral stability. This approach allows the identification of processes that facilitate or inhibit Sn enrichment in granitic melts.

## 2.2. Geological background

The Iberian Massif offers insight into a suite of mainly Paleozoic and Ediacaran rocks. The Central Iberian Zone is special, as it exposes both, shallow and deep crustal

levels, i.e., the level of granite emplacement and the levels of crustal melting to form the granitic melts (Escuder Viruete et al., 1997; Castro et al., 2002). In the northern to central part of the Central Iberian Zone, there occur voluminous migmatites that formed under

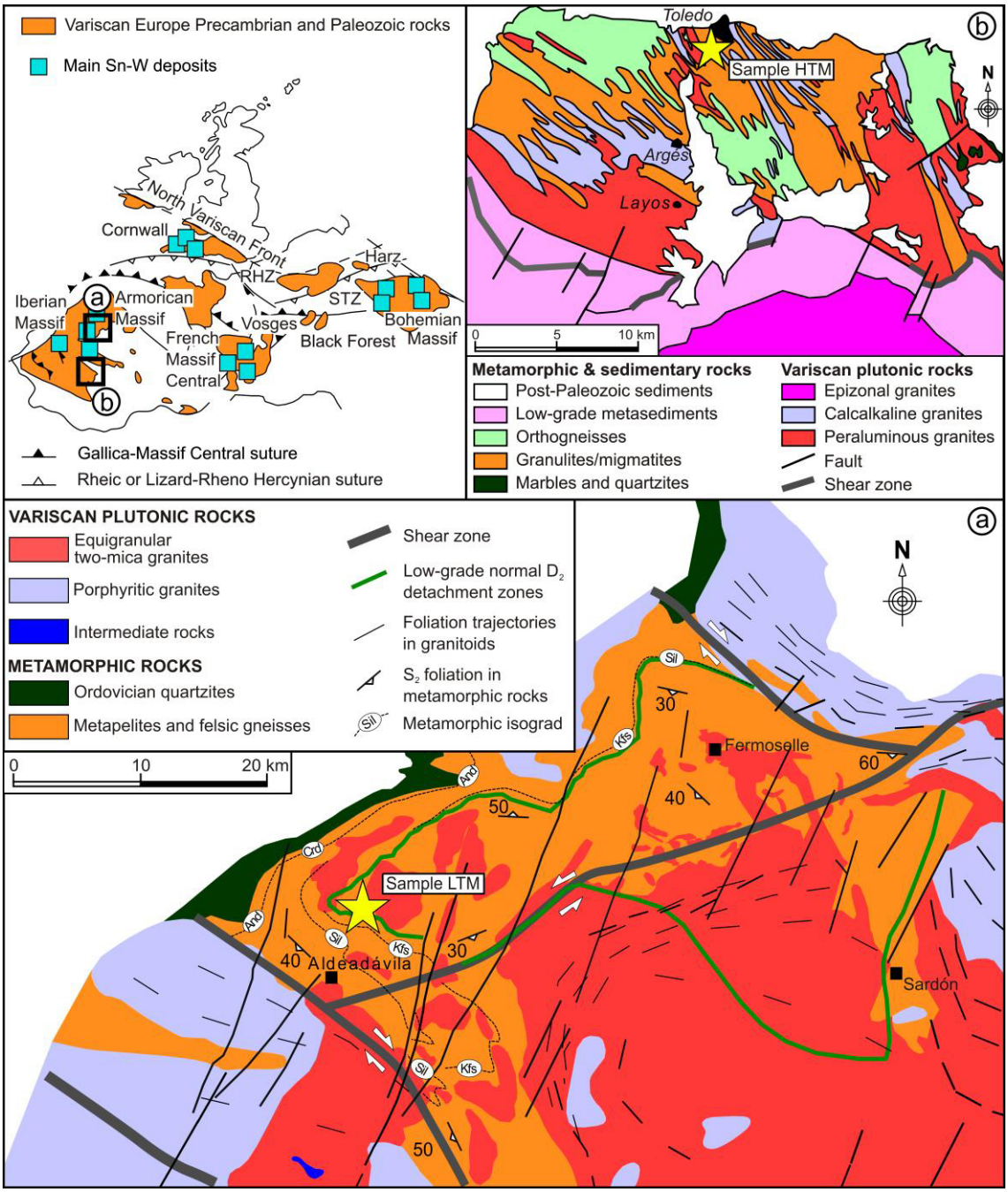


Fig. 2.1. Schematic map of the Variscan orogen in Europe (based on Franke, 1989). (a) Geological map of the Tormes dome area. Asterisk marks the sample location for the studied low-temperature migmatite (LTM; adapted from López-Moro et al., 2012). (b) Detailed geological map of the Anatectic Complex of Toledo. Asterisk marks the sample location of the high-temperature migmatite (HTM) formed by biotite dehydration melting (adapted from Barbero and Villaseca, 1992; Barbero and Villaseca, 2004).

muscovite dehydration melting conditions (~750 °C), whereas the migmatites in the southern part were generated under higher-temperatures, reaching biotite dehydration melting conditions (>800 °C). Migmatites from the corresponding areas were sampled in the Tormes Dome and the Anatectic Complex of Toledo, respectively.

### *2.2.1. Geology of the Tormes Dome*

The Tormes Dome (Fig. 2.1a) represents the southernmost prolongation of the "plutono-metamorphic belt" of the NW Iberian Massif, a zone characterized by structurally controlled extensive Variscan partial melting and multiple granitic intrusions. The structurally lower units of the belt include migmatized felsic gneisses and migmatized Neoproterozoic-Lower Cambrian sandstones and pelites (Ibarguchi and Martinez, 1982; López-Moro and López-Plaza, 1993; Bea et al., 2006), whereas the upper units consist of a monotonous sequence of Lower Cambrian low to medium grade slates and schists. Barrovian-type upper amphibolite facies metamorphism (700-740 °C and 8-9 kbar, Escuder Viruete et al., 2000) in this part of the Central Iberian Zone peaked at 337-329 Ma (Valverde-Vaquero, 1997; Valverde-Vaquero et al., 2007). Subsequent extensional tectonics resulted in nearly isothermal decompression (700-740 °C at 3 kbar) that triggered extensive migmatization and anatexis by muscovite dehydration melting (Escuder Viruete et al., 1994; Escuder Viruete et al., 2000). The migmatites yield ages of 325-320 Ma (Valverde-Vaquero et al., 2007). Late Variscan granitoid intrusions (316-310 Ma, López-Moro et al., 2012) are closely related to the NNE-SSW compressional tectonics affecting the Central Iberian Zone.

### *2.2.2. Geology of the Anatectic Complex of Toledo*

The Anatectic Complex of Toledo (Fig. 2.1b) represents the southernmost outcrops of the Spanish Central System, which is part of the Central Iberian Zone. The Anatectic Complex of Toledo is a granulitic migmatite area with the highest metamorphic grade of the Central Iberian Zone (Barbero and Villaseca, 2000) and consists of metamorphic rocks, calc-alkaline granitoids with associated mafic rocks, and abundant restite-rich peraluminous leucogranites. Peak metamorphic pressure in this area was below 8-10 kbar, as rutile, kyanite, and staurolite are absent and sillimanite inclusions in garnet are present (Barbero and Villaseca, 2000). Biotite dehydration melting was triggered by a nearly isothermal decompression to 4-6 kbar at 800 ± 25 °C (Barbero, 1995) leading to intense migmatization. Depending on the pressure conditions garnet +

alkali feldspar + melt or garnet + cordierite + alkali feldspar + melt formed as peritectic products of anatexis (Barbero and Villaseca, 2000). Migmatization in this area occurred between 315 Ma and 310 Ma (Castiñeiras et al., 2008).

### 2.3. Sample description

The nomenclature used in this paper follows the suggestions of (Sawyer, 2008). BSE images can be found in appendix A. Low-temperature migmatites (LTM) were sampled in the Tormes Dome anatectic region. Temperatures of metamorphism did not exceed 740 °C at 3 kbar, triggering muscovite dehydration melting (Escuder Viruete et al., 2000). The folded metapelitic migmatite (Fig. 2.2a and b) consists of a leucosome (LTM-L), a melanosome (LTM-M), and mesocratic residuum (LTM-R). The leucosome is separated from the melanosome by a rim of quartz that is concentrated in fold hinges. The leucosome contains coarse grained plagioclase together with quartz and rare, small biotite flakes. Sillimanite is partially replaced by secondary muscovite at the contact between leucosome and melanosome. The melanosome consists of coarse biotite flakes with abundant zircon inclusions, plagioclase, fractured tourmaline and quartz. The mesocratic residual part of this sample consists of biotite, plagioclase, quartz, and local zones with strongly fractured tourmaline. Plagioclase ($An_{10-13}$) and biotite do not show any systematic compositional variation over the three domains. Tourmaline in the melanosome and the residuum is chemically zoned with Fe-rich cores and Mg-rich rims.

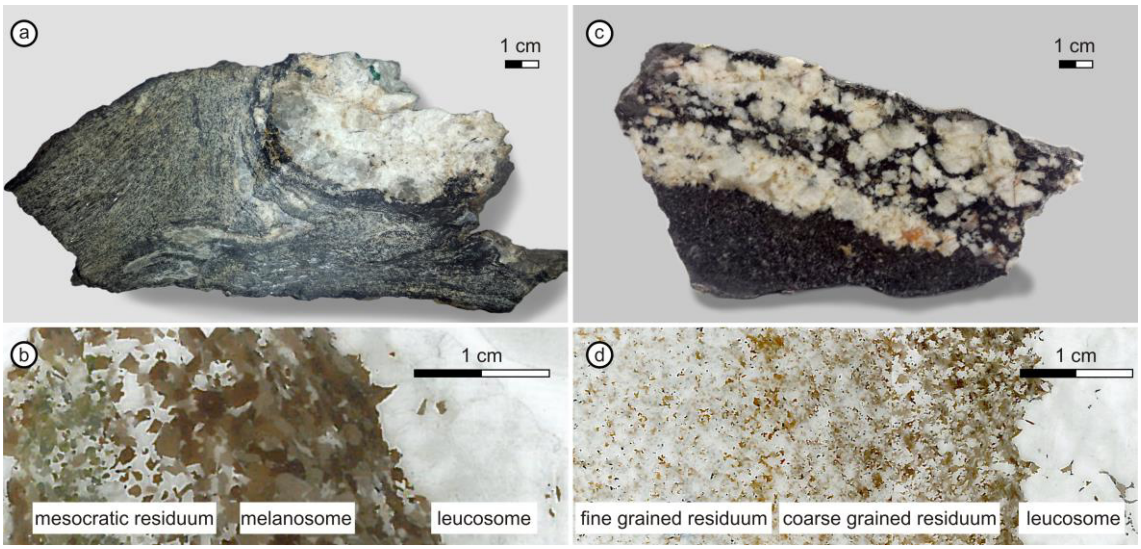


Fig. 2.2. (a) Hand specimen and (b) thin section profile of the low-temperature migmatite (LTM) from the Tormes Dome. Leucosome (top right in the hand specimen), melanosome, and mesocratic residuum were manually separated for analysis. (c) Hand specimen and (d) thin section profile of the high-temperature migmatite (HTM) from the Anatectic Complex of Toledo. The fine and coarse grained residue (both in the lower, dark part), and the leucosome (bright part) were manually separated for analysis. Note the increasing grain size and change in mineralogy from residuum to leucosome.

Sample HTM originates from the Anatectic Complex of Toledo and represents a high temperature, low pressure migmatite (Fig. 2.2c). Peak metamorphic conditions in this complex reached 800 ± 50 °C at 4-6 kbar (Barbero, 1995) and anatexis involved the incomplete breakdown of biotite. The sample shows three domains (Fig. 2.2d) including a leucosome (HTM-L), a coarse grained residuum (HTM-CR), and a fine grained residuum (HTM-FR). The mineral assemblage of the fine grained residuum consists of plagioclase, amphibole (cummingtonite-grunerite), irregularly shaped fine grained biotite, and accessory apatite, zircon, and ilmenite. Toward the coarse grained residuum, grain size generally increases and amphibole disappears. Plagioclase, K-feldspar, fine and coarse grained biotite together with quartz dominate the assemblage. The leucosome consists of mainly coarse grained plagioclase, K-feldspar, quartz, minor biotite, garnet ($Alm_{72-76}$) with inclusions of biotite and quartz, and small amounts of apatite and ilmenite. $X_{Mg}$ and F content of biotite decrease from the residuum to the leucosome, whereas Ti and Al in biotite increase. The anorthite content in plagioclase decreases from the residuum ($An_{80-85}$) to the leucosome ($An_{30-35}$).

## 2.4. Methods

Samples with clear transitions between leucosome, mesosome, and melanosome were selected and slices were cut from different domains. The fragments were visually checked to avoid contamination from adjacent domains and several 100 grams of each domain were used for rock powder preparation. Major elements were determined using XRF. Trace elements were analyzed using ICP-MS and XRF. REE were analyzed by ICP-AES. For a detailed description of the analytical protocols see (Romer and Hahne, 2010) and references therein. The data are shown in Table C.1 of the appendix C.

Phase equilibria calculations were performed using Domino/Theriak (De Capitani and Petrakakis, 2010) and the internally consistent dataset of Holland and Powell (1998). Calculations were performed in the system $Na_2O$ - CaO - $K_2O$ - FeO - MgO - $Al_2O_3$ - $SiO_2$ - $H_2O$ - $TiO_2$ - $Fe_2O_3$ (NCKFMASHTO). The considered phases and activity-composition (a-x) models include K-feldspar and plagioclase (Holland and Powell, 2003), ilmenite - hematite, spinel, biotite, garnet, and melt (White et al., 2007), orthopyroxene (Powell and Holland, 1999), white mica (Coggon and Holland, 2002), cordierite and epidote (Holland and Powell, 1998) and hornblende (Diener et al., 2007). Aluminosilicates, quartz, titanite, rutile, and aqueous fluid are treated as pure

endmembers. Equilibrium phase diagrams were calculated under reducing conditions (all Fe as $Fe^{2+}$) and at elevated oxygen fugacities ($fO_2$ = OHM = hematite-magnetite-buffer) and for different protolith compositions (altered shale and unaltered shale, see also section 2.5.2.) in order to assess their influence on mineral stability, melting conditions, and amount of melt. Fluid absent melting (i.e. dehydration melting by mica breakdown) was modeled by adjusting bulk water content in such a way that no free fluid phase is present (i.e. all the water is stored in hydrous minerals) during the onset of melting at 5 kbar.

## 2.5. Results

### *2.5.1. Chemical composition of the two migmatites*

The compositions of leucosome, melanosome, and residuum of the low- and high-temperature migmatites normalized to upper continental crust (Rudnick and Gao, 2003) are shown in Figs. 2.3a and b. The distinct patterns of leucosome and melanosome/residuum of the two samples reflect the contrasting mineralogy of the rocks, which is a function of pressure and temperature at melting conditions and of bulk composition of the protoliths. Recalculation of the weighted proportions of the different domains shows that the protoliths of the low-temperature and high-temperature migmatites had different chemical compositions. These samples are used to examine Sn distribution between the different domains within a sample, thus, the relative distribution of Sn is compared which is largely unaffected by differences in whole rock composition.

The integrated bulk composition of the low-temperature migmatite shows enrichment in Li and Be and low concentrations of Na, P, Ca, Pb, and Sr. The high-temperature migmatite has elevated P, Ca, and Ti contents, reflecting the abundance of apatite, plagioclase, and Ti-oxides. The sedimentary protolith of the high-temperature migmatite did not experience as intense chemical alteration as the one of the low-temperature migmatite (e.g. lower contents of plagioclase-bound elements). The low contents of Sb, W, and Th in all domains of the high-temperature migmatite, mostly reflect their low contents in the sedimentary protolith rather than mobilization during partial melting.

#### *2.5.1.1 Partitioning in the low-temperature migmatite*

The relative concentrations of trace elements in the leucosome and the residual parts reflect the contrasting mineralogical compositions of the different domains and,

thus, the mineralogically controlled partitioning behavior of respective element during melt generation. Element concentrations of the melanosome in the low-temperature migmatite fall between the mesocratic residuum and leucosome, except for Na, Ca, Sr, Cd, and Pb that are enriched and Bi that is depleted in the melanosome relative to the leucosome and residuum. Due to late quartz segregation, $SiO_2$ contents in the leucosome are unusually high (88 wt%; Table C.1, appendix), diluting the contents of other elements in the leucosome. Thus, elements that have similar concentrations in the leucosome and the residual parts, actually partition into the melt rather than into the restite. This is especially true for Na, Ca, Sr, Mo, Cd, Sb, Pb, and Bi (Fig. 2.3a). The other elements show a clear preference for the residuum. This distribution illustrates that their host phases remain stable during muscovite dehydration melting. Particularly, mica-hosted trace elements (Li, V, Cr, Zn, Rb, Nb, and Cs) follow the same trend as Sn with significant enrichment in the restite. The Rb/Sr ratios in the low-temperature migmatite show a broad range from 0.35 in the leucosome to 8.32 in the residuum.

*2.5.1.2. Partitioning in the high-temperature migmatite*

The coarse and fine grained residual parts of the high-temperature migmatite show very similar chemical compositions. Na, P, Y, Cd, Sn, $REE^{3+}$, Pb, Bi, and U show a clear preference to partition into the leucosome. Mg, Ti, Mn, Fe, Li, Be, Sc, V, Cr, Co, Ni, Zn, Mo, Ba, and Th, are retained in the residual part of the migmatite (Fig. 2.3b). Na enrichment in the leucosome is attributed to the higher modal abundance of plagioclase, whereas Fe and Mg accumulation in the restite is controlled by the ferromagnesian phases (biotite and amphibole). HREE are enriched over LREE in the leucosome. For the other analyzed elements, no distinct preference can be seen. Interestingly, those trace elements that follow the same trend as Sn in the low-temperature sample (Li, V, Cr, Zn, and Rb and to a lesser extent Nb and Cs) do not show the same behavior in the high-T sample. This may result from differences in Kd for these trace elements and, thus, fractionation during incomplete breakdown of biotite and/or due to differences in restite mineralogy (e.g. ilmenite in the restite). Rb/Sr ratios in the high-temperature migmatite show little variation between residuum and leucosome (0.31 – 0.65), compared to the low-temperature migmatite.

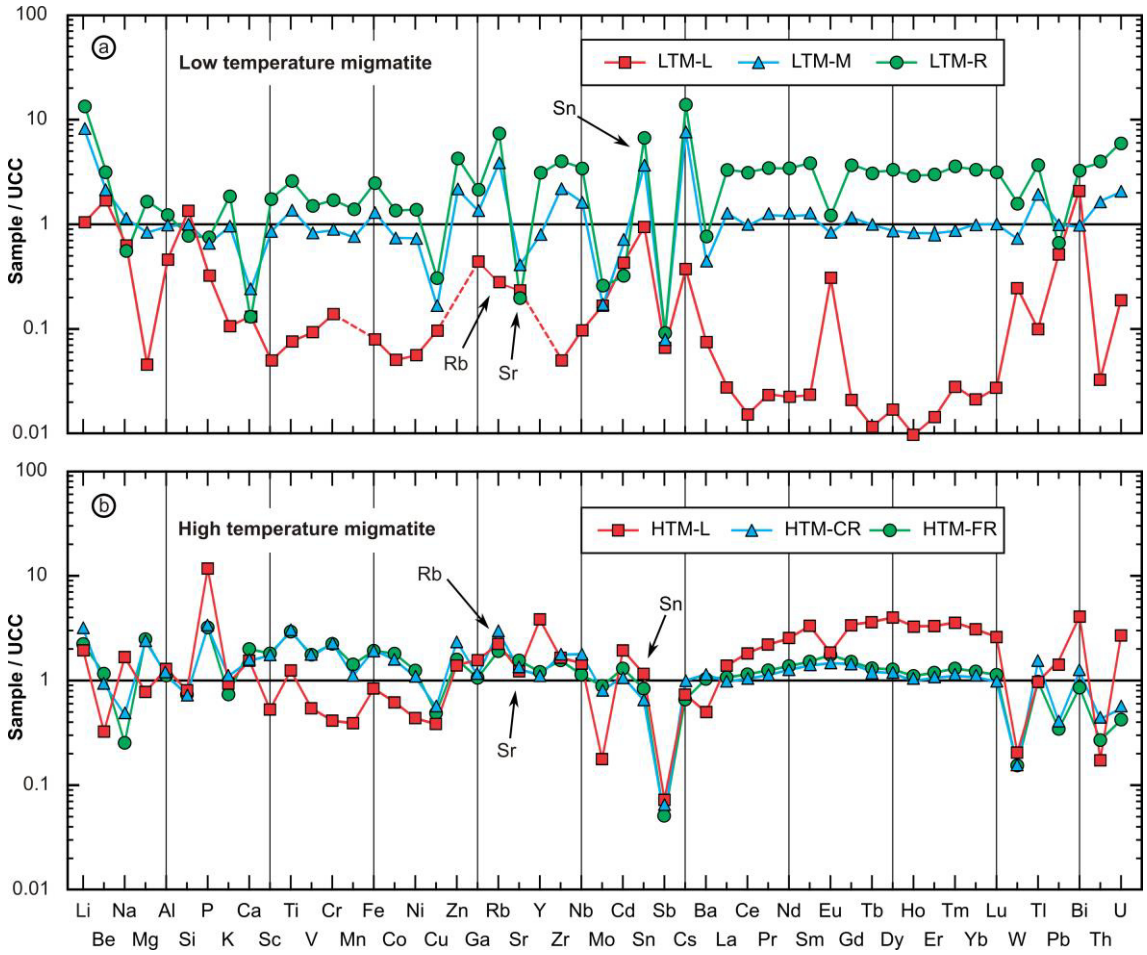


Fig. 2.3. The different domains of the migmatite samples have been separated for whole rock chemical analysis. The whole rock chemical composition of low-temperature migmatite (LTM-L, LTM-M, and LTM-R) and high-temperature migmatite (HTM-L, HTM-CR, and HTM-FR) is normalized to upper continental crust (Rudnick and Gao, 2003). The contrasting patterns of the two samples reflect the different mineralogy of the protoliths and melting phases. (a) In the high-temperature migmatite, Na, Mg, P, Y, REE, Bi, and U partition preferentially into the leucosome. The mesosome and residuum are enriched in Ti, V, Cr, Mn, Fe, Co, and Ni in comparison to the leucosome. (b) For the low-temperature migmatite, Be, Mo, and Bi are the only trace elements that partition into the melt. Note the accumulation of Sn in the mesosome and residuum of the low-temperature migmatite whereas Sn is slightly enriched in the leucosome of the high-temperature migmatite. The Rb/Sr ratios in the three domains of the high-temperature sample show little variation whereas in the low-temperature sample Rb/Sr ratios in the mesosome and residuum are much higher than in the leucosome.

### *2.5.2. Equilibrium phase diagram modeling*

Phase diagrams were calculated for three different cases:

1. a deeply altered Paleozoic shale (APS; feldspar-poor)
2. a deeply altered shale with additional Si (APS+Si)
3. an unaltered shale (UAS; feldspar-rich)

Sample APS (Romer and Hahne, 2010) is a deeply weathered shale from the Paleozoic sedimentary record of the Saxo-Thuringian Zone. As a result of intense weathering, these rocks show a strong depletion in Ca, Na, and Sr due to the

decomposition of feldspar and a relative enrichment in Sn, W, B, Rb, Cs, and Tl. The bulk composition of APS (Table C.1 in the appendix) in moles is Si(49.835), Al(31.732), Mg(1.824), Ca(0.388), Fe(2.703), Na(0.190), Ti(0.891), K(12.428), and H(7.56). Oxygen concentration is adjusted for different oxygen fugacities. The water content corresponds to 1.3 wt%.

Shales are often intercalated with quartzites, thus the $SiO_2$ concentration for sample APS was increased to examine the effect of elevated $SiO_2$ concentrations. The silica enriched composition of APS+Si in moles is Si(79.835), Al(31.732), Mg(1.824), Ca(0.388), Fe(2.703), Na(0.190), Ti(0.891), K(12.428), and H(19.814). As this specific composition generates more mica, the water content of the rock corresponds to 2.3 wt%.

An unaltered shale (UAS, Table C.1 in the appendix) has been modeled to compare the phase assemblage and melt production to the strongly weathered protolith. The composition in moles of the UAS sample is Si(61.974), Al(22.789), Mg(2.528), Ca(0.170), Fe(4.685), Na(2.134), Ti(0.761), K(4.959), and H(6.414). The water content corresponds to 1.0 wt%.

*2.5.2.1. Sample APS*

The equilibrium phase diagram for the sample APS under reducing conditions is shown in Fig. 2.4a. Figure 2.4b shows the same diagram contoured for melt volume. The onset of melting due to the breakdown of muscovite lies between 700 °C at 5 kbar and 785 °C at 10 kbar. Muscovite dehydration melting leads to the generation of 10 vol% melt. The resulting phase assemblage consists of melt, Kfs, Sil, Plg, Bt, and Ilm (+ Grt at elevated pressure). The stability limit of biotite lies between 775 °C and 975 °C for pressures between 3 and 9 kbar. At pressures above 9 kbar, the thermal stability of biotite decreases. After biotite breakdown, the phase assemblage consists of melt, Kfs, Crd, Crn, Ilm (+ Grt, Spl, depending on P and T). As the biotite-out reaction is shifted to higher temperatures with increasing pressure, the amount of melt present during the breakdown varies significantly. At low pressures (e.g. 3.5 kbar) and, thus, low temperatures, 20 vol% of melt formed before the onset of the biotite-out reaction, whereas as much as 45 vol% melt formed before the onset of the biotite-out reaction at 7 kbar.

Equilibrium phase diagrams for the sample APS were calculated with a fixed $fO_2$ at the hematite-magnetite buffer (OHM; see Fig. 2.4c and d). The stability of muscovite and, thus, the onset of melting are not influenced by elevated $fO_2$ values. In contrast to reduced conditions, rutile becomes stable around 600 °C, replacing ilmenite. Garnet and

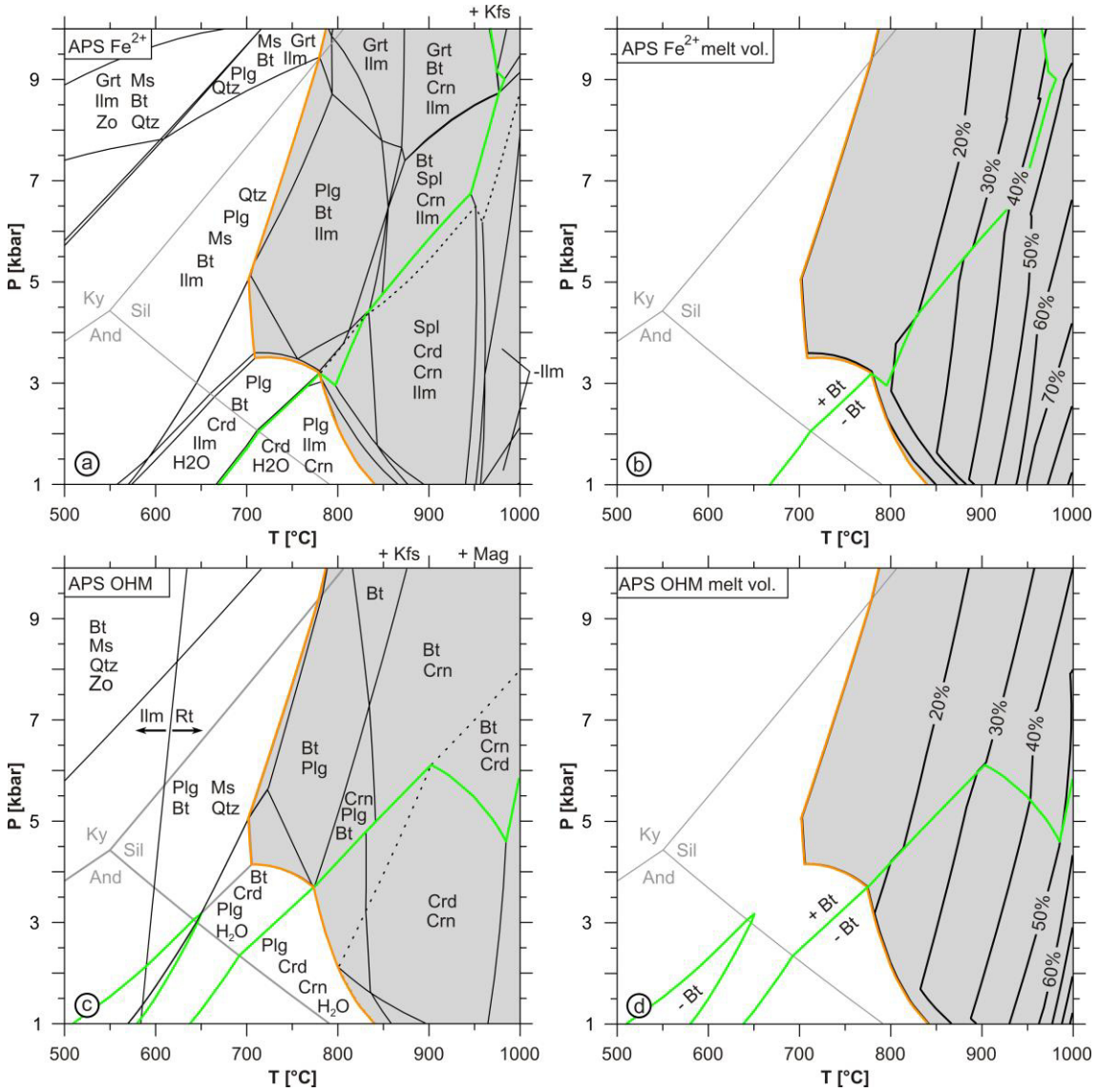


Fig. 2.4. Simplified equilibrium phase diagrams for a strongly weathered shale (APS) illustrating the influence of oxygen fugacity on mineral assemblage, melting conditions and melt production. The green line denotes the Bt-out line and the orange line represents the solidus. The shaded fields contain melt. Fig. 2.4a and c show the phase assemblages under different conditions, Fig. 2.4b and d are contoured for melt volume. The dashed line in the right part of (a) and (c) denotes the Als-out lines, all other fields contain Als. Phases indicated at the top right of each diagram are stable over the whole diagram unless specified otherwise. The fully labelled diagrams are shown in appendix B. (a) Phase diagram under reducing conditions. Biotite stability above the solidus increases with pressure. Early generated melts at pressures above 3 kbar (fields between the orange and green line) coexist with biotite. (b) Melt generation starts between 700 °C and 790 °C, depending on pressure. Muscovite dehydration melting leads to the generation of 10 vol% melt. Melt volume after the breakdown of biotite varies between 20 vol% at low pressure and 45 vol% at elevated pressure. (c) Equilibrium phase diagram at elevated oxygen fugacity (OHM-buffer). The Bt-out reaction is shifted to lower temperatures at low pressures. At pressures above 6 kbar biotite stability exceeds 1000 °C. Ilmenite is replaced by rutile at temperatures above ~600 °C. Melts generated at low temperature and elevated pressures coexist with biotite. Magnetite is stable over the whole modeled P-T space. (d) The onset of melting is not influenced by higher oxygen fugacity. Below 900 °C, melt volumes are slightly higher compared to reduced conditions. The melt volume during biotite breakdown varies between 10 vol% at low pressure and 50 vol% at high pressure.

spinel are not stable within the modeled boundaries. At OHM-buffer conditions, the biotite stability is shifted to lower temperatures than for reducing conditions at pressures below 6 kbar. The maximum difference is around 35 °C at low/intermediate pressures and decreases with increasing pressure. At pressures above 6 kbar, biotite stability is extended to temperatures exceeding 1000 °C. At more oxidizing conditions, the melt volume is slightly higher at temperatures below 900 °C. At higher temperatures, the oxidized rock has a lower fertility, resulting in smaller melt volumes than for reducing conditions. The main difference in mineral assemblage under more oxidizing conditions in comparison with reducing conditions is the absence of garnet and spinel and the presence of magnetite and rutile.

### *2.5.2.2. Sample APS+Si*

The equilibrium phase diagram for the sample APS+Si under reducing conditions is shown in Fig. 2.5a and the corresponding melt volumes are shown in Fig. 2.5b. Melting starts with the breakdown of muscovite at 700 °C and 5 kbar and at 790 °C and 10 kbar. Up to 30 vol% of melt are produced over a narrow temperature interval. The resulting

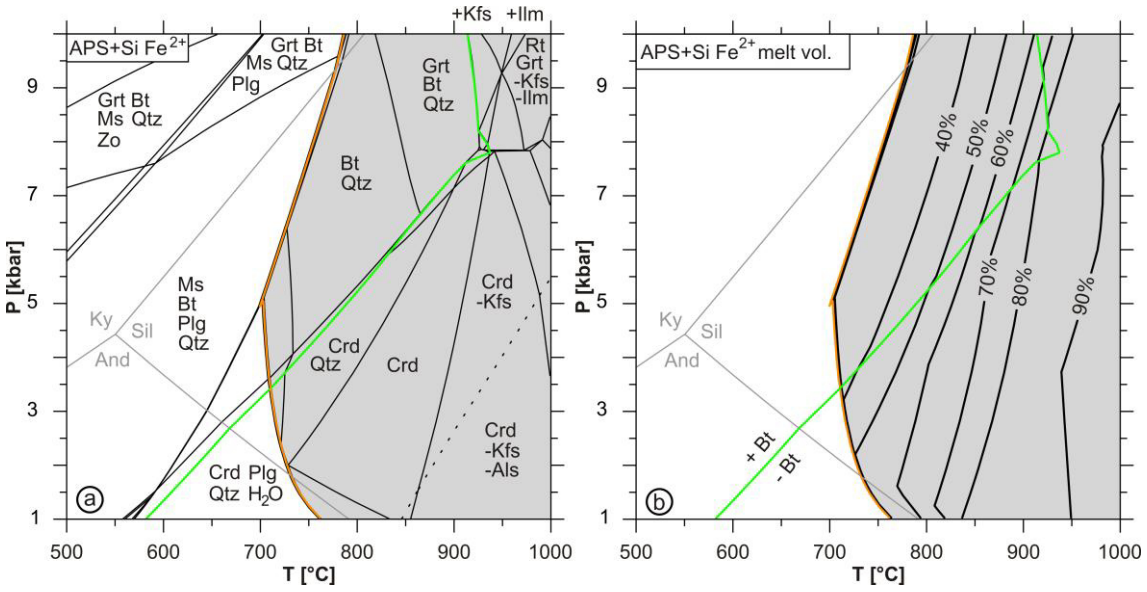


Fig. 2.5. Simplified equilibrium phase diagrams under reducing conditions for a strongly weathered shale with additional Si (APS + Si) illustrating the influence of quartz content on mineral assemblage and melt production. The green line denotes the Bt-out line and the orange line represents the solidus. The dashed line in the right part of (a) denotes the Als-out lines, all other fields contain Als. Phases indicated at the top right of each diagram are stable over the whole diagram unless specified otherwise. The shaded fields contain melt. The fully labelled diagrams are shown in appendix B. (a) Equilibrium phase diagram for sample APS + Si. Muscovite dehydration melting starts at around 700 °C at low pressure and 790 °C at high pressure. Biotite stability varies between 680 °C at low pressure and 925 °C at pressures above 7.5 kbar. (b) The breakdown of muscovite leads to the generation of up to 30 vol% of melt over a narrow temperature interval. During the breakdown of biotite between 40 vol% and 80 vol% of melt are present.

phase assemblage consists of melt, Kfs, Sil, Qtz, Bt, and Ilm. Biotite stability rises with increasing pressure to higher temperatures from 680 °C at 3.5 kbar to temperatures around 925 °C at pressures above 7.5 kbar. As the biotite-out reaction is shifted to higher temperatures with increasing pressure, the amount of melt present during biotite-breakdown varies significantly. At 3.5 kbar, 30 vol% of melt formed before the breakdown of biotite, whereas at 7 kbar as much as 70 vol% melt are produced. At pressures above 7 kbar, the biotite-out reaction crosses lower melt volume contours, resulting in smaller melt volumes at biotite-breakdown (e.g. 60 vol% at 10 kbar).

### *2.5.2.3. Sample UAS*

The equilibrium phase diagram for sample UAS, an unaltered shale, is shown in Fig. 2.6a with the corresponding melt volumes in Fig. 2.6b. Melt generation starts between 650 °C at 3.5 kbar and 750 °C at 10 kbar with the breakdown of muscovite. The mineral assemblage consists of melt, Plg, Kfs, Bt, Qtz, and Ilm (+ Grt at elevated pressure) right after the onset of melting at pressures above 3 kbar. The biotite-out line lies between 680 °C at 3 kbar and 850 °C at pressures above 7 kbar. During the breakdown of biotite above 4 kbar, garnet is stable in the resulting phase assemblage. The melt volumes produced during the breakdown of muscovite remain below 10 vol% at pressures above 2.5 kbar. Melt volumes during biotite-breakdown are between 7 vol% at 3 kbar and 26 vol% at 7 kbar.

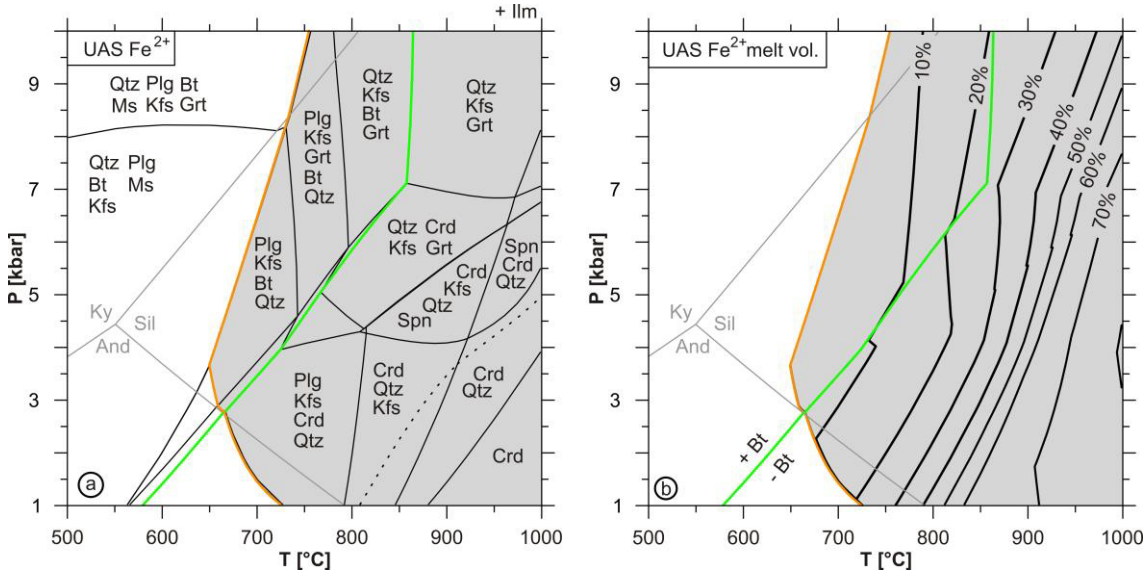


Fig. 2.6. Equilibrium phase diagrams for sample UAS, representing an unaltered shale. The green line denotes biotite-out line. The orange line represents the solidus and shaded fields contain melt. The dashed line in the lower right corner denotes the Als-out line, all other fields contain Als. Phases indicated at the top right of each diagram are stable over the whole diagram unless specified otherwise. The fully labelled diagrams are shown in appendix B. (a) Muscovite breakdown occurs between 650 °C at low pressure and

*Fig. 2.6. continued:*750 °C at elevated pressures. Biotite breakdown with the presence of melt occurs at 680 °C at 3 kbar and 850 °C at pressure above 7 kbar. (b) Melt production at low temperature is very limited with melt volumes below 10 vol% during muscovite dehydration melting. Between 7 vol% and 26 vol% melt are present during the breakdown of biotite.

### *2.5.2.4. Partial melt extraction*

The foregoing diagrams were calculated assuming closed system conditions. As natural rocks are unlikely to hold high amounts of melt (Arzi, 1978), the effects of a hypothetical melt extraction of 90% of the generated melt (20 vol%) at 840 °C and 7 kbar have been modeled for the sample APS. The bulk rock composition after the melt extraction is Si(40.856), Al(28.839), Mg(1.801), Ca(0.201), Fe(2.538), Na(0.125), Ti(0.891), K(10.716), and H(2.815). The recalculated equilibrium phase diagram is shown in Figure 2.7a. The modeled extraction of melt has only minor influence on the melt bearing fields of the system. The main difference compared to the undepleted system is the shift of the corundum-in and plagioclase-out line to lower temperatures. The stability of biotite is shifted to slightly higher temperatures at low pressure. The onset of melting shows no difference at pressures above 3 kbar, whereas at lower pressures, the onset of melting is shifted by ~25 °C to higher temperatures. The melt volumes, however, show significant response to the extraction of melt. The extraction of melt (90% of the available melt at 840 °C and 7 kbar) removes large proportions of water from the system and, therefore, lowers the fertility of the restitic rock significantly, resulting in 50-70% lower melt volume compared to the system without melt extraction at the same P-T conditions (appendix B). The mineral assemblage is only little affected by the modeled melt extraction but the relative proportions of the phases show changes (Fig. 2.7b). Kfs, Als, and Spl show an increase in modal abundance. The modal abundances of Ilm and Bt are marginally influenced.

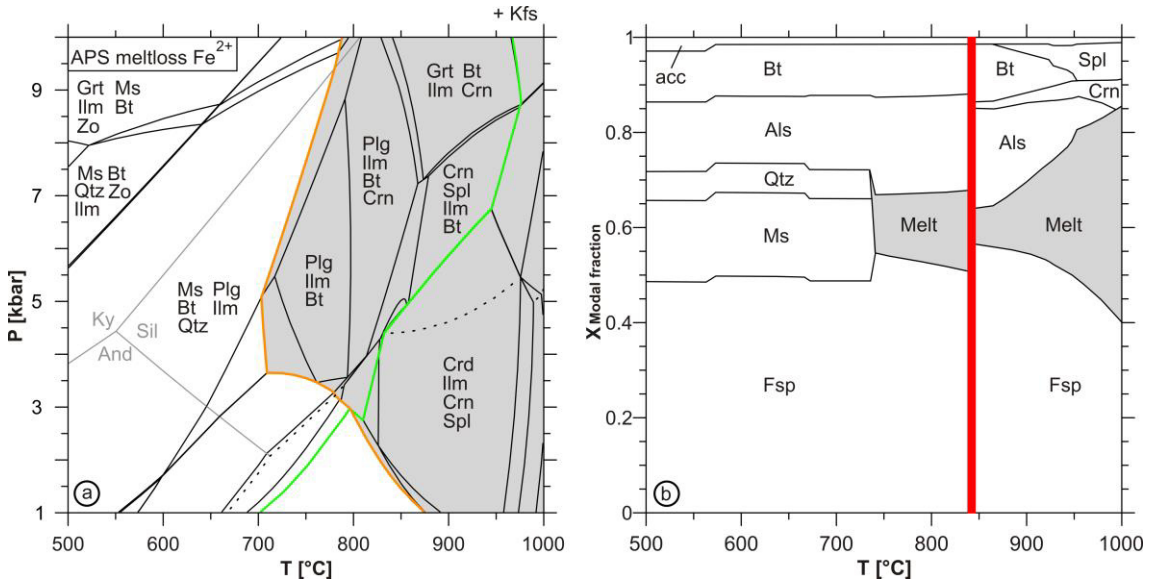


Fig. 2.7. Influence of a melt extraction on mineral assemblage and modal proportions of the phases. The fully labelled diagrams are shown in appendix B. (a) Equilibrium phase diagram for sample APS after 90% of the generated melt at 840 °C and 7 kbar have been extracted from the bulk composition. The green line denotes biotite stability limits. The orange line represents the solidus of the system and shaded fields contain melt. The dashed line in the lower right corner denotes the Als-out line. The phase assemblage is only little affected by the modified bulk composition. The stability limit of plagioclase is shifted towards lower temperatures whereas corundum is stabilized towards lower temperatures compared to the undepleted system (Fig. 2.4a). Biotite-out reaction and melt-in reaction at low pressures are shifted to slightly higher temperatures. (b) Diagram showing the modal amount of the phases stable along an isobaric profile at 7 kbar. The red bar marks a hypothetical melt extraction event of 90% of the generated melt (20 vol%) at 840 °C. The modal fractions before melt extraction are calculated with the original composition of sample APS. The modal amounts after the melt extraction are calculated with the depleted bulk rock composition from Fig. 2.7a. Accessory phases with <1 vol% are added together and labelled with "acc". The main effect of the melt extraction is the relative increase in Sil and Qtz and the smaller volume of melt. Tin released from the breakdown of biotite after the melt extraction partitions into a smaller amount of melt.

## 2.6. Discussion

### *2.6.1. Tin in low-temperature melts*

The decomposition of feldspars in shales during intense chemical alteration results in the loss of Ca and Na and the relative enrichment of K (Nesbitt and Young, 1982). Metamorphism of such rocks results in muscovite- and biotite-rich schists. Fluid absent melting in these rocks starts at 650 °C, depending on rock composition and pressure, with the breakdown of muscovite. The low Ca and Na shales, similar to sample APS, produce large amounts of biotite and muscovite during prograde metamorphism. As dehydration melting involves the breakdown of hydrous phases, together with quartz and feldspar, muscovite-rich shales may produce large amounts of melt over a small temperature interval. This effect is even more pronounced if quartz is added as for sample APS+Si. In this case, up to 40 vol% of muscovite can be produced before the onset of melting, resulting in up to 30 vol% low-temperature melt.

Muscovite melting, however, does not generally result in Sn enrichment in the melt because: (i) enrichment of muscovite-hosted Sn in the melt is limited (e.g. a factor of 2.5 at 40% melting), (ii) available Sn from muscovite is diluted by feldspar and quartz that are involved in melting, and (iii) Sn released from muscovite may strongly partition into restitic phases such as biotite, ilmenite, or rutile.

The element distribution from the LTM together with the modeling results shows, that partial melting by muscovite breakdown leads to a Sn-enriched restite, rather than a Sn-enriched melt. This results from the stability of Sn-sequestering phases in the restite. These effects are well visible in the normalized trace element diagram for the LTM from the Tormes dome (Fig. 2.3b). Although rutile has the potential to host significant amounts of Sn, it is of minor importance under the considered conditions as its stability is restricted to higher pressures. One noteworthy exception is the modeled case with elevated oxygen fugacity (Fig. 2.4c). In that scenario, rutile becomes stable even before the onset of partial melting and remains stable during prograde metamorphism. Low-temperature melting would therefore also result in restite enrichment. This is well in line with the observation that Sn granites are reduced (e.g. Ishihara, 1978).

### *2.6.2. Tin in high-temperature melts*

During high temperature metamorphism, biotite is progressively consumed during biotite dehydration melting. Batch melting of Sn-enriched restitic biotite should result in increased Sn concentrations in the melt, although significant amounts of Sn may remain in the restite as long as biotite is not completely consumed. Provided no other Sn-sequestering phase is stable, biotite breakdown will release Sn into the melt. In the case of the APS sample, biotite breakdown occurs between 775 °C and 950 °C for pressures between 3 and 7 kbar. Final breakdown of biotite in high-temperature migmatites has a high potential to produce melts that are enriched in Sn. The slight enrichment of Sn in the leucosome of the HTM from the Anatectic Complex of Toledo reflects this process (Fig. 2.3b); even though for higher melting temperatures the enrichment of Sn is expected to be more pronounced. Elevated oxygen fugacities stabilize rutile towards low temperatures and pressures (Fig. 2.4c). Under such conditions rutile is stable during high-temperature melting and would inhibit Sn partitioning into the melt. As Ti is currently not included in thermodynamic melt models, care must be taken regarding the stability of Ti-oxide stability from phase equilibria modeling. However, rutile stability can exhibit profound influence on Sn distribution.

### *2.6.3. Effects of melt extraction on tin distribution*

Depending on pressure, temperature and extracted melt volume, bulk rock chemistry changes to variable extent. In the modeled case (20 vol% melt available, 90 % of it extracted at 840°C and 7 kbar) there is only minor impact on the mineral assemblage in the restite. Particularly the stability limits of Sn-sequestering phases (e.g. biotite, muscovite) and, thus, the behavior of Sn, which is concentrated in the restite, are not changed. The most prominent change is the decrease in water and, thus, in melt production. As low-temperature melts have low Sn contents, single or multiple melt extractions of low-temperature melt, i.e. melts that formed by muscovite dehydration melting, result in an increase of Sn content in the restite. Most importantly, the Sn content of later melts that formed by biotite dehydration melting is not diluted by low-Sn melts that formed at lower temperatures. Actually, if high-temperature melts partition some Sn into biotite-bearing restite, the loss of early high-temperature melts also would increase the Sn content of the residue. High Sn contents, however, may be obtained for small volume melts that consume the last Sn-hosting phases (e.g. biotite). In a simplified, hypothetic case with assumed complete partitioning of Sn into restite, 50% of melting at low-temperature and complete melt loss may double the Sn content of the restite. Subsequent 20% high-temperature melting of the remaining restite with a complete transfer of Sn into the melt would result in a melt that has up to five times higher Sn contents than its restite precursor. Thus, such a multi-stage process could result in one order of magnitude higher Sn contents in the melt relative to the starting lithology. Above considerations indicate that multiple melt extraction is a highly efficient process to produce Sn-rich melts without magmatic fractionation. The lack of experimental data on Sn-partitioning between melts and minerals, however, does not allow quantifying the process at the moment.

### *2.6.4. Role of protolith composition on tin distribution between melt and restite*

Protolith composition defines the mineral assemblage and the modal proportions during metamorphism. The mineral phases, in turn, control (a) distribution of tin during partial melting and (b) melting conditions and melt amount. Tin may form phases on its own as for example in cassiterite, it may be hosted in accessory phases (e.g. rutile or titanite), or it can be incorporated in rock forming minerals (e.g. muscovite or biotite). The whole rock Sn budget is controlled by the amount of Sn that is incorporated in a

mineral and the modal abundance of that phase in the rock. Breakdown of the host phases, as during melting reactions, leads to redistribution of Sn among stable phases and eventually to the release of Sn into the melt. The stability of a Sn-sequestering phase during the release of Sn from another mineral prevents enrichment in the melt and leads to Sn enrichment in the restite.

Intensely weathered shales have a high potential for the generation of vast amounts of granitic melts. Shales that experienced extreme chemical alteration at the surface have a Chemical Index of Alteration (CIA = $\left[\frac{Al_2O_3}{(Al_2O_3+CaO^*+Na_2O+K_2O)}\right]\times100$, where CaO* is the calcium content of silicates; Nesbitt and Young, 1982) of >95, which largely reflects the loss of the feldspar bound elements Na, Ca, and Sr and a relative gain in K and Rb that are retained in secondary minerals. This specific rock composition, i.e., low Na and Ca and high K contents, allows for high modal abundances of muscovite and biotite, which both incorporate significant amounts of Sn and which control dehydration melting reactions at different temperatures. Residual enrichment in intensely weathered shales may double the Sn contents relative to the protolith. Although, pre-metamorphic enrichment in the protolith reduces the volume of melt necessary to mobilize a particular amount of Sn, the importance of chemical alteration is not related to this residual enrichment, but to the loss of Ca and Na that affects the metamorphic mineralogy and the melting behavior of the rock, in particular the amount of melt produced at low temperature by muscovite dehydration melting and, thus, the potential of low-Sn low-temperature melts to leave the migmatite source.

Phase diagram modeling of the unaltered shale sample shows that biotite breakdown occurs in average shale at distinctly lower temperatures than in strongly weathered shale. However, melt volumes produced until the final breakdown of biotite is much lower in the average shale. This makes the extraction of significant amounts of melt prior to Sn-mobilization unlikely. Additionally, average shale has much lower Sn content. For instance UAS only has 2.1 to 5.5 ppm Sn (e.g. Taylor and McLennan, 1995; Rudnick and Gao, 2003), whereas highly altered shale with CIA > 95 have Sn contents as high as 7 to 13 ppm (Romer and Hahne, 2010). Thus, to mobilize the same amount of Sn from an unaltered protolith, twice the amount of material must undergo partial melting.

## 2.7. Conclusions

Melt generation in the crust is mainly controlled by source rock composition, pressure, temperature, and the content of hydrous minerals in the source rock (Clemens and Vielzeuf, 1987). Strongly weathered shales have a high content of K and low contents of Na and Ca, which leads to high modal amounts of muscovite and biotite during prograde metamorphism. Thus, these rocks are fertile and large amounts of melt are produced if these protoliths reach appropriate temperature conditions. Sn-specific granites are widely believed to be derived from the melting of sedimentary protoliths (Lehmann, 1990). Our modeling shows that the specific protolith composition and the heat source play an important role. Protolith composition plays an important role in a double sense, (i) by its major element composition that controls mineralogy and, thus, melting conditions and amount of melt and (ii) by its initial Sn content. One lithology of particular interest are intensely altered shales (CIA >95). Tin concentrations in intensely altered shales are higher than in average crustal sediments because of residual enrichment. Although these concentrations are beyond any economic interest, even small levels of enrichment in the protolith become important for the formation of mineralization: higher concentrations of Sn in the protolith require a smaller melt volume to mobilize a particular amount of Sn and, thus, need less energy. Alternatively, a particular rock volume that undergoes melting may result in a distinctly larger amount of Sn that is mobilized. Multistage melting of an enriched protolith can generate melts that show a significant enrichment of Sn even before fractionation starts. Multistage melt extraction with Sn enrichment in late melts is in line with field observations. For instance, the Sn-specific granites of the Erzgebirge (i) show geochemical fingerprints that may be obtained by high temperature melting of chemically intensely altered shales (e.g. Romer and Kroner, 2014), (ii) even the least fractionated granites are geochemically highly evolved (Förster and Romer, 2010), and (iii) Sn mineralization is related to late intrusions within the same magmatic complex (Tischendorf and Förster, 1990; Förster et al., 1999), a feature also found in other major tin provinces (De Laeter and Blockley, 1972; Searle et al., 2012).

**Acknowledgment**

Many thanks to Uwe Kroner and Miguel López Plaza for their help in the field and to Carlos Villaseca for his information about the ACT outcrops. Furthermore we thank Andrea Gottsche, Sabine Tonn, Heike Rothe, and Bettina Hübner for their support in the laboratory for the major and trace element data.

# Chapter 3: Isotope disequilibrium during partial melting of metasedimentary rocks


## Abstract

The chemical composition of partial melts is buffered by the rock forming minerals that participate in the melting reactions and by the solubility of accessory phases in the melts. Both depend on the melting conditions. The chemical composition of restite depends on the restite mineralogy and may be highly variable. Partial melts and restite show contrasting Sr and Nd isotopic compositions if the various mineral phases of the protolith have developed contrasting Sr and Nd isotopic compositions by radiogenic in situ ingrowth, which depends on the parent-to-daughter ratios and time. We present chemical and isotopic data from different leucosome-restite pairs that differ by 13 to 67 εSr-units and 0.2 to 6.2 εNd-units, respectively. As the Sr and Nd isotopic composition of the partial melts shows little variation for comparable protoliths, the difference in Sr and Nd isotopic composition is related to the restites, whose variable compositions largely reflects variations in the mineral assemblage.

We present Li and B concentration and isotope data from a smallscale profile across the contact between leucosome and restite. Lithium has systematically lower concentrations and higher $\delta^7$Li in the leucosome than in the restite. There is a sharp change in $\delta^7$Li at the contact between restite and leucosome. In contrast, B shows only minor variations in concentration and isotopic composition across the contact zone. Our data indicate that (i) the Li and B isotopic compositions of the leucosome is controlled by different minerals (ii) isotope fractionation of Li and B by diffusion processes is of subordinate importance on the handspecimen scale, even at magmatic conditions.

## 3.1. Introduction

The isotopic composition of magmatic rocks is widely used to trace the protoliths of melts and to quantify the relative contributions of isotopically contrasting end-member reservoirs (DePaolo and Wasserburg, 1979; McCulloch and Chappell, 1982; Lesher, 1990; Chappell, 1996). The basic assumption for this type of geochemical tracing of the magma sources is that the partial melts have the same isotopic composition as their protoliths. The fundamental requirement for mass-balance estimates for magma mixing or wallrock assimilation is that the isotopic compositions and the elemental concentrations of the involved end-member reservoirs are reasonably well known. Both geochemical tracing and mass-balance estimates commonly treat the mobilization of partial melts from a source as bulk processes with isotopic compositions and element contents of the mobilized material being similar to those of the protoliths (Fig. 3.1a). These simplifications disregard that trace elements partition between melt and restite material and that there may be no chemical or isotopic equilibration between restite minerals and melt. The prime example for such a lack of equilibration is the older age of inherited zircon in the restite. There may be many other minerals that do not equilibrate either. Thus, the assumption of the melt composition being representative for the protolith represents a simplification that may point toward the wrong source or the isotopic composition of the melt does not reflect the correct relative contributions of different sources properly.

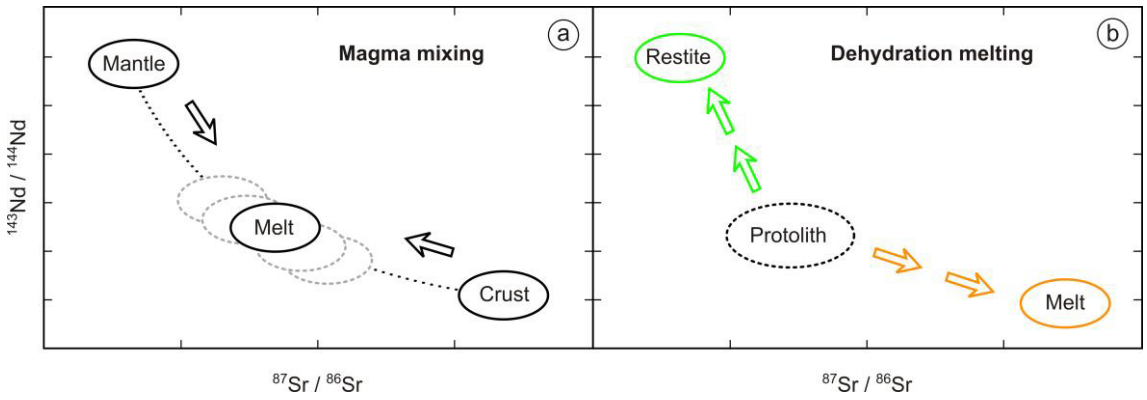


Fig. 3.1. Schematic $^{143}Nd/^{144}Nd$ – $^{87}Sr/^{86}Sr$ diagram for magma mixing and partial melting. (a) Variable mixing of melts from two end-member reservoirs leads to a hyperbolic trend with the isotopic composition of individual samples representing the weighted contribution of each reservoir. (b) As rock-forming minerals may have a broad range of radioactive parent-to-daughter element ratios, the isotopic composition of the daughter element eventually differs among the various minerals. Partial melting does not involve all minerals and, therefore, the isotopic composition of partial melts may differ from that of the bulk sample and among subsequent melt batches. The contrast in the Sr and Nd isotopic composition of melt and restite depend on the nature of the melting phases and their age.

Dehydration melting is controlled by the nature and proportion of the hydrous phases (muscovite, biotite, amphibole) and the modal abundance of quartz and feldspar (Thompson, 1982; Vielzeuf and Holloway, 1988; Vielzeuf and Montel, 1994). The nature of the OH-bearing minerals controls the melting conditions, whereas its modal abundance influences the amount of melt that can be produced (Le Breton and Thompson, 1988). Thus, the major element composition of the melt is largely buffered by the rock forming minerals involved in the melting reaction (e.g. muscovite, biotite, feldspar, quartz). The trace element content of the melt is controlled by three factors: (i) the trace element inventory of minerals that melt, (ii) the degree of saturation of the melt in P, Ti, and Zr for elements that are dominantly bound to minerals of these elements, i.e., phosphates (apatite, monazite, xenotime), Ti-minerals (titanite, ilmenite, rutile), and zircon (Watson and Harrison, 1983; Rapp and Watson, 1986), and (iii) partitioning between melt and restite. The situation is considerably more complicated for the isotopic composition of melt and restite for elements with radiogenic isotopes, as the various minerals have different parent-to-daughter ratios (P/D) and, thus, the elements with radiogenic ingrowth (e.g. Sr, Nd, Pb) develop contrasting isotopic compositions with time. The isotopic composition of partial melt and restite reflects the weighted average P/D of the minerals that are melted and the minerals that remain in the restite, respectively. Figure 3.1b shows schematically how the partial melting of an old rock involving feldspar and mica that have high Rb/Sr and low Sm/Nd ratios eventually results in a melt with higher $^{87}Sr/^{86}Sr$ and lower $^{143}Nd/^{144}Nd$ than the corresponding restite that is dominated by minerals that have lower Rb/Sr and higher Sm/Nd ratios.

We present chemical and isotopic data from melt and restite pairs from migmatites that formed at different conditions and show that partial melting under mid crustal conditions may lead to contrasting isotopic signatures in melt and restite that are both different from the protolith. We show that the isotopic composition of the melt is buffered by the nature of the melting phases, which leads to relatively homogeneous isotopic fingerprints in the leucosome domains of different samples. The isotopic composition of the residual material, however, is determined by the modal composition of the restite and, therefore, may be very variable. Furthermore, we show that isotopic disequilibrium between melt and restite is not restricted to radiogenic isotopes, it is to variable extent also observed for the stable isotopes, as for instance for Li and B.

## 3.2. Samples and geological context

Four high-temperature (HTM_1 – 4) and one low-temperature (LTM) leucosome-melanosome pairs from different migmatites were analyzed for their chemical, isotopic, and mineralogical composition. Leucosome and melanosome were separated manually and several hundred grams of material of each sample were processed for chemical and isotopic analysis. For the low-temperature sample, a profile over the three different domains (leucosome, melanosome, and mesocratic residuum) was prepared and subdivided into seven segments to document potential spatial variations in Li and B isotopic composition across the contact. The leucosome and mesocratic residuum segments were analyzed as whole rock samples, whereas minerals fractions were prepared from the contact (melanosome) segment and analyzed separately.

### *3.2.1. High-temperature samples*

High temperature schollen migmatite samples were collected from the Anatectic Complex of Toledo (ACT), part of the Central Iberian Zone, Spain. In the ACT there occur high-grade metasedimentary and meta-igneous rocks, calc-alkaline granitoids with associated mafic rocks, and restite-rich peraluminous leucogranites (Barbero and Villaseca, 2000). During the Variscan orogeny, the area experienced high-T, low-P (800 ± 25 °C at 4–6 kbar) conditions that triggered anatexis controlled by biotite dehydration melting (Barbero, 1995; Castiñeiras et al., 2008). The leucosome domains of the high-T samples (Fig. 3.2a) consist of coarse-grained K-feldspar, plagioclase, quartz, minor biotite, apatite, zircon, and small amounts of ilmenite. The residual domains contain plagioclase, quartz, biotite, and accessory apatite, zircon, and ilmenite. The residuum of HTM_3 additionally contains amphibole and HTM_4 has some garnet in the restite. Grain size in the residual domains is generally smaller and increases towards the leucosome domains. $X_{Mg}$ and F content of biotite decrease continuously, whereas Ti and Al contents increase towards the leucosome. The anorthite component of plagioclase decreases from residuum ($An_{80–85}$) to the leucosome ($An_{30–35}$).

### *3.2.2. Low-temperature sample*

The folded metapelitic low-temperature stromatic migmatite (Fig. 3.2d) was sampled in the Tormes Dome anatectic region, located in the northwestern part of the Iberian Massif. Isothermal exhumation of these rocks (700–740 °C at 3 kbar) triggered extensive migmatization and anatexis by muscovite dehydration melting between 325 and

320 Ma (Escuder Viruete et al., 2000; Valverde-Vaquero et al., 2007). The low temperature migmatite (LTM) contains a mesocratic residuum, a melanosome, and a leucosome (Fig 3.2e). The leucosome domain is mainly composed of coarse-grained plagioclase and quartz with minor, small biotite flakes (Fig. 3.2f). Sillimanite in the leucosome is partially replaced by secondary muscovite. The melanosome is dominated by biotite with abundant zircon and monazite inclusions, plagioclase, tourmaline, and quartz. The mesocratic residuum part of the sample contains biotite, plagioclase, quartz, and tourmaline (Fig. 3.2f).

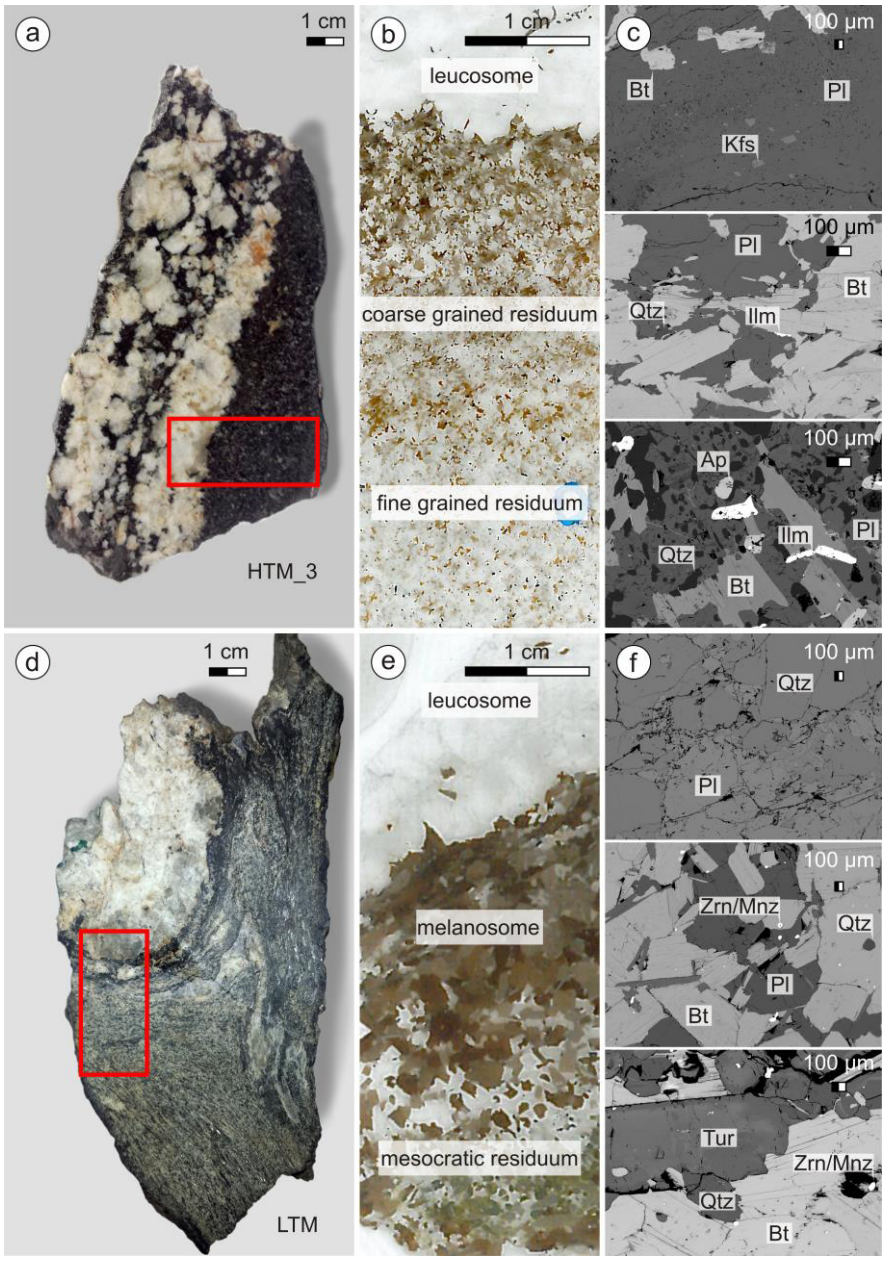


Fig. 3.2. Hand specimen, thin section, and BSE pictures from high- (a-c; sample HTM_3) and low-temperature (d-e; sample LTM) migmatites. Red frames show the location of the thin sections. Grain size and mineralogy in the high-temperature sample (HTM_3) show distinct changes from restite to leucosome.

## 3.3. Methods

### *3.3.1. Whole rock chemistry*

Major element oxides ($SiO_2$, $Al_2O_3$, $Fe_2O_3$, MnO, CaO, $K_2O$, $TiO_2$, $Na_2O$, $P_2O_5$) and some trace elements (V, Cr, Ni, Zn, Ga, Y, Zr, Nb, and Ba) were analyzed on fused glass disks using a PANalytical® AXIOS Advanced X-ray fluorescence (XRF) spectrometer. The instrument is equipped with a rhodium anode end-window X-ray tube operated at 2.7 kW. Whole rock samples were crushed and powdered in an agate disc mill, and sieved to < 63 μm grain size. The powdered samples were dried in an oven at 105 °C over night. Platinum vessels were filled with 1.0 g of the powdered sample, mixed with 6.0 g of lithium tetraborate as fluxing agent and 0.5 – 0.7 g ammonium nitrate as oxidizer. The vessels were heated in several steps (400 °C – 1150 °C) to prepare fused lithium tetraborate discs (see Romer and Hahne, 2010 and references therein for more analytical details).

Sample digestion for REE analysis was done by the $Na_2O_2$ sinter digestion method (Zuleger and Erzinger, 1988). 1.0 g of rock powder (<63 μm) was mixed with 3.0 g $Na_2O_2$ in a platinum crucible, covered with 1.0 g $Na_2O_2$ and placed in a muffle furnace at 480 °C for one hour. The sinter cake was transferred into tubes and centrifuged with distilled water twice to wash out sodium hydroxide and soluble silica salts. The remaining sinter cake was then dissolved in ~100 ml 1mol/l HCl. REE separation and concentration was done by ion exchange columns (diameter 20 mm), using 31.5 $cm^3$ Dowex® 50-WX-8 (200–400 mesh) resin. After washing and conditioning, major and trace elements were washed out using 500 ml 1.7 mol/l HCl. REE and Y were then eluted quantitatively with 500 ml 4 mol/l HCl. After filtering and drying, the residue was dissolved in 10 ml 10% HCl and measured using an Agilent Technologies® 5110 ICP-OES.

For trace element determination, 125 mg of rock powder (<63 μm) were digested with 2 ml concentrated HF and 2 ml aqua regia in closed Savillex vials on the heating plate (160 °C) for several hours. Further digestion steps involved addition of 1 ml concentrated $HClO_4$ followed by another evaporation step, addition of 2 ml $H_2O$ and 1 ml concentrated $HNO_3$, and after drying again, addition of 1 ml concentrated $HNO_3$ and 5 ml $H_2O$. Beakers were then put on the heating plate for another 10 h (100 °C). The solution was diluted (1:2000) with 2% $HNO_3$ for trace element determination using a Thermo Fisher® Element 2XR.

### *3.3.2. Radiogenic and stable isotopes*

Sample dissolution, separation, and concentration of Sr, Nd, and Pb were done using HF digestion and ion-exchange chromatography. For analytical details see Table 3.1 and Romer et al. (2005).

Lithium sample dissolution of 0.08 – 0.1 g of rock powder and mineral separates was done with concentrated HF. The sample was taken up in 2N $HNO_3$ and gently dried to decompose and dissolve fluorides. The samples were then dissolved in 6N HCl and heated for several hours until a clear solution was obtained. Dissolution of tourmaline was done by closed vessel pressure digestion with HF. Lithium purification involved two steps, using 1N $HNO_3$ in 80% methanol on BioRad AG 50 W-X8 200–400 mesh exchange resin and 1N HCl in 80% methanol on BioRad AG 50 W-X12 200–400 mesh exchange resin. Details on column separation and analytical procedure are described in Table 3.1 and in Romer et al. (2014).

Boron sample dissolution and ion-exchange chromatography were done following the slightly modified approach of Tonarini et al. (1997) and Kasemann et al. (2001) described in Romer et al. (2014). Sample powders were fused together with $K_2CO_3$ in platinum crucibles. Melt cakes were dissolved in ultrapure water, centrifuged, and transferred into Savillex beakers. The residual material was washed several times to ensure that boron is transferred quantitatively. A boron specific resin (Amberlite 743) was added to the samples. Purification and separation of boron was achieved in two steps. In a first step, elements that are highly soluble under alkaline conditions were washed out using BioRad polyprep columns. Adsorbed boron was eluted with 12 ml of 0.5N HCl. 100 µl of Mannitol were added to avoid boron loss during drying. The second purification step was done using BioRad polyprep columns filled with 2 ml BioRad AG 50W-X8 resin. Adsorbed boron-mannitol complexes were washed out using 8 ml 0.02N HCl while unwanted cations remained on the resin. Analytical details are given in Table 3.1 and in Romer et al. (2014).

Table 3.1. Whole-rock Sr, Nd, Pb, Li, and B isotope data of analyzed migmatites.

| Sample[a] | Age (Ma) | $^{87}Sr/^{86}Sr$ [b] | $^{87}Sr/^{86}Sr_{(T)}$ [c] | $^{143}Nd/^{144}Nd$ [b] | $\varepsilon Nd_{(T)}$ [c] | $^{206}Pb/^{204}Pb$ [d] | $^{207}Pb/^{204}Pb$ [d] | $^{208}Pb/^{204}Pb$ [d] | $^{206}Pb/^{204}Pb$ [e] | $^{207}Pb/^{204}Pb$ [e] | $^{208}Pb/^{204}Pb$ [e] | $\delta^7Li$ [f] ±2 SE | Li [g] [ppm] | $\delta^{11}B$ [h] ±2 SE | B [i] [ppm] |
|---|---|---|---|---|---|---|---|---|---|---|---|---|---|---|---|
| High-temperature samples | | | | | | | | | | | | | | | |
| HTM_1 L | 320 | 0.713996±5 | 0.70989±17 | 0.512147±3 | –7.2 | 18.518 | 15.651 | *39.078* | 18.20 | 15.63 | *39.04* | 0.82±0.09 | 20 | –8.91±0.33 | 4.0 |
| HTM_1 R | 320 | 0.723495±6 | 0.70625±72 | 0.512299±3 | –4.1 | 18.654 | 15.667 | 38.442 | 18.06 | 15.64 | 38.32 | –1.55±0.09 | 59 | –9.93±0.09 | 2.1 |
| HTM_2 L | 320 | 0.712760±6 | 0.70989±12 | 0.512132±6 | –7.1 | 18.575 | 15.649 | 38.346 | 18.27 | 15.63 | 38.29 | 0.78±0.16 | 13 | –9.27±0.26 | 4.5 |
| HTM_2 R | 320 | 0.723682±6 | 0.70895±61 | 0.512149±3 | –6.9 | 19.007 | 15.676 | 38.555 | 18.10 | 15.63 | 38.26 | 0.67±0.17 | 69 | –10.16±0.08 | 1.7 |
| HTM_3 R1 | 320 | 0.708748±5 | 0.70450±18 | 0.512439±2 | –0.6 | 18.623 | 15.670 | 38.659 | 18.06 | 15.64 | 38.19 | –1.13±0.18 | 41 | 0.57±0.07 | 4.2 |
| HTM_3 R2 | 320 | 0.712890±4 | 0.70653±27 | 0.512413±4 | –1.1 | 18.721 | 15.664 | 38.770 | 18.02 | 15.63 | 38.09 | –0.93±0.07 | 59 | 3.27±0.09 | 3.8 |
| HTM_3 L | 320 | 0.715592±6 | 0.70925±27 | 0.512167±5 | –6.8 | 18.917 | 15.679 | 38.390 | 18.01 | 15.63 | 38.32 | 0.52±0.10 | 34 | –7.05±0.10 | 3.7 |
| HTM_4 L | 320 | 0.710747±4 | 0.709353±68 | 0.512121±4 | –5.7 | 18.335 | 15.647 | 38.863 | 18.11 | 15.64 | 38.06 | 2.24±0.33 | 7.7 | 2.32±0.05 | 7.7 |
| HTM_4 R | 320 | 0.715640±3 | 0.70736±35 | 0.512109±5 | –5.2 | 18.793 | 15.684 | *43.477* | 18.10 | 15.65 | *36.97* | –1.51±0.13 | 29 | –1.99±0.06 | 4.3 |
| Low-temperature samples | | | | | | | | | | | | | | | |
| LTM L | 320 | 0.723487±3 | 0.71936±18 | 0.512058±9 | –7.7 | 18.427 | 15.631 | 38.274 | 18.23 | 15.62 | 38.23 | 3.13±0.11 | 19 | See profile data Table 3.3 | |
| LTM M | 320 | 0.748563±7 | 0.7188±12 | 0.512064±4 | –7.6 | 19.169 | 15.715 | 39.377 | 18.13 | 15.66 | 38.28 | –7.03±0.09 | 123 | See profile data Table 3.3 | |
| LTM R | 320 | 0.826820±4 | 0.7171±35 | 0.512071±3 | –7.9 | 22.322 | 15.866 | *41.506* | 18.15 | 15.65 | *37.39* | –7.61±0.12 | 269 | See profile data Table 3.3 | |

**a** Samples were dissolved with concentrated HF for four days at 160°C on the hot plate. Digested samples were dried and taken up in 6N HCl. Strontium and Nd were separated and purified using ion-exchange chromatography as described in Romer et al. (2005). L = leucosome, M = melanosome, R = restite.

**b** $^{87}Sr/^{86}Sr$ and $^{143}Nd/^{144}Nd$, normalized to $^{86}Sr/^{88}Sr = 0.1194$ and $^{146}Nd/^{144}Nd = 0.7219$, respectively. Strontium and Nd isotope data were analyzed on a Triton multi-collector mass-spectrometer, using dynamic multicollection. Rb/Sr and Sm/Nd ratios are shown in Table 3.2. Analytical uncertainties are given at $2\sigma_m$ level.

**c** $^{87}Sr/^{86}Sr_{(T)}$ and $\varepsilon Nd_{(T)}$ were calculated for migmatization age using $\lambda^{87}Rb = 1.3972E\text{-}11\ y^{-1}$ and $\lambda^{147}Sm = 6.54E\text{-}12\ y^{-1}$, $(^{147}Sm/^{144}Nd)^0_{CHUR} = 0.1967$, and $(^{143}Nd/^{144}Nd)^0_{CHUR} = 0.512638$, respectively, and the concentration data given in Table 3.2. Uncertainties for initial 87Sr/86Sr isotopic compositions include propagated uncertainties of $^{87}Rb/^{86}Sr$ ratios (±3%) and of the absolute age of migmatization (320 Ma ±3%).

**d** Lead isotope data corrected for mass discrimination with 0.1% / A.M.U. Reproducibility at $2\sigma$ level is better than 0.1%.

**e** Lead isotope data recalculated to the time of migmatization using the contents of Pb, Th, and U (Table 3.2) and the constants recommended by IUGS: $\lambda^{232}Th = 4.9475E\text{-}11\ y^{-1}$, $\lambda^{235}U = 9.848E\text{-}10\ y^{-1}$, and $\lambda^{238}U = 1.55125E\text{-}10\ y^{-1}$. Recalculated values given in italics seem geologically unreasonably low due to post-migmatization disturbance of their U–Th–Pb systematics.

*Table 3.1. continued:*

**f** Lithium isotopes were analyzed on a MC-ICP-MS Neptune (Thermo Fisher Scientific, TFS) using the standard–sample bracketing method and NIST8545 as reference solution. The internal precision of repeatedly analyzed sample solution is given as 2 SE. Independent replicates of reference materials show an external reproducibility of better than 0.4‰ For analytical details see text and Romer et al. (2014).

**g** Lithium content was determined on a MC-ICP MS Neptune (TFS) on aliquots of the same sample solution that was used for isotope analysis. The data of independently analyzed reference materials replicate well within 10% (2 SD).

**h** Boron isotope ratios were measured on a MC-ICP-MS Neptune (TFS) using the standard-sample-standard bracketing method and NBS951 reference material. Sample and standards were diluted to 50 ppb with 2% $HNO_3$. Boron isotope ratios are expressed in the delta notation relative to measured NBS951. Independent replicates show an external reproducibility of better than 0.4‰. For analytical details see text and Electronic Annex 3 in Romer et al. (2014).

**i** Boron content was determined by MC-ICP-MS on aliquots of the same sample solution, which was used for isotope analysis. Completely independent replicates show a reproducibility of better than 10% (2 SD).

## 3.4. Results

### *3.4.1. Whole rock chemistry*

The major element composition of restite and leucosome domains from high-T and low-temperature migmatites are shown in Table 3.2 and Fig. 3.3a. Weighted recombination of restite and leucosome to a "bulk" sample reveals that high- and low-temperature samples had slightly different protoliths. The high-T migmatites have higher Ca, Na, Ti, and P contents. For the present study, this variation in protolith chemistry is not critical as we are interested in the distribution of elements between melt and restite. It means, however, that the trace element inventory of low-temperature and high-temperature melts or restites are not directly comparable. It is noteworthy that phosphorus contents in the high-temperature samples are relatively high, and P concentration in the leucosomes is above apatite saturation (calculated after Bea et al., 1992). This is attributed to the entrainment of restitic "biotite-schlieren", including apatite grains, into the leucosome.

The distinct compositions of leucosome and restite domains (Table 3.2 and Fig. 3.3a) reflect the mineralogy of the melting and restite phases, respectively, and the redistribution of elements between melt and stable restite minerals. For instance, Rb and Ba released from melting phases may partition into restitic biotite. The elements Si, Al, and Na in the leucosomes are controlled by the melting phases quartz, feldspar, and mica. The distribution of Ca does not show a clear preference for leucosome or restite, whereas the contents of K in most leucosome samples are lower than would be expected for minimum melts in a haplogranitic system (e.g. Patiño Douce and Johnston, 1991). The elements Ti, Fe, Mn, Mg, and K are predominantly hosted in restitic phases, in particular in biotite. Therefore, they are depleted in the leucosomes and their variable contents in leucosomes of the high-temperature migmatites may reflect variable degrees of biotite-dehydration melting as well as mineralogical or modal heterogeneities in the leucosomes on a local scale.

#### *3.4.1.1. High-temperature migmatites*

Trace element distribution between leucosome and restite for high-temperature migmatites is shown in Table 3.2 and Fig. 3.4a. The trace element distribution is controlled by contributions from the melting rock-forming minerals, in which trace elements substitute for major elements, and the solubility of accessory phases, which

strongly enrich some of the trace elements, as well as the partitioning of trace elements between melt and restite minerals. The trace elements Li, Sc, V, Cr, Co, Ni, Cu, Zn, Mo, Ba, and Th show a clear preference for the restite in high-temperature samples, whereas Be, Ga, Rb, Zr, Nd, Cs, and Tl show a more variable behavior even though they are generally enriched in the restite. Strontium, Cd, Sn, and W typically partition preferentially into the leucosome. Lead and Sb are the only trace elements that are enriched in the leucosome of all analyzed high-temperature samples. Yttrium, Bi, and U show no clear preference for leucosome or restite. There are two pattern of REE distribution between leucosome and restite: (i) REE are enriched in the leucosome (HTM_1 and 3) and (ii) REE are enriched in the restite (HTM_2 and 4; Fig. 3.3b).

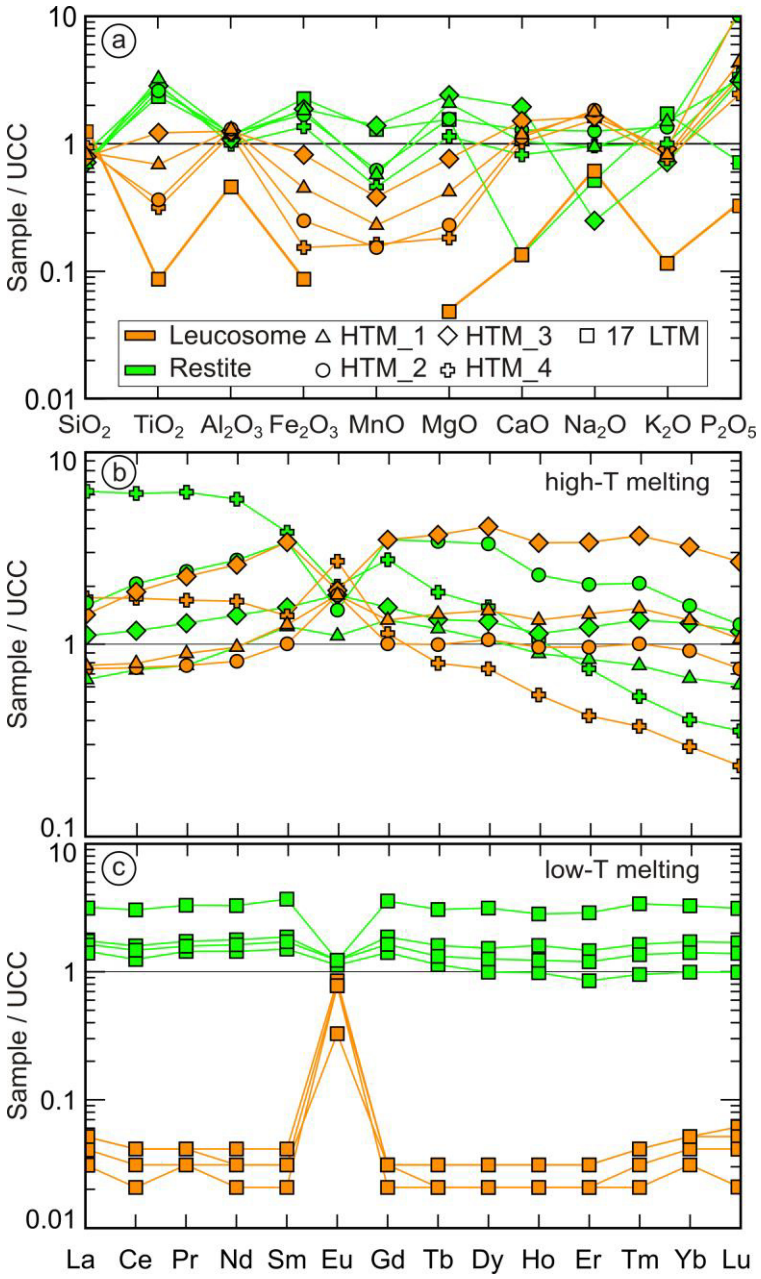


Fig. 3.3. (a) Major element concentrations of high- and low temperature migmatites normalized to upper continental crust (UCC; Rudnick and Gao, 2003). Leucosome-melanosome pairs from the same migmatic complex show similar major element pattern, compositional differences may be explained by differences in modal mineralogy and/or local entrainment of restitic material into the leucosome. Chemical differences between high- and low-temperature migmatites are due to differences in protolith compositions. (b) UCC normalized REE distribution between leucosome and restite pairs for high-temperature samples is contrasting between different samples reflecting different accessory phase inventory. (c) UCC normalized REE concentrations from low-temperature leucosome-restite pairs. Accumulation of REE in the restite is attributed to the almost exclusive occurrence of accessories, predominantly monazite and zircon, in the restite.

Table 3.2. Major and trace element data for high- and low temperature migmatite samples

| | HTM_1 L | HTM_1 R | HTM_2 L | HTM_2 R | HTM_3 R1 | HTM_3 R2 | HTM_3 L | HTM_4 L | HTM_4 R | LTM L | LTM M | LTM R |
|---|---|---|---|---|---|---|---|---|---|---|---|---|
| $SiO_2$(wt%) | 60.2 | 48.6 | 62.4 | 48.2 | 50.2 | 49.6 | 55.0 | 66.6 | 59.9 | 88.4 | 66.5 | 52.4 |
| $TiO_2$ | 0.46 | 2.19 | 0.24 | 1.76 | 1.91 | 1.97 | 0.82 | 0.22 | 1.99 | 0.055 | 0.87 | 1.58 |
| $Al_2O_3$ | 20.9 | 19.1 | 21.1 | 19.6 | 17.6 | 18.0 | 20.4 | 19.1 | 16.1 | 7.40 | 14.7 | 18.6 |
| $Fe_2O_3$ | 2.39 | 9.70 | 1.32 | 8.95 | 9.93 | 10.1 | 4.33 | 0.81 | 7.29 | 0.45 | 6.45 | 11.9 |
| MnO | 0.024 | 0.060 | 0.016 | 0.065 | 0.15 | 0.11 | 0.040 | 0.017 | 0.048 | bdl | 0.076 | 0.14 |
| MgO | 1.10 | 5.44 | 0.60 | 4.10 | 6.31 | 6.02 | 1.98 | 0.46 | 3.00 | 0.13 | 2.08 | 4.03 |
| CaO | 4.44 | 3.90 | 4.24 | 4.86 | 7.35 | 5.66 | 5.71 | 3.89 | 3.11 | 0.52 | 0.90 | 0.49 |
| $Na_2O$ | 6.12 | 3.24 | 6.32 | 4.32 | 0.85 | 1.58 | 5.59 | 5.30 | 3.31 | 2.10 | 3.67 | 1.78 |
| $K_2O$ | 2.42 | 4.40 | 2.33 | 3.97 | 2.11 | 3.16 | 2.68 | 2.25 | 2.97 | 0.33 | 2.68 | 5.08 |
| $P_2O_5$ | 0.70 | 0.51 | 0.53 | 1.68 | 0.49 | 0.50 | 1.81 | 0.39 | 0.56 | 0.051 | 0.10 | 0.11 |
| $H_2O$ | 0.8 | 1.75 | 0.59 | 1.64 | 1.91 | 2.06 | 0.98 | 0.63 | 1.54 | 0.50 | 1.52 | 3.01 |
| $CO_2$ | 0.19 | 0.06 | 0.08 | 0.07 | 0.34 | 0.24 | 0.08 | 0.14 | 0.14 | 0.05 | 0.06 | 0.07 |
| Total | **99.7** | **98.9** | **99.8** | **99.2** | **99.2** | **99.0** | **99.4** | **99.8** | **99.4** | **100.0** | **99.6** | **99.2** |
| Li(ppm)[a] | 20.8 | 59.4 | 13.5 | 69.9 | 41.6 | 59.7 | 34.4 | 7.70 | 29.2 | 19.8 | 123 | 270 |
| Be | 0.8 | 1.0 | 0.8 | 0.5 | 2.5 | 2.0 | 0.7 | 2.3 | 1.4 | 3.5 | 4.4 | 6.5 |
| Sc | 4.3 | 20 | 2.3 | 15 | 26 | 25 | 7.4 | 1.3 | 7.6 | 0.8 | 12 | 24 |
| V[b] | 26 | 191 | 18 | 119 | 175 | 168 | 54 | bdl | 83 | 10 | 81 | 142 |
| Cr[b] | 26 | 183 | 14 | 110 | 211 | 215 | 39 | 1.2 | 14 | 14 | 81 | 153 |
| Co | 6 | 27 | 5 | 23 | 32 | 28 | 11 | 1.8 | 20 | 1.3 | 13 | 23 |
| Ni[b] | 12 | 52 | 11 | 49 | 60 | 52 | 21 | 2.6 | 23 | 3[c] | 35 | 64 |
| Cu | 2 | 17 | 4 | 43 | 14 | 16 | 11 | 2.6 | 6.4 | 2.6 | 5.1 | 9.1 |
| Zn[b] | 56 | 231 | 31 | 216 | 109 | 162 | 97 | 13 | 119 | bdl | 138 | 268 |
| Ga[b] | 28 | 32 | 28 | 35 | 19 | 20 | 28 | 20 | 26 | 8[c] | 23 | 36 |
| Rb | 138 | 410 | 99 | 349 | 164 | 252 | 193 | 61 | 205 | 25 | 306 | 565 |
| Sr | 444 | 314 | 456 | 313 | 510 | 423 | 402 | 578 | 327 | 80 | 136 | 68 |
| Y[b] | 40 | 27 | 26 | 66 | 29 | 31 | 98 | 15 | 25 | bdl | 27 | 74 |
| Zr[b] | 95 | 366 | 225 | 335 | 308 | 348 | 327 | 104 | 516 | 11 | 413 | 726 |
| Nb[b] | 9.6[c] | 31 | 5.2[c] | 40 | 14 | 22 | 18 | 3.5[c] | 28 | 1.3[c] | 19 | 39 |
| Mo | 0.1 | 0.6 | 0.2 | 0.7 | 1.0 | 0.9 | 0.2 | 0.1 | 0.3 | 0.2 | 0.2 | 0.3 |
| Cd | 0.12 | 0.08 | 0.11 | 0.17 | 0.12 | 0.10 | 0.18 | 0.09 | 0.08 | 0.04 | 0.06 | 0.03 |
| Sn | 2.0 | 2.1 | 2.8 | 2.7 | 1.8 | 1.4 | 2.5 | – | – | 2.0 | 7.3 | 13 |
| Sb | 0.06 | 0.02 | 0.02 | 0.01 | 0.02 | 0.02 | 0.03 | 0.08 | 0.03 | 0.03 | 0.04 | 0.04 |
| Cs | 2.3 | 9.4 | 1.3 | 7.5 | 3.3 | 5.0 | 3.7 | 1.9 | 4.3 | 1.9 | 34.4 | 59.7 |
| Ba[b] | 307 | 708 | 305 | 411 | 661 | 731 | 319 | 573 | 585 | 52 | 283 | 473 |
| La | 24 | 20 | 23 | 49 | 34 | 31 | 44 | 54 | 194 | 1.0[c] | 39 | 97 |
| Ce | 50 | 46 | 47 | 130 | 74 | 67 | 118 | 109 | 385 | 1.2[c] | 61 | 188 |
| Pr | 6.3 | 5.5 | 5.5 | 17 | 9.1 | 8.2 | 16 | 12 | 44 | 0.20[c] | 8.6 | 23 |
| Nd | 26 | 26 | 22 | 74 | 38 | 35 | 70 | 45 | 154 | 0.72[c] | 32 | 87 |

*Table 3.2 continued:*

| | | | | | | | | | | | | |
|---|---|---|---|---|---|---|---|---|---|---|---|---|
| Sm | 5.9 | 5.8 | 4.7 | 16 | 7.3 | 6.7 | 16 | 6.6 | 18 | 0.13[c] | 5.7 | 17 |
| Eu | 1.8 | 1.1 | 1.8 | 1.5 | 1.8 | 1.5 | 1.9 | 2.7 | 2.0 | 0.32[c] | 0.83 | 1.2 |
| Gd | 5.3 | 5.3 | 4.0 | 14 | 6.2 | 5.9 | 14 | 4.5 | 11 | 0.10[c] | 4.6 | 14 |
| Tb | 1.0 | 0.84 | 0.69 | 2.4 | 0.94 | 0.87 | 2.6 | 0.55 | 1.3 | 0.01[c] | 0.69 | 2.1 |
| Dy | 5.8 | 4.1 | 4.1 | 13 | 5.1 | 4.7 | 16 | 2.9 | 6.1 | 0.08[c] | 3.4 | 12 |
| Ho | 1.1 | 0.74 | 0.80 | 1.9 | 0.94 | 0.84 | 2.8 | 0.45 | 0.87 | 0.01[c] | 0.69 | 2.3 |
| Er | 3.3 | 1.9 | 2.2 | 4.7 | 2.8 | 2.5 | 7.8 | 0.97 | 1.7 | 0.04[c] | 1.9 | 6.5 |
| Tm | 0.46 | 0.23 | 0.30 | 0.62 | 0.4 | 0.34 | 1.1 | 0.11 | 0.16 | 0.01[c] | 0.26 | 1 |
| Yb | 2.6 | 1.3 | 1.8 | 3.1 | 2.5 | 2.2 | 6.3 | 0.57 | 0.79 | 0.05[c] | 2.0 | 6.3 |
| Lu | 0.33 | 0.19 | 0.23 | 0.39 | 0.36 | 0.31 | 0.83 | 0.07 | 0.11 | 0.01[c] | 0.31 | 0.95 |
| W | 0.5 | 0.5 | 0.5 | 0.4 | 0.3 | 0.3 | 0.4 | – | – | 0.5 | 1.4 | 2.9 |
| Tl | 0.6 | 2.2 | 0.4 | 1.9 | 0.86 | 1.4 | 0.92 | 0.3 | 0.9 | 0.11 | 1.7 | 3.1 |
| Pb | 31 | 14 | 35 | 19 | 6.5 | 7.2 | 27 | 29 | 18 | 9.0 | 17 | 11 |
| Bi | 0.38 | 0.29 | 0.31 | 0.54 | 0.14 | 0.20 | 0.67 | 0.02 | 0.07 | 0.33 | 0.15 | 0.51 |
| Th | 1.2 | 1.5 | 1.9 | 6.0 | 2.9 | 4.6 | 1.9 | 22 | 104 | 0.4 | 17 | 38 |
| U | 3.0 | 2.5 | 3.3 | 7.0 | 1.1 | 1.5 | 7.5 | 2.0 | 3.6 | 0.55 | 5.3 | 15 |
| Rb/Sr | 0.31 | 1.31 | 0.22 | 1.12 | 0.32 | 0.60 | 0.48 | 0.11 | 0.63 | 0.31 | 2.25 | 8.31 |
| Sm/Nd | 0.23 | 0.22 | 0.21 | 0.22 | 0.19 | 0.19 | 0.23 | 0.15 | 0.12 | 0.18 | 0.18 | 0.20 |

Notes: Unless otherwise specified, major elements were measured with XRF, trace elements with ICP-MS, and REE with ICP-AES. HTM= high-temperature migmatite, LTM= low-temperature migmatite, L = leucosome, M = melanosome, R = restite.

[a] Measured on a MC-ICP MS NEPTUNE (TFS) on aliquots of the same sample solution that was used for isotope analysis.

[b] Measured with XRF.

[c] Measured with ICP-MS

bdl = Below detection limit.

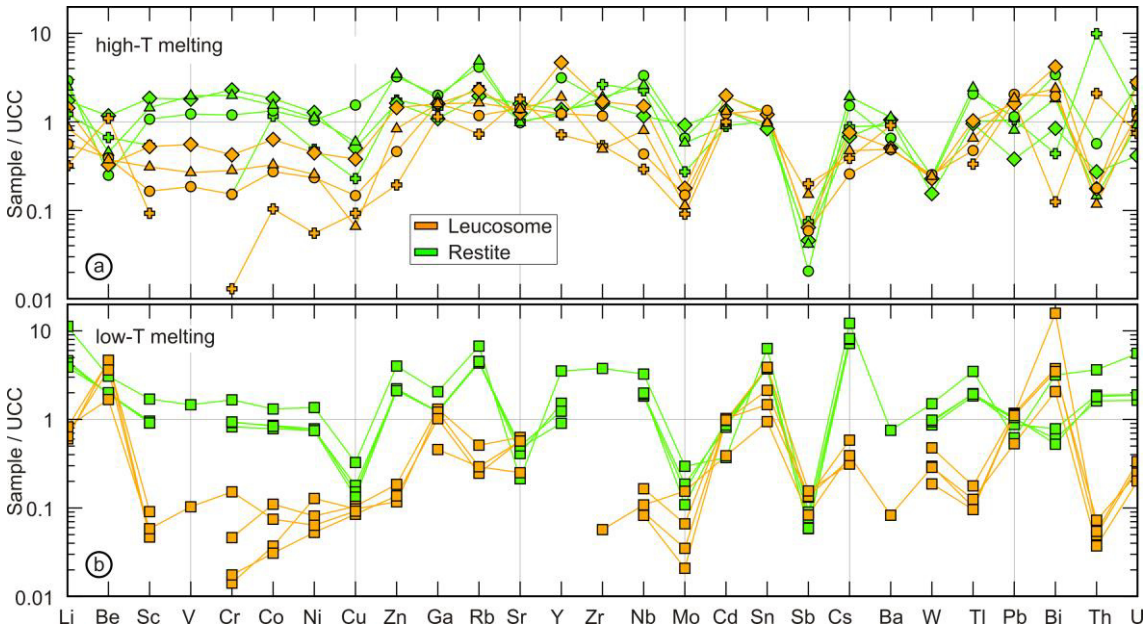


Fig. 3.4. (a) and (b) UCC normalized trace element composition of the analyzed leucosome-restite pairs for high- and low-temperature sample, respectively. Trace elements may be available to partition into the melt if host accessory phases or rock forming minerals are involved in melting. Trace element fractionation between leucosome and restite is less pronounced in the analyzed high temperature samples than in the low temperature sample. See text for a detailed description. Symbols as in Fig. 3.3.

### *3.4.1.2. Low-temperature migmatite*

Trace element compositions for the low-temperature migmatite are shown in Fig. 3.4b. Beryllium, Sr, Bi, and Sb are the only trace elements that are clearly enriched in the leucosome of the low-temperature migmatite. For Pb, Ga, and Cd there is no clear preference. All other analyzed trace elements are enriched in the restitic part of the migmatite. The REE show a flat upper continental crust normalized pattern (Fig. 3.3c) with a distinct negative Eu anomaly in the restite and a pronounced complementary positive Eu anomaly in the leucosome. The restitic domain is enriched in REE, reflecting the high abundance of accessories, whereas the leucosome has low REE concentrations. In general, partitioning between leucosome and restite is much more pronounced in the low-T migmatite than in the high-T migmatites. This difference, which in part may be due to differences in protolith chemistry and, thus, protolith mineralogy, seems to be related to melting temperature as the solubility of many trace-element sequestering accessory phases in granitic melt increases with temperature (Watson and Harrison, 1983; Rapp and Watson, 1986).

### *3.4.2. Radiogenic isotopes*

#### *3.4.2.1. Strontium*

Measured $^{87}Sr/^{86}Sr$ ratios of leucosome and restite samples of the high-temperature migmatites range between 0.708748±5 and 0.723682±6 and recalculated initial $^{87}Sr/^{86}Sr$ (for T=320 Ma) range between 0.70450±18 and 0.70989±61 (Fig. 3.5 and Table 3.1). Commonly, the initial Sr isotopic composition of the leucosome is more radiogenic than the corresponding restite, although the absolute difference may be rather variable. For instance, sample HTM_2 shows only a small difference, which is, however, significant (0.70989±12 vs. 0.70895±61, absolute difference = 0.00094 or 13 εSr-units) between leucosome and melanosome, whereas sample HTM_3 has a pronounced difference (0.70925±27 vs. 0.70450±18; absolute difference = 0.0048 or 67 εSr-units). The leucosomes of the high-temperature samples have relatively radiogenic and uniform initial Sr isotopic compositions that cluster around 0.7095 (Fig. 3.5). In contrast, the initial Sr isotopic composition of the various high-temperature restite domains is more variable (0.70450±18 and 0.70895±61 for restites of samples HTM_3 and HTM_2). The low-temperature migmatite (LTM) has a more radiogenic initial Sr isotopic composition than the high-temperature migmatites, largely reflecting protolith nature. The different domains of the low-temperature sample do not show a significant difference in their initial $^{87}Sr/^{86}Sr$ isotopic composition.

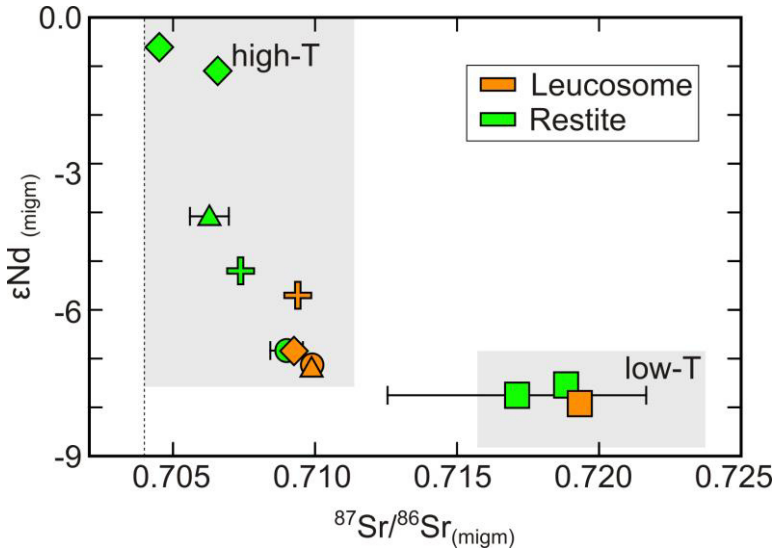


Fig. 3.5. εNd *vs.* $^{87}Sr/^{86}Sr$ diagram for the high- and low-temperature migmatites. The Nd and Sr isotopic compositions of the various leucosomes of the high-temperature samples fall in a narrow range, suggesting they are buffered by minerals that participate in the melting reactions and the solubility of accessory phases in the melt. The Nd and Sr isotopic compositions of restite samples are more variable, reflecting the contrasting mineral assemblages and modal differences in the restite. Note that there is no pronounced difference in the Nd and Sr isotopic composition of melt and restite in the low-temperature restite. Unless shown otherwise, uncertainties (2SD) are smaller than symbol size. Symbols as in Fig. 3.3.

*3.4.2.2. Lead*

The results of Pb isotope analyses are shown in Table 3.1 and calculated initial (320 Ma) isotopic compositions are shown in Fig. 3.6. In the $^{206}Pb/^{204}Pb$ vs $^{208}Pb/^{204}Pb$ diagram, the Pb data look more scattered because of three samples that do not fall on a common Pb trend (Fig. 3.6a). The concentrations of Pb, U, and Th (Table 3.2) and the isotopic composition of Pb were determined on different solutions. Therefore, deviation of the initial Pb isotopic composition from the common Pb trend may result from nugget effects (Th concentration controlled by monazite) and under- or overcorrection of *in situ* $^{208}Pb$ ingrowth. In the $^{206}Pb/^{204}Pb$ vs $^{207}Pb/^{204}Pb$ diagram, the data plot along a trend parallel to typical crustal Pb growth curves (Fig. 3.6b). There is some difference between most leucosome-melanosome pairs of the high-temperature and low-temperature migmatites, with leucosomes commonly having slightly higher $^{206}Pb/^{204}Pb$ values.

*3.4.2.3. Neodymium*

The high temperature leucosome-melanosome pairs show a broad variation in the Nd isotopic composition with only small differences between melanosome and leucosome for sample HTM_2 ($\varepsilon Nd_{(t)}$ = -7.1 vs. -6.9) and a significant difference for sample HTM_3 with -6.8 for the leucosome and -0.6 for the restite. With the exception of sample HTM_4 ($\varepsilon Nd_{(t)}$ = -5.7), the high-temperature leucosomes have uniform $\varepsilon Nd_{(t)}$ values around $\varepsilon Nd_{(t)}$ = -7.0 that are systematically, although to different extent, less radiogenic than the corresponding restite domains. As for the Sr isotopic composition of the low-temperature sample, $\varepsilon Nd_{(t)}$ values of leucosome and restite are very similar ($\varepsilon Nd_{(t)}$ = -7.7 and -7.9).

*3.4.3. Stable isotopes*

*3.4.3.1. Li and B in high-temperature samples*

Lithium and B isotopes do not behave very systematic in high-temperature samples. Three different cases can be distinguished for fractionation behavior of Li and B (Fig. 3.7a–d; Table 3.1): (i) there is almost no fractionation in the isotopic composition between leucosome and melanosome (similar $\delta^7Li$ and $\delta^{11}B$ values in sample HTM_2), (ii) fractionation of the Li isotopic composition (2.4 $\delta^7Li$-units; HTM_1) with little or no fractionation of the B isotopic composition (unchanged $\delta^{11}B$), and (iii) fractionation of the Li isotopic composition (up to 3.7 $\delta^7Li$ -units; sample HTM_4) and the B isotopic composition (up to 10.3 $\delta^{11}B$ -units; sample HTM_3). With the exception of sample

HTM_4, all the analyzed high-temperature leucosomes have relatively uniform $\delta^7$Li and $\delta^{11}$B values ranging between 0.52 – 0.82 (sample HTM_4 = 2.24) $\delta^7$Li and -7.05 – -9.93 (sample HTM_4 = 2.32) $\delta^{11}$B, respectively. The high-temperature leucosomes tend to have heavier Li compositions and lower Li contents than their corresponding melanosomes (Fig. 3.7a) whereas the B isotopic compositions and B contents show no systematic variation (Fig. 3.7c). The B concentrations in the high temperature samples are rather low (up to 5 ppm), which may reflect either the overall lower B content of the protolith or B loss during prograde metamorphism.

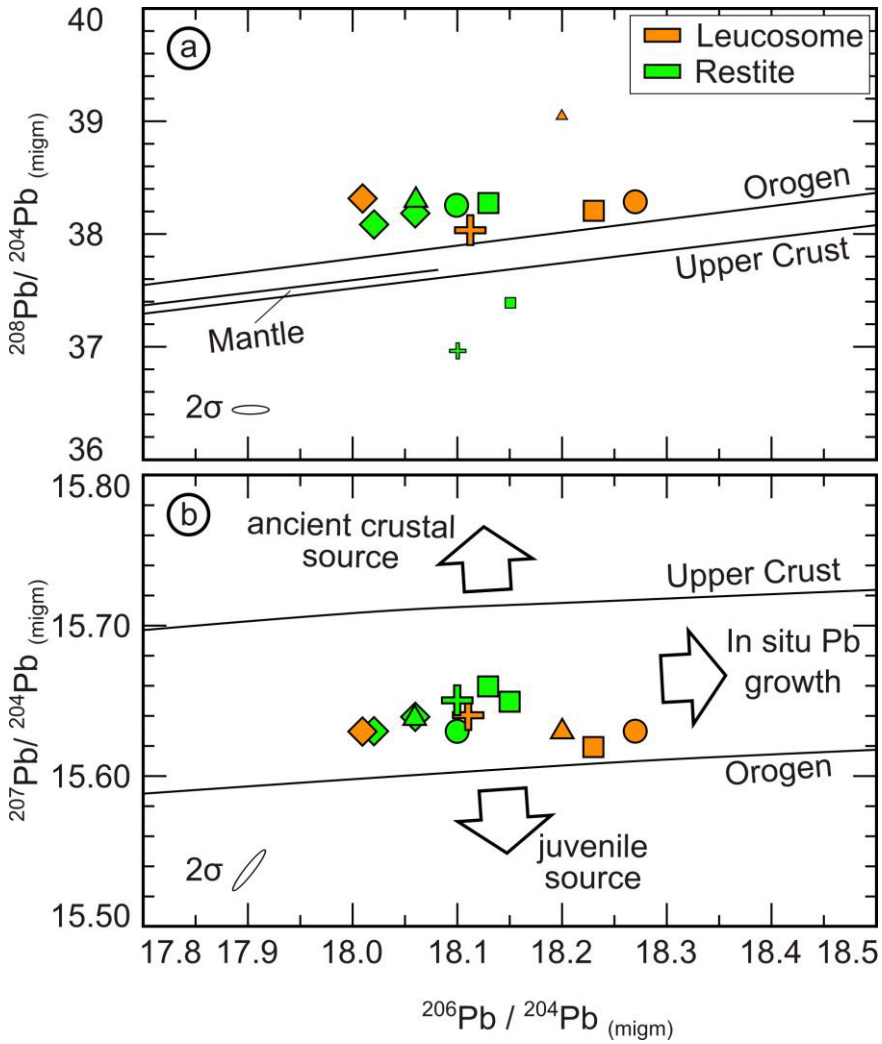


Fig. 3.6. (a) $^{206}$Pb/$^{204}$Pb *vs* $^{208}$Pb/$^{204}$Pb diagram for high- and low- temperature migmatites. There is no systematic difference between restite and melt, although the Pb isotopic compositions of the melts tend to be slightly more radiogenic. The scatter in $^{208}$Pb/$^{204}$Pb for some samples (smaller symbol size) is most likely an artifact from over- and under correction of *in situ* Pb growth due to nugget effects (e.g. monazite) affecting Th concentrations. (b) $^{206}$Pb/$^{204}$Pb *vs* $^{207}$Pb/$^{204}$Pb diagram for high- and low- temperature migmatite samples. All samples plot parallel to a crustal *in situ* Pb growth curve. Standard deviation (2σ) is indicated by the error ellipse. Growth curves for different Pb reservoirs according to Zartman and Doe (1981). Symbols as in Fig. 3.3.

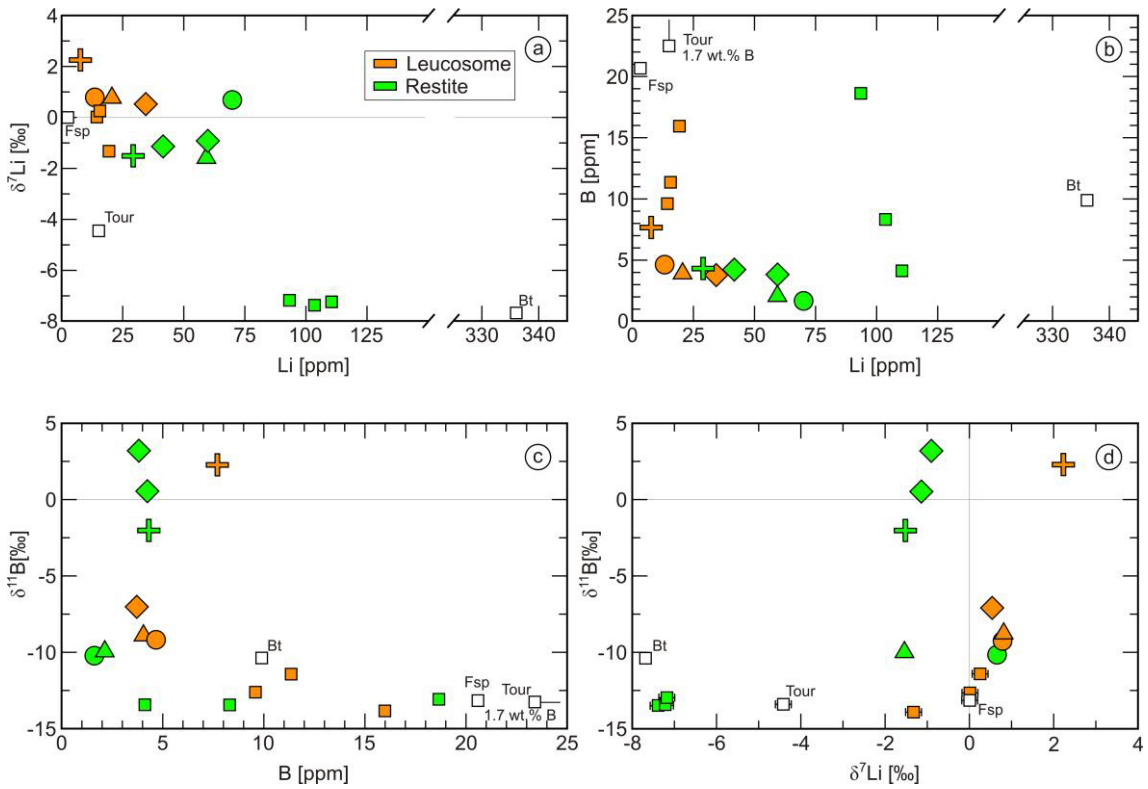


Fig. 3.7. Isotopic and concentration data of high- and low-temperature samples. Squares represent low-temperature migmatite data from the profile (Table 3.3 and Fig. 3.8, open symbols = mineral separates). (a) Li concentration vs $\delta^7$Li diagram. There is a clear trend for higher $\delta^7$Li values and lower Li concentrations in the melt. The overall higher Li concentrations in the low-temperature sample, however, reflect differences in protolith composition. (b) Li vs B concentration diagram. In high- and low-T samples, Li is enriched in the restite relative to the melt. Boron is slightly depleted in the restite relative to the melt in high-T samples. Most of the leucosome domains in the low-T sample have slightly higher B concentrations (c) B concentration vs $\delta^{11}$B diagram. The low-temperature sample has higher B concentrations than high-temperature samples and shows little variation in $\delta^{11}$B. The high-temperature leucosome-restite pairs show a tendency to higher $\delta^{11}$B values in the leucosome. (d) $\delta^7$Li vs $\delta^{11}$B values for high- and low-temperature migmatites. Note, in the low-T sample, the Li isotopic composition of the leucosomes and restites closely match the composition of fsp and biotite, respectively, from the contact zone (Fig. 3.8). Symbols as in Fig. 3.3.

### *3.4.3.2. Li and B in low-temperature profile*

Lithium and B isotope data for the small-scale profile of the low-temperature sample (Fig. 3.8 and Table 3.3) have been determined for three leucosome whole-rock segments, three mesocratic residuum whole-rock segments, and for mineral separates from the melanosome separating leucosome and residuum. The melanosome contact zone contains quartz, feldspar, biotite, and tourmaline. The Li isotopic composition of the mesocratic residuum shows little variation ($\delta^7$Li: -7.17 – -7.37). Whole rock Li isotopic composition and concentrations of the melanosome are $\delta^7$Li = -7.03 and 123 ppm, respectively (Table 3.1). Minerals from the melanosome domain show a broad range of Li isotopic compositions ranging from $\delta^7$Li = -7.68 for biotite and -4.43 for tourmaline up to $\delta^7$Li = 0.00 for feldspar. The Li isotopic composition of the feldspar-dominated

leucosome samples range between -1.33 proximal to the contact and 0.25, distal to it ("distal" here refers to few centimeters; Figs. 3.2b and 3.8). The contrast in Li content between the residuum (~100 ppm) and leucosome (~15 ppm) is directly linked to the biotite and feldspar content. The lower Li contents in the leucosome are correlated with heavier $\delta^7$Li values. The slightly lower $\delta^7$Li and slightly higher Li concentration in the leucosome segment (L1) closest to the contact zone may result from the entrainment/contamination of minor biotite flakes from the restite.

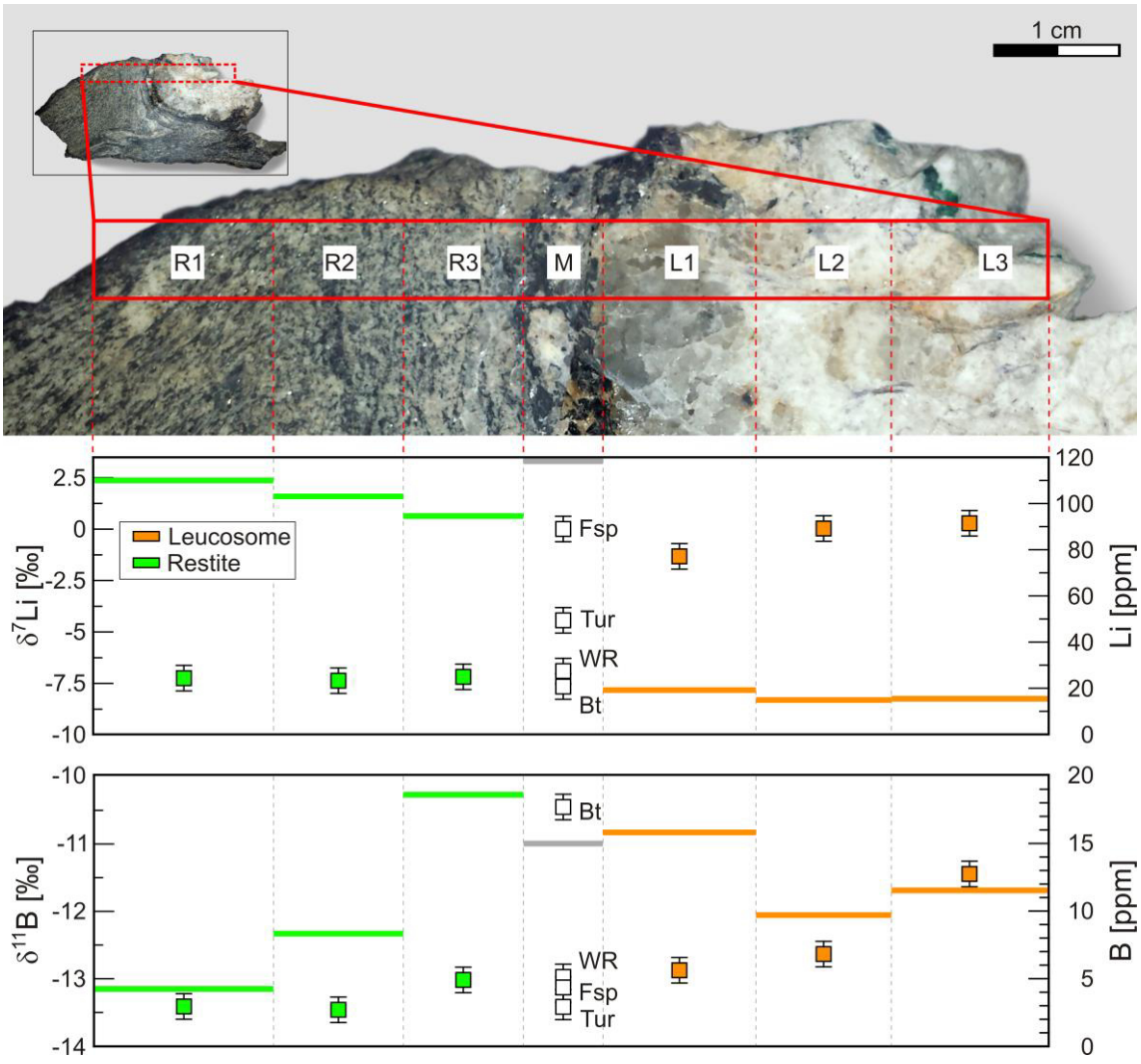


Fig. 3.8. Picture of the low-temperature migmatite sample showing the position of the segments used for Li and B isotope analysis. The $\delta^7$Li values show a step between restite and leucosome whereas $\delta^{11}$B values do not change significantly. Colored bars show B and Li concentrations of the corresponding segments.

The B isotopic composition varies only little among the different domains of the low-temperature sample. There is, however, a tendency for slightly lighter $\delta^{11}$B in the residual domain (average $\delta^{11}$B = -13.3) than in the leucosome (average $\delta^{11}$B = -12.3). This pattern closely resembles that of the Li isotopic composition, although the difference in $\delta^{11}$B is smaller and the "proximal" samples next to the contact do not show a distinct

step in $\delta^{11}B$ (see also Figs. 3.7c and 3.8). Among the individual minerals, biotite has the lightest B isotopic composition ($\delta^{11}B$ = -10.4), whereas feldspar and tourmaline have similar compositions ($\delta^{11}B$ = -13.1 and $\delta^{11}B$ = -13.4). Calculated temperatures with the tourmaline-biotite thermometer using the equations of Wunder et al. (2005) and Kowalski and Wunder (2018) gives unreasonably high temperatures (in excess of 1000 °C), which indicates that the minerals in this domain are not in isotopic equilibrium with each other. The contact zone rather represents a mixture of restitic material (mainly biotite) that is diluted/contaminated by feldspar and quartz from the leucosome. Simple mass balance using the modal abundance of these minerals and their B composition and content (Table 3.3) shows that the transition zone has calculated $\delta^{11}B$ = ~ -13 and B concentration of 15 ppm. There is a slight trend to higher B concentrations in the leucosome samples, which reflects both their modal composition and the higher B contents in feldspar than in biotite (Table 3.3). Minute contamination with entrapped tourmaline from the melanosome also would increase B contents of the sample at the contact to the melanosome (e.g. profile sample L1).

Table 3.3. Li and B data of low-T migmatite (LTM) profile.

| Sample[a] | $\delta^7$Li ±2 SE | Li [ppm] | $\delta^{11}$B ±2 SE | B [ppm] |
|---|---|---|---|---|
| R1 | –7.23±0.11 | 110 | –13.42±0.05 | 4.1 |
| R2 | –7.37±0.05 | 103 | –13.46±0.04 | 8.3 |
| R3 | –7.17±0.18 | 94 | –13.02±0.14 | 18.6 |
| M Tur | –4.43±0.07 | 15 | –13.41±0.03 | 1.7[b] |
| M Bt | –7.68±0.06 | 336 | –10.44±0.16 | 9.9 |
| M Fsp | 0.00±0.11 | 2.5 | –13.14±0.16 | 20.6 |
| L1 | –1.33±0.15 | 19 | –12.88±0.11 | 15.9 |
| L2 | 0.02±0.18 | 15 | –12.63±0.14 | 9.6 |
| L3 | 0.25±0.10 | 16 | –11.44±0.14 | 11.4 |

[a] for sample location refer to Fig. 3.8.
[b] in wt%
For analytical procedure see Table 3.1.

### 3.5. Discussion

Disequilibrium of radiogenic isotopes develops during partial melting, if the protolith minerals (i) had distinct parent-to-daughter nuclide ratios and (ii) enough time to develop contrasting isotopic compositions depending on their parent-to-daughter ratio (Harris and Ayres, 1998). Among the studied samples, the low-temperature sample does not show significant disequilibrium for radiogenic isotopes, possibly due to the young age

of the protolith minerals at the time of melting, "smoothing" of the original heterogeneity during the prograde growth of the metamorphic minerals, or equilibration during/after partial melting. Therefore, the discussion of the radiogenic systems Rb–Sr, Sm–Nd, and U,Th–Pb bases mainly on the results from high-temperature samples that show larger isotopic contrasts between melt and restite. For these samples, the precursor minerals apparently were sufficiently old to have developed significant differences in the isotopic composition of Sr, Nd, and Pb. In contrast, fractionation of Li and B is strongly controlled by contrasting coordination of these elements in different minerals and fluid/melt and by temperature (Wunder et al., 2005; Wunder et al., 2006).

### *3.5.1. Sr, Pb, Nd radiogenic isotopes*

#### *3.5.1.1. Rb-Sr system*

Major and trace element pattern of leucosome and melanosome reflect the differences in the mineralogical and modal compositions of the two domains. Leucosomes from the various high-temperature migmatite samples have similar chemical compositions, implying that the same melting reaction controlled anatexis in all samples. Weighted combination of leucosome and melanosome pairs indicates that all high-temperature migmatites were derived from similar protoliths. The Sr isotopic composition of individual high-temperature leucosome-melanosome pairs, however, is variable, with most samples having a distinctly less radiogenic Sr isotopic composition in the restites than in the corresponding leucosomes and only one sample having similar $^{87}Sr/^{86}Sr$ ratios for the leucosome and the corresponding residuum (HTM_2).

The analyzed leucosomes have similar Sr isotopic compositions (Fig. 3.5), which in combination with the chemical composition of the leucosomes implies that both the Sr isotopic and the chemical composition are controlled by the melting reaction. For the chemical composition of the leucosomes, broadly similar major and trace element patterns for the various leucosomes are expected, as melting involves the same reactant phases at the same proportions. The Sr isotopic composition of the phases taking part in the melting reaction is very variable, depending on their Rb/Sr and age. For instance, biotite has much higher Rb/Sr ratios than the other minerals involved in bt-dehydration melting and, therefore, develops with time the highest $^{87}Sr/^{86}Sr$ ratios. Nonetheless, the Sr isotopic composition of the leucosomes is relatively homogeneous, reflecting that the stoichiometry of the melting reaction(s) also buffers the Sr isotopic composition. As the

melting phases on average have higher Rb/Sr and therefore higher $^{87}Sr/^{86}Sr$ than the restite phases, the leucosome has a more radiogenic $^{87}Sr/^{86}Sr$ isotopic composition. Whether this general relation results in resolvable differences in the Sr isotopic composition of melt and restite depends to a large extent on the metamorphic history of the protolith. If isotopic contrasts on the mineral scale persist during progressive metamorphism, partial melting of such rocks results in Sr isotopic contrasts between melt and restite. Under these conditions the chemical and Sr isotopic composition of the melt may not represent the chemical and Sr isotopic composition of the protolith (Figs. 3.3a and 3.5). If, however, isotopic homogenization is achieved during prograde metamorphism shortly prior to partial melting, melt and restite will not show significant Sr isotopic differences.

In contrast to the leucosomes, the restite domains show large variations in their Sr isotopic composition that follow a trend to less radiogenic $^{87}Sr/^{86}Sr$ isotopic compositions than that of the melt, reflecting both (i) the restite mineral assemblage differs from the melting assemblage and (ii) modal differences in the restite mineral assemblages in the various samples, or the contrasting extent of melt removal from the restite. Variations in the restite Sr isotopic composition may result from differences in restite mineralogy or modal differences that arise from slight differences in protolith chemistry or from inclusion of older minerals in later ones. Sample HTM_3, which shows the largest difference in Sr isotopic composition between leucosome and melanosome, contains restitic amphibole. As amphibole hosts significant amounts of Sr while commonly having a low to very low Rb/Sr, the presence of amphibole shifts the Sr isotopic composition of the restite to less radiogenic values. Thus, if different restite minerals at the time of melting are sufficiently old to have developed contrasting Sr isotopic compositions, differences in the restite mineral assemblage or the modal composition of the restites result in different Sr isotopic compositions of the restites.

Melting of an isotopically heterogeneous source may not only produce a melt that is distinct in Sr isotopic composition from its source, but may produce, for systems with multiple melt extractions, a series of melt batches, each with a distinct isotopic signature. Farina and Stevens (2011) showed that progressive (dehydration-) melting of a single source is able to produce magma batches with contrasting $^{87}Sr/^{86}Sr$ ratios due to variation in mineral Rb/Sr ratios and changes in the stoichiometry of the melting reactions with changing temperature and pressure. Using K-feldspar megacrysts as proxy for the changing melt composition, Farina et al. (2014) argued that decreasing $^{87}Sr/^{86}Sr$ ratios

from core to rim record the decreasing biotite to plagioclase ratio of the melting reaction with increasing temperature (Montel and Vielzeuf, 1997), as biotite and plagioclase have contrasting Rb/Sr and, thus, $^{87}Sr/^{86}Sr$ ratios. Similarly, McLeod et al. (2012) documented Sr isotopic disequilibrium in anatectic melts that resulted from differences in $^{87}Sr/^{86}Sr$ of the melting phases and their ratios during melt generation. An alternative process resulting in contrasting isotopic composition is dehydration melting with early melt batches controlled by the consumption of muscovite and later ones by the consumption of biotite.

*3.5.1.2. U,Th-Pb system*

The Pb whole rock budget of common granitic rocks and their metasedimentary source rocks is controlled by rock-forming minerals, most importantly (potassic) feldspar. The main carriers of Th and U, however, are accessory phases (Bea, 1996; Förster, 1998a; Förster, 1998b), which therefore strongly influence Pb isotopic compositions (Romer, 2001; Romer and Rötzler, 2011). The solubility of accessory phases in a melt is mainly controlled by the chemical composition of the melt and increases with temperature (Watson and Harrison, 1983; Rapp and Watson, 1986; Boehnke et al., 2013). The trace element budget of melts, however, does not only depend on melt composition and melting temperature alone, but also on the nature and abundance of the accessory phases. For instance, the dissolution behavior of zircon, titanite, monazite, xenotime, and apatite is controlled by the solubility of Zr, Ti, P, and REE in the melt. Thus, the REE budget is potentially controlled by several minerals. As long as the melt is saturated in these elements, the REE- hosting accessory phases are stable and may concentrate in the restite. The accessory phases zircon, monazite, xenotime, and apatite are also important hosts of Th and U in many granitic and sedimentary rocks. Thus, the amount of U, Th, and radiogenic Pb that may enter the melt is controlled by the solubility of these phases in the melt. Using these considerations, Hogan and Sinha (1991) argued that the Pb budget and the initial Pb isotopic composition of multiple batches of low-temperature melt is dominated by feldspar, which is participating in the melting reaction, whereas contributions of radiogenic lead derived from accessory minerals (zircon, monazite) are small. The transition from minimum melting (i.e. ms-dehydration melting) to high temperature melting (bt-dehydration melting) not only results in melts of different chemical composition, but also enhances the solubility of accessory phases, which increases the contribution of radiogenic Pb from accessory phases to the melt. Hogan and

Sinha (1991) demonstrated that biotite-dehydration melting of a metasedimentary protolith with complete dissolution of zircon in the source and residual monazite in the source may result in the decoupling of $^{206}Pb$ and $^{207}Pb$ from $^{208}Pb$ as U and Th are preferentially hosted in different accessory phases.

The Pb isotopic data from melanosome-leucosome pairs from the same outcrop show Pb isotopic disequilibrium during partial melting (Fig. 3.6). The relation between the Pb isotopic composition of the analyzed leucosome and restite pairs does not fully agree with the decoupling of $^{206}Pb$ and $^{207}Pb$ from $^{208}Pb$ in the Hogan and Sinha (1991) model, as $^{207}Pb/^{204}Pb$ and $^{206}Pb/^{204}Pb$ of the leucosomes do not show the relations observed in their conceptional model, possibly due to (i) the contrasting spatial distribution of different kinds of accessory minerals and (ii) the simplified assumption in their model, using zircon and monazite as the only accessory phases contributing radiogenic Pb. Titanite and apatite are accessory phases that also may significantly contribute to the U and Th budget of a rock and, thus, host significant portions of the in situ produced Pb.

The textural position of accessory phases may play a crucial role whether they are available to dissolve in the melt or not (Watson et al., 1989). Apatite in migmatites is preferentially located at major mineral boundaries and, therefore, is available for dissolution by the melt (Bea, 1996). Thus, if apatite hosts a significant portion of U and Th of the rock, apatite also is a major source of radiogenic Pb. In contrast, as much as 70% of monazite, xenotime, and zircon occur as inclusions in biotite, where they are shielded from dissolution (Bea, 1996). If these minerals are the major hosts of REE, Y, Th, U, (and radiogenic Pb), their behavior during anatexis may be controlled by biotite stability rather than by their saturation in the melt. Finally, the entrainment of restitic biotite flakes (with zircon, monazite, and/or xenotime inclusions) in the partial melt also may affect the trace element and Pb isotopic composition of some leucosomes. One additional complication may arise from the behavior of U,Th-hosting accessory phases during prograde metamorphic reactions. For instance, consumption of titanite to form Ti-oxides or Ti-rich biotite during progressive metamorphism releases U, Th, and radiogenic Pb. The radiogenic Pb may not be incorporated into the Ti-oxide or Ti-rich biotite, but is instead incorporated into feldspar. Incipient melting consumes feldspar and eventually introduces radiogenic Pb originally derived from titanite into the melt. In such a scenario, the melts may have more radiogenic Pb isotopic compositions than the restite.

*3.5.1.3. Sm-Nd system*

Rock-forming minerals generally incorporate limited amounts of REE, whereas accessory phases may have several orders of magnitude higher REE contents. In some accessory minerals, REE even represent an essential structural component (e.g. in Ce-, La-, Nd-, Sm-Monazite). Therefore, a significant portion of the REE budget of rocks is bound to accessory phases. Most rock-forming minerals in granitic systems have smooth chondrite-normalized LREE-enriched pattern. Hornblende and garnet represent notable exceptions as they typically have variably MREE- and strongly HREE-enriched pattern, respectively (Irving and Frey, 1978; Dorais and Tubrett, 2012; Taylor et al., 2015). In contrast, accessory phases exhibit a variety of REE pattern. Titanite, allanite, and monazite preferentially incorporate LREE. Xenotime and zircon show HREE enrichment (Rubatto, 2002; Whitehouse, 2003). Apatite may show a broad range of different REE pattern, including pattern with MREE enrichment relative to LREE and HREE, leading to a bell-like REE pattern. Minerals with different REE pattern have different Sm/Nd ratios and, thus, develop with time different Nd isotopic compositions. The range of Nd isotopic compositions of minerals within a rock depends on the Sm/Nd ratios of different minerals and becomes more pronounced with increasing time after the last isotopic homogenization (Fig. 3.9).

Prograde metamorphism that eventually reaches conditions of partial melting commonly results in a series of different mineral assemblages before melting starts. Prograde mineral reactions result in the redistribution of material from precursor minerals to product minerals and, thereby, also result in a reduction of Nd isotopic contrasts present between different minerals (Fig. 3.9a). If the prograde mineral assemblages form during the same metamorphic cycle that eventually leads to partial melting, the isotopic heterogeneity among minerals that take part in the melting reaction may be small. Hence, the isotopic composition of the melt and protolith may be nearly identical (Fig. 3.9a). Such prograde homogenization of the isotopic composition may be particularly pervasive during metamorphism of fine-grained sedimentary rocks with a high portion of authigenic minerals that do not stand temperature and pressure conditions of medium and higher-grade metamorphism. In contrast, if the protolith is dominated by minerals that formed at magmatic or metamorphic conditions, prograde metamorphism may not result in significant mineral reactions (as the precursor minerals remain stable) and there is limited redistribution of material.

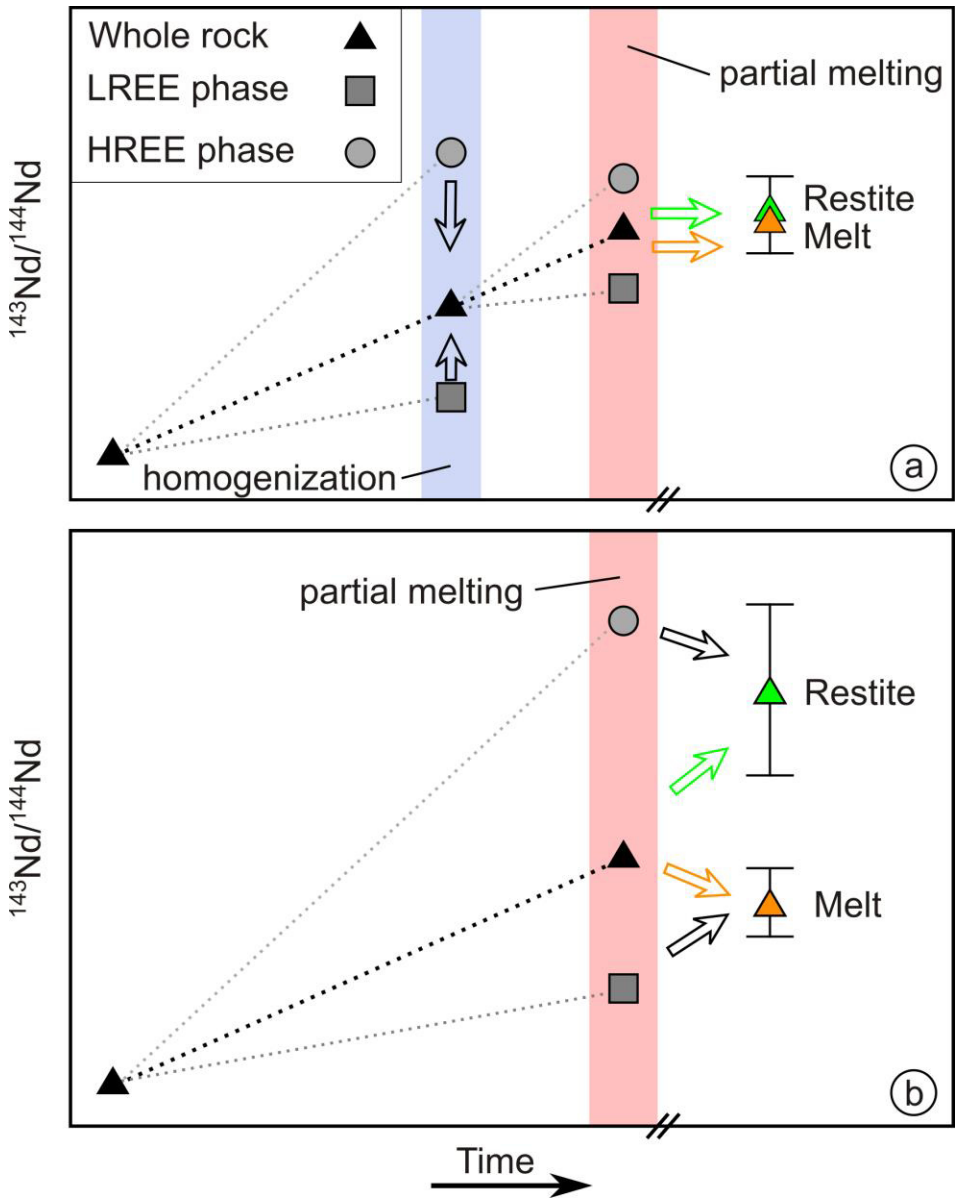


Fig. 3.9. Conceptual illustration of Nd radiogenic isotope systematics and evolution for different protoliths. LREE phases: apatite, monazite, most rock forming minerals. HREE phases: zircon, xenotime, allanite, garnet, amphibole. (a) Sedimentary rocks that undergo pervasive recrystallization during prograde metamorphism are likely to have homogenized isotopic compositions on the mineral scale. Melts derived from protoliths with such "young" minerals will have the same radiogenic isotope signature as their restites. (b) Isotopic differences may persist up to partial melting conditions in rocks that do not completely recrystallize and lead to isotopically distinct signatures in the melt and restite.

In such a scenario, the isotopic composition of minerals of the protolith may be very variable at the time of melting and, thus, the isotopic composition of protolith and partial melt may differ significantly (Fig. 3.9b). Protoliths that are likely to show significant isotopic heterogeneity at the onset of partial melting could be geologically old magmatic and metamorphic rocks, as well as any rock that contains significant amounts of inherited materials. For examples, gneisses of the Western Gneiss Region (Norway) have experienced a Grenville/Sveconorwegian (~950 Ma) granulite facies metamorphism and

a Caledonian (~400 Ma) eclogite facies metamorphism. Erambert and Austrheim (1993) showed that garnet in many of the eclogites is actually a relic phase after granulite facies metamorphism. Thus, garnet is more than 500 Ma older than the matrix eclogite facies minerals and, thus, is unlikely to have homogenized its Nd isotopic composition with the eclogite facies minerals. Similarly, there are numerous studies on the provenance of zircon in magmatic and metamorphic rocks. The commonly observed large age range of inherited zircon in magmatic and metamorphic rocks clearly shows that these zircon crystals did neither equilibrate during metamorphism nor during their entrainment in the melts. In analogy to inherited zircon and garnet, REE concentration and pattern in apatite and, thus, also its Nd isotopic composition may show large variation. Bingen et al. (1996) have shown that MREE-and HREE-concentrations in apatite strongly increase with metamorphic grade, resulting not only in higher REE concentrations but also modifying the REE pattern. Similarly, Janots et al. (2018) have shown that apatite grown during particular metamorphic and orogenic events may have different REE concentrations and pattern. The effect of contrasting REE pattern on the Nd isotopic composition is most pronounced for apatite that did not equilibrate during metamorphism because of the absence of a fluid phase or that forms inclusions in other phases and, therefore, is shielded from equilibration (Janots et al., 2018).

The low-temperature sample does not show significant Nd isotopic variation between leucosome and restite ($\varepsilon Nd_{(t)}$ = -7.7 and -7.9; Fig. 3.5). Melting under low-temperature conditions is expected to result in limited accessory phase solubility. Therefore, the Nd isotopic composition of the melt will be controlled by rock forming minerals that participate in melting reaction rather than buffered by accessory phases. Actually, accessory phases in the low temperature sample are almost exclusively concentrated in the restite. This is also reflected by the elevated REE concentrations of the restite relative to the leucosome (Fig. 3.3c). Microprobe analysis in combination with elevated Zr concentrations in the restite and rather low P concentrations indicate that the REE budget is controlled by monazite and, for the HREE, also zircon. As there is no significant Nd isotopic difference between melt and restite, phases with high $^{147}Sm/^{144}Nd$ do not contribute significantly to the whole rock Nd budget. Inherited zircon that is on average 500 Ma older than the other minerals would have an εNd that is about 22 ε-units higher than the LREE-enriched melting phases. As zircon strongly enriches HREE (but not Sm or Nd) it does not contribute significantly to the Nd budget of the whole rock sample and does not affect the Nd isotopic composition of the restite significantly.

For instance, model calculations using 3 ppm Nd in zircon and the Zr content of the rock (500 ppm) as proxy for the amount of zircon present, indicates that less than 0.05% of the bulk Nd (6 ppm) is hosted in zircon. Thus, even if zircon has an ε-value that is 22 units higher than the bulk sample, it does not shift the WR ε-value significantly (less than 0.02 ε-units). Furthermore, if the protolith of the low-temperature migmatite consists of sedimentary rocks that had not experienced older metamorphism, the prograde metamorphic mineral reactions may have wiped out some of the initial heterogeneity prior to partial melting (Fig. 3.9a).

In our sample set, the high-temperature leucosomes have peraluminous compositions and formed by biotite-dehydration melting. As the solubility of accessory phases depends on melt composition and increases with temperature (Watson and Harrison, 1983), the REE budget of high-temperature melts as those of the high-temperature leucosomes is likely to be controlled by contributions from accessory phases. This expectation is supported by elevated (L)REE and P concentrations in the melt domains relative to the corresponding restites, which are well above contributions from rock forming minerals alone (Table 3.2). The relatively uniform εNd values between -6.8 and -7.2 (Fig. 3.5) in the leucosome domains reflect the preferential melting of minerals that preferentially incorporate LREE (such as feldspar, muscovite, and biotite) and more importantly contributions from LREE enriched accessory phases (such as apatite and monazite). The relatively homogeneous Nd isotopic composition of the leucosome domains has two possible explanations: (i) minerals contributing significantly to the LREE budget of the melt all have similar REE pattern and age and, therefore, similar Nd isotopic compositions; (ii) the contribution of apatite and monazite to the Nd budget is buffered by the solubility of these minerals in the partial melt, which would imply that the various minerals contributed in relatively constant proportions to the melt.

In contrast to the partial melts, the restite domains of the high-temperature migmatites exhibit large variations in εNd between -0.6 to -6.9. The scattering of εNd in the restites reflects differences in their inventory of accessory minerals. HREE- and MREE-enriched rock-forming minerals (e.g. garnet and amphibole; Cruciani et al., 2014), as well as accessory phases (most importantly xenotime, apatite, and zircon; Bea, 1996; Hoskin and Schaltegger, 2003) will develop with time distinctly more radiogenic Nd isotopic compositions than other phases as they have higher Sm/Nd ratios. The whole rock isotopic Nd composition is therefore controlled by the relative abundance of accessory phases, their contribution to whole rock Nd, and their Nd isotopic composition,

which in turn depends on $^{147}Sm/^{144}Nd$ and age. If the REE budget of the restite is controlled by the same REE enriched accessory phases that also buffer the REE budget of the melt (apatite and monazite), the restite has a similar Nd isotopic composition as the melt. This is the case for the restite of sample HTM_2, which has a much higher P concentration in the restite than the leucosome. Restites with lower P contents (HTM_1 and 3) than the melt show significantly more radiogenic Nd isotopic compositions, which may reflect the decreasing contribution of LREE accessories to the REE budget or changes in their isotopic composition. The Nd isotopic composition of the melt may be buffered by apatite (with contributions of monazite) that preferentially occurs at grain boundaries and, therefore, is available for dissolution and may contribute significantly to the Nd budget of the melt. The restite may contain apatite that occurs as inclusions in other phases. If this apatite had a higher Sm/Nd than apatite from grain boundaries and contributes significantly to the Nd budget of the restite, the Nd isotopic composition of the restite may be markedly more radiogenic than the melt. Similar effects may be expected for increasing contributions of HREE enriched phases such as zircon and xenotime that also may have considerably more radiogenic Nd compositions. Although Zr/P ratios are higher in restite samples with more radiogenic Nd compositions (Table 3.2), contributions of zircon to the whole rock Nd budget, however, are not likely to result in a detectable effect on the ε-Nd value due to its low LREE content. The high concentrations of REE in xenotime could influence the whole rock Nd isotopic composition. Significant contributions of xenotime, however, also would be associated with elevated Y concentration in the whole rock sample, which is not observed for the HTM samples.

The modification of the restite (protolith minus partial melt) isotopic composition by partial melting may have important consequences. As after a first melting event Nd of the restite shows a more radiogenic isotopic composition than the original protolith, melting of restite material after loss of early melts will generate melts that have more radiogenic Nd isotopic compositions than earlier melt batches. Such a difference in the Nd isotopic composition of subsequent melt batches may incorrectly be interpreted to reflect increasing contributions of mantle material to crustal melts.

### *3.5.2. Li-B stable isotopes*

#### *3.5.2.1. Li-B in high-temperature samples*

Mg-bearing phyllosilicates are the most important Li host in sedimentary rocks of pelitic compositions. Conversion of clay minerals into chlorite, muscovite, and biotite during prograde metamorphism does not result in significant Li loss from these rocks as the newly formed sheet silicates incorporate Li released from the consumed clay minerals (Qiu et al., 2011). The behavior of Li in higher-grade metamorphic rocks is controlled by the behavior of the Li host (e.g. Romer and Meixner, 2014). Even during migmatization, the concentration of Li in high-temperature leucosome-restite pairs (7–34 ppm and 29–70 ppm, respectively) largely reflects the higher modal abundance of biotite in the restitic domains. Interestingly all of the analyzed leucosomes have lower Li concentrations and variably, although generally slightly higher $\delta^7$Li values than the corresponding restites (Fig. 3.7a). Experimental work indicates that Li isotopic fractionation at elevated temperatures is not insignificant (Bryant et al., 2004; Wunder et al., 2006; Wunder et al., 2007). Therefore, Qiu et al. (2011) speculated that elevated $\delta^7$Li values in leucosomes may result from Li isotopic fractionation during crystallization as Li enters two- and four-fold coordinated sites in quartz (Sartbaeva et al., 2004), whereas in most other minerals Li partitions into higher coordinated sites (Teng et al., 2006). Teng et al. (2006) also pointed out that the influence of quartz on the whole rock Li budget is insignificant due to low Li concentrations in quartz and that the heavier Li isotopic composition of granitic intrusions may result from the lower coordination of Li in the melt and, thus, result from isotopic fractionation with increasing magmatic differentiation. Alternatively, Li isotopic fractionation may already occur during partial melting if a Li rich phase with a distinct Li isotopic composition remains stable in the source rock (Romer et al., 2014; Sun et al., 2016). This may apply for the analyzed leucosome-restite pairs that show varying Li isotopic pattern. Actually the sample pair with the most pronounced difference (almost 4 $\delta^7$Li units in sample HTM_4) is the only one with garnet as a restitic phase. Sun et al. (2016) have shown that elevated $\delta^7$Li and Li depletion in the melt may result from Li fractionation in a garnet- and biotite-rich restite. Due to the eightfold coordination of Li in garnet (Halama et al., 2011; Cahalan et al., 2014), this phase may cause Li isotopic fractionation, if it is stable in the restite or occurs as a peritectic phase during partial melting reaction, resulting in a heavier $\delta^7$Li signature in the melt.

Isotopic fractionation of B is controlled by two factors: (i) differences in bond strength, and therefore differences in B coordination, among different phases and (ii) temperature (Kakihana et al., 1977; Marschall and Foster, 2018). The heavier B isotope preferentially partitions into sites with lower coordination which leads to different B isotopic compositions of cogenetic phases with different B coordination. Fractionation strongly depends on temperature and is most pronounced at low temperature and becomes increasingly smaller at higher temperatures. Tonarini et al. (2003) have shown that magmatic B isotopic fractionation between biotite and volcanic glass also depends on the $K_2O$ concentration in the melt and that increasing $K_2O$ contents in the melt decrease the portion of trigonally coordinated B. Therefore, B isotopic fractionation is expected to be more pronounced at low $K_2O$ concentrations.

The observed variation in B concentration and B isotopic composition in the analyzed high-temperature migmatite samples are less systematic than for Li. With the exception of sample HTM_4, there is a slight tendency to higher B concentrations and higher $\delta^{11}B$ values in the leucosomes (Figs. 3.7c and 3.8). This observation is basically in line with experimental data showing that the lower coordination of B in fluids/melts leads to heavier B isotopic composition in those phases, and preferred partitioning of B into the melt (Trumbull and Slack, 2018) resulting in higher B concentrations in the melt. The overall low $K_2O$ concentrations in the analyzed high-temperature samples, that are significantly below those observed by Tonarini et al. (2003) who observed B isotopic fractionation between rhyolitic glass and biotite. The low $K_2O$ concentrations in the leucosomes may account for continuous/persistent B isotopic fractionation at high-temperature, as B in low $K_2O$ melt has a lower coordination than coexisting minerals during partial melting. Using the equation of Wunder et al. (2005) under the assumption that B isotope fractionation systematics for $^{[4]}B$ solid - $^{[3]}B$ fluid also apply for $^{[4]}B$ solid - $^{[3]}B$ melt, a B isotopic difference of $\delta^{11}B$ = -5.6 to -6.0 (800 – 850 °C) between restite and melt is expected. Measured B isotopic differences of the high-temperature sample pairs are significantly smaller (differences between 0.9 and 4 $\delta^{11}B$-units, Fig. 3.7c) than calculated isotopic fractionation. This discrepancy may arise from the inaccurate assumption that B in a high $K_2O$ granitic melt is entirely trigonally coordinated. Actually, using the equation of Meyer et al. (2008), calculated B isotopic fractionation under the assumption that B is trigonally coordinated in both phases results in a difference of only 0.4 $\delta^{11}B$-units. The observed deviation from calculated B isotopic fractionation may result from a mixture of tetragonal and trigonal coordinated B sites in granitic melts whereas B

in the restite silicates is tetrahedrally coordinated. Whether such "mixed" B coordination results from differences in $K_2O$ contents or if additional factors influence B coordination in the melt is unclear. Contamination of the leucosome domain by entrained restitic biotite flakes could also dilute the heavier B isotopic composition of the leucosomes. Considering that most of the restite domains have lower overall B concentrations, entrainment of restitic biotite into the melt, however, seems not to contribute sufficient B to explain the measured $\delta^{11}B$ differences.

*3.5.2.2. Li-B in the low-temperature profile*

Lithium isotopic composition in the analyzed profile shows a step like contrast at the contact between restite and leucosome. The restite and leucosome segments at the contact differ by 5.8 $\delta^7Li$ units with the lighter Li isotopic compositions in the restite (Fig. 3.8). In the leucosome, which is mainly composed of feldspar and quartz, feldspar is the main Li host. In contrast, in the restite, which is dominated by biotite, feldspar, and quartz with minor tourmaline, biotite is the most important Li host. Therefore, the Li isotopic composition of the whole rock restite sample is controlled by the isotopic composition of biotite. Interestingly, leucosome and restite isotopic signatures closely match those of feldspar and biotite from the contact zone. Experimental work has shown that Li diffusion in hydrous silicic melts may result in significant Li isotope fractionation (Holycross et al., 2018). This process may work reasonably well for experimental melting of rhyolitic glasses, with a homogeneous Li isotopic composition, as this may be treated as a bulk process, therefore mobilizing Li with the same isotopic composition. Dehydration melting, in contrast, is a process that selectively involves protolith minerals depending on the melting reaction. As minerals in the protolith may have different Li isotopic compositions before melting, partial melting mobilizes Li with a distinct isotopic composition. Such a mineralogically controlled mobilization of Li may explain the observed sharp change in $\delta^7Li$ between restite and leucosome during muscovite-dehydration melting. Therefore, isotopic fractionation by other processes (e.g. diffusive fractionation) is of subordinate importance during water undersaturated partial melting conditions. It is important to note that this kind of selective Li mobilization does result in isotopic disequilibria between melt and restite minerals. For instance, experimental data (equation of Wunder et al., 2007) for Li isotopic fractionation between mica-melt (assuming the fractionation is similar to the one between mica-fluid) suggest that there is no significant fractionation of Li. In the natural example, however, there is a difference of

5.8 $\delta^7$Li-units (Fig. 3.8) between the leucosome and restite segments that are directly at the contact. Therefore, the $\delta^7$Li isotopic composition of the leucosome may reflect that of phases involved in the muscovite-dehydration melting reaction (i.e. feldspar and muscovite). With biotite not being involved in the low-temperature melting reaction and the high fraction of whole rock Li hosted in biotite, the stability of this phase may be responsible for the distinctly lower $\delta^7$Li values in the restite.

Boron concentrations and B isotopic composition of the low temperature profile shows only little variation which is in line with the observations made for tourmaline bearing migmatites in other studies (Kasemann et al., 2000). The boron isotopic composition of minerals from the contact zone of leucosome and restite, however, do show differences of up to 3‰ between tourmaline and biotite. (London et al., 1996) pointed out that tourmaline controls B in the melt if it remains stable until anatexis. The almost identical B isotopic signature of leucosome, restite, feldspar and tourmaline suggests that (i) whole rock B isotopic composition of the restite is controlled by tourmaline and (ii) B isotopic composition of the melt is buffered by tourmaline (Fig. 3.8 and Table 3.3). If biotite had a significant influence on the B isotopic composition, whole rock B isotopic composition of the restite segments would be shifted to heavier values. During melt generation in the presence of a B-rich phase (generally tourmaline, but also dumortierite, kornerupine, and ilvaite), the B isotopic compositions among different melt batches will not vary, even if the character of the melting reaction changes. Once tourmaline is exhausted in the source and melts that are buffered by the B isotopic composition of tourmaline have been extracted, subsequent biotite-dehydration melting is likely to result in melts with a distinctly higher $\delta^{11}$B isotopic composition due to the heavier B isotopic composition of biotite.

### 3.6. Summary

During migmatization, the character of melt producing reactions depends on pressure, fluid availability, temperature, and mineral assemblage of the protolith. The chemical composition of the melt is buffered by the partial melting reaction and by the composition of the minerals that participate in the melting reaction. This applies particularly for major elements and those trace elements that are predominantly hosted in rock forming minerals. In contrast, the concentration of trace elements that are mostly hosted in accessory phases is controlled by the solubility of these minerals and their

availability for dissolution in the melt. Different P/D ratios of radiogenic isotopes in different phases lead to contrasting isotopic compositions in these minerals. If minerals in a protolith are homogenized before partial melting, melt and restite will have the same isotopic compositions. If, however, isotopic differences persist up to partial melting conditions, the melt and restite will have isotopic compositions different from their bulk source. For isotopic systems that are mainly controlled by major phases, as for instance the Rb/Sr system, the partial melting reaction controls the isotopic composition of the melt. For Nd, accessory phases contribute most of the whole rock Nd budget. Therefore, the Nd isotopic composition of the melt is controlled by the solubility of accessory phases and their isotopic compositions. Partial melting also influences the restite as modal variation in the major and accessory phase inventory may lead to variations in isotopic composition. Melting of restite after earlier melt extraction leads to contrasting isotopic compositions in later melt batches that may be misinterpreted to represent higher contributions from a different source.

Although equilibrium isotopic fractionation of Li and B is expected to be insignificant at magmatic temperatures, the presence of minerals with contrasting Li or B isotopic compositions may lead to isotopic contrasts between melt and restite. In our samples, the leucosomes have high $\delta^7$Li values. This effect may be more pronounced if a low-$\delta^7$Li phase (e.g. garnet) is stable in the restite. The sharp variation in $\delta^7$Li at the contact between melt and restite highlights the mineralogical control on the Li isotope distribution and that diffusive fractionation is of subordinate importance. The B isotopic composition also shows some variation, most pronounced in systems with low bulk B, although the fractionation is less systematic than for Li. For partial melting systems with a B-rich phase (e.g. tourmaline), the B isotopic signature of the system is buffered by this phase. Loss on B or exhaustion of the B-rich phase may result in distinct B isotopic signatures for later melt batches.

**Acknowledgments**

We thank Bettina Hübner, Andrea Gottsche, Heike Rothe, and Sabine Tonn for analytical assistance. We also thank A. Schleicher and Ch. Kusebauch for discussion.

# Chapter 4: Partitioning of Sn, W, Nb, and Ta during partial melting – a controlling factor for rare metal mineralization

**Abstract**

Intrusions of highly specialized rare metal granites may show late stage magmatic and hydrothermal mineralization and pegmatites. Whether mineralization grade enrichment in these melts eventually occurs largely depends on the behavior of economically important trace elements (Sn, W, Nb, Ta) during melt generation. The chemical composition of the melt depends on the partial melting reaction(s) as well as the mineral assemblage of the melting rock. If Sn, W, Nb, and/or Ta are preferentially incorporated into restitic phases, the partial melts are depleted in these elements. Breakdown of phases enriched in Sn, W, Nd, and/or Ta during later melting events, may results in melts strongly enriched in these rare metals. As the Sn, W, Nb, and Ta budget of the melting rock is controlled by different minerals, partial melting represents a mechanism to fractionate those elements from each other. Such mineral-controlled selective mobilization of rare elements may play an important role for the spatial and temporal distribution of mineralization of these elements.

We present trace element data from *in situ* analysis of restite minerals from different migmatites and discuss different scenarios of Sn, W, Nb, and/or Ta enrichment in melts and their consequence for the potential of granitic melts to develop mineralization and rare element enriched pegmatites. This work highlights the paramount role of source-related processes for the entire sequence of rare element enrichment in granitic melts.

## 4.1. Introduction

The generation of granitic melts in the crust represents a first order process for the differentiation of the crust (Brown and Rushmer, 2006). During partial melting, major and trace elements are available for redistribution between melt and restite. The chemical composition of the melt depends on the nature of the partial melting reaction and on the chemical composition of the rock forming minerals that are involved in the melting reactions (Montel and Vielzeuf, 1997). This applies in particular for major elements and trace elements that are mainly hosted in rock-forming minerals. Some trace elements are preferentially hosted in accessory phases. Whether trace elements predominantly hosted in accessory phases become available for partitioning into the melt depends on the solubility of the host phase in the melt as well as whether the host is accessible for melting or is shielded by other phases (e.g. apatite inclusions in biotite). Monazite, zircon, and rutile are import hosts for LREE, HREE, as well as several trace metals, respectively. The partitioning of these elements into the melt mainly depends on the saturation of the melt in P, Zr, and Ti which are major constituents of these minerals (Watson and Harrison, 1983; Rapp and Watson, 1986; Ryerson and Watson, 1987).

The generation of granitic melts in the continental crust commonly takes place in the absence of a free fluid phase (Clemens, 1984; Clemens and Vielzeuf, 1987; Holtz and Johannes, 1991; Sawyer et al., 2011). Instead, water is contributed from OH-bearing minerals as for instance muscovite, biotite, and amphibole (Thompson, 1982; Vielzeuf and Holloway, 1988; Vielzeuf and Montel, 1994). These phases play a crucial role in the production of crustally derived granitic melts as their modal abundances, together with feldspar and quartz, control the fertility of rocks and the conditions under which melts are formed. Partial melting that involves hydrous phases takes place in several temperature ranges. In the upper and middle crust, first melt(s) is generated by muscovite dehydration melting between 700 °C and 750 °C (e.g. Le Breton and Thompson, 1988; Vielzeuf and Holloway, 1988). At higher temperatures, melt production is controlled by biotite-dehydration melting (800°C to 1000°C; Vielzeuf and Holloway, 1988; Vielzeuf and Montel, 1994). Besides their role in partial melting, biotite and muscovite may host significant amounts of trace elements that also are of economic interest (Bea et al., 1994; Neves, 1997; Van Lichtervelde et al., 2008). In combination with accessory phases, that may host significant amounts of trace metals, micas may exhibit a first order control on the enrichment/depletion of trace metals in granitic melts during partial melting.

The behavior of micas in different source rocks and at different metamorphic conditions therefore has a critical influence on the potential of granitic melt to eventually develop rare metal mineralization.

The potential of a granitic melt to form mineralization is critically influenced by the conditions of partial melting. If ore elements are not mobilized during partial melting, the potential to form mineralization during later fractional crystallization and fluid-melt separation is small. In contrast, enrichment of ore elements in partial melts increases the potential to concentrate metals during fractional crystallization to a sufficient extent to form mineralization (Romer and Kroner, 2014). The behavior of the ore elements Sn, W, Ta, and Nb in crustal metasedimentary rocks is to a large extent controlled by the major and accessory phases muscovite, biotite, titanite, ilmenite, rutile, and magnetite. Depending on protolith history (influencing its chemical composition), pressure, and temperature, different mineral assemblages will be stable during prograde metamorphism and partial melting. The breakdown of the host phases of Sn, W, Nb, and Ta, during partial melting makes these elements available for redistribution. Whether these elements remain in the melt or are partitioned into the restite depends on the mineral assemblage of the restite. The presence of trace element "sequestering" phases in the restite may prevent partitioning of a specific trace element into the melt and instead lead to its enrichment in the restite. Mineralization of Sn, W, Ta, and Nb is related to similar types of granites. These elements do, however, commonly not form mineralization together, but seem to be separated geographically or – if they occur in the same area – differ systematically in age. Differences in the stable mineral assemblage during melt generation may in part explain the contrasting prevalent occurrence of particular ore elements in different regions.

## 4.2. Sample description

Migmatites that formed under different metamorphic conditions were sampled and analyzed for their chemical compositions. The trace element contents of biotite, ilmenite, and tourmaline were analyzed by LA-ICP-MS in leucosome and restite domains of three high-temperature samples (HTM_1, HTM_3 and HTM_5) and one low-temperature sample (LTM). Sample HTM_3 contains two chemically and mineralogically distinct restite domains (R1, distal to the leucosome; R2, proximal to the leucosome) that were analyzed separately. The other samples all contain one leucosome and one restite domain.

### *4.2.1. Low-temperature sample*

A low temperature metapelitic migmatite (LTM) was sampled in the Tormes Dome anatectic area in northwestern Spain. Migmatization and anatexis by muscovite dehydration melting in these rocks were triggered by nearly isothermal exhumation (700 °C – 740 °C at 3 kbar) between 325 and 320 Ma (Escuder Viruete et al., 2000; Valverde-Vaquero et al., 2007). The low temperature sample is composed of three different domains: a mesocratic residuum, a melanosome, and a leucosome. The leucosome domain contains coarse grained plagioclase and quartz with minor, small biotite flakes. The restite domain is composed of coarse biotite flakes, plagioclase, quartz, and locally strongly fractured tourmaline. Biotite at the contact to the leucosome has abundant inclusions of zircon and monazite.

### *4.2.2. High-temperature samples*

High temperature migmatites were sampled from the Anatectic Complex of Toledo (ACT), which is part of the Central Iberian Zone, Spain. Migmatization in these rocks was triggered during Variscan high-T, low-P (800 ± 25 °C at 4–6 kbar) metamorphism. Melt production was controlled by biotite-dehydration melting (Barbero, 1995; Castiñeiras et al., 2008). All high temperature migmatite samples are composed of a leucosome and a restite domain. One sample (HTM_3) has an additional, mineralogically distinct restite domain (fine grained restite; R1). The leucosome domains are mainly composed of plagioclase and quartz (up to 1 mm). Biotite occurs as isolated grains and as aggregates (up to 2 mm) that were entrained into the leucosome. In some of the leucosomes, apatite may be present as accessory phase, forming inclusions in plagioclase and biotite. The restite domains contain plagioclase (up to 300 μm). Biotite occurs as idiomorphic flakes of up to 500 μm, sometimes containing inclusions of zircon or xenotime, and as smaller, partially reabsorbed grains. Quartz grains vary in grain size between 50 and 100 μm and may occur as rounded inclusions in plagioclase. Accessory apatite (and ilmenite in HTM_3) is present in the restite domains of the samples. The additional restite domain of sample HTM_3 (R1) contains small (80 μm) biotite and plagioclase (150 μm) grains and irregularly shaped amphibole grains (200 μm). Amphibole is observed only in this sample.

## 4.3. Methods

### *4.3.1. LA-ICP-MS*

Analyses were performed at GeoRessources (Nancy, France), using a LA-ICPMS system composed of a GeoLas excimer laser (ArF, 193 nm, Microlas) coupled to a conventional transmitted and reflected light microscope (Olympus BX51) for sample observation and laser beam focusing onto the sample and an Agilent 7500c quadrupole ICP-MS. The LA-ICPMS system was optimized to have high sensitivity on the entire mass range for all elements (from $^{7}$Li to $^{238}$U), ThO/Th ratio < 0.5% and Th/U ratio of ~1. Samples were ablated with laser spot sizes of 44, 60, 90 or 120 µm, depending on the size of the analyzed minerals. A fluence of ~ 8 J/cm$^{-2}$ and a repetition rate of 5 Hz were used. The carrier gas used was helium (0.5 L/min), which was mixed to argon (0.5 L/min) gas before entering the ICP-MS. The ICP-MS settings were the following: ICP RF Power at 1550 W, cooling gas (Ar) at 15 L/min, and auxiliary gas (Ar) at 0.9 L/min. Dual detector mode was used. For each analysis, acquisition time was 30 s for background, 40 s for external (NIST SRM 610 and NIST SRM 612 silicate glasses (Jochum et al., 2011) and cross-calibration standards, and between 40 to 60 s for the minerals. The analytical procedure for the analytical session was the following: analyses of NIST SRM 612 or NIST SRM 610 (external standard, choice of the external standard based on the diameter of the ablation spot analyses of NIST SRM 612 or NIST SRM 614 (cross-calibration samples, choice based on the chosen external standard), analyses of the minerals, analyses of the chosen cross-calibration sample and analyses of the chosen external standard. $^{28}$Si was used as internal standard for the micas and tourmalines and $^{47}$Ti for ilmenite. NIST SRM 612 and 614 silicate glass were analyzed and considered as cross-calibration samples to control the quality of the analyses (precision, accuracy, repeatability) and to correct for possible drift during the analytical session. Si (for silicates) contents in each zones of the minerals analyzed by LA-ICP-MS were measured before by electron microprobe, except for rutiles for which a stoichiometric value for Ti ($TiO_2$ = 52 wt. %) was used. Average $SiO_2$ concentrations from representative microprobe analysis of each sample were used for internal standardization; average concentrations vary from 34.88 to 37.75 wt. % $SiO_2$ (Table 4.1.). The measured elements were: $^{23}$Na, $^{24}$Mg, $^{28}$Si, $^{39}$K, $^{44}$Ca, $^{45}$Sc, $^{47}$Ti, $^{51}$V, $^{53}$Cr, $^{57}$Fe, $^{66}$Zn, $^{71}$Ga, $^{72}$Ge, $^{75}$As, $^{95}$Mo, $^{115}$In, $^{118}$Sn, $^{139}$La, $^{140}$Ce, $^{141}$Pr, $^{146}$Nd, $^{147}$Sm, $^{153}$Eu, $^{157}$Gd, $^{159}$Tb, $^{163}$Dy, $^{165}$Ho, $^{166}$Er, $^{169}$Tm, $^{172}$Yb, $^{175}$Lu, $^{181}$Ta, $^{182}$W, $^{208}$Pb, $^{209}$Bi, $^{232}$Th and $^{238}$U. An acquisition time of 10 ms was selected for all isotopes

measured. Total cycle time was 449 ms. Precision was better than 15% for Na, Mg, K and Ca, and better than 10% for the other elements. Data treatment was done using the software "Iolite" (Paton et al., 2011), following Longerich et al. (1996) for data reduction.

### *4.3.2. Electron microprobe*

The chemical composition of biotite, tourmaline, and ilmenite, were analyzed on polished thin sections by electron microprobe using a JEOL Superprobe JXA-8230 at GFZ Potsdam. The instrument is equipped with a $LaB_6$-cathode and 5 wavelength-dispersive spectrometers. Standard operating conditions were 15 kV acceleration voltage and 20 nA beam current. Beam diameter for the analysis of biotite and tourmaline was 5 µm and for ilmenite 1 µm. The following standards were used: Orthoclase (Si, Al, K), diopside (Ca, Mg), albite (Na), rutile (Ti), magnetite (Fe), rhodonite (Mn), $BiSi_2O_5$ (Ba), apatite (P) fluorite (F), and tugtupite (Cl). Counting times for the different elements were 10s (Si, Al, K, Fe, Mn) and 20s (F, Ca, Cl, Ba, Mn, Mg, P, Ti). Backgrounds were acquired using half the counting time on the peaks.

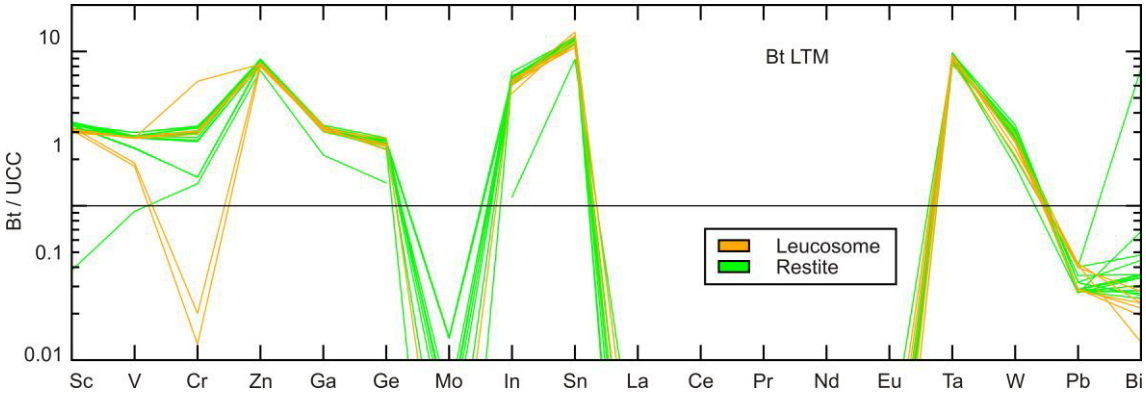


Fig. 4.1. UCC (Rudnick and Gao, 2003) normalized LA-ICP-MS trace element data for biotite from the low-temperature sample.

## 4.4. Results

### *4.4.1. LA-ICP-MS of the low-temperature sample*

Trace element compositions of biotite from the low-temperature migmatite are shown in Fig. 4.1. To facilitate comparison between different samples, all compositional data are normalized against upper continental crust (Rudnick and Gao, 2003), rather than against the immediate host rock because of the following reasons: (i) normalization to the respective whole rock data of the corresponding domains would produce apparent enrichment of some trace elements in minerals that are hosted in domains with low overall concentration of these elements and (ii) trace element pattern of the minerals from

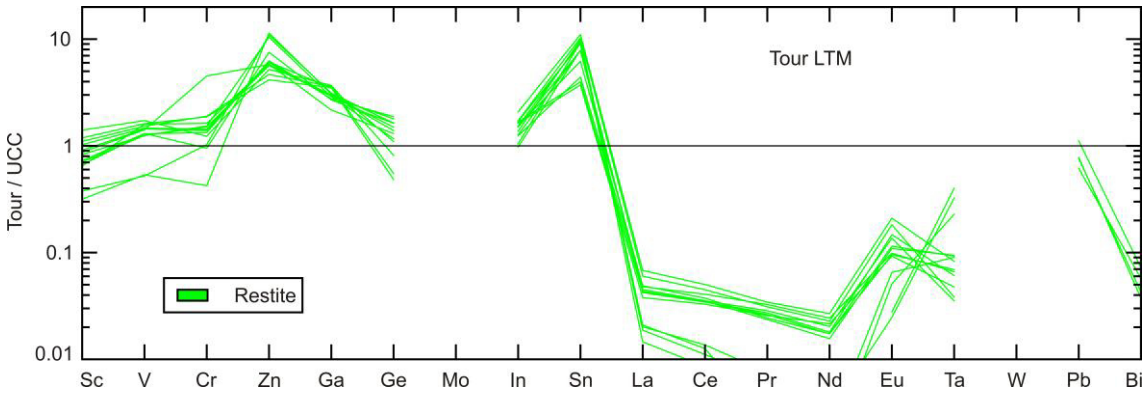


Fig. 4.2. UCC (Rudnick and Gao, 2003) normalized LA-ICP-MS trace element data for tourmaline from the low-temperature sample. While Sn may be readily hosted by tourmaline, W is below LOD in all analyses.

different domains would not be comparable. The most striking difference between biotite from the restite and leucosomes are the lower content of V, Cr and Bi of biotite from the leucosome. All other analyzed trace elements do not show large differences between biotite from the restite and biotite close to or in the leucosome. The concentration of REE in low temperature biotite is always below limit of detection. Restitic tourmaline in the low temperature migmatite sample has elevated contents of Zn and Sn. The REE pattern show a slight enrichment of LREE and a positive Eu anomaly (Fig. 4.2).

### *4.4.2. LA-ICP-MS of the high-temperature samples*

Trace element content of biotite from the high temperature samples are shown in Fig. 4.3. In general, biotite from the restite domains has higher V, Cr, (and Sn in samples HTM_3 and 5) contents than biotite closer to the leucosome or in the leucosome. For Sc, Ge, Pb, and Bi, there is no significant difference between leucosome and restite biotite. The elements Zn, Ga, Mo, In, Ta, and W are generally enriched in biotite that is closer to the leucosome or in the leucosome. Biotite from the "distal" restite (R1) of sample HTM_3 has markedly higher V and Cr contents and distinctly lower contents of Zn, Ga, Ge, In, Ta, and W than biotite from the other domains. The REE pattern of biotite are flat and REE concentrations are low with no clear preference for restite or leucosome biotite.

Table 4.1. Representative averaged EMPA analyses used as internal standards for LA-ICP-MS

| Mineral | Bt | | | | | | | | Ilm | | Tour |
|---|---|---|---|---|---|---|---|---|---|---|---|
| Sample | HTM_1a | HTM_1b | HTM_3a | HTM_3b | HTM_3c | HTM_5a | HTM_5b | LTM | HTM_3a | HTM_3b | LTM |
| n | 24 | 9 | 22 | 11 | 10 | 4 | 6 | 11 | 3 | 5 | 7 |
| $SiO_2$ | 34.88 | 36.47 | 35.84 | 35.52 | 37.75 | 36.43 | 36.20 | 35.88 | – | – | 36.80 |
| $TiO_2$ | 4.84 | 4.51 | 4.40 | 4.16 | 3.12 | 4.52 | 4.42 | 2.97 | 52.99 | 52.76 | 0.88 |
| $Al_2O_3$ | 16.55 | 17.02 | 16.32 | 16.31 | 14.39 | 17.13 | 16.86 | 19.98 | – | – | 33.82 |
| MgO | 10.85 | 10.04 | 11.66 | 11.34 | 15.38 | 10.34 | 10.86 | 7.67 | – | – | 4.35 |
| CaO | 0.27 | 0.01 | 0.04 | 0.04 | 0.05 | 0.03 | 0.03 | 0.02 | – | – | 0.30 |
| MnO | 0.12 | 0.13 | 0.18 | 0.12 | 0.07 | 0.12 | 0.10 | 0.31 | 2.22 | 1.76 | 0.09 |
| FeO | 18.55 | 19.09 | 18.12 | 18.72 | 14.66 | 18.41 | 17.91 | 20.53 | 44.37 | 44.77 | 10.09 |
| BaO | 0.26 | 0.21 | 0.26 | 0.23 | 0.51 | 0.20 | 0.20 | 0.20 | – | – | 2.04 |
| $Na_2O$ | 0.19 | 0.15 | 0.21 | 0.20 | 0.55 | 0.18 | 0.17 | 0.25 | – | – | 0.05 |
| $K_2O$ | 8.87 | 9.60 | 9.16 | 8.80 | 8.95 | 9.55 | 9.55 | 9.06 | – | – | – |
| $B_2O_3$ [(a)] | – | – | – | – | – | – | – | – | – | – | 10.79 |
| $H_2O$ [(a)] | 3.44 | 3.55 | 3.45 | 3.44 | 3.16 | 3.78 | 3.70 | 3.79 | – | – | – |
| F- | 1.00 | 0.94 | 1.08 | 1.03 | 1.72 | 0.44 | 0.57 | 0.43 | – | – | – |
| Cl- | 0.08 | 0.08 | 0.06 | 0.08 | 0.16 | 0.09 | 0.07 | 0.02 | – | – | – |
| Total | 99.46 | 101.39 | 100.31 | 99.54 | 99.70 | 101.00 | 100.93 | 100.93 | 99.58 | 99.29 | 99.21 |

(a) = calculated

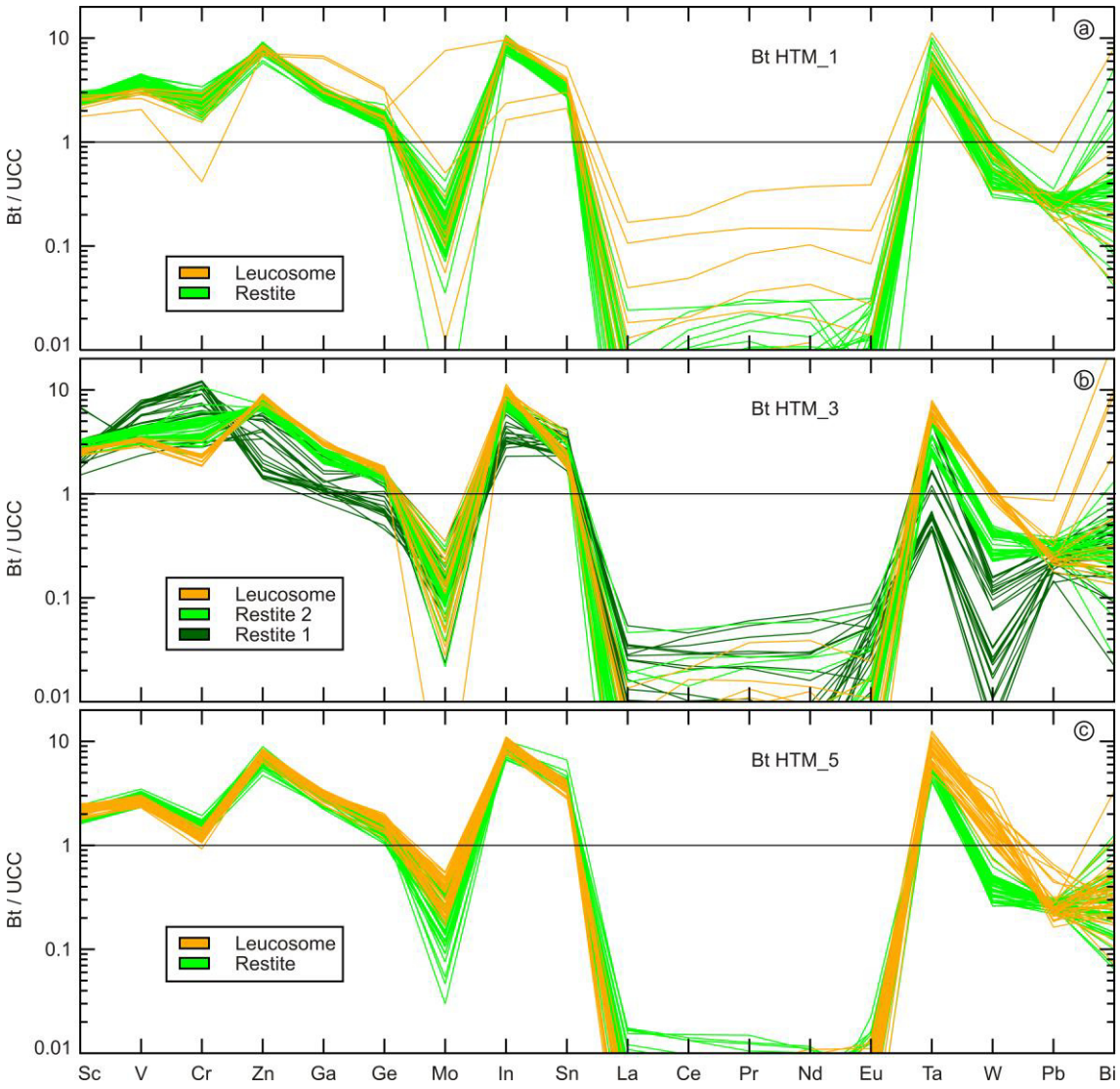


Fig. 4.3. UCC (Rudnick and Gao, 2003) normalized LA-ICP-MS trace element data for biotite from different high-temperature migmatites. Note the depletion in Ta and W for biotite in restite domains where ilmenite is stable (b).

The "proximal" restite (R2) of sample HTM_3 contains relatively rare ilmenite grains. Trace element content of ilmenite crystals that are large enough for analysis by LA-ICP-MS are shown in Fig. 4.4. Ilmenite has elevated contents of Sc, V, In, Sn, and Ta. The pattern of REE in ilmenite is flat and concentrations are generally very low.

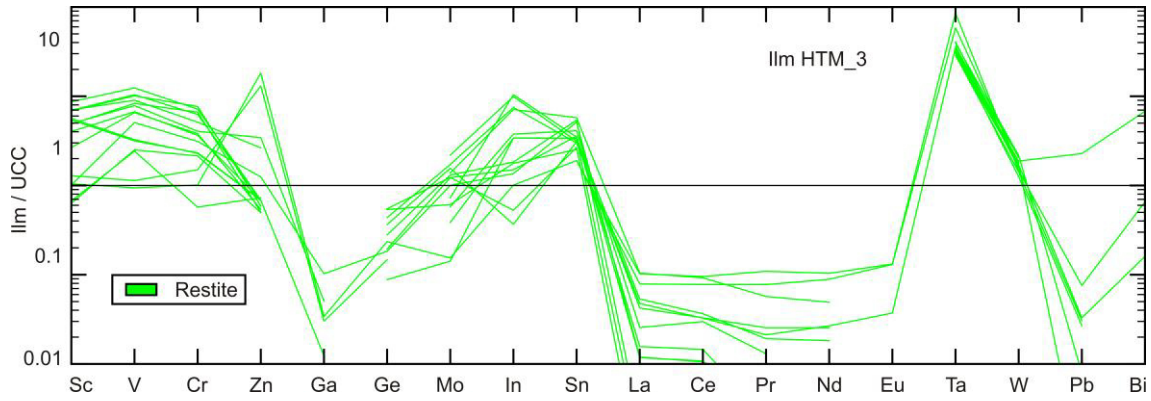


Fig. 4.4. UCC (Rudnick and Gao, 2003) normalized LA-ICP-MS trace element data for ilmenite from sample HTM_3. Note the enrichment in Ta.

## 4.5. Discussion

The elements Sn, W, Nb, and Ta may form phases of their own (e.g. cassiterite, wolframite, columbite) in rare metal granites, pegmatites, and quartz veins (Lehmann, 1985; Linnen and Williams-Jones, 1993; Marignac and Cuney, 1999; Černý et al., 2004). In sedimentary rocks and their metamorphic equivalents, however, these elements occur only in trace amounts and are hosted in rock-forming minerals (e.g. micas) or accessory phases (e.g. Ti-oxides; Cave et al., 2017). The formation of a hydrothermal, magmatic, or magmatic-hydrothermal mineral deposit, starting from a sedimentary source rock, involves a wide range of processes that may result in a wide range of different types of mineralization and metal assemblages. These processes include prograde metamorphism and devolatilization (Cuney et al., 1990), partial melting (Simons et al., 2017; Wolf et al., 2018), fractional crystallization (Gomes and Neiva, 2002; Groves and McCarthy, 1978; Lehmann, 1982), fluid-melt separation (Lehmann and Mahawat, 1989; Thomas et al., 2005; Webster et al., 2004), and fluid-rock interaction (Eugster, 1985; Meinert, 1992). These processes represent (i) critical steps for the formation of a mineralization and (ii) may lead to fractionation/separation of Sn, W, Nb, and Ta. We discuss processes that may influence the budget of Sn, W, Nb, and Ta during different stages and processes.

### *4.5.1. Sedimentary source*

Long-term, intense weathering of crustal sediments leads the decomposition of feldspar which eventually results in the loss of Na, Ca, Sr, and Pb that are not incorporated into authigenic minerals to a significant extent, whereas K, Al, and Rb may be incorporated into clay minerals. Other elements released from feldspar and other readily altered minerals also may be lost (e.g. Mo, V, U) or they are incorporated or

adsorbed on clay minerals and Fe-oxyhydroxides. Elements that belong to this second group are Li, Cs, Sn, W, and Ta. In contrast, elements that are mobilized and transported away from the source may be enriched in a different depositional environment. For instance, Mo, V, and U may be concentrated in reduced environments, closed basins, reduced sediments (i.e. black shales) or calcrete rocks (Fyffe and Pickerill, 1993; Kyser and Cuney, 2008; Romer and Cuney, 2018; Romer and Hahne, 2010). The weathering history of a sedimentary source rock is important in two ways: (i) source rocks of granitic melts may already have enhanced concentrations in Sn, W, Ta, and Nb due to relative enrichment and (ii) the specific chemical composition of the weathered shale (high K, Al, low Na, Ca) eventually affects the melting behavior, in particular the amount of melt produced at a given temperature, that may lead to enhanced ore element contents in partial melts (Romer and Kroner, 2014; Wolf et al., 2018).

### *4.5.2. Low-grade metamorphism*

The solubility of different trace metals in aqueous solutions may depend on multiple factors, most importantly pH, type and concentration of ligands, temperature, and/or pressure (Barnes, 1979; Gibert et al., 1998; Seward, 1973). The concentration of Sn in an aqueous fluid seems to be mainly controlled by the concentration of HCl in the fluid (Schmidt, 2018), whereas the solubility of W in an aqueous solution increases with increasing NaCl concentrations and temperature and decreasing pH (Wood and Samson, 2000). In contrast, Nb and Ta solubility is very low for average crustal fluids as Nb and Ta transport requires concentrated fluoride solutions (Timofeev et al., 2017, 2015; Zaraisky et al., 2010). Compaction of sedimentary rocks during burial and diagenesis reduces the pore space in these rocks and fluid is expelled from the sediments. With the onset of low grade metamorphism, clay minerals progressively recrystallize to sheet silicates resulting in further devolatilization of the (meta-) sedimentary rocks. Schmidt (2018) has shown that Sn is highly soluble in an HCl-rich fluid at relatively low temperatures. Depending on the composition of the fluid and the form in which metal ions are present in the rock, Sn and/or W may be mobilized into the fluid phase. For instance, if Sn and W are predominantly adsorbed on clay minerals, these elements may readily partition into a fluid of appropriate composition. This may have two important consequences: (i) potential source rocks may become depleted in Sn and/or W and (ii) focused flow of metal enriched fluids may lead to precipitation of Sn and/or W in overlying units. Such enriched rocks also provide a source for Sn and/or W enriched

granitic melts. An example of such a low-grade metamorphic mobilization of W is given by Cave et al. (2015). In their samples, detrital rutile hosts a significant amount of W that is mobilized and partially lost from the source rock during prograde metamorphism and formation of titanite at the expense of rutile.

*4.5.3. Low-temperature melting with sequestering phases in the restite*

Comparison of the trace element partitioning (Sn and W) in leucosome restite pairs of low-temperature and high-temperature migmatites indicates that the partitioning behavior is controlled by the melting temperature and restite mineralogy (e.g. Bea et al., 1994; Gómez and Alonso, 2000; Neves, 1997; Wolf et al., 2018). Deeply weathered sediments develop high modal amounts of muscovite and biotite during prograde metamorphism that eventually reaches partial melting conditions. Although these phases do not have particularly high contents of Sn, W, Nb, and Ta, they may host a large portion of the whole rock budget of Sn, W, Nb, and Ta budget due to their high modal abundance. Under low-pressure fluid-absent conditions, muscovite-dehydration melting takes place around 700 °C. If Sn, W, Nb, and Ta are released during the breakdown of muscovite they may either partition into the melt or they may be redistributed into restitic or peritectic phases. The elevated $D_{Nb}^{Bt-melt}/D_{Ta}^{Bt-melt}$ 1.8 – 4.8, and high $D_{Nb}^{Bt-melt}$ of 3.6 – 9 (Acosta-Vigil et al., 2010; Nash and Crecraft, 1985) suggest that partial melting will result in elevated Nb concentrations in the restitic biotite as well as higher Nb/Ta ratios in the restite (Stepanov and Hermann, 2013). At the same time, Ta (together with Li and Cs from muscovite) may, to some extent, be partitioned into the melt. Such low-temperature melts eventually may develop into LCT-type pegmatites (Romer and Kroner, 2014). Biotite from the analyzed low-temperature migmatite has between 18 and 28 ppm Sn and 3.4 to 6.3 ppm W. The whole rock concentrations for these elements are 13 and 3 ppm, respectively. Biotite, being the most abundant phase in the restite, may therefore account for the entire whole rock W budget of the restite, whereas some Sn may also be incorporated into other phases (e.g. tourmaline 7.8 – 27 ppm). Whether W was already present in biotite during prograde metamorphism or if W in biotite was sequestered during muscovite-breakdown is unclear. Data on partitioning coefficients between biotite and granitic melt for W are scarce. If $D_W^{Bt-melt}$ is close to unity or below, low temperature melting by muscovite-dehydration provides a mechanism to mobilize W into the melt if no other W sequestering phases are stable. For instance, Ti-phases such as rutile may

incorporate significant amounts of W and therefore prevent W enrichment in the melt (Zack et al., 2002). If, however, Ti concentration in the protolith is relatively low, the stability of biotite suppresses saturation of Ti-oxide phases (Stepanov et al., 2014) and W may partition into the melt. This process also results in the fractionation of Sn and Nb, hosted in restitic biotite, from Ta and W.

### *4.5.4. Low-temperature melting without sequestering phases*

In contrast to above scenario, protolith rocks that have (very) low Fe and Mg (and Ti) contents will only develop little or no biotite during prograde metamorphism. Melt production by the breakdown of muscovite will mobilize Sn, W, Nb, and Ta that are incorporated in muscovite. In the absence minerals that act as sequestering phases (e.g. biotite and Ti-phases), these elements may not be redistributed into the restite and will remain in the melt. Melts generated under such conditions could mobilize Sn, W, Nb, and Ta together with Li and Cs. Such an ore element inventory closely resembles that of some LCT-pegmatites with associated Sn and W in peripheral quartz veins (Cuney et al., 1990; Linnen et al., 2014). The role of source composition for the generation of rare metal pegmatites has been debated since a long time (Deveaud et al., 2015; London, 2005; Shaw et al., 2016). Low-temperature melting of a metasedimentary source without a sequestering phase for Sn, W, Nb, and Ta may explain both, pegmatite formation in association with highly specialized granitic melts (Martins et al., 2012) as well as pegmatite formation that is not correlated with a parental granitic intrusion (Melleton et al., 2012; Müller et al., 2015).

### *4.5.5. High-temperature melting with sequestering phases in the restite*

At high temperatures, progressive breakdown of biotite, which may host significant amounts of Sn, Nb and Ta, releases a significant portion of Sn, Nb, and Ta whole rock budget into the melt. With increasing temperature during prograde metamorphism, Ti is increasingly incorporated in biotite (Guidotti, 1984). Decomposition of biotite, therefore, not only releases Sn, Nb, and Ta but also Ti. As granitic melts can dissolve only limited amounts of Ti (Ryerson and Watson, 1987), breakdown of biotite at high temperature may lead to the formation of peritectic Ti-phases (e.g. rutile, ilmenite, or Ti-magnetite; Luvizotto and Zack, 2009). For instance, Sn, Nb, and Ta are moderately compatible in ilmenite during melt generation (D > 1), whereas W is little compatible ($D_W^{Ilm-melt}$ < 1; Klemme et al., 2006). In rutile, Nb, Ta, and W are highly compatible

(D >> 1). There is no data available for Sn, but $D_{Sn}^{Rt-melt}$ is likely to be smaller than for Nb, Ta, and W (Green and Pearson, 1987; Hart et al., 2018; Horng and Hess, 2000; Mallmann et al., 2014). It is important to note that these systematic differences may show significant variation depending on the melt composition (Horng and Hess, 2000). In the presence of an accessory Ti-phase (i.e. ilmenite, rutile, Ti-magnetite, titanite), a large portion of Sn, W, Nb, and Ta from biotite may be sequestered in these accessory phases, preventing their enrichment in the melt. Actually, the restite domain of sample HTM_3 (R2) contains abundant ilmenite grains. Biotite in this domain has distinctly lower Ta and W contents (Fig. 4.3b), which may be explained by the strong preference of ilmenite (Ti-phases in general) for Ta and W. In contrast, Sn concentrations in biotite are not lower in the presence of ilmenite compared to biotite without ilmenite. Melt formed under high-temperature conditions in the presence of a Ti-phase, therefore, may have a limited potential to develop significant enrichment of Sn, W, Nb, and Ta by fractional crystallization as these elements may be retained in restitic/peritectic Ti-phases.

### *4.5.6. High-temperature melting after low-temperature melting and melt extraction*

The restites of metasedimentary rocks that have experienced muscovite dehydration melting followed by loss of the low-temperature melt in one or several extraction events may undergo further prograde metamorphism. With increasing temperatures melt production changes from muscovite- to biotite-dehydration melting. Biotite may sequester Sn and Nb and, to a lesser extent, W and Ta that were released during low-temperature melting. As the low-temperature melts have been extracted from the system, these rocks are relatively enriched in the Sn, W, Nb, and Ta. The process of restite enrichment by sequestration of the ore elements in biotite may continue during early high-temperature melting if some of the released trace elements are partitioned back into restitic biotite. Extraction of these early high-temperature melts would then further enhance the Sn, W, Nb, and Ta concentrations in the restite. Volumetrically small melt batches that consume the last biotite, thus, may have particularly high contents in Sn, W, Nb, and/or Ta. The precondition for this process to work efficiently is that Sn, W, Nb, and Ta released by the breakdown of biotite are not sequestered by stable restite phases (e.g. rutile, ilmenite). Melts that are generated by the described sequence of processes may have significantly higher Sn, W, Nb, and Ta contents than their original protoliths or average crustal sedimentary sources in general. These high “starting”-concentrations

make further accumulation by fractional crystallization particularly efficient, as the extent of fractional crystallization to reach concentrations of Sn, W, Nb, or Ta in the melt sufficiently high to form mineralization, is dramatically reduced.

### 4.6. Implications

Granite related Sn and W mineralization commonly occurs along distinct belts (Romer and Kroner, 2016; Schuiling, 1967). Deposits of Sn-W often show predominance of one of these ore elements. This predominance may also be observed on a larger scale. For instance, in southern China, W-mineralization is mainly restricted to the eastern part whereas Sn-mineralization is mainly found in the western part (Mao et al., 2013). Mineralization of different ore elements (e.g. Sn and W) may not only be separated in space, but also in time (Breiter et al., 1997; Cheng et al., 2018; Raimbault et al., 1995). Such observations may in part be explained by the above discussed scenarios. The source rocks for granitic intrusions in areas that predominantly host W mineralization may have experienced lower temperature regimes and biotite remained stable and did not release Sn. Alternatively, the protolith composition may have led the formation of peritectic phases that sequester Sn. Similar considerations hold true for the separation of Sn and W mineralization in time. While W may be mobilized during low-temperature melting in an early stage of the metamorphic cycle, Sn mobilization may be delayed as high-temperature melting conditions were reached later or Sn was mobilized from restitic material during a second metamorphic cycle.

It is important to note that the above discussed scenarios do not implicitly lead to mineralization in granitic intrusions or rare metal pegmatites. If mineralization and/or pegmatite formation eventually takes place is critically depending on subsequent fractional crystallization processes (López-Moro et al., 2017; Stilling et al., 2006) and magmatic/hydrothermal processes (Heinrich, 1990; Lehmann, 1990). Source processes that control whether rare metals are mobilized into the melt or not, provide key constraints to estimate the **potential** of these melts to generate economically important deposits.

**Acknowledgments**

We thank Andrea Gottsche, Sabine Tonn, Heike Rothe, and Bettina Hübner for their support in the laboratory for the major and trace element data and Oona Appelt for help during microprobe analysis.

# Chapter 5: Discussion

The generation of granitic melts by partial melting of metasediments in the crust has profound consequences for the trace element budget and the isotopic composition of melt and restite. The partial melting reactions control the major element composition of granitic melts. The trace element inventories of melt and restite, however, depend on the minerals, particularly accessory phases, that are stable during melt generation. Understanding of these systematics becomes especially important in the context of trace metals that are of economic interest and for elements whose isotopes are used as geochemical tracers: (i) trace metals may be enriched in the restite, resulting in high starting concentrations in the melt during remelting and (ii) variations of the isotopic compositions of different melt batches may erroneously be interpreted to reflect variable contributions from different sources.

## 5.1. Sn mineralization as the result of multiple processes

The generation of Sn-specific granitic melts is subjected to a sequence of processes. Traditionally, fractional crystallization and late magmatic/hydrothermal processes were considered as the most significant or exclusive processes that control Sn enrichment (Lehmann, 1987; Heinrich, 1990). A more comprehensive model by Romer and Kroner (2015) explains the formation of Sn and W mineralization as the result of a sequence of superimposed processes (alteration and redistribution of source rocks, partial melting at different conditions, melt extraction) that are all ultimately controlled by a large scale tectonic framework. The results of this work illustrate the role of source rock composition, prograde metamorphism with melt formation at different temperatures, and the mode of melt extraction for the generation of Sn enriched granitic melts.

### *5.1.1. Distribution of Sn between melt and restite*

Trace element analyses from different migmatites show that Sn mobilization into the melt is strongly controlled by the stability of micas. In low-temperature migmatites, Sn concentrations are distinctly higher in the restite than in the leucosome. In contrast, biotite-dehydration melting results in Sn enrichment in the leucosome. The observations from natural samples together with thermodynamic modeling show that intensely weathered metasediments represent particularly important source rocks. Decomposition

of feldspar in these sediments leads to a depletion in Ca, Na, Sr, and Pb and a relative enrichment in Al, K, Rb, and Sn. This specific chemical composition stabilizes large amounts of muscovite and biotite during prograde metamorphism. These minerals are important for two reasons: (i) they incorporate significant amounts of Sn and control the distribution of Sn and (ii) they control dehydration melting reactions.

### *5.1.2. Melt production and extraction*

During low-temperature melt generation by muscovite-dehydration melting, large amounts of melt are generated over a limited temperature interval. If melt generation occurs in the presence of biotite, a significant portion of Sn released from muscovite will be sequestered in restitic biotite and therefore retained in the source. Under closed system conditions, the release of sequestered Sn during high-temperature melting does not result in Sn enriched melt as high amounts of low-temperature (low Sn) melts are present. Natural rocks are, however, unlikely to hold high amounts of melt (Arzi, 1978; Vigneresse et al., 1996). Therefore, the large volume of melt produced during low-temperature melting is extracted from the source. Extraction of material from the source represents a relative increase in Sn concentration in the remaining rock (i.e. restite). With increasing temperature, melt generation shifts from muscovite- to biotite-dehydration melting. If Sn behaves similar as during muscovite-dehydration melting, biotite gets increasingly enriched in Sn with increasing temperature and melt production. Breakdown of such strongly enriched biotite releases significant amounts of Sn into the melt. This effect may be particularly efficient, if melt extraction occurs shortly before consumption of the last remaining Sn-host (e.g. biotite). Such Sn enriched, small-volume, high-temperature melts are particularly suited for subsequent formation of mineralization as less extensive fractional crystallization is necessary to reach mineralization grade Sn concentrations.

## 5.2. Ti-phases and the distribution of Sn, W, Nb, and Ta

Besides muscovite and biotite, accessory phases such as rutile, ilmenite, and titanite may also act as important hosts for Sn and other trace metals, specifically W, Nb, and Ta (Zack et al., 2002; Klemme et al., 2006; Cave et al., 2017). As the different minerals incorporate Sn, W, Nb, and Ta in variable amounts, the mineral assemblage that is stable during melt generation may lead to decoupling of these elements from each other, resulting in different degrees of enrichment of these metals in the melt. Their

behavior during partial melting is therefore critical for the mobilization or retention of these elements into the melt or restite, respectively. Which specific phases are stable during melt generation depends on the chemical composition of the protolith and the metamorphic conditions under which melt generation takes place. Whether or not a granitic melt develops rare metal mineralization is therefore in part controlled by source-related processes.

### *5.2.1. Metal mobilization during low-grade metamorphism*

The trace element budget (Sn, W, Nb, Ta) of a (meta)-sedimentary source rock may be modified during different stages from sedimentation up to partial melt generation. A first modification of the rare metal budget may already occur during chemical alteration of the sedimentary source. For instance, Mo, V, and U may be lost during intense weathering whereas other elements (e.g. Li, Cs, Sn, W, and Ta) may be adsorbed on clay minerals and Fe-oxyhydroxides and, therefore, show a relative enrichment. During diagenesis and low-grade metamorphism, pore space in (meta)-sedimentary rocks decreases progressively and a fluid phase is expelled. The solubilities of Sn, W, Nb, and Ta in aqueous fluids depend on different parameters. While Sn is readily soluble in aqueous fluids that have high HCl contents (Schmidt, 2018), the solubility of W is mainly controlled by the concentration of NaCl in the fluid. Depending on the composition of the formation water Sn and/or W may already be mobilized during low-grade metamorphism. This may result in (i) depletion of the corresponding elements in the source rock and (ii) enrichment in other source rocks where Sn or W may be precipitated from enriched fluids. In contrast, the solubility of Nb and Ta in average crustal fluids is restricted as they require high HF concentrations in the fluid to be soluble (Zaraisky et al., 2010; Timofeev et al., 2015; Timofeev et al., 2017). Therefore, Nb and Ta are expected to be rather immobile during low-grade metamorphism and devolatilization.

### *5.2.2. Generation of melts with distinct Sn, W, Nb, and Ta contents*

Breakdown of muscovite during low-temperature melt generation releases Sn, W, Nb, and Ta. Whether these elements partition into the melt or restite depends on the restite mineral assemblage and the partitioning coefficient ($D_{Sn,W,Nb,Ta}^{mineral-melt}$). For instance biotite has elevated $D_{Nb}^{Bt-melt}/D_{Ta}^{Bt-melt}$ of 1.8 – 4.8, and high $D_{Nb}^{Bt-melt}$ of 3.6 – 9 (Nash and Crecraft, 1985; Acosta-Vigil et al., 2010). If restitic biotite is present during low-

temperature melt generation, the restite will be enriched in Nb, whereas the melt will have elevated Ta (together with Li and Cs) contents. Such a trace metal inventory in the melt may eventually lead to the formation of rare metal enriched pegmatites of the LCT-type (Romer and Kroner, 2014). Similar mechanisms may influence the trace metal budget of the melt if Ti-phases (e.g. rutile, ilmenite, titanite) are stable. However, for protoliths with relatively low Ti contents, biotite will incorporate most of the available Ti, thereby suppressing the saturation of Ti-phases (Stepanov et al., 2014). Breakdown of biotite at elevated temperatures not only releases Sn, W, Nb, and Ta but also Ti and, therefore, may form peritectic Ti-phases (Luvizotto and Zack, 2009). As these phases strongly incorporate Sn, W, Nb, and/or Ta (Green and Pearson, 1987; Zack et al., 2002; Klemme et al., 2006; Hart et al., 2018), melts that are generated in the presence of a Ti-phase have a restricted potential to develop significant mineralization. In contrast, melts generated from an enriched restite without a trace metal sequestering phase have a high potential to develop mineralization and/or rare metal enriched pegmatites. Further enrichment of trace metals by fractional crystallization in these melts is particularly efficient as these melts already have elevated concentrations in Sn, W, Nb, and/or Ta.

## 5.3. Effects of partial melting on radiogenic isotope systematics

Partial melting also has profound consequences for the stable and radiogenic isotope systematics of the melt and the restite (Harris and Ayres, 1998; Farina et al., 2014). The radiogenic isotope composition of different minerals may show significant variation depending on their P/D ratio and age. If the isotopic compositions of the minerals homogenize before partial melting, melt and restite have the same isotopic composition. If, however, isotopic differences persist up to partial melting conditions, melt and restite have different isotopic compositions. For isotopic systems that are mainly controlled by rockforming minerals, as for instance Rb/Sr (muscovite, biotite, feldspar), the isotopic composition of the melt mainly depends on the partial melting reaction and the rockforming phases involved in the melting reaction. In contrast, accessory phases control the Nd budget of most rocks. The Nd isotopic composition of the melt, therefore, strongly depends on the solubility of accessory phases.

### *5.3.1. The Rb/Sr system*

The analyzed leucosomes from the high-temperature samples have relatively homogeneous and more radiogenic Sr isotopic compositions. This observation suggests

that the isotopic composition of the melt is buffered by the biotite-dehydration melting reaction. In contrast, the corresponding restite domains have variable and less radiogenic $^{87}Sr/^{86}Sr$ isotopic compositions. These observations may be explained by differences in the restite mineral assemblage that reflect chemical variations in the protolith or different degrees of melt extraction. For instance, the sample with amphibole in the restite has a distinctly less radiogenic Sr isotopic composition. Amphibole commonly has a low Rb/Sr ratio and, therefore, less radiogenic Sr isotopic composition. Its stability in the restite shifts the whole rock Sr isotopic composition to less radiogenic values. Melting of such restites with variable $^{87}Sr/^{86}Sr$ leads to melt batches with distinct Sr isotopic compositions.

*5.3.2. The Sm/Nd system*

The whole rock Nd data show a similar pattern as $^{87}Sr/^{86}Sr$. Leucosome domains have almost homogeneous εNd values whereas the corresponding restites have variable and more radiogenic Nd isotopic compositions. For the analyzed samples, apatite is the most important Nd host phase. LREE- and MREE-pattern in apatite may vary during prograde metamorphism resulting in different Sm/Nd ratios and, therefore, different $^{143}Nd/^{144}Nd$. Additionally, isotopic equilibration of apatite is largely suppressed under fluid absent conditions (Bingen et al., 1996; Janots et al., 2018). For protoliths that contain different types of apatite with different Sm/Nd ratios, one type (lower Sm/Nd) of apatite may preferentially be located at grain boundaries whereas the other type (higher Sm/Nd) mainly occurs as inclusions in other phases. Dissolution of accessory phases during melt generation in such a protolith will mainly affect low Sm/Nd (less radiogenic $^{143}Nd/^{144}Nd$) apatite, resulting in a homogeneous (less radiogenic) $\varepsilon Nd_{(t)}$ in the leucosome. In contrast, the Nd isotopic composition of the restites may be variably influenced by the additional high Sm/Nd apatite. Restitic domains may therefore have variable and $\varepsilon Nd_{(t)}$ values that are different from $\varepsilon Nd_{(t)}$ of the melt.

## 5.4. Effects of partial melting on stable isotopes

*5.4.1. Li isotope systematics during partial melting*

The observed differences in Li isotopic composition in the high-temperature leucosome-restite pairs are in contradiction to the generally assumed isotopic equilibration of Li isotopes at high temperatures. The observed trend for elevated $\delta^7Li$ values and lower Li concentrations in the melt may be explained by residual Li-rich

phases that also have lower $\delta^7$Li (e.g. garnet and biotite) values (Sun et al., 2016). Similar observations are made for the low temperature profile. The lower $\delta^7$Li composition of the restite closely matches the Li isotopic composition of biotite, suggesting that restitic biotite dominates the Li budget of the restite domains, whereas $\delta^7$Li values of the leucosome correspond to that of feldspar. This suggests a strong mineralogical control on the Li budget and isotopic fractionation during melt generation. The spatial variation in $\delta^7$Li, showing a sharp change between leucosome and restite, illustrate that Li isotopic fractionation by diffusion is of subordinate importance during water undersaturated melting.

### *5.4.2. B isotope systematics during partial melting*

The behavior of Boron in the high-temperature migmatites is less systematic than for Li. The slight trend to higher $\delta^{11}$B values and higher B concentrations in the melt is in agreement with experimental work (Trumbull and Slack, 2018). However, measured B isotopic composition of leucosome and restite does not fit well with theoretical calculations that assume either different coordination of B (i.e. trigonal and tetragonal) between melt and restite or the same coordination (i.e. trigonal) in both phases. This discrepancy may be explained by a mixture of trigonally and tetragonally coordinated B in granitic melts. For instance, Tonarini et al. (2003) have shown that with increasing $K_2O$ content of the melt the portion of trigonally coordinated B decreases. The small variation in B isotopic composition between melt and restite of the low-temperature samples suggests that the B isotopic composition of the melt is buffered by a B-rich phase. Actually, this sample has restitic tourmaline stable and $\delta^{11}$B values of restite and leucosome domains closely correspond to that of tourmaline. Therefore, if a B-rich phase is stable, $\delta^{11}$B values of different melt batches will be buffered by that phase. Exhaustion of the B-rich phase in the source may result in melt batches with distinct $\delta^{11}$B values.

## 5.5. Summary

The presented work highlights the importance of source related processes, specifically the mineralogical control, on trace element and isotope systematics during partial melting. In the context of granite related mineralization, the findings provide insight into the mechanisms that control mobilization or retention of economically important metals (Sn, W, Nb, and Ta). Mobilization of trace elements from their source strongly depends on the mineral assemblage that is present during melt generation as well

as the conditions of melt generation. Furthermore, the understanding of trace metal distribution between different phases during partial melting events may also explain temporal and spatial variations of different mineralization and fractionation of certain metal elements in specific areas. Therefore, the formation of granite-related mineral deposits may best be explained as a multistage process rather than an end-member scenario (e.g. source anomaly *vs.* fractional crystallization). Application of these results in a geotectonic framework provides a promising tool to distinguish areas that potentially host important mineralization from barren ones.

The assumption of complete isotopic equilibration at partial melting conditions in fluid absent systems does not entirely hold true. The isotopic composition of radiogenic (Sr, Nd, and Pb) isotopes in melt and restite are controlled by a combination of source history, mineral assemblage, and melting reaction. This may result in isotopic differences between melt and restite, which in turn may result in incorrect assumptions for the source of granitic intrusions or wrong estimations for the contribution of different sources to a granitic melt. Lithium and B isotope systematics may display significant mineralogically controlled fractionation if phases with different distinct Li and/or B isotopic compositions are present. Therefore, other fractionation processes are of subordinate importance during fluid absent melting.

# 6. References


Acosta-Vigil A., Buick I., Hermann J., Cesare B., Rubatto D., London D. and Morgan G. B. (2010) Mechanisms of Crustal Anatexis: a Geochemical Study of Partially Melted Metapelitic Enclaves and Host Dacite, SE Spain. *Journal of Petrology* **51**, 785–821.

Arzi A. A. (1978) Critical phenomena in the rheology of partially melted rocks. *Tectonophysics* **44**, 173–184.

Ayres M. and Harris N. (1997) REE fractionation and Nd-isotope disequilibrium during crustal anatexis: constraints from Himalayan leucogranites. *Chemical Geology* **139**, 249–269.

Barbero L. (1995) Granulite-facies metamorphism in the Anatectic Complex of Toledo, Spain: late Hercynian tectonic evolution by crustal extension. *Journal of the Geological Society* **152**, 365–382.

Barbero L. and Villaseca C. (2000) Eclogite facies relics in metabasites from the Sierra de Guadarrama (Spanish Central System): P-T estimations and implications for the Hercynian evolution. *Mineralogical Magazine* **64**, 815–836.

Barbero L. and Villaseca C. (2004) El macizo de Toledo. In *Geología de España* (ed. J. A. Vera). SGE-IGME. pp. 110–115.

Barbero L. and Villaseca C. (1992) The Layos Granite, Hercynian Complex of Toledo (Spain): an example of parautochthonous restite-rich granite in a granulitic area. *Earth and Environmental Science Transactions of The Royal Society of Edinburgh* **83**, 127–138.

Barnes H. L. (1979) Solubilities of Ore Minerals. In *Geochemistry of hydrothermal ore deposits 2nd Edition* (ed. H. L. Barnes). Wiley, New York. pp. 404–454.

Bea F. (1996) Residence of REE, Y, Th and U in granites and crustal protoliths; Implications for the chemistry of crustal melts. *Journal of Petrology*. **37**, 521–552.

Bea F., Fershtater G. and Corretgé L. G. (1992) The geochemistry of phosphorus in granite rocks and the effect of aluminium. *Lithos* **29**, 43–56.

Bea F., Montero P., Talavera C. and Zinger T. (2006) A revised Ordovician age for the Miranda do Douro orthogneiss, Portugal. Zircon U-Pb ion-microprobe and LA-ICPMS dating. *Geologica Acta* **4**, 395–401.

Bea F., Pereira M. D. and Stroh A. (1994) Mineral/leucosome trace-element partitioning in a peraluminous migmatite (a laser ablation-ICP-MS study). *Chemical Geology* **117**, 291–312.

Bingen B., Demaiffe D. and Hertogen J. (1996) Redistribution of rare earth elements, thorium, and uranium over accessory minerals in the course of amphibolite to granulite facies metamorphism: The role of apatite and monazite in orthogneisses from southwestern Norway. *Geochimica et Cosmochimica Acta* **60**, 1341–1354.

Boehnke P., Watson E. B., Trail D., Harrison T. M. and Schmitt A. K. (2013) Zircon saturation re-revisited. *Chemical Geology* **351**, 324–334.

Bowen N. L. and Tuttle O. F. (1950) The System $NaAlSi_3O_8$-$KAlSi_3O_8$-$H_2O$. *The Journal of Geology* **58**, 489–511.

Breiter K., Frýda J., Seltmann R. and Thomas R. (1997) Mineralogical Evidence for Two Magmatic Stages in the Evolution of an Extremely Fractionated P-rich Rare-metal Granite: the Podlesí Stock, Krušné Hory, Czech Republic. *Journal of Petrology* **38**, 1723–1739.

Brown G. C. and Fyfe W. S. (1970) The production of granitic melts during ultrametamorphism. *Contributions to Mineralogy and Petrology.* **28**, 310–318.

Brown M. and Rushmer T. (2006) *Evolution and Differentiation of the Continental Crust*. eds. M. Brown and T. Rushmer, Cambridge University Press, Cambridge.

Bryant C. J., Chappell B. W., Bennett V. C. and McCulloch M. T. (2004) Lithium isotopic compositions of the New England Batholith: correlations with inferred source rock compositions. *Transactions of the Royal Society of Edinburgh: Earth Sciences* **95**, 199–214.

Cahalan R. C., Kelly E. D. and Carlson W. D. (2014) Rates of Li diffusion in garnet: Coupled transport of Li and Y+REEs. *American Mineralogist* **99**, 1676–1682.

Castiñeiras P., Villaseca C., Barbero L. and Romera C. M. (2008) SHRIMP U–Pb zircon dating of anatexis in high-grade migmatite complexes of Central Spain: implications in the Hercynian evolution of Central Iberia. *International Journal of Earth Sciences (Geologische Rundschau)* **97**, 35–50.

Castro A., Corretege L. G., De la Rosa J., Enrique P., Martinez F. J., Pascual E., Lago M., Arranz E., Gale C., Fernandez C., Donaire T. and Lopez S. (2002) Palaeozoic Magmatism. In *The Geology of Spain* (eds. W. Gibbons and T. Moreno). Geological Society of London, London. pp. 117–154.

Cave B. J., Pitcairn I. K., Craw D., Large R. R., Thompson J. M. and Johnson S. C. (2017) A metamorphic mineral source for tungsten in the turbidite-hosted orogenic gold deposits of the Otago Schist, New Zealand. *Mineralium Deposita* **52**, 515–537.

Cave B. J., Stepanov A. S., Craw D., Large R. R., Halpin J. A. and Thompson J. (2015) Release of trace elements through the sub-greenschist facies breakdown of detrital rutile to metamorphic titanite in the Otago schist, New Zealand. *The Canadian Mineralogist* **53**, 379–400.

Černý P., Chapman R., Ferreira K. and Smeds S.-A. (2004) Geochemistry of oxide minerals of Nb, Ta, Sn, and Sb in the Varuträsk granitic pegmatite, Sweden: The case of an "anomalous" columbite-tantalite trend. *American Mineralogist* **89**, 505–518.

Chappell B. W. (1996) Magma mixing and the production of compositional variation within granite suites: Evidence from the granites of southeastern Australia. *Journal of Petrology* **37**, 449–470.

Cheng Y., Spandler C., Chang Z. and Clarke G. (2018) Volcanic–plutonic connections and metal fertility of highly evolved magma systems: A case study from the Herberton Sn–W–Mo Mineral Field, Queensland, Australia. *Earth and Planetary Science Letters* **486**, 84–93.

Chorlton L. B. and Martin R. F. (1978) The effect of boron on the granite solidus. *Candian Mineralogist* **16**, 239–244.

Clemens J. D. (1984) Water contents of silicic to intermediate magmas. *Lithos* **17**, 273–287.

Clemens J. D. and Vielzeuf D. (1987) Constraints on melting and magma production in the crust. *Earth and Planetary Science Letters* **86**, 287–306.

Coggon R. and Holland T. (2002) Mixing properties of phengitic micas and revised garnet-phengite thermobarometers. *Journal of Metamorphic Geology* **20**, 683–696.

Cruciani G., Franceschelli M., Foley S. F. and Jacob D. E. (2014) Anatectic amphibole and restitic garnet in Variscan migmatite from NE Sardinia, Italy: insights into partial melting from mineral trace elements. *European Journal of Mineralogy* **26**, 381–395.

Cuney M., Friedrich M., Blumenfeld P., Bourguignon A., Boiron M. C., Vigneresse J. L. and Poty B. (1990) Metallogenesis in the French part of the Variscan orogen. Part I: U preconcentrations in pre-Variscan and Variscan formations — a comparison with Sn, W and Au. *Tectonophysics* **177**, 39–57.

De Capitani C. and Petrakakis K. (2010) The computation of equilibrium assemblage diagrams with Theriak/Domino software. *American Mineralogist* **95**, 1006–1016.

De Laeter J. R. and Blockley J. G. (1972) Granite ages within the Archaean Pilbara Block, Western Australia. *Journal of the Geological Society of Australia* **19**, 363–370.

De Wit M. J., Thiart C., Doucouré M. and Wilsher W. (1999) Scent of a supercontinent: Gondwana's ores as chemical tracers—tin, tungsten and the Neoproterozoic Laurentia-Gondwana connection. *Journal of African Earth Sciences* **28**, 35–51.

DePaolo D. J. and Wasserburg G. J. (1979) Petrogenetic mixing models and Nd-Sr isotopic patterns. *Geochimica et Cosmochimica Acta* **43**, 615–627.

Deveaud S., Millot R. and Villaros A. (2015) The genesis of LCT-type granitic pegmatites, as illustrated by lithium isotopes in micas. *Chemical Geology* **411**, 97–111.

Diener J. F. A., Powell R., White R. W. and Holland T. (2007) A new thermodynamic model for clino- and orthoamphiboles in the system $Na_2O$–CaO–FeO–MgO–$Al_2O_3$–$SiO_2$–$H_2O$–O. *Journal of Metamorphic Geology* **25**, 631–656.

Dorais M. J. and Tubrett M. (2012) Detecting Peritectic Garnet in the Peraluminous Cardigan Pluton, New Hampshire. *Journal of Petrology* **53**, 299–324.

Erambert M. and Austrheim H. (1993) The effect of fluid and deformation on zoning and inclusion patterns in poly-metamorphic garnets. *Contributions to Mineralogy and Petrology* **115**, 204–214.

Escuder Viruete J., Arenas R. and Martínez Catalán J. R. (1994) Tectonothermal evolution associated with Variscan crustal extension in the Tormes Gneiss Dome (NW Salamanca, Iberian Massif, Spain). *Tectonophysics* **238**, 117–138.

Escuder Viruete J., Indares A. and Arenas R. (1997) P-T path determinations in the Tormes Gneissic Dome, NW Iberian Massif, Spain. *Journal of Metamorphic Geology* **15**, 645–663.

Escuder Viruete J., Indares A. and Arenas R. (2000) P–T paths derived from garnet growth zoning in an extensional setting: an example from the Tormes Gneiss Dome (Iberian Massif, Spain). *Journal of Petrology* **41**, 1489–1515.

Eugster H. P. (1985) Granites and hydrothermal ore deposits: a geochemical framework. *Mineralogical Magazine* **49**, 7–23.

Farina F., Dini A., Rocchi S. and Stevens G. (2014) Extreme mineral-scale Sr isotope heterogeneity in granites by disequilibrium melting of the crust. *Earth and Planetary Science Letters* **399**, 103–115.

Farina F. and Stevens G. (2011) Source controlled $^{87}Sr/^{86}Sr$ isotope variability in granitic magmas: The inevitable consequence of mineral-scale isotopic disequilibrium in the protolith. *Lithos* **122**, 189–200.

Förster H.-J. (1998a) The chemical composition of REE-Y-Th-U-rich accessory minerals in peraluminous granites of the Erzgebirge-Fichtelgebirge region, Germany; Part I, The monazite-(Ce)-brabantite solid solution series. *American Mineralogist* **83**, 259–272.

Förster H.-J. (1998b) The chemical composition of REE-Y-Th-U-rich accessory minerals in peraluminous granites of the Erzgebirge-Fichtelgebirge region, Germany; Part II, Xenotime. *American Mineralogist* **83**, 1302–1315.

Förster H.-J. and Romer R. L. (2010) Carboniferous magmatism. In *Pre-Mesozoic Geology of Saxo-Thuringia* (eds. U. Linnemann and R. L. Romer). Schweizerbart, Stuttgart. pp. 287–308.

Förster H.-J., Tischendorf G., Trumbull R. B. and Gottesmann B. (1999) Late-Collisional Granites in the Variscan Erzgebirge, Germany. *Journal of Petrology* **40**, 1613–1645.

Franke W. (1989) Variscan plate tectonics in Central Europe—current ideas and open questions. *Tectonophysics* **169**, 221–228.

Fyffe L. R. and Pickerill R. K. (1993) Geochemistry of Upper Cambrian-Lower Ordovician black shale along a northeastern Appalachian transect. *Geological Society of America Bulletin* **105**, 897–910.

Gibert F., Pascal M.-L. and Pichavant M. (1998) Gold solubility and speciation in hydrothermal solutions: experimental study of the stability of hydrosulphide complex of gold (AuHS°) at 350 to 450°C and 500 bars. *Geochimica et Cosmochimica Acta* **62**, 2931–2947.

Gomes M. E. P. and Neiva A. M. R. (2002) Petrogenesis of Tin-bearing Granites from Ervedosa, Northern Portugal: The Importance of Magmatic Processes. *Geochemistry (Chemie der Erde )***62**, 47–72.

Gómez M. D. P. and Alonso M. D. R. (2000) Duality of cordierite granites related to melt-restite segregation in the Pena Negra anatectic complex, central Spain. *The Canadian Mineralogist* **38**, 1329–1346.

Green T. H. and Pearson N. J. (1987) An experimental study of Nb and Ta partitioning between Ti-rich minerals and silicate liquids at high pressure and temperature. *Geochimica et Cosmochimica Acta* **51**, 55–62.

Groves D. I. and McCarthy T. S. (1978) Fractional crystallization and the origin of tin deposits in granitoids. *Mineralium Deposita* **13**, 11–26.

Guidotti C. V. (1984) Micas in metamorphic rocks. *Reviews in Mineralogy and Geochemistry* **13**, 357–467.

Halama R., John T., Herms P., Hauff F. and Schenk V. (2011) A stable (Li, O) and radiogenic (Sr, Nd) isotope perspective on metasomatic processes in a subducting slab. *Chemical Geology* **281**, 151–166.

Halliday A. N. (1980) The timing of early and main stage ore mineralization in Southwest Cornwall. *Economic Geology* **75**, 752–759.

Harris N. and Ayres M. (1998) The implications of Sr-isotope disequilibrium for rates of prograde metamorphism and melt extraction in anatectic terrains. *Geological Society of London, Special Publications* **138**, 171–182.

Hart E., Storey C., Harley S. L. and Fowler M. (2018) A window into the lower crust: Trace element systematics and the occurrence of inclusions/intergrowths in granulite-facies rutile. *Gondwana Research* **59**, 76–86.

Hedenquist J. W. and Lowenstern J. B. (1994) The role of magmas in the formation of hydrothermal ore deposits. *Nature* **370**, 519–527.

Heinrich C. A. (1990) The chemistry of hydrothermal tin(-tungsten) ore deposition. *Economic Geology* **85**, 457–481.

Hogan J. P. and Sinha A. K. (1991) The effect of accessory minerals on the redistribution of lead isotopes during crustal anatexis: A model. *Geochimica et Cosmochimica Acta* **55**, 335–348.

Holland T. and Powell R. (2003) Activity–composition relations for phases in petrological calculations: an asymmetric multicomponent formulation. *Contributions to Mineralogy and Petrology* **145**, 492–501.

Holland T. and Powell R. (1998) An internally consistent thermodynamic data set for phases of petrological interest. *Journal of Metamorphic Geology* **16**, 309–343.

Holtz F. and Johannes W. (1991) Genesis of Peraluminous Granites I. Experimental Investigation of Melt Compositions at 3 and 5 kb and Various $H_2O$ Activities. *Journal of Petrology* **32**, 935–958.

Holycross M. E., Watson E. B., Richter F. M. and Villeneuve J. (2018) Diffusive fractionation of Li isotopes in wet, silicic melts. *Geochemical Perspectives Letters* ***6***, 39–42.

Horng W.-S. and Hess P. C. (2000) Partition coefficients of Nb and Ta between rutile and anhydrous haplogranite melts. *Contributions to Mineralogy and Petrology* **138**, 176–185.

Hoskin P. W. O. and Schaltegger U. (2003) The composition of zircon and igneous and metamorphic petrogenesis. *Reviews in Mineralogy and Geochemistry* **53**, 27–62.

Huang W. L. and Wyllie P. J. (1973) Muscovite dehydration and melting in deep crust and subducted oceanic sediments. *Earth and Planetary Science Letters* **18**, 133–136.

Huang W.-L. and Wyllie P. J. (1975) Melting Reactions in the System $NaAlSi_3O_8$-$KAlSi_3O_8$-$SiO_2$ to 35 Kilobars, Dry and with Excess Water. *Journal of Geology* **83**, 737–748.

Ibarguchi J. I. G. and Martinez F. J. (1982) Petrology of garnet — cordierite — sillimanite gneisses from the El Tormes thermal dome, Iberian Hercynian foldbelt (W Spain). *Contributions to Mineralogy and Petrology* **80**, 14–24.

Irving A. J. and Frey F. A. (1978) Distribution of trace elements between garnet megacrysts and host volcanic liquids of kimberlitic to rhyolitic composition. *Geochimica et Cosmochimica Acta* **42**, 771–787.

Ishihara S. (1978) Metallogenesis in the Japanese island arc system. *Journal of the Geological Society of London* **135**, 389–406.

Janots E., Austrheim H., Spandler C., Hammerli J., Trepmann C. A., Berndt J., Magnin V. and Kemp A. I. S. (2018) Rare earth elements and Sm-Nd isotope redistribution in apatite and accessory minerals in retrogressed lower crust material (Bergen Arcs, Norway). *Chemical Geology* **484**, 120–135.

Jochum K. P., Weis U., Stoll B., Kuzmin D., Yang Q., Raczek I., Jacob D. E., Stracke A., Birbaum K., Frick D. A., Günther D. and Enzweiler J. (2011) Determination of Reference Values for NIST SRM 610–617 Glasses Following ISO Guidelines. *Geostandards and Geoanalytical Research* **35**, 397–429.

Kakihana H., Kotaka M., Satoh S., Nomura M. and Okamoto M. (1977) Fundamental studies on the ion-exchange separation of boron isotopes. *Bulletin of the Chemical Society of Japan* **50**, 158–163.

Kasemann S., Erzinger J. and Franz G. (2000) Boron recycling in the continental crust of the central Andes from the Palaeozoic to Mesozoic, NW Argentina. *Contributions to Mineralogy and Petrology* **140**, 328–343.

Kasemann S., Meixner A., Rocholl A., Vennemann T., Rosner M., Schmitt A. K. and Wiedenbeck M. (2001) Boron and oxygen isotope composition of certified reference materials NIST SRM 610/612 and reference materials JB-2 and JR-2. *Geostandards Newsletter* **25**, 405–416.

Klemme S., Günther D., Hametner K., Prowatke S. and Zack T. (2006) The partitioning of trace elements between ilmenite, ulvospinel, armalcolite and silicate melts with implications for the early differentiation of the moon. *Chemical Geology* **234**, 251–263.

Knesel K. M. and Davidson J. P. (2002) Insights into Collisional Magmatism from Isotopic Fingerprints of Melting Reactions. *Science* **296**, 2206–2208.

Kowalski P. M. and Wunder B. (2018) Boron Isotope Fractionation Among Vapor–Liquids–Solids–Melts: Experiments and Atomistic Modeling. In *Boron Isotopes – The Fifth Element* (eds. H. R. Marschall and G. L. Foster). Advances in Isotope Geochemistry. Springer, Cham. pp. 33–69.

Kronberg B. I., Fyfe W. S., McKinnon B. J., Couston J. F., Filho B. S. and Nash R. A. (1982) Model for bauxite formation: Paragominas (Brazil). *Chemical Geology* **35**, 311–320.

Kyser K. and Cuney M. (2008) Sandstone-hosted uranium deposits. In *Recent and not-so-recent developments in uranium deposits and implications for exploration* Mineralogical Association of Canada Short course series. Mineralogical Association of Canada, Québec. pp. 221–237.

Le Breton N. and Thompson A. B. (1988) Fluid-absent (dehydration) melting of biotite in metapelites in the early stages of crustal anatexis. *Contributions to Mineralogy and Petrology* **99**, 226–237.

Lehmann B. (1985) Formation of the strata-bound Kellhuani tin deposits, Bolivia. *Mineralium Deposita* **20**, 169–176.

Lehmann B. (1990) *Metallogeny of Tin.*, Springer, Berlin, Heidelberg.

Lehmann B. (1982) Metallogeny of tin; magmatic differentiation versus geochemical heritage. *Economic Geology* **77**, 50–59.

Lehmann B. (1987) Tin granites, geochemical heritage, magmatic differentiation. *Geologische Rundschau* **76**, 177–185.

Lehmann B. and Mahawat C. (1989) Metallogeny of tin in central Thailand: A genetic concept. *Geology* **17**, 426–429.

Lesher C. E. (1990) Decoupling of chemical and isotopic exchange during magma mixing. *Nature* **344**, 235–237.

Linnen R. L., Samson I. M., Williams-Jones A. E. and Chakhmouradian A. R. (2014) 13.21 - Geochemistry of the Rare-Earth Element, Nb, Ta, Hf, and Zr Deposits. In *Geochemistry of mineral deposits* (eds. H. D. Holland and K. K. Turekian). Treatise on Geochemistry (Second Edition). Elsevier, Oxford. pp. 543–568.

Linnen R. L. and Williams-Jones A. E. (1993) Mineralogical constraints on magmatic and hydrothermal Sn-W-Ta-Nb mineralization at the Nong Sua aplite-pegmatite, Thailand. *European Journal of Mineralogy* **5**, 721–736.

London D. (2005) Granitic pegmatites: an assessment of current concepts and directions for the future. *Lithos* **80**, 281–303.

London D., Morgan G. B. and Wolf M. B. (1996) Boron in granitic rocks and their contact aureoles. In *Boron: mineralogy, petrology and geochemistry in the Earth's crust.* (eds. E. Grew and L. Anovitz). Reviews in Mineralogy. Mineralogical Society of America, Washington, D.C. pp. 299–325.

Longerich H. P., Jackson S. E. and Günther D. (1996) Inter-laboratory note. Laser ablation inductively coupled plasma mass spectrometric transient signal data acquisition and analyte concentration calculation. *Journal of Analytical Atomic Spectrometry* **11**, 899–904.

López-Moro F. J., García Polonio F., Llorens González T., Sanz Contreras J. L., Fernández Fernández A. and Moro Benito M. C. (2017) Ta and Sn concentration by muscovite fractionation and degassing in a lens-like granite body: The case study of the Penouta rare-metal albite granite (NW Spain). *Ore Geology Reviews* **82**, 10–30.

López-Moro F. J. and López-Plaza M. (1993) Geology of the basement in the Miranda do Douro antiform (Western sector of Zamora). *Studia Geologica Salmanticensia* **28**, 103–140.

López-Moro F. J., López-Plaza M. and Romer R. L. (2012) Generation and emplacement of shear-related highly mobile crustal melts: the synkinematic leucogranites from the Variscan Tormes Dome,

Western Spain. *International Journal of Earth Sciences (Geologische Rundschau)* **101**, 1273–1298.

Luvizotto G. L. and Zack T. (2009) Nb and Zr behavior in rutile during high-grade metamorphism and retrogression: An example from the Ivrea–Verbano Zone. *Chemical Geology* **261**, 303–317.

Mallmann G., Fonseca R. O. C., Silva A. B., Mallmann G., Fonseca R. O. C. and Silva A. B. (2014) An experimental study of the partitioning of trace elements between rutile and silicate melt as a function of oxygen fugacity. *Anais da Academia Brasileira de Ciências* **86**, 1609–1629.

Manning D. A. C. and Pichavant M. (1983) The role of fluorine and boron in the generation of granitic melts. In *Migmatites, Melting and Metamorphism* (eds. M. P. Atherton and C. D. Gribble). Shiva Publishing Unlimited, Nantwich. pp. 94–109.

Mao J., Yanbo C., Maohong C. and Pirajno F. (2013) Major types and time–space distribution of Mesozoic ore deposits in South China and their geodynamic settings. *Mineralium Deposita* **48**, 267–294.

Marignac C. and Cuney M. (1999) Ore deposits of the French Massif Central: insight into the metallogenesis of the Variscan collision belt. *Mineralium Deposita* **34**, 472–504.

Marschall H. R. and Foster G. L. (2018) Boron Isotopes in the Earth and Planetary Sciences—A Short History and Introduction. In *Boron Isotopes – The Fifth Element* (eds. H. R. Marschall and G. L. Foster). Advances in Isotope Geochemistry. Springer, Cham. pp. 1–11.

Martins T., Roda-Robles E., Lima A. and Parseval P. de (2012) Geochemistry and evolution of micas in the Barroso-alvao pegmatite field, northern. *The Canadian Mineralogist* **50**, 1117–1129.

McCulloch M. T. and Chappell B. W. (1982) Nd isotopic characteristics of S- and I-type granites. *Earth and Planetary Science Letters* **58**, 51–64.

McLeod C. L., Davidson J. P., Nowell G. M. and Silva S. L. de (2012) Disequilibrium melting during crustal anatexis and implications for modeling open magmatic systems. *Geology* **40**, 435–438.

Mehnert K. R., Büsch W. and Schneider G. (1973) Initial melting at grain boundaries of quartz and feldspar in gneisses and granulites. *Neues Jahrbuch für Mineralogie*, *Monatshefte* 165–183.

Meinert L. D. (1992) Skarns and Skarn Deposits. *Geoscience Canada* **19**.

Melleton J., Gloaguen E., Frei D., Novák M. and Breiter K. (2012) How are the emplacement of rare-element pegmatites, regional metamorphism and magmatism interrelated in the Moldanubian domain of the variscan bohemian massif, Czech Republic? *The Canadian Mineralogist* **50**, 1751–1773.

Meyer C., Wunder B., Meixner A., Romer R. L. and Heinrich W. (2008) Boron-isotope fractionation between tourmaline and fluid: an experimental re-investigation. *Contributions to Mineralogy and Petrology* **156**, 259–267.

Montel J.-M. and Vielzeuf D. (1997) Partial melting of metagreywackes, Part II. Compositions of minerals and melts. *Contributions to Mineralogy and Petrology* **128**, 176–196.

Müller A., Ihlen P. M., Snook B., Larsen R. B., Flem B., Bingen B. and Williamson B. J. (2015) The Chemistry of Quartz in Granitic Pegmatites of Southern Norway: Petrogenetic and Economic Implications. *Economic Geology* **110**, 1737–1757.

Nash W. P. and Crecraft H. R. (1985) Partition coefficients for trace elements in silicic magmas. *Geochimica et Cosmochimica Acta* **49**, 2309–2322.

Neiva A. M. R. (2002) Portuguese granites associated with Sn-W and Au mineralizations. *Bulletin of the Geological Society of Finland* **74**, 79–101.

Neiva A. M. R. (1998) Trace Element Partitioning Between Coexisting Biotite and Muscovite of Portuguese Granitic Differentiation Series. *Mineralogical Magazine* **62A**, 1069–1070.

Nesbitt H. W. and Young G. M. (1982) Early Proterozoic climates and plate motions inferred from major element chemistry of lutites. *Nature* **299**, 715–717.

Neves L. J. P. F. (1997) Trace element content and partitioning between biotite and muscovite of granitic rocks; a study in the Viseu region (central Portugal). *European Journal of Mineralogy* **9**, 849–857.

Patiño Douce A. E. and Johnston A. D. (1991) Phase equilibria and melt productivity in the pelitic system: implications for the origin of peraluminous granitoids and aluminous granulites. *Contributions to Mineralogy and Petrology* **107**, 202–218.

Paton C., Hellstrom J., Paul B., Woodhead J. and Hergt J. (2011) Iolite: Freeware for the visualisation and processing of mass spectrometric data. *Journal of Analytical Atomic Spectrometry* **26**, 2508–2518.

Petö P. (1976) An experimental investigation of melting relations involving muscovite and paragonite in the silica-saturated portion of the system $K_2O$-$Na_2O$-$Al_2O_3$-$SiO_2$-$H_2O$. *Progress in Experimental Petrology* **3**, 41–45.

Pichavant M. (1981) An experimental study of the effect of boron on a water saturated haplogranite at 1 Kbar vapour pressure. *Contributions to Mineralogy and Petrology* **76**, 430–439.

Plimer I. R. (1980) Exhalative Sn and W deposits associated with mafic volcanism as precursors to Sn and W deposits associated with granites. *Mineralium Deposita* **15**, 275–289.

Powell R. and Holland T. (1999) Relating formulations of the thermodynamics of mineral solid solutions; activity modeling of pyroxenes, amphiboles, and micas. *American Mineralogist* **84**, 1–14.

Qiu L., Rudnick R. L., McDonough W. F. and Bea F. (2011) The behavior of lithium in amphibolite- to granulite-facies rocks of the Ivrea–Verbano Zone, NW Italy. *Chemical Geology* **289**, 76–85.

Raimbault L., Cuney M., Azencott C., Duthou J.-L. and Joron J. L. (1995) Geochemical evidence for a multistage magmatic genesis of Ta-Sn-Li mineralization in the granite at Beauvoir, French Massif Central. *Economic Geology* **90**, 548–576.

Rapp R. P. and Watson E. B. (1986) Monazite solubility and dissolution kinetics: implications for the thorium and light rare earth chemistry of felsic magmas. *Contributions to Mineralogy and Petrology* **94**, 304–316.

Romer R. L. (2001) Lead incorporation during crystal growth and the misinterpretation of geochronological data from low-$^{238}U/^{204}Pb$ metamorphic minerals. *Terra Nova* **13**, 258–263.

Romer R. L. and Cuney M. (2018) Phanerozoic uranium mineralization in Variscan Europe – More than 400 Ma of tectonic, supergene, and climate-controlled uranium redistribution. *Ore Geology Reviews* **102**, 474–504.

Romer R. L. and Hahne K. (2010) Life of the Rheic Ocean: Scrolling through the shale record. *Gondwana Research* **17**, 236–253.

Romer R. L., Heinrich W., Schröder-Smeibidl B., Meixner A., Fischer C.-O. and Schulz C. (2005) Elemental dispersion and stable isotope fractionation during reactive fluid-flow and fluid immiscibility in the Bufa del Diente aureole, NE-Mexico: evidence from radiographies and Li, B, Sr, Nd, and Pb isotope systematics. *Contributions to Mineralogy and Petrology* **149**, 400–429.

Romer R. L. and Kroner U. (2016) Phanerozoic tin and tungsten mineralization—Tectonic controls on the distribution of enriched protoliths and heat sources for crustal melting. *Gondwana Research* **31**, 60–95.

Romer R. L. and Kroner U. (2014) Sediment and weathering control on the distribution of Paleozoic magmatic tin–tungsten mineralization. *Mineralium Deposita* **50**, 327–338.

Romer R. L. and Meixner A. (2014) Lithium and boron isotopic fractionation in sedimentary rocks during metamorphism – The role of rock composition and protolith mineralogy. *Geochimica et Cosmochimica Acta* **128**, 158–177.

Romer R. L., Meixner A. and Hahne K. (2014) Lithium and boron isotopic composition of sedimentary rocks — The role of source history and depositional environment: A 250 Ma record from the Cadomian orogeny to the Variscan orogeny. *Gondwana Research* **26**, 1093–1110.

Romer R. L. and Rötzler J. (2011) The role of element distribution for the isotopic dating of metamorphic minerals. *European Journal of Mineralogy* **23**, 17–33.

Rose A. W., Hawkes H. E. and Webb J. S. (1979) *Geochemistry in mineral exploration*. Academic press, London.

Rubatto D. (2002) Zircon trace element geochemistry: partitioning with garnet and the link between U–Pb ages and metamorphism. *Chemical Geology* **184**, 123–138.

Rudnick R. L. and Gao S. (2003) Composition of the Continental Crust. In *Treatise on Geochemistry* (eds. H. D. Holland and K. K. Turekian). Pergamon, Oxford. pp. 1–64.

Ryerson F. J. and Watson E. B. (1987) Rutile saturation in magmas: implications for Ti-Nb-Ta depletion in island-arc basalts. *Earth and Planetary Science Letters* **86**, 225–239.

Sartbaeva A., Wells S. A. and Redfern S. A. T. (2004) Li + ion motion in quartz and β-eucryptite studied by dielectric spectroscopy and atomistic simulations. *Journal of Physics: Condensed Matter* **16**, 8173.

Sawyer E. W. (2008) *Atlas of Migmatites*. NRC Research Press.

Sawyer E. W., Cesare B. and Brown M. (2011) When the Continental Crust Melts. *Elements* **7**, 229–234.

Schmidt C. (2018) Formation of hydrothermal tin deposits: Raman spectroscopic evidence for an important role of aqueous Sn(IV) species. *Geochimica et Cosmochimica Acta* **220**, 499–511.

Schuiling R. D. (1967) Tin belts on the continents around the Atlantic Ocean. *Economic Geology* **62**, 540–550.

Searle M. P., Whitehouse M. J., Robb L. J., Ghani A. A., Hutchison C. S., Sone M., Ng S. W.-P., Roselee M. H., Chung S.-L. and Oliver G. J. H. (2012) Tectonic evolution of the Sibumasu–Indochina terrane collision zone in Thailand and Malaysia: constraints from new U–Pb zircon chronology of SE Asian tin granitoids. *Journal of the Geological Society of London* **169**, 489–500.

Seward T. M. (1973) Thio complexes of gold and the transport of gold in hydrothermal ore solutions. *Geochimica et Cosmochimica Acta* **37**, 379–399.

Shaw R. A., Goodenough K. M., Roberts N. M. W., Horstwood M. S. A., Chenery S. R. and Gunn A. G. (2016) Petrogenesis of rare-metal pegmatites in high-grade metamorphic terranes: A case study from the Lewisian Gneiss Complex of north-west Scotland. *Precambrian Research* **281**, 338–362.

Simons B., Andersen J. C. Ø., Shail R. K. and Jenner F. E. (2017) Fractionation of Li, Be, Ga, Nb, Ta, In, Sn, Sb, W and Bi in the peraluminous Early Permian Variscan granites of the Cornubian Batholith: Precursor processes to magmatic-hydrothermal mineralisation. *Lithos* **278–281**, 491–512.

Spear F. S. (1995) *Metamorphic Phase Equilibria and Pressure-Temperature-Time Paths*. 2nd ed., Mineralogical Society of America, Washington, D.C.

Štemprok M. (1995) A comparison of the Krusne hory-Erzgebirge (Czech Republic-Germany) and Cornish (UK) granites and their related mineralisation. *Proceedings of the Ussher Society* **8**, 347–356.

Štemprok M. (1990) Intrusion sequences within ore-bearing granitoid plutons. *Geological Journal* **25**, 413–417.

Stepanov A., A. Mavrogenes J., Meffre S. and Davidson P. (2014) The key role of mica during igneous concentration of tantalum. *Contributions to Mineralogy and Petrology* **167**, 1009.

Stepanov A. S. and Hermann J. (2013) Fractionation of Nb and Ta by biotite and phengite: Implications for the "missing Nb paradox." *Geology* **41**, 303–306.

Stilling A., Ćerný P. and Vanstone P. J. (2006) The Tanco pegmatite at Bernic Lake, Manitoba. XVI. Zonal and bulk composition and their petrogenetic. *The Canadian Mineralogist* **44**, 599–623.

Sun H., Gao Y., Xiao Y., Gu H. and Casey J. F. (2016) Lithium isotope fractionation during incongruent melting: Constraints from post-collisional leucogranite and residual enclaves from Bengbu Uplift, China. *Chemical Geology* **439**, 71–82.

Taylor R. J. M., Harley S. L., Hinton R. W., Elphick S., Clark C. and Kelly N. M. (2015) Experimental determination of REE partition coefficients between zircon, garnet and melt: a key to understanding high-T crustal processes. *Journal of Metamorphic Geology* **33**, 231–248.

Taylor S. R. and McLennan S. M. (1995) The geochemical evolution of the continental crust. *Reviews of Geophysics* **33**, 241–265.

Teng F.-Z., McDonough W. F., Rudnick R. L. and Walker R. J. (2006) Diffusion-driven extreme lithium isotopic fractionation in country rocks of the Tin Mountain pegmatite. *Earth and Planetary Science Letters* **243**, 701–710.

Thomas R., Förster H.-J., Rickers K. and Webster J. D. (2005) Formation of extremely F-rich hydrous melt fractions and hydrothermal fluids during differentiation of highly evolved tin-granite magmas: a melt/fluid-inclusion study. *Contributions to Mineralogy and Petrology* **148**, 582–601.

Thompson A. B. (1982) Dehydration melting of pelitic rocks and the generation of $H_2O$-undersaturated granitic liquids. *American Journal of Science* **282**, 1567–1595.

Timofeev A., Migdisov A. A. and Williams-Jones A. E. (2015) An experimental study of the solubility and speciation of niobium in fluoride-bearing aqueous solutions at elevated temperature. *Geochimica et Cosmochimica Acta* **158**, 103–111.

Timofeev A., Migdisov A. A. and Williams-Jones A. E. (2017) An experimental study of the solubility and speciation of tantalum in fluoride-bearing aqueous solutions at elevated temperature. *Geochimica et Cosmochimica Acta* **197**, 294–304.

Tischendorf G. and Förster H.-J. (1990) Acid magmatism and related metallogenesis in the Erzgebirge. *Geological Journal* **25**, 443–454.

Tischendorf G., Förster H.-J. and Gottesmann B. (2001) Minor- and trace-element composition of trioctahedral micas: a review. *Mineralogical Magazine* **65**, 249–276.

Tonarini S., Forte C., Petrini R. and Ferrara G. (2003) Melt/biotite $^{11}B/^{10}B$ isotopic fractionation and the boron local environment in the structure of volcanic glasses. *Geochimica et Cosmochimica Acta* **67**, 1863–1873.

Tonarini S., Pennisi M. and Leeman W. P. (1997) Precise boron isotopic analysis of complex silicate (rock) samples using alkali carbonate fusion and ion-exchange separation. *Chemical Geology* **142**, 129–137.

Trumbull R. B. and Slack J. F. (2018) Boron Isotopes in the Continental Crust: Granites, Pegmatites, Felsic Volcanic Rocks, and Related Ore Deposits. In *Boron Isotopes – The Fifth Element* (eds. H. R. Marschall and G. L. Foster). Advances in Isotope Geochemistry. Springer, Cham. pp. 249–272.

Tuttle O. F. and Bowen N. L. (1958) Origin of Granite in the Light of Experimental Studies in the System $NaAlSi_3O_8$–$KAlSi_3O_8$–$SiO_2$–$H_2O$. *Geological Society of America Memoir* **74**.

Valverde-Vaquero P. (1997) An integrated field, geochemical and U-Pb geochronological study of the southwest Hermitage Flexure (Newfoundland Appalachians, Canada) and the Sierra De Guadarrama (Iberian Massif, Central Spain) : a contribution to the understanding of the geological evolution of circum-Atlantic Peri-Gondwana. Thesis, Memorial University of Newfoundland.

Valverde-Vaquero P., Díez Balda M. A., Díez Montes A., Dörr W., Escuder Viruete J., González Clavijo E., Maluski H., Rodríguez Fernández L. R., Rubio F. and Villar P. (2007) The "hot orogen": two separate Variscan low-pressure metamorphic events in the Central Iberian Zone. In *Mechanics of Variscan Orogeny: A Modern View on Orogenic Research* (eds. M. Faure, J. M. Lardeaux, P. Ledru, A. Peschler, and K. Schulmann). Géologie de la France. Societé Géologique de France and Bureau de Recherches Géologiques et Minières. p. 168.

Van Lichtervelde M., Grégoire M., Linnen R. L., Béziat D. and Salvi S. (2008) Trace element geochemistry by laser ablation ICP-MS of micas associated with Ta mineralization in the Tanco pegmatite, Manitoba, Canada. *Contributions to Mineralogy and Petrology* **155**, 791–806.

Vielzeuf D., Clemens J. D., Pin C. and Moinet E. (1990) Granites, Granulites, and Crustal Differentiation. In *Granulites and Crustal Evolution* (eds. D. Vielzeuf and P. Vidal). NATO ASI Series. Springer Netherlands, Dordrecht. pp. 59–85.

Vielzeuf D. and Holloway J. R. (1988) Experimental determination of the fluid-absent melting relations in the pelitic system. *Contributions to Mineralogy and Petrology* **98**, 257–276.

Vielzeuf D. and Montel J. M. (1994) Partial melting of metagreywackes. Part I. Fluid-absent experiments and phase relationships. *Contributions to Mineralogy and Petrology* **117**, 375–393.

Vigneresse J. L., Barbey P. and Cuney M. (1996) Rheological Transitions During Partial Melting and Crystallization with Application to Felsic Magma Segregation and Transfer. *Journal of Petrology* **37**, 1579–1600.

Wang R. C., Xie L., Chen J., Yu A., Wang L., Lu J. and Zhu J. (2013) Tin-carrier minerals in metaluminous granites of the western Nanling Range (southern China): Constraints on processes of tin mineralization in oxidized granites. *Journal of Asian Earth Sciences* **74**, 361–372.

Watson E. B. and Harrison T. M. (1983) Zircon saturation revisited: temperature and composition effects in a variety of crustal magma types. *Earth and Planetary Science Letters* **64**, 295–304.

Watson E. B., Vicenzi E. P. and Rapp R. P. (1989) Inclusion/host relations involving accessory minerals in high-grade metamorphic and anatectic rocks. *Contributions to Mineralogy and Petrology* **101**, 220–231.

Webster J., Thomas R., Förster H.-J., Seltmann R. and Tappen C. (2004) Geochemical evolution of halogen-enriched granite magmas and mineralizing fluids of the Zinnwald tin-tungsten mining district, Erzgebirge, Germany. *Mineralium Deposita* **39**, 452–472.

White R. W., Powell R. and Holland T. J. B. (2007) Progress relating to calculation of partial melting equilibria for metapelites. *Journal of Metamorphic Geology* **25**, 511–527.

Whitehouse M. J. (2003) Rare earth elements in zircon: a review of applications and case studies from the Outer Hebridean Lewisian Complex, NW Scotland. *Geological Society of London, Special Publications* **220**, 49–64.

Wolf M., Romer R. L., Franz L. and López-Moro F. J. (2018) Tin in granitic melts: The role of melting temperature and protolith composition. *Lithos* **310–311**, 20–30.

Wood S. A. and Samson I. M. (2000) The Hydrothermal Geochemistry of Tungsten in Granitoid Environments: I. Relative Solubilities of Ferberite and Scheelite as a Function of T, P, pH, and mNaCl. *Economic Geology* **95**, 143–182.

Wunder B., Meixner A., Romer R. L., Feenstra A., Schettler G. and Heinrich W. (2007) Lithium isotope fractionation between Li-bearing staurolite, Li-mica and aqueous fluids: An experimental study. *Chemical Geology* **238**, 277–290.

Wunder B., Meixner A., Romer R. L. and Heinrich W. (2006) Temperature-dependent isotopic fractionation of lithium between clinopyroxene and high-pressure hydrous fluids. *Contributions to Mineralogy and Petrology* **151**, 112–120.

Wunder B., Meixner A., Romer R. L., Wirth R. and Heinrich W. (2005) The geochemical cycle of boron: Constraints from boron isotope partitioning experiments between mica and fluid. *Lithos* **84**, 206–216.

Wyllie P. J. (1977) Crustal anatexis: An experimental review. *Tectonophysics* **43**, 41–71.

Yang P. and Rivers T. (2000) Trace element partitioning between coexisting biotite and muscovite from metamorphic rocks, Western Labrador: structural, compositional and thermal controls. *Geochimica et Cosmochimica Acta* **64**, 1451–1472.

Zack T., Kronz A., Foley S. F. and Rivers T. (2002) Trace element abundances in rutiles from eclogites and associated garnet mica schists. *Chemical Geology* **184**, 97–122.

Zaraisky G. P., Korzhinskaya V. and Kotova N. (2010) Experimental studies of $Ta_2O_5$ and columbite–tantalite solubility in fluoride solutions from 300 to 550°C and 50 to 100 MPa. *Mineralogy and Petrology* **99**, 287–300.

Zartman R. E. and Doe B. R. (1981) Plumbotectonics—the model. *Tectonophysics* **75**, 135–162.

Zhao W. W. and Zhou M.-F. (2015) In-situ LA–ICP-MS trace elemental analyses of magnetite: The Mesozoic Tengtie skarn Fe deposit in the Nanling Range, South China. *Ore Geology Reviews* **65**, **Part 4**, 872–883.

Zuleger E. and Erzinger J. (1988) Determination of the REE and Y in silicate materials with ICP-AES. *Fresenius Zeitschrift für Analytische Chemie*. **332**, 140–143.

# Appendix A: BSE images of low- and high-temperature migmatite samples

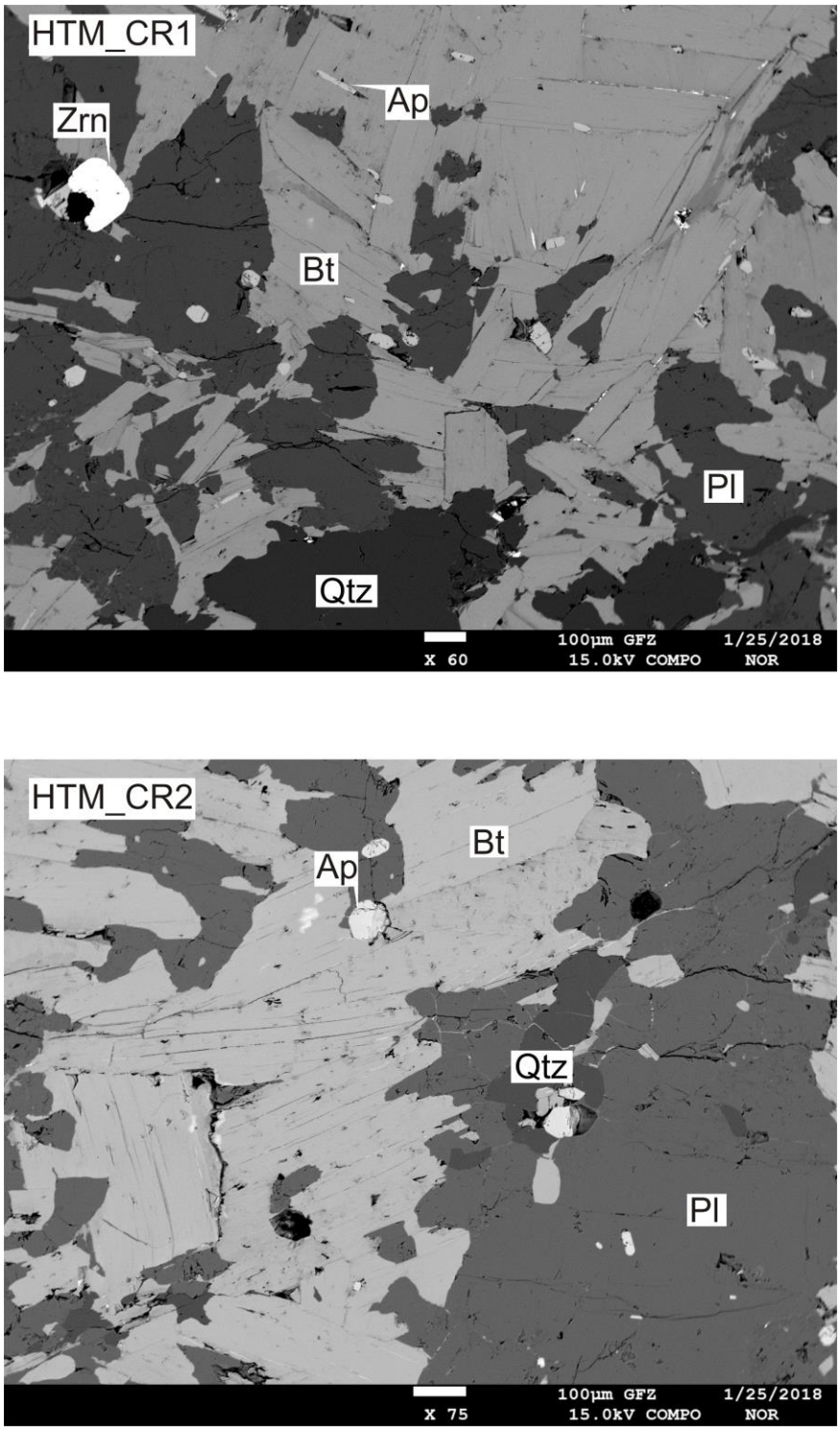


**Fig. A.1.** BSE images of the high-T coarse grained residuum. Bt = Biotite, Pl = Plagioclase, Qtz = Quartz, Ap = Apatite, Zrn = Zircon.

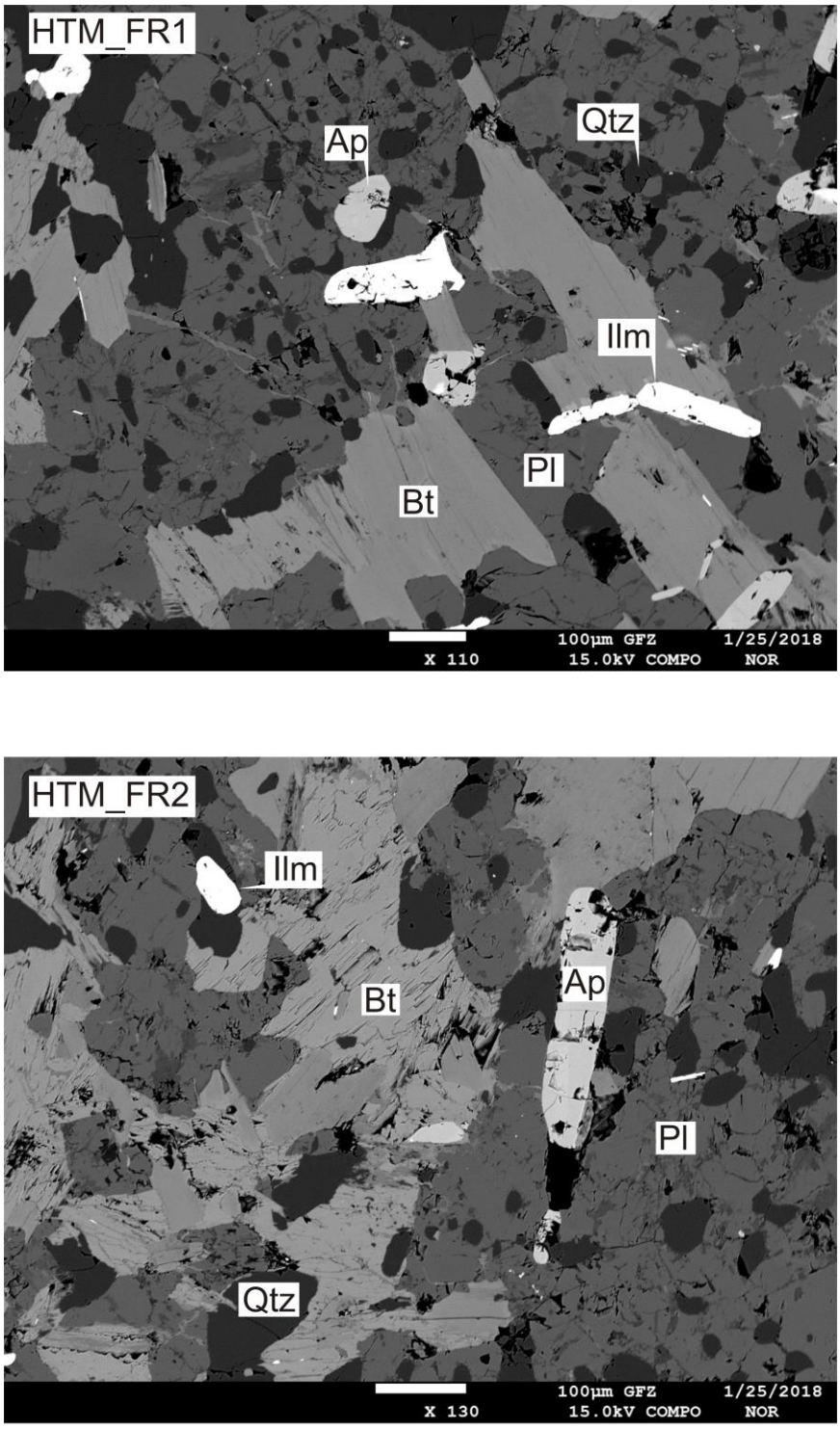


**Fig. A.2.** BSE images of the high-T fine grained residuum. Bt = Biotite, Pl = Plagioclase, Qtz = Quartz, Ap = Apatite, Ilm = Ilmenite.

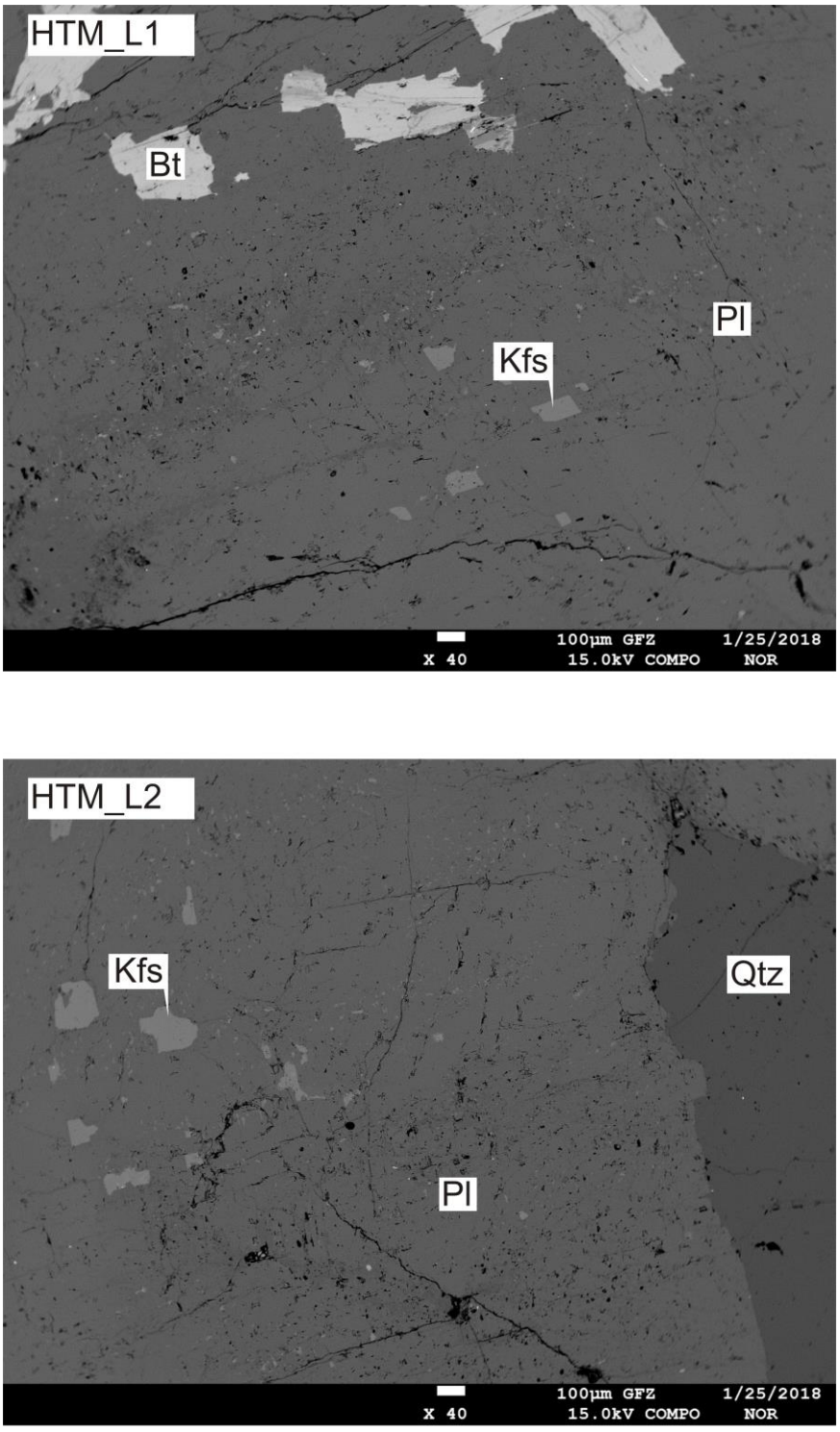


**Fig. A.3.** BSE images of the high-T leucosome. Bt = Biotite, Pl = Plagioclase, Qtz = Quartz, Kfs = K-feldspar.

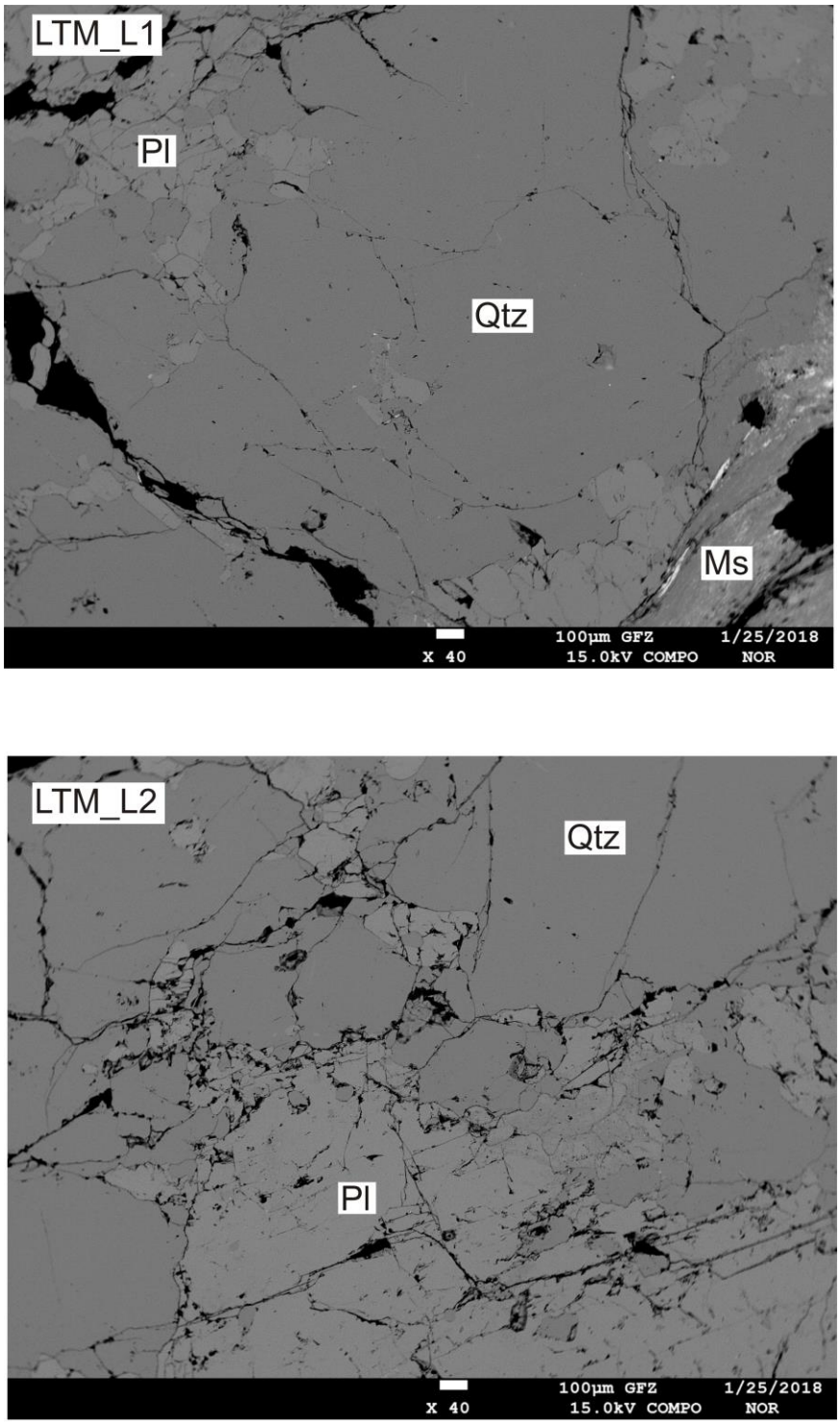


**Fig. A.4.** BSE imagse of the low-T leucosome. Pl = Plagioclase, Qtz = Quartz, Ms = Muscovite.

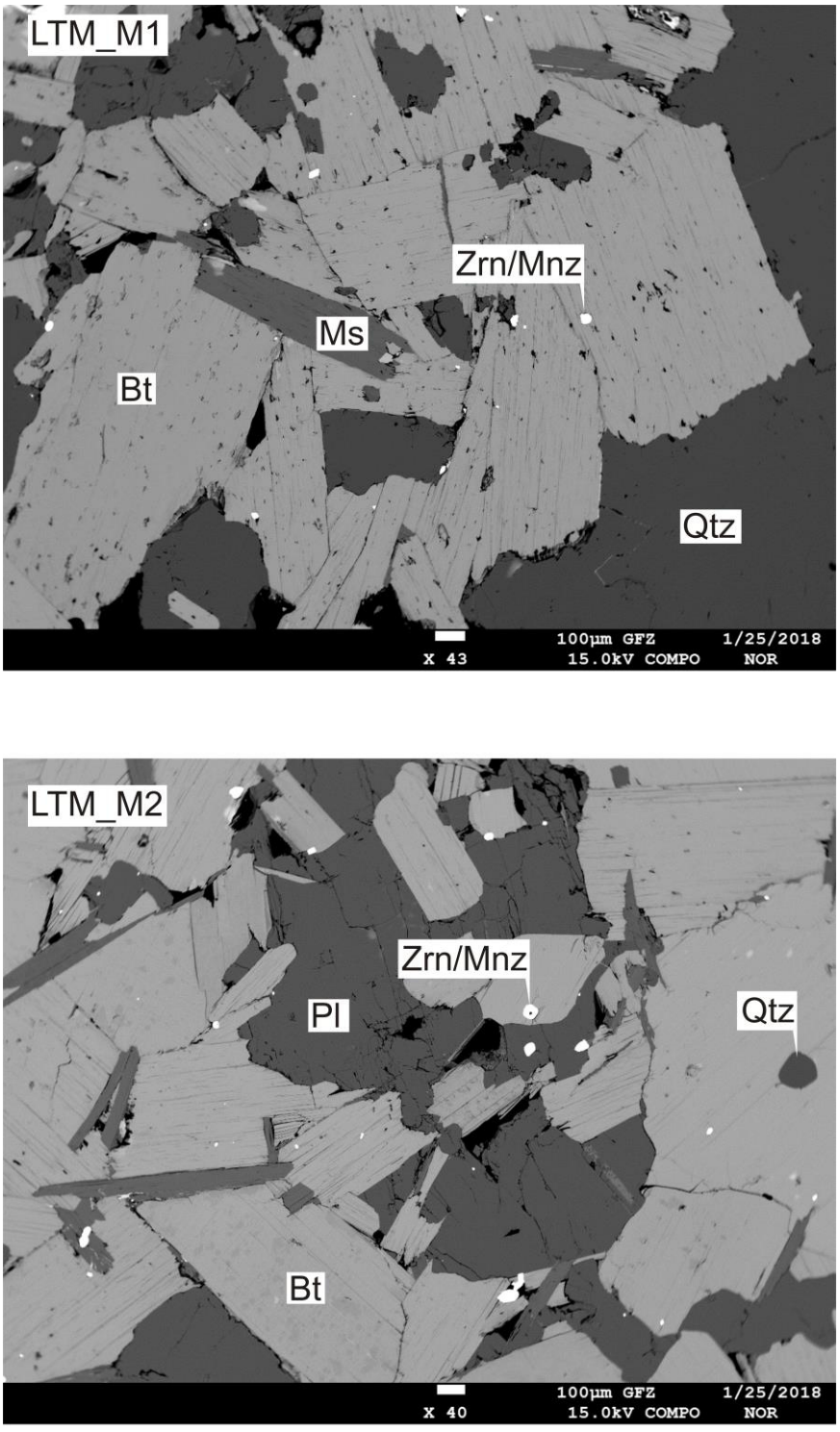


**Fig. A.5.** BSE images of the low-T melanosome. Bt = Biotite, Pl = Plagioclase, Qtz = Quartz, Ms = Muscovite, Zrn = Zircon, Mnz = Monazite.

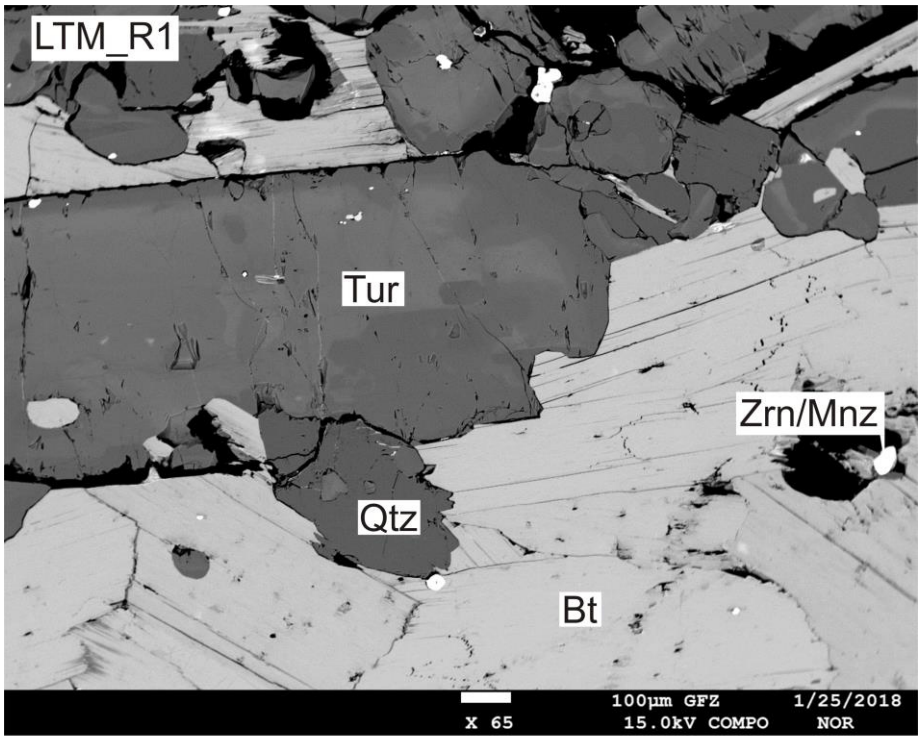


BSE image of the low-T residuum. Bt = Biotite, Tur = Tourmaline, Qtz = Quartz, Zrn = Zircon, Mnz = Monazite.

**Fig. A.6.** BSE image of the low-T residuum. Bt = Biotite , Tur = Tourmaline, Qtz = Quartz, Zrn = Zircon, Mnz = Monazite.

# Appendix B: Phase diagrams with complete labeling

## B.1. Sample APS $Fe^{2+}$

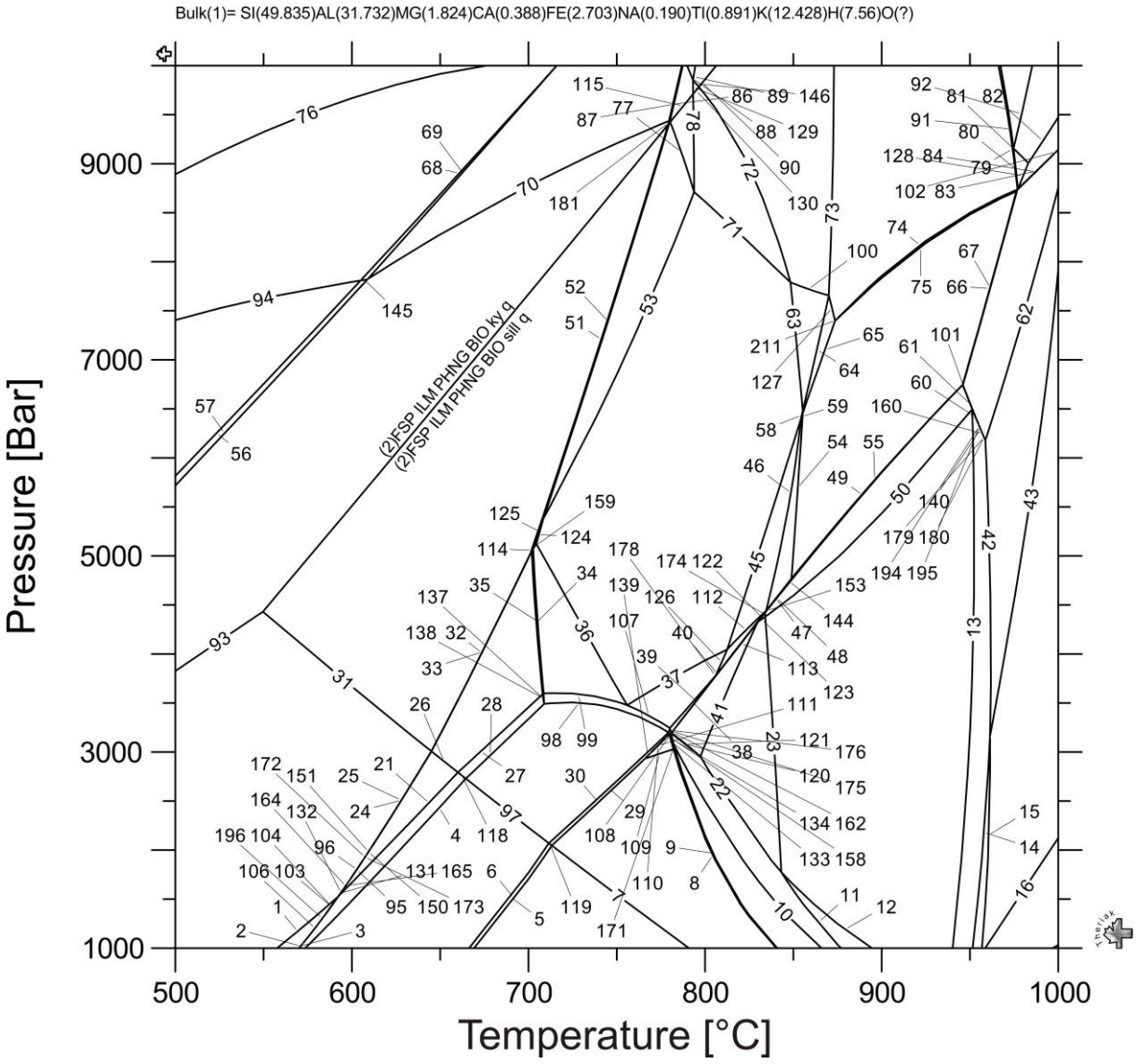


1): (2)FSP ILM PHNG BIO and q = (2)FSP ILM PHNG BIO CORD and q
2): (2)FSP ILM PHNG BIO CORD and q = (2)FSP ILM PHNG BIO CORD and q H2O
3): (2)FSP ILM PHNG BIO CORD and q H2O = (2)FSP ILM BIO CORD and q H2O
4): (2)FSP ILM BIO CORD and q H2O = (2)FSP ILM BIO CORD and H2O
5): (2)FSP ILM BIO CORD and H2O = (2)FSP ILM BIO CORD and cor H2O
6): (2)FSP ILM BIO CORD and cor H2O = (2)FSP ILM CORD and cor H2O
7): (2)FSP ILM CORD and cor H2O = (2)FSP ILM CORD sill cor H2O
8): (2)FSP ILM CORD sill cor H2O = (2)FSP ILM CORD LIQtc sill cor H2O
9): (2)FSP ILM CORD LIQtc sill cor H2O = (2)FSP ILM CORD LIQtc cor H2O
10): (2)FSP ILM CORD LIQtc cor H2O = (2)FSP ILM CORD SPIN LIQtc cor H2O
11): (2)FSP ILM CORD SPIN LIQtc cor H2O = FSP ILM CORD SPIN LIQtc cor H2O
12): FSP ILM CORD SPIN LIQtc cor H2O = FSP ILM CORD SPIN LIQtc cor
13): FSP ILM CORD SPIN LIQtc cor = FSP ILM CORD SPIN LIQtc ru cor
14): FSP ILM CORD SPIN LIQtc ru cor = FSP CORD SPIN LIQtc ru cor
15): FSP CORD SPIN LIQtc ru cor = FSP SPIN LIQtc ru cor
16): FSP SPIN LIQtc ru cor = FSP SPIN LIQtc ru
17): FSP SPIN LIQtc ru = FSP ILM SPIN LIQtc ru
18): (2)FSP ILM PHNG BIO and q = (2)FSP ILM BIO and q H2O
19): (2)FSP ILM PHNG BIO and q = (2)FSP ILM BIO and q H2O
20): (2)FSP ILM PHNG BIO and q = (2)FSP ILM BIO and q H2O
21): (2)FSP ILM BIO and q H2O = (2)FSP ILM BIO CORD and q H2O
22): (2)FSP ILM CORD SPIN LIQtc cor = (2)FSP ILM CORD SPIN LIQtc cor H2O
23): (2)FSP ILM CORD SPIN LIQtc cor = FSP ILM CORD SPIN LIQtc cor
24): (2)FSP ILM PHNG BIO and q = (2)FSP ILM PHNG BIO and q H2O
25): (2)FSP ILM PHNG BIO and q H2O = (2)FSP ILM BIO and q H2O
26): (2)FSP ILM BIO and q H2O = (2)FSP ILM BIO sill q H2O

27): (2)FSP ILM BIO sill q H2O = (2)FSP ILM BIO CORD sill q H2O
28): (2)FSP ILM BIO CORD sill q H2O = (2)FSP ILM BIO CORD sill H2O
29): (2)FSP ILM BIO CORD sill H2O = (2)FSP ILM BIO CORD sill cor H2O
30): (2)FSP ILM BIO CORD sill cor H2O = (2)FSP ILM CORD sill cor H2O
31): (2)FSP ILM PHNG BIO and q = (2)FSP ILM PHNG BIO sill q
32): (2)FSP ILM PHNG BIO sill q = (2)FSP ILM PHNG BIO sill q H2O
33): (2)FSP ILM PHNG BIO sill q H2O = (2)FSP ILM BIO sill q H2O
34): (2)FSP ILM BIO sill q H2O = (2)FSP ILM BIO LIQtc sill q H2O
35): (2)FSP ILM BIO LIQtc sill q H2O = (2)FSP ILM BIO LIQtc sill H2O
36): (2)FSP ILM BIO LIQtc sill H2O = (2)FSP ILM BIO LIQtc sill
37): (2)FSP ILM BIO LIQtc sill = (2)FSP ILM BIO CORD LIQtc sill
38): (2)FSP ILM BIO CORD LIQtc sill = (2)FSP ILM BIO CORD LIQtc sill cor
39): (2)FSP ILM BIO CORD LIQtc sill cor = (2)FSP ILM BIO CORD SPIN LIQtc sill cor
40): (2)FSP ILM BIO CORD SPIN LIQtc sill cor = (2)FSP ILM BIO CORD SPIN LIQtc cor
41): (2)FSP ILM BIO CORD SPIN LIQtc cor = (2)FSP ILM CORD SPIN LIQtc cor
42): FSP ILM CORD SPIN LIQtc ru cor = FSP ILM SPIN LIQtc ru cor
43): FSP ILM SPIN LIQtc ru cor = FSP SPIN LIQtc ru cor
44): (2)FSP ILM PHNG BIO ky q = (2)FSP ILM PHNG BIO sill q
45): (2)FSP ILM BIO LIQtc sill = (2)FSP ILM BIO SPIN LIQtc sill
46): (2)FSP ILM BIO SPIN LIQtc sill = (2)FSP ILM BIO SPIN LIQtc sill cor
47): (2)FSP ILM BIO SPIN LIQtc sill cor = (2)FSP ILM BIO CORD SPIN LIQtc sill cor
48): (2)FSP ILM BIO CORD SPIN LIQtc sill cor = FSP ILM BIO CORD SPIN LIQtc sill cor
49): FSP ILM BIO CORD SPIN LIQtc sill cor = FSP ILM CORD SPIN LIQtc sill cor
50): FSP ILM CORD SPIN LIQtc sill cor = FSP ILM CORD SPIN LIQtc cor
51): (2)FSP ILM PHNG BIO sill q = (2)FSP ILM PHNG BIO LIQtc sill q
52): (2)FSP ILM PHNG BIO LIQtc sill q = (2)FSP ILM BIO LIQtc sill q
53): (2)FSP ILM BIO LIQtc sill q = (2)FSP ILM BIO LIQtc sill
54): (2)FSP ILM BIO SPIN LIQtc sill cor = FSP ILM BIO SPIN LIQtc sill cor
55): FSP ILM BIO SPIN LIQtc sill cor = FSP ILM BIO CORD SPIN LIQtc sill cor
56): FSP ILM PHNG BIO ky zo q = (2)FSP ILM PHNG BIO ky zo q
57): (2)FSP ILM PHNG BIO ky zo q = (2)FSP ILM PHNG BIO ky q
58): (2)FSP ILM BIO LIQtc sill = (2)FSP ILM BIO LIQtc sill cor
59): (2)FSP ILM BIO LIQtc sill cor = (2)FSP ILM BIO SPIN LIQtc sill cor
60): FSP ILM CORD SPIN LIQtc sill ru cor = FSP ILM CORD SPIN LIQtc ru cor
61): FSP ILM SPIN LIQtc sill ru cor = FSP ILM CORD SPIN LIQtc sill ru cor
62): FSP ILM SPIN LIQtc sill ru cor = FSP ILM SPIN LIQtc ru cor
63): (2)FSP ILM BIO LIQtc sill = FSP ILM BIO LIQtc sill
64): FSP ILM BIO LIQtc sill = FSP ILM BIO LIQtc sill cor
65): FSP ILM BIO LIQtc sill cor = FSP ILM BIO SPIN LIQtc sill cor
66): FSP ILM BIO SPIN LIQtc sill cor = FSP ILM BIO SPIN LIQtc sill ru cor
67): FSP ILM BIO SPIN LIQtc sill ru cor = FSP ILM SPIN LIQtc sill ru cor
68): FSP ILM GARNET PHNG BIO ky zo q = (2)FSP ILM GARNET PHNG BIO ky zo q
69): (2)FSP ILM GARNET PHNG BIO ky zo q = (2)FSP ILM GARNET PHNG BIO ky q
70): (2)FSP ILM GARNET PHNG BIO ky q = (2)FSP ILM PHNG BIO ky q
71): (2)FSP ILM GARNET BIO LIQtc sill = (2)FSP ILM BIO LIQtc sill
72): (2)FSP ILM GARNET BIO LIQtc sill = FSP ILM GARNET BIO LIQtc sill
73): FSP ILM GARNET BIO LIQtc sill = FSP ILM GARNET BIO LIQtc sill cor
74): FSP ILM GARNET BIO LIQtc sill cor = FSP ILM GARNET BIO SPIN LIQtc sill cor
75): FSP ILM GARNET BIO SPIN LIQtc sill cor = FSP ILM BIO SPIN LIQtc sill cor
76): FSP ILM GARNET PHNG BIO ky q = FSP ILM GARNET PHNG BIO ky zo q
77): (2)FSP ILM GARNET BIO LIQtc sill q = (2)FSP ILM BIO LIQtc sill q
78): (2)FSP ILM GARNET BIO LIQtc sill q = (2)FSP ILM GARNET BIO LIQtc sill
79): FSP ILM GARNET BIO LIQtc sill cor = FSP ILM GARNET BIO LIQtc sill ru cor
80): FSP ILM GARNET BIO LIQtc sill ru cor = FSP ILM GARNET BIO LIQtc ru cor
81): FSP ILM GARNET LIQtc ru cor = FSP ILM GARNET BIO LIQtc ru cor
82): FSP ILM GARNET LIQtc ru cor = FSP ILM GARNET SPIN LIQtc ru cor
83): FSP ILM GARNET SPIN LIQtc ru cor = FSP ILM GARNET SPIN LIQtc sill ru cor
84): FSP ILM GARNET SPIN LIQtc sill ru cor = FSP ILM SPIN LIQtc sill ru cor
85): FSP ILM GARNET PHNG BIO ky zo q = (2)FSP ILM GARNET PHNG BIO ky q
86): (2)FSP ILM GARNET PHNG BIO ky q = (2)FSP ILM GARNET PHNG BIO LIQtc ky q
87): (2)FSP ILM GARNET PHNG BIO LIQtc ky q = (2)FSP ILM GARNET BIO LIQtc ky q
88): (2)FSP ILM GARNET BIO LIQtc ky q = FSP ILM GARNET BIO LIQtc ky q
89): FSP ILM GARNET BIO LIQtc ky q = FSP ILM GARNET BIO LIQtc ky
90): FSP ILM GARNET BIO LIQtc ky = FSP ILM GARNET BIO LIQtc sill
91): FSP ILM GARNET BIO LIQtc sill ru cor = FSP ILM GARNET LIQtc sill ru cor
92): FSP ILM GARNET LIQtc sill ru cor = FSP ILM GARNET LIQtc ru cor
93): (2)FSP ILM PHNG BIO ky q = (2)FSP ILM PHNG BIO and q
94): FSP ILM GARNET PHNG BIO ky zo q = FSP ILM PHNG BIO ky zo q
95): (2)FSP ILM PHNG BIO and q H2O = (2)FSP ILM BIO and q H2O
96): (2)FSP ILM PHNG BIO and q = (2)FSP ILM PHNG BIO and q H2O
97): (2)FSP ILM BIO CORD sill H2O = (2)FSP ILM BIO CORD and H2O
98): (2)FSP ILM BIO CORD LIQtc sill H2O = (2)FSP ILM BIO CORD sill H2O
99): (2)FSP ILM BIO LIQtc sill H2O = (2)FSP ILM BIO CORD LIQtc sill H2O
100): FSP ILM GARNET BIO LIQtc sill = FSP ILM BIO LIQtc sill
101): FSP ILM CORD SPIN LIQtc sill cor = FSP ILM CORD SPIN LIQtc sill ru cor

102): FSP ILM SPIN LIQtc sill ru cor = FSP ILM GARNET SPIN LIQtc ru cor
103): (2)FSP ILM PHNG BIO CORD and q = (2)FSP ILM PHNG BIO CORD and q H2O
104): (2)FSP ILM PHNG BIO CORD and q H2O = (2)FSP ILM BIO CORD and q H2O
105): (2)FSP ILM PHNG BIO CORD and q H2O = (2)FSP ILM BIO CORD and q H2O
106): (2)FSP ILM BIO CORD and q H2O = (2)FSP ILM PHNG BIO CORD and q
107): (2)FSP ILM BIO CORD LIQtc sill = (2)FSP ILM BIO CORD LIQtc sill H2O
108): (2)FSP ILM BIO CORD LIQtc sill cor = (2)FSP ILM BIO CORD SPIN LIQtc cor
109): (2)FSP ILM CORD SPIN sill cor H2O = (2)FSP ILM CORD sill cor H2O
110): (2)FSP ILM BIO CORD SPIN sill cor H2O = (2)FSP ILM CORD SPIN sill cor H2O
111): (2)FSP ILM BIO CORD SPIN sill cor H2O = (2)FSP ILM BIO CORD sill cor H2O
112): (2)FSP ILM BIO SPIN LIQtc sill = (2)FSP ILM BIO CORD SPIN LIQtc sill
113): (2)FSP ILM BIO CORD SPIN LIQtc sill = (2)FSP ILM BIO CORD SPIN LIQtc sill cor
114): (2)FSP ILM PHNG BIO LIQtc sill q = (2)FSP ILM BIO LIQtc sill q H2O
115): (2)FSP ILM GARNET BIO LIQtc ky q = (2)FSP ILM GARNET BIO LIQtc sill q
116): (2)FSP ILM PHNG BIO and q = (2)FSP ILM BIO and q H2O
117): (2)FSP ILM PHNG BIO and q = (2)FSP ILM BIO and q H2O
118): (2)FSP ILM BIO CORD sill q H2O = (2)FSP ILM BIO CORD and q H2O
119): (2)FSP ILM BIO CORD and cor H2O = (2)FSP ILM BIO CORD sill cor H2O
120): (2)FSP ILM BIO CORD SPIN LIQtc cor H2O = (2)FSP ILM CORD SPIN LIQtc cor H2O
121): (2)FSP ILM BIO CORD SPIN LIQtc cor = (2)FSP ILM BIO CORD SPIN LIQtc cor H2O
122): (2)FSP ILM BIO CORD SPIN LIQtc sill cor = (2)FSP ILM CORD SPIN LIQtc sill cor
123): (2)FSP ILM CORD SPIN LIQtc sill cor = (2)FSP ILM CORD SPIN LIQtc cor
124): (2)FSP ILM PHNG BIO LIQtc sill q = (2)FSP ILM PHNG BIO LIQtc sill
125): (2)FSP ILM PHNG BIO LIQtc sill = (2)FSP ILM BIO LIQtc sill
126): (2)FSP ILM BIO CORD LIQtc sill = (2)FSP ILM BIO CORD SPIN LIQtc sill
127): FSP ILM BIO LIQtc sill cor = FSP ILM GARNET BIO LIQtc sill cor
128): FSP ILM GARNET BIO LIQtc ru cor = FSP ILM GARNET SPIN LIQtc ru cor
129): (2)FSP ILM GARNET BIO LIQtc ky q = (2)FSP ILM GARNET BIO LIQtc ky
130): (2)FSP ILM GARNET BIO LIQtc ky = (2)FSP ILM GARNET BIO LIQtc sill
131): (2)FSP ILM PHNG BIO and q = (2)FSP ILM PHNG BIO and q H2O
132): (2)FSP ILM PHNG BIO and q H2O = (2)FSP ILM BIO and q H2O
133): (2)FSP ILM CORD SPIN LIQtc sill cor H2O = (2)FSP ILM CORD SPIN sill cor H2O
134): (2)FSP ILM CORD SPIN LIQtc sill cor H2O = (2)FSP ILM CORD SPIN LIQtc cor H2O
135): (2)FSP ILM BIO CORD LIQtc cor = (2)FSP ILM BIO CORD SPIN LIQtc cor H2O
136): (2)FSP ILM BIO CORD LIQtc sill cor = (2)FSP ILM BIO CORD LIQtc cor
137): (2)FSP ILM BIO CORD sill q H2O = (2)FSP ILM BIO CORD LIQtc sill q H2O
138): (2)FSP ILM BIO CORD LIQtc sill q H2O = (2)FSP ILM BIO CORD LIQtc sill H2O
139): (2)FSP ILM CORD SPIN sill cor H2O = (2)FSP ILM BIO CORD sill cor H2O
140): FSP ILM CORD SPIN LIQtc ru cor = FSP ILM SPIN LIQtc sill ru cor
141): FSP ILM CORD SPIN LIQtc ru cor = FSP ILM SPIN LIQtc sill ru cor
142): FSP ILM CORD SPIN LIQtc sill ru cor = FSP ILM CORD SPIN LIQtc ru cor
143): FSP ILM SPIN LIQtc sill ru cor = FSP ILM CORD SPIN LIQtc sill ru cor
144): (2)FSP ILM BIO SPIN LIQtc sill cor = FSP ILM BIO CORD SPIN LIQtc sill cor
145): (2)FSP ILM GARNET PHNG BIO ky zo q = (2)FSP ILM PHNG BIO ky zo q
146): (2)FSP ILM GARNET BIO LIQtc ky = FSP ILM GARNET BIO LIQtc ky
147): (2)FSP ILM BIO CORD and q H2O = (2)FSP ILM PHNG BIO CORD and q
148): (2)FSP ILM PHNG BIO CORD and q H2O = (2)FSP ILM BIO CORD and q H2O
149): (2)FSP ILM PHNG BIO CORD and q = (2)FSP ILM PHNG BIO CORD and q H2O
150): (2)FSP ILM PHNG BIO and q H2O = (2)FSP ILM BIO and q H2O
151): (2)FSP ILM PHNG BIO and q = (2)FSP ILM PHNG BIO and q H2O
152): (2)FSP ILM BIO CORD SPIN LIQtc cor = (2)FSP ILM CORD SPIN LIQtc cor H2O
153): (2)FSP ILM BIO CORD SPIN LIQtc sill cor = FSP ILM CORD SPIN LIQtc sill cor
154): (2)FSP ILM BIO SPIN LIQtc sill = (2)FSP ILM BIO CORD SPIN LIQtc sill cor
155): (2)FSP ILM BIO CORD sill cor H2O = (2)FSP ILM BIO CORD LIQtc sill cor H2O
156): (2)FSP ILM BIO CORD LIQtc sill cor H2O = (2)FSP ILM BIO CORD LIQtc cor H2O
157): (2)FSP ILM BIO CORD LIQtc cor H2O = (2)FSP ILM BIO CORD LIQtc cor
158): (2)FSP ILM CORD SPIN sill cor H2O = (2)FSP ILM BIO CORD sill cor H2O
159): (2)FSP ILM PHNG BIO LIQtc sill = (2)FSP ILM BIO LIQtc sill H2O
160): FSP ILM CORD SPIN LIQtc ru cor = FSP ILM SPIN LIQtc sill ru cor
161): (2)FSP ILM BIO LIQtc sill cor = FSP ILM BIO SPIN LIQtc sill cor
162): (2)FSP ILM BIO CORD LIQtc cor = (2)FSP ILM BIO CORD SPIN LIQtc cor
163): (2)FSP ILM PHNG BIO and q = (2)FSP ILM BIO and q H2O
164): (2)FSP ILM PHNG BIO and q H2O = (2)FSP ILM BIO and q H2O
165): (2)FSP ILM PHNG BIO and q = (2)FSP ILM PHNG BIO and q H2O
166): (2)FSP ILM BIO CORD and q H2O = (2)FSP ILM PHNG BIO CORD and q
167): (2)FSP ILM PHNG BIO CORD and q H2O = (2)FSP ILM BIO CORD and q H2O
168): (2)FSP ILM PHNG BIO CORD and q = (2)FSP ILM PHNG BIO CORD and q H2O
169): (2)FSP ILM PHNG BIO and q H2O = (2)FSP ILM BIO CORD and q H2O
170): (2)FSP ILM PHNG BIO and q = (2)FSP ILM PHNG BIO CORD and q H2O
171): (2)FSP ILM CORD SPIN LIQtc sill cor H2O = (2)FSP ILM CORD LIQtc sill cor H2O
172): (2)FSP ILM PHNG BIO and q = (2)FSP ILM PHNG BIO and q H2O
173): (2)FSP ILM PHNG BIO and q H2O = (2)FSP ILM BIO and q H2O
174): (2)FSP ILM CORD SPIN LIQtc sill cor = FSP ILM CORD SPIN LIQtc sill cor
175): (2)FSP ILM BIO CORD LIQtc sill H2O = (2)FSP ILM BIO CORD LIQtc sill cor H2O
176): (2)FSP ILM BIO CORD LIQtc sill cor H2O = (2)FSP ILM BIO CORD LIQtc sill cor

177): (2)FSP ILM PHNG BIO sill q H2O = (2)FSP ILM PHNG BIO LIQtc sill q
178): (2)FSP ILM BIO CORD LIQtc sill = (2)FSP ILM BIO CORD SPIN LIQtc sill cor
179): FSP ILM CORD SPIN LIQtc ru cor = FSP ILM CORD SPIN LIQtc sill ru cor
180): FSP ILM CORD SPIN LIQtc sill ru cor = FSP ILM SPIN LIQtc sill ru cor
181): (2)FSP ILM PHNG BIO ky q = (2)FSP ILM PHNG BIO LIQtc ky q
182): (2)FSP ILM PHNG BIO LIQtc ky q = (2)FSP ILM PHNG BIO LIQtc sill q
183): (2)FSP ILM GARNET PHNG BIO LIQtc ky q = (2)FSP ILM PHNG BIO LIQtc ky q
184): (2)FSP ILM BIO LIQtc sill = FSP ILM BIO LIQtc sill cor
185): FSP ILM GARNET BIO SPIN LIQtc sill cor = FSP ILM GARNET SPIN LIQtc sill ru cor
186): FSP ILM BIO SPIN LIQtc sill ru cor = FSP ILM GARNET BIO SPIN LIQtc sill cor
187): (2)FSP ILM PHNG BIO and q = (2)FSP ILM BIO and q H2O
188): (2)FSP ILM PHNG BIO and q H2O = (2)FSP ILM BIO and q H2O
189): (2)FSP ILM PHNG BIO and q = (2)FSP ILM PHNG BIO and q H2O
190): (2)FSP ILM BIO CORD LIQtc sill cor H2O = (2)FSP ILM CORD SPIN sill cor H2O
191): (2)FSP ILM PHNG BIO and q = (2)FSP ILM BIO and q H2O
192): (2)FSP ILM PHNG BIO and q H2O = (2)FSP ILM BIO and q H2O
193): (2)FSP ILM PHNG BIO and q = (2)FSP ILM PHNG BIO and q H2O
194): FSP ILM CORD SPIN LIQtc sill ru cor = FSP ILM CORD SPIN LIQtc ru cor
195): FSP ILM CORD SPIN LIQtc sill ru cor = FSP ILM SPIN LIQtc sill ru cor
196): (2)FSP ILM BIO CORD and q H2O = (2)FSP ILM PHNG BIO CORD and q
197): (2)FSP ILM PHNG BIO CORD and q H2O = (2)FSP ILM BIO CORD and q H2O
198): (2)FSP ILM PHNG BIO CORD and q = (2)FSP ILM PHNG BIO CORD and q H2O
199): (2)FSP ILM BIO CORD and q H2O = (2)FSP ILM PHNG BIO CORD and q
200): FSP ILM CORD SPIN LIQtc ru cor = FSP SPIN LIQtc ru cor
201): (2)FSP ILM BIO LIQtc sill q H2O = (2)FSP ILM BIO CORD LIQtc sill q H2O
202): FSP ILM SPIN LIQtc sill ru cor = FSP ILM CORD SPIN LIQtc ru cor
203): (2)FSP ILM BIO SPIN LIQtc sill cor = FSP ILM BIO CORD SPIN LIQtc sill cor
204): (2)FSP ILM BIO CORD SPIN LIQtc sill cor = FSP ILM BIO CORD SPIN LIQtc sill cor
205): (2)FSP ILM BIO SPIN LIQtc sill cor = (2)FSP ILM BIO CORD SPIN LIQtc sill cor
206): (2)FSP ILM PHNG BIO LIQtc sill q = (2)FSP ILM BIO LIQtc sill
207): (2)FSP ILM PHNG BIO LIQtc ky q = (2)FSP ILM BIO LIQtc ky q
208): (2)FSP ILM BIO LIQtc ky q = (2)FSP ILM GARNET BIO LIQtc sill q
209): (2)FSP ILM BIO LIQtc sill cor = FSP ILM BIO LIQtc sill cor
210): (2)FSP ILM BIO LIQtc sill = FSP ILM GARNET BIO LIQtc sill
211): FSP ILM GARNET BIO LIQtc sill cor = FSP ILM BIO SPIN LIQtc sill cor
212): FSP ILM GARNET BIO LIQtc ru cor = FSP ILM GARNET BIO SPIN LIQtc ru cor
213): FSP ILM GARNET BIO SPIN LIQtc ru cor = FSP ILM GARNET SPIN LIQtc ru cor
214): (2)FSP ILM PHNG BIO and q = (2)FSP ILM PHNG BIO and q H2O
215): (2)FSP ILM PHNG BIO and q H2O = (2)FSP ILM BIO and q H2O
216): (2)FSP ILM BIO CORD LIQtc sill cor H2O = (2)FSP ILM CORD SPIN LIQtc sill cor H2O
217): (2)FSP ILM BIO CORD and q H2O = (2)FSP ILM PHNG BIO CORD and q
218): (2)FSP ILM PHNG BIO CORD and q H2O = (2)FSP ILM BIO CORD and q H2O
219): (2)FSP ILM PHNG BIO CORD and q = (2)FSP ILM PHNG BIO CORD and q H2O
220): (2)FSP ILM BIO CORD and q H2O = (2)FSP ILM PHNG BIO CORD and q
221): (2)FSP ILM PHNG BIO CORD and q H2O = (2)FSP ILM BIO CORD and q H2O
222): (2)FSP ILM PHNG BIO CORD and q = (2)FSP ILM PHNG BIO CORD and q H2O

## B.2. Sample APS OHM (hematite-magnetite buffer)

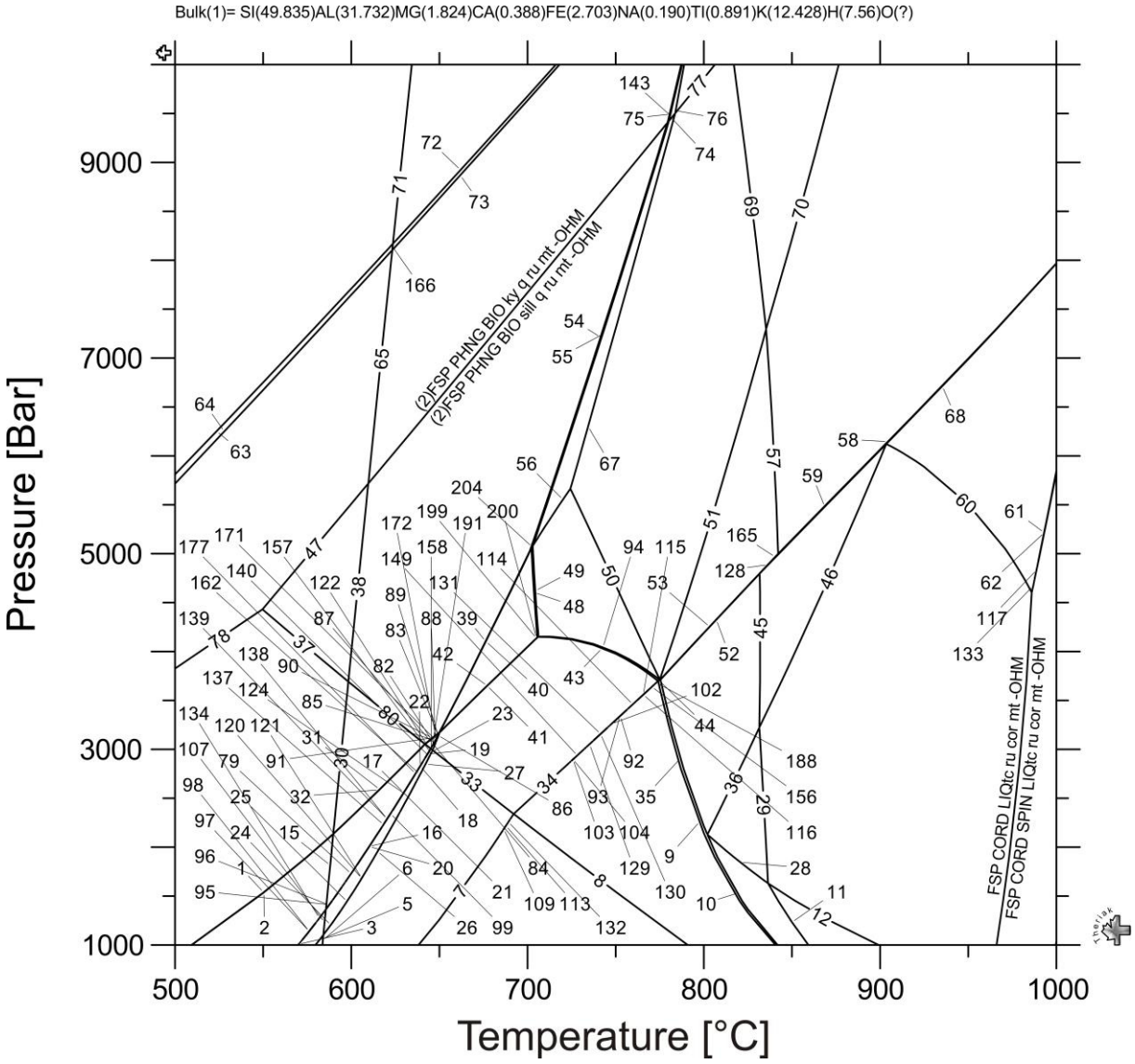


1): (2)FSP ILM PHNG BIO and q mt -OHM = (2)FSP ILM PHNG BIO CORD and q mt -OHM
2): (2)FSP ILM PHNG BIO CORD and q mt -OHM = (2)FSP ILM PHNG CORD and q mt -OHM
3): (2)FSP ILM PHNG CORD and q mt -OHM = (2)FSP ILM PHNG CORD and mt H2O -OHM
4): (2)FSP ILM PHNG CORD and q mt -OHM = (2)FSP ILM PHNG CORD and mt H2O -OHM
5): (2)FSP ILM PHNG CORD and mt H2O -OHM = (2)FSP ILM BIO CORD and mt H2O -OHM
6): (2)FSP ILM BIO CORD and mt H2O -OHM = (2)FSP BIO CORD and ru mt H2O -OHM
7): (2)FSP BIO CORD and ru mt H2O -OHM = (2)FSP CORD and ru cor mt H2O -OHM
8): (2)FSP CORD and ru cor mt H2O -OHM = (2)FSP CORD sill ru cor mt H2O -OHM
9): (2)FSP CORD sill ru cor mt H2O -OHM = (2)FSP CORD LIQtc sill ru cor mt H2O -OHM
10): (2)FSP CORD LIQtc sill ru cor mt H2O -OHM = (2)FSP CORD LIQtc ru cor mt H2O -OHM
11): (2)FSP CORD LIQtc ru cor mt H2O -OHM = FSP CORD LIQtc ru cor mt H2O -OHM
12): FSP CORD LIQtc ru cor mt H2O -OHM = FSP CORD LIQtc ru cor mt -OHM
13): FSP CORD LIQtc ru cor mt -OHM = FSP CORD SPIN LIQtc ru cor mt -OHM
14): FSP CORD SPIN LIQtc ru cor mt -OHM = FSP SPIN LIQtc ru cor mt -OHM
15): (2)FSP ILM PHNG CORD and q mt -OHM = (2)FSP PHNG CORD and q ru mt -OHM
16): (2)FSP PHNG CORD and q ru mt -OHM = (2)FSP PHNG CORD and q ru mt H2O -OHM
17): (2)FSP PHNG CORD and q ru mt -OHM = (2)FSP PHNG CORD and q ru mt H2O -OHM
18): (2)FSP PHNG CORD and q ru mt -OHM = (2)FSP PHNG CORD and q ru mt H2O -OHM
19): (2)FSP PHNG CORD and q ru mt -OHM = (2)FSP PHNG CORD and q ru mt H2O -OHM
20): (2)FSP PHNG CORD and q ru mt H2O -OHM = (2)FSP PHNG CORD and ru mt H2O -OHM
21): (2)FSP PHNG CORD and q ru mt H2O -OHM = (2)FSP PHNG CORD and ru mt H2O -OHM
22): (2)FSP PHNG CORD and q ru mt H2O -OHM = (2)FSP PHNG CORD and ru mt H2O -OHM
23): (2)FSP PHNG CORD and q ru mt H2O -OHM = (2)FSP PHNG CORD and ru mt H2O -OHM
24): (2)FSP PHNG CORD and ru mt H2O -OHM = (2)FSP BIO CORD and ru mt H2O -OHM
25): (2)FSP PHNG CORD and ru mt H2O -OHM = (2)FSP BIO CORD and ru mt H2O -OHM
26): (2)FSP PHNG CORD and ru mt H2O -OHM = (2)FSP BIO CORD and ru mt H2O -OHM

27): (2)FSP PHNG CORD and ru mt H2O -OHM = (2)FSP BIO CORD and ru mt H2O -OHM
28): (2)FSP CORD LIQtc ru cor mt H2O -OHM = (2)FSP CORD LIQtc ru cor mt -OHM
29): (2)FSP CORD LIQtc ru cor mt -OHM = FSP CORD LIQtc ru cor mt -OHM
30): (2)FSP ILM PHNG BIO and q mt -OHM = (2)FSP PHNG BIO and q ru mt -OHM
31): (2)FSP PHNG BIO and q ru mt -OHM = (2)FSP PHNG BIO CORD and q ru mt -OHM
32): (2)FSP PHNG BIO CORD and q ru mt -OHM = (2)FSP PHNG CORD and q ru mt -OHM
33): (2)FSP BIO CORD sill ru mt H2O -OHM = (2)FSP BIO CORD and ru mt H2O -OHM
34): (2)FSP BIO CORD sill ru mt H2O -OHM = (2)FSP CORD sill ru cor mt H2O -OHM
35): (2)FSP CORD LIQtc sill ru cor mt H2O -OHM = (2)FSP CORD LIQtc sill ru cor mt -OHM
36): (2)FSP CORD LIQtc sill ru cor mt -OHM = (2)FSP CORD LIQtc ru cor mt -OHM
37): (2)FSP ILM PHNG BIO and q mt -OHM = (2)FSP ILM PHNG BIO sill q mt -OHM
38): (2)FSP ILM PHNG BIO sill q mt -OHM = (2)FSP PHNG BIO sill q ru mt -OHM
39): (2)FSP PHNG BIO sill q ru mt -OHM = (2)FSP PHNG BIO sill q ru mt H2O -OHM
40): (2)FSP PHNG BIO sill q ru mt H2O -OHM = (2)FSP BIO sill q ru mt H2O -OHM
41): (2)FSP BIO sill q ru mt H2O -OHM = (2)FSP BIO CORD sill q ru mt H2O -OHM
42): (2)FSP BIO CORD sill q ru mt H2O -OHM = (2)FSP BIO CORD sill ru mt H2O -OHM
43): (2)FSP BIO CORD sill ru mt H2O -OHM = (2)FSP BIO CORD LIQtc sill ru mt H2O -OHM
44): (2)FSP BIO CORD LIQtc sill ru mt H2O -OHM = (2)FSP CORD LIQtc sill ru cor mt H2O -OHM
45): (2)FSP CORD LIQtc sill ru cor mt -OHM = FSP CORD LIQtc sill ru cor mt -OHM
46): FSP CORD LIQtc sill ru cor mt -OHM = FSP CORD LIQtc ru cor mt -OHM
47): (2)FSP ILM PHNG BIO ky q mt -OHM = (2)FSP ILM PHNG BIO sill q mt -OHM
48): (2)FSP BIO sill q ru mt H2O -OHM = (2)FSP BIO LIQtc sill q ru mt H2O -OHM
49): (2)FSP BIO LIQtc sill q ru mt H2O -OHM = (2)FSP BIO LIQtc sill ru mt H2O -OHM
50): (2)FSP BIO LIQtc sill ru mt -OHM = (2)FSP BIO LIQtc sill ru mt H2O -OHM
51): (2)FSP BIO LIQtc sill ru mt -OHM = (2)FSP BIO LIQtc sill ru cor mt -OHM
52): (2)FSP BIO LIQtc sill ru cor mt -OHM = (2)FSP BIO CORD LIQtc sill ru cor mt -OHM
53): (2)FSP BIO CORD LIQtc sill ru cor mt -OHM = (2)FSP CORD LIQtc sill ru cor mt -OHM
54): (2)FSP PHNG BIO sill q ru mt -OHM = (2)FSP PHNG BIO LIQtc sill q ru mt -OHM
55): (2)FSP PHNG BIO LIQtc sill q ru mt -OHM = (2)FSP PHNG BIO LIQtc sill ru mt -OHM
56): (2)FSP PHNG BIO LIQtc sill ru mt -OHM = (2)FSP BIO LIQtc sill ru mt H2O -OHM
57): (2)FSP BIO LIQtc sill ru cor mt -OHM = FSP BIO LIQtc sill ru cor mt -OHM
58): FSP BIO LIQtc sill ru cor mt -OHM = FSP BIO CORD LIQtc sill ru cor mt -OHM
59): FSP BIO CORD LIQtc sill ru cor mt -OHM = FSP CORD LIQtc sill ru cor mt -OHM
60): FSP BIO CORD LIQtc ru cor mt -OHM = FSP CORD LIQtc ru cor mt -OHM
61): FSP BIO CORD LIQtc ru cor mt -OHM = FSP BIO CORD SPIN LIQtc ru cor mt -OHM
62): FSP BIO CORD SPIN LIQtc ru cor mt -OHM = FSP CORD SPIN LIQtc ru cor mt -OHM
63): FSP ILM PHNG BIO ky zo q mt -OHM = (2)FSP ILM PHNG BIO ky zo q mt -OHM
64): (2)FSP ILM PHNG BIO ky zo q mt -OHM = (2)FSP ILM PHNG BIO ky q mt -OHM
65): (2)FSP ILM PHNG BIO ky q mt -OHM = (2)FSP PHNG BIO ky q ru mt -OHM
66): (2)FSP PHNG BIO ky q ru mt -OHM = (2)FSP PHNG BIO sill q ru mt -OHM
67): (2)FSP PHNG BIO LIQtc sill ru mt -OHM = (2)FSP BIO LIQtc sill ru mt -OHM
68): FSP BIO CORD LIQtc sill ru cor mt -OHM = FSP BIO CORD LIQtc ru cor mt -OHM
69): (2)FSP BIO LIQtc sill ru mt -OHM = FSP BIO LIQtc sill ru mt -OHM
70): FSP BIO LIQtc sill ru mt -OHM = FSP BIO LIQtc sill ru cor mt -OHM
71): FSP ILM PHNG BIO ky zo q mt -OHM = FSP PHNG BIO ky zo q ru mt -OHM
72): FSP PHNG BIO ky zo q ru mt -OHM = (2)FSP PHNG BIO ky zo q ru mt -OHM
73): (2)FSP PHNG BIO ky zo q ru mt -OHM = (2)FSP PHNG BIO ky q ru mt -OHM
74): (2)FSP PHNG BIO ky q ru mt -OHM = (2)FSP PHNG BIO LIQtc ky q ru mt -OHM
75): (2)FSP PHNG BIO LIQtc ky q ru mt -OHM = (2)FSP PHNG BIO LIQtc ky ru mt -OHM
76): (2)FSP PHNG BIO LIQtc ky ru mt -OHM = (2)FSP BIO LIQtc ky ru mt -OHM
77): (2)FSP BIO LIQtc ky ru mt -OHM = (2)FSP BIO LIQtc sill ru mt -OHM
78): (2)FSP ILM PHNG BIO ky q mt -OHM = (2)FSP ILM PHNG BIO and q mt -OHM
79): (2)FSP PHNG CORD and q ru mt -OHM = (2)FSP PHNG CORD and ru mt H2O -OHM
80): (2)FSP PHNG BIO sill q ru mt -OHM = (2)FSP PHNG BIO and q ru mt -OHM
81): (2)FSP BIO CORD sill ru mt H2O -OHM = (2)FSP PHNG CORD sill ru mt H2O -OHM
82): (2)FSP PHNG CORD sill ru mt H2O -OHM = (2)FSP BIO CORD sill ru mt H2O -OHM
83): (2)FSP BIO CORD sill ru mt H2O -OHM = (2)FSP PHNG CORD sill ru mt H2O -OHM
84): (2)FSP PHNG CORD sill q ru mt H2O -OHM = (2)FSP PHNG CORD sill ru mt H2O -OHM
85): (2)FSP PHNG CORD sill ru mt H2O -OHM = (2)FSP PHNG CORD sill q ru mt H2O -OHM
86): (2)FSP PHNG CORD sill q ru mt H2O -OHM = (2)FSP PHNG CORD sill ru mt H2O -OHM
87): (2)FSP PHNG CORD sill q ru mt H2O -OHM = (2)FSP PHNG CORD sill q ru mt -OHM
88): (2)FSP PHNG CORD sill q ru mt H2O -OHM = (2)FSP PHNG CORD sill q ru mt -OHM
89): (2)FSP PHNG CORD sill q ru mt -OHM = (2)FSP PHNG CORD sill q ru mt H2O -OHM
90): (2)FSP PHNG BIO CORD sill q ru mt -OHM = (2)FSP PHNG CORD sill q ru mt -OHM
91): (2)FSP PHNG BIO sill q ru mt -OHM = (2)FSP PHNG BIO CORD sill q ru mt -OHM
92): (2)FSP CORD sill ru cor mt H2O -OHM = (2)FSP BIO CORD sill ru cor mt H2O -OHM
93): (2)FSP BIO CORD sill ru cor mt H2O -OHM = (2)FSP BIO CORD sill ru mt H2O -OHM
94): (2)FSP BIO LIQtc sill ru mt H2O -OHM = (2)FSP BIO CORD LIQtc sill ru mt H2O -OHM
95): (2)FSP PHNG CORD and q ru mt -OHM = (2)FSP PHNG CORD and q ru mt H2O -OHM
96): (2)FSP PHNG CORD and q ru mt H2O -OHM = (2)FSP PHNG CORD and ru mt H2O -OHM
97): (2)FSP ILM PHNG CORD and mt H2O -OHM = (2)FSP ILM PHNG CORD and q mt H2O -OHM
98): (2)FSP ILM PHNG CORD and q mt H2O -OHM = (2)FSP ILM PHNG CORD and q mt -OHM
99): (2)FSP PHNG CORD and ru mt H2O -OHM = (2)FSP PHNG CORD and q ru mt -OHM
100): (2)FSP PHNG CORD and ru mt H2O -OHM = (2)FSP PHNG BIO CORD and ru mt H2O -OHM
101): (2)FSP PHNG BIO CORD and ru mt H2O -OHM = (2)FSP BIO CORD and ru mt H2O -OHM

102): (2)FSP BIO CORD sill ru mt H2O -OHM = (2)FSP CORD sill ru cor mt H2O -OHM
103): (2)FSP BIO CORD sill ru cor mt H2O -OHM = (2)FSP CORD sill ru cor mt H2O -OHM
104): (2)FSP BIO CORD sill ru cor mt H2O -OHM = (2)FSP BIO CORD sill ru mt H2O -OHM
105): (2)FSP PHNG BIO LIQtc sill q ru mt -OHM = (2)FSP BIO sill q ru mt H2O -OHM
106): (2)FSP BIO LIQtc sill q ru mt H2O -OHM = (2)FSP BIO CORD LIQtc sill ru mt H2O -OHM
107): (2)FSP ILM PHNG CORD and mt H2O -OHM = (2)FSP PHNG CORD and ru mt H2O -OHM
108): (2)FSP BIO CORD and ru mt H2O -OHM = (2)FSP BIO CORD and ru cor mt H2O -OHM
109): (2)FSP BIO CORD and ru mt H2O -OHM = (2)FSP BIO CORD and ru cor mt H2O -OHM
110): (2)FSP BIO CORD and ru mt H2O -OHM = (2)FSP BIO CORD and ru cor mt H2O -OHM
111): (2)FSP BIO CORD and ru cor mt H2O -OHM = (2)FSP CORD and ru cor mt H2O -OHM
112): (2)FSP BIO CORD and ru cor mt H2O -OHM = (2)FSP CORD and ru cor mt H2O -OHM
113): (2)FSP BIO CORD and ru cor mt H2O -OHM = (2)FSP CORD and ru cor mt H2O -OHM
114): (2)FSP BIO CORD sill ru mt H2O -OHM = (2)FSP CORD sill ru cor mt H2O -OHM
115): (2)FSP BIO CORD sill ru cor mt H2O -OHM = (2)FSP CORD sill ru cor mt H2O -OHM
116): (2)FSP BIO CORD sill ru mt H2O -OHM = (2)FSP BIO CORD sill ru cor mt H2O -OHM
117): FSP BIO CORD LIQtc ru cor mt -OHM = FSP CORD SPIN LIQtc ru cor mt -OHM
118): FSP BIO CORD SPIN LIQtc ru cor mt -OHM = FSP CORD SPIN LIQtc ru cor mt -OHM
119): FSP BIO CORD LIQtc ru cor mt -OHM = FSP BIO CORD SPIN LIQtc ru cor mt -OHM
120): (2)FSP PHNG CORD and ru mt H2O -OHM = (2)FSP PHNG BIO CORD and ru mt H2O -OHM
121): (2)FSP PHNG BIO CORD and ru mt H2O -OHM = (2)FSP BIO CORD and ru mt H2O -OHM
122): (2)FSP PHNG CORD and q ru mt -OHM = (2)FSP PHNG CORD sill q ru mt -OHM
123): (2)FSP PHNG CORD sill q ru mt -OHM = (2)FSP PHNG CORD sill ru mt H2O -OHM
124): (2)FSP PHNG CORD and ru mt H2O -OHM = (2)FSP BIO CORD and ru mt H2O -OHM
125): (2)FSP PHNG BIO CORD and ru mt H2O -OHM = (2)FSP BIO CORD and ru mt H2O -OHM
126): (2)FSP PHNG CORD and ru mt H2O -OHM = (2)FSP PHNG BIO CORD and ru mt H2O -OHM
127): (2)FSP BIO CORD LIQtc sill ru cor mt -OHM = FSP CORD LIQtc sill ru cor mt -OHM
128): FSP BIO CORD LIQtc sill ru cor mt -OHM = (2)FSP BIO CORD LIQtc sill ru cor mt -OHM
129): (2)FSP BIO CORD sill ru mt H2O -OHM = (2)FSP CORD sill ru cor mt H2O -OHM
130): (2)FSP BIO CORD sill ru cor mt H2O -OHM = (2)FSP CORD sill ru cor mt H2O -OHM
131): (2)FSP BIO CORD sill ru mt H2O -OHM = (2)FSP BIO CORD sill ru cor mt H2O -OHM
132): (2)FSP BIO CORD and ru mt H2O -OHM = (2)FSP CORD and ru cor mt H2O -OHM
133): FSP BIO CORD LIQtc ru cor mt -OHM = FSP CORD SPIN LIQtc ru cor mt -OHM
134): (2)FSP ILM PHNG CORD and q mt -OHM = (2)FSP ILM PHNG CORD and mt H2O -OHM
135): (2)FSP ILM PHNG CORD and q mt -OHM = (2)FSP ILM PHNG CORD and mt H2O -OHM
136): (2)FSP PHNG CORD and ru mt H2O -OHM = (2)FSP PHNG CORD and q ru mt -OHM
137): (2)FSP PHNG CORD and ru mt H2O -OHM = (2)FSP PHNG CORD and q ru mt -OHM
138): (2)FSP PHNG CORD and q ru mt H2O -OHM = (2)FSP PHNG CORD and ru mt H2O -OHM
139): (2)FSP PHNG CORD and q ru mt -OHM = (2)FSP PHNG CORD and q ru mt H2O -OHM
140): (2)FSP PHNG CORD and ru mt H2O -OHM = (2)FSP BIO CORD and ru mt H2O -OHM
141): (2)FSP PHNG BIO CORD and ru mt H2O -OHM = (2)FSP BIO CORD and ru mt H2O -OHM
142): (2)FSP PHNG CORD and ru mt H2O -OHM = (2)FSP PHNG BIO CORD and ru mt H2O -OHM
143): (2)FSP PHNG BIO LIQtc ky ru mt -OHM = (2)FSP PHNG BIO LIQtc sill ru mt -OHM
144): (2)FSP PHNG CORD and ru mt H2O -OHM = (2)FSP PHNG CORD and q ru mt -OHM
145): (2)FSP PHNG CORD and q ru mt H2O -OHM = (2)FSP PHNG CORD and ru mt H2O -OHM
146): (2)FSP PHNG CORD and q ru mt -OHM = (2)FSP PHNG CORD and q ru mt H2O -OHM
147): (2)FSP PHNG CORD and ru mt H2O -OHM = (2)FSP PHNG BIO CORD and ru mt H2O -OHM
148): (2)FSP PHNG BIO CORD and ru mt H2O -OHM = (2)FSP BIO CORD and ru mt H2O -OHM
149): (2)FSP BIO CORD sill ru mt H2O -OHM = (2)FSP CORD sill ru cor mt H2O -OHM
150): (2)FSP CORD sill ru cor mt H2O -OHM = (2)FSP BIO CORD sill ru cor mt H2O -OHM
151): (2)FSP BIO CORD sill ru cor mt H2O -OHM = (2)FSP CORD sill ru cor mt H2O -OHM
152): (2)FSP BIO CORD sill ru cor mt H2O -OHM = (2)FSP BIO CORD sill ru mt H2O -OHM
153): (2)FSP BIO CORD sill ru mt H2O -OHM = (2)FSP BIO CORD sill ru cor mt H2O -OHM
154): (2)FSP BIO CORD and ru mt H2O -OHM = (2)FSP BIO CORD and ru cor mt H2O -OHM
155): (2)FSP BIO CORD and ru cor mt H2O -OHM = (2)FSP CORD and ru cor mt H2O -OHM
156): (2)FSP BIO CORD sill ru mt H2O -OHM = (2)FSP CORD sill ru cor mt H2O -OHM
157): (2)FSP PHNG CORD and ru mt H2O -OHM = (2)FSP PHNG BIO CORD and ru mt H2O -OHM
158): (2)FSP PHNG BIO CORD and ru mt H2O -OHM = (2)FSP BIO CORD and ru mt H2O -OHM
159): (2)FSP PHNG CORD and ru mt H2O -OHM = (2)FSP BIO CORD and ru mt H2O -OHM
160): (2)FSP PHNG BIO CORD and ru mt H2O -OHM = (2)FSP BIO CORD and ru mt H2O -OHM
161): (2)FSP PHNG CORD and ru mt H2O -OHM = (2)FSP PHNG BIO CORD and ru mt H2O -OHM
162): (2)FSP PHNG CORD and ru mt H2O -OHM = (2)FSP BIO CORD and ru mt H2O -OHM
163): (2)FSP PHNG BIO CORD and ru mt H2O -OHM = (2)FSP BIO CORD and ru mt H2O -OHM
164): (2)FSP PHNG CORD and ru mt H2O -OHM = (2)FSP PHNG BIO CORD and ru mt H2O -OHM
165): (2)FSP BIO LIQtc sill ru cor mt -OHM = FSP BIO CORD LIQtc sill ru cor mt -OHM
166): (2)FSP ILM PHNG BIO ky zo q mt -OHM = (2)FSP PHNG BIO ky zo q ru mt -OHM
167): (2)FSP PHNG CORD and ru mt H2O -OHM = (2)FSP PHNG CORD and q ru mt -OHM
168): (2)FSP PHNG CORD and ru mt H2O -OHM = (2)FSP PHNG CORD and q ru mt -OHM
169): (2)FSP PHNG CORD and q ru mt H2O -OHM = (2)FSP PHNG CORD and ru mt H2O -OHM
170): (2)FSP PHNG CORD and q ru mt -OHM = (2)FSP PHNG CORD and q ru mt H2O -OHM
171): (2)FSP PHNG CORD sill ru mt H2O -OHM = (2)FSP PHNG BIO CORD sill ru mt H2O -OHM
172): (2)FSP PHNG BIO CORD sill ru mt H2O -OHM = (2)FSP BIO CORD sill ru mt H2O -OHM
173): (2)FSP PHNG CORD and q ru mt -OHM = (2)FSP PHNG CORD and q ru mt H2O -OHM
174): (2)FSP PHNG CORD and q ru mt H2O -OHM = (2)FSP PHNG CORD and ru mt H2O -OHM
175): (2)FSP PHNG CORD and ru mt H2O -OHM = (2)FSP PHNG CORD and q ru mt -OHM
176): (2)FSP BIO CORD and ru mt H2O -OHM = (2)FSP CORD and ru cor mt H2O -OHM

177): (2)FSP PHNG CORD and ru mt H2O -OHM = (2)FSP PHNG CORD and q ru mt -OHM
178): (2)FSP PHNG CORD and ru mt H2O -OHM = (2)FSP PHNG CORD and q ru mt -OHM
179): (2)FSP ILM PHNG CORD and q mt H2O -OHM = (2)FSP ILM PHNG CORD and mt H2O -OHM
180): (2)FSP ILM PHNG CORD and q mt -OHM = (2)FSP ILM PHNG CORD and q mt H2O -OHM
181): (2)FSP ILM PHNG CORD and q mt H2O -OHM = (2)FSP ILM PHNG CORD and q mt -OHM
182): (2)FSP ILM PHNG CORD and q mt H2O -OHM = (2)FSP ILM PHNG CORD and mt H2O -OHM
183): (2)FSP BIO CORD and ru mt H2O -OHM = (2)FSP CORD and ru cor mt H2O -OHM
184): (2)FSP BIO CORD sill ru cor mt H2O -OHM = (2)FSP CORD sill ru cor mt H2O -OHM
185): (2)FSP BIO CORD sill ru mt H2O -OHM = (2)FSP BIO CORD sill ru cor mt H2O -OHM
186): (2)FSP BIO CORD sill ru cor mt H2O -OHM = (2)FSP BIO CORD sill ru mt H2O -OHM
187): (2)FSP CORD sill ru cor mt H2O -OHM = (2)FSP BIO CORD sill ru cor mt H2O -OHM
188): (2)FSP BIO CORD sill ru mt H2O -OHM = (2)FSP CORD sill ru cor mt H2O -OHM
189): (2)FSP ILM PHNG CORD and q mt -OHM = (2)FSP PHNG CORD and q ru mt H2O -OHM
190): (2)FSP PHNG CORD and ru mt H2O -OHM = (2)FSP PHNG CORD and q ru mt -OHM
191): (2)FSP PHNG CORD sill ru mt H2O -OHM = (2)FSP PHNG CORD and ru mt H2O -OHM
192): (2)FSP PHNG CORD sill ru mt H2O -OHM = (2)FSP PHNG CORD sill q ru mt H2O -OHM
193): (2)FSP PHNG CORD sill q ru mt H2O -OHM = (2)FSP PHNG CORD sill q ru mt -OHM
194): (2)FSP PHNG CORD and ru mt H2O -OHM = (2)FSP PHNG CORD and q ru mt -OHM
195): (2)FSP CORD LIQtc sill ru cor mt -OHM = FSP CORD LIQtc ru cor mt -OHM
196): (2)FSP PHNG BIO CORD and q ru mt -OHM = (2)FSP PHNG CORD sill q ru mt -OHM
197): (2)FSP PHNG BIO LIQtc sill q ru mt -OHM = (2)FSP PHNG BIO sill q ru mt H2O -OHM
198): (2)FSP BIO sill q ru mt H2O -OHM = (2)FSP BIO CORD sill ru mt H2O -OHM
199): (2)FSP BIO CORD sill q ru mt H2O -OHM = (2)FSP BIO CORD sill ru mt H2O -OHM
200): (2)FSP BIO sill q ru mt H2O -OHM = (2)FSP BIO CORD sill q ru mt H2O -OHM
201): (2)FSP BIO CORD LIQtc sill ru cor mt -OHM = FSP CORD LIQtc sill ru cor mt -OHM
202): FSP BIO CORD LIQtc sill ru cor mt -OHM = FSP CORD LIQtc sill ru cor mt -OHM
203): FSP BIO CORD LIQtc sill ru cor mt -OHM = (2)FSP BIO CORD LIQtc sill ru cor mt -OHM
204): (2)FSP PHNG BIO LIQtc sill q ru mt -OHM = (2)FSP BIO LIQtc sill q ru mt H2O -OHM
205): (2)FSP PHNG BIO LIQtc ky q ru mt -OHM = (2)FSP PHNG BIO LIQtc sill q ru mt -OHM
206): (2)FSP PHNG CORD sill q ru mt -OHM = (2)FSP PHNG CORD sill ru mt H2O -OHM
207): (2)FSP BIO CORD and ru mt H2O -OHM = (2)FSP CORD and ru cor mt H2O -OHM
208): (2)FSP BIO CORD sill ru mt H2O -OHM = (2)FSP CORD sill ru cor mt H2O -OHM
209): (2)FSP CORD sill ru cor mt H2O -OHM = (2)FSP BIO CORD sill ru cor mt H2O -OHM
210): (2)FSP BIO CORD sill ru cor mt H2O -OHM = (2)FSP BIO CORD sill ru mt H2O -OHM
211): (2)FSP ILM PHNG CORD and q mt -OHM = (2)FSP ILM PHNG CORD and mt H2O -OHM
212): (2)FSP ILM PHNG CORD and q mt H2O -OHM = (2)FSP ILM PHNG CORD and mt H2O -OHM
213): (2)FSP ILM PHNG CORD and q mt -OHM = (2)FSP ILM PHNG CORD and q mt H2O -OHM
214): (2)FSP PHNG CORD and ru mt H2O -OHM = (2)FSP PHNG CORD and q ru mt -OHM
215): (2)FSP PHNG CORD and q ru mt H2O -OHM = (2)FSP PHNG CORD and ru mt H2O -OHM
216): (2)FSP PHNG CORD and q ru mt -OHM = (2)FSP PHNG CORD and q ru mt H2O -OHM
217): (2)FSP PHNG CORD and ru mt H2O -OHM = (2)FSP PHNG CORD and q ru mt -OHM
218): (2)FSP PHNG CORD and q ru mt H2O -OHM = (2)FSP PHNG CORD and ru mt H2O -OHM
219): (2)FSP PHNG CORD and q ru mt -OHM = (2)FSP PHNG CORD and q ru mt H2O -OHM
220): (2)FSP PHNG CORD and ru mt H2O -OHM = (2)FSP PHNG CORD and q ru mt -OHM
221): (2)FSP PHNG CORD and q ru mt H2O -OHM = (2)FSP PHNG CORD and ru mt H2O -OHM
222): (2)FSP PHNG CORD and q ru mt -OHM = (2)FSP PHNG CORD and q ru mt H2O -OHM
223): (2)FSP PHNG CORD and ru mt H2O -OHM = (2)FSP PHNG CORD and q ru mt -OHM
224): (2)FSP PHNG CORD and q ru mt H2O -OHM = (2)FSP PHNG CORD and ru mt H2O -OHM
225): (2)FSP PHNG CORD and q ru mt -OHM = (2)FSP PHNG CORD and q ru mt H2O -OHM
226): (2)FSP PHNG CORD and ru mt H2O -OHM = (2)FSP BIO CORD and ru mt H2O -OHM
227): (2)FSP BIO CORD sill ru cor mt H2O -OHM = (2)FSP BIO CORD sill ru mt H2O -OHM
228): (2)FSP CORD sill ru cor mt H2O -OHM = (2)FSP BIO CORD sill ru cor mt H2O -OHM
229): (2)FSP BIO CORD sill ru mt H2O -OHM = (2)FSP CORD sill ru cor mt H2O -OHM
230): (2)FSP BIO LIQtc sill ru mt H2O -OHM = (2)FSP BIO LIQtc sill ru cor mt -OHM
231): (2)FSP PHNG BIO LIQtc ky q ru mt -OHM = (2)FSP PHNG BIO LIQtc sill ru mt -OHM
232): (2)FSP PHNG CORD sill q ru mt -OHM = (2)FSP PHNG CORD sill ru mt H2O -OHM
233): (2)FSP PHNG CORD and ru mt H2O -OHM = (2)FSP PHNG CORD and q ru mt -OHM
234): (2)FSP PHNG CORD and q ru mt H2O -OHM = (2)FSP PHNG CORD and ru mt H2O -OHM
235): (2)FSP PHNG CORD and q ru mt -OHM = (2)FSP PHNG CORD and q ru mt H2O -OHM
236): (2)FSP ILM PHNG CORD and q mt H2O -OHM = (2)FSP ILM PHNG CORD and q mt -OHM
237): (2)FSP ILM PHNG CORD and mt H2O -OHM = (2)FSP ILM PHNG CORD and q mt H2O -OHM
238): (2)FSP ILM PHNG CORD and q mt -OHM = (2)FSP ILM PHNG CORD and mt H2O -OHM
239): (2)FSP ILM PHNG CORD and q mt H2O -OHM = (2)FSP ILM PHNG CORD and mt H2O -OHM
240): (2)FSP ILM PHNG CORD and q mt -OHM = (2)FSP ILM PHNG CORD and q mt H2O -OHM
241): (2)FSP BIO CORD sill ru cor mt H2O -OHM = (2)FSP BIO CORD sill ru mt H2O -OHM
242): (2)FSP CORD sill ru cor mt H2O -OHM = (2)FSP BIO CORD sill ru cor mt H2O -OHM
243): (2)FSP BIO CORD sill ru mt H2O -OHM = (2)FSP CORD sill ru cor mt H2O -OHM
244): (2)FSP PHNG CORD sill ru mt H2O -OHM = (2)FSP PHNG BIO CORD sill ru mt H2O -OHM
245): (2)FSP PHNG BIO CORD sill ru mt H2O -OHM = (2)FSP BIO CORD sill ru mt H2O -OHM
246): (2)FSP PHNG CORD and q ru mt H2O -OHM = (2)FSP PHNG CORD and ru mt H2O -OHM
247): (2)FSP PHNG CORD and q ru mt -OHM = (2)FSP PHNG CORD and q ru mt H2O -OHM
248): (2)FSP BIO CORD sill ru mt H2O -OHM = (2)FSP CORD sill ru cor mt H2O -OHM
249): (2)FSP PHNG CORD and q ru mt -OHM = (2)FSP PHNG CORD and q ru mt H2O -OHM
250): (2)FSP PHNG CORD and q ru mt H2O -OHM = (2)FSP PHNG CORD and ru mt H2O -OHM
251): (2)FSP PHNG CORD and q ru mt H2O -OHM = (2)FSP PHNG CORD and ru mt H2O -OHM

## B.3. Sample APS+Si $Fe^{2+}$

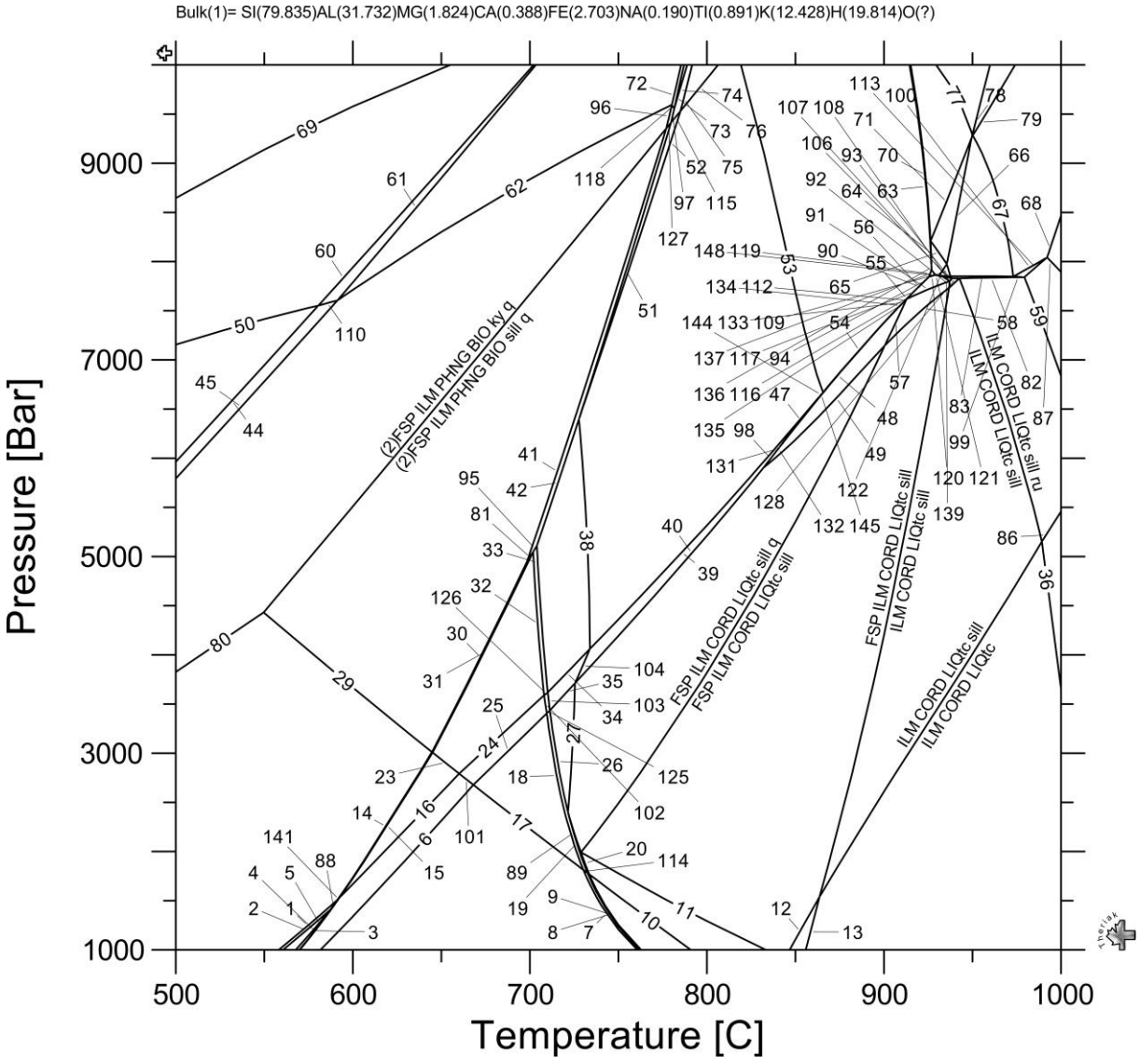


1): (2)FSP ILM PHNG BIO and q = (2)FSP ILM PHNG BIO CORD and q
2): (2)FSP ILM PHNG BIO CORD and q = (2)FSP ILM PHNG BIO CORD q
3): (2)FSP ILM PHNG BIO CORD q = (2)FSP ILM PHNG BIO CORD q H2O
4): (2)FSP ILM PHNG BIO CORD q H2O = (2)FSP ILM PHNG BIO CORD and q H2O
5): (2)FSP ILM PHNG BIO CORD and q H2O = (2)FSP ILM BIO CORD and q H2O
6): (2)FSP ILM BIO CORD and q H2O = (2)FSP ILM CORD and q H2O
7): (2)FSP ILM CORD and q H2O = (2)FSP ILM CORD LIQtc and q H2O
8): (2)FSP ILM CORD LIQtc and q H2O = FSP ILM CORD LIQtc and q H2O
9): FSP ILM CORD LIQtc and q H2O = FSP ILM CORD LIQtc and H2O
10): FSP ILM CORD LIQtc and H2O = FSP ILM CORD LIQtc sill H2O
11): FSP ILM CORD LIQtc sill H2O = FSP ILM CORD LIQtc sill
12): FSP ILM CORD LIQtc sill = FSP ILM CORD LIQtc
13): FSP ILM CORD LIQtc = ILM CORD LIQtc
14): (2)FSP ILM PHNG BIO and q = (2)FSP ILM PHNG BIO and q H2O
15): (2)FSP ILM PHNG BIO and q H2O = (2)FSP ILM BIO and q H2O
16): (2)FSP ILM BIO and q H2O = (2)FSP ILM BIO CORD and q H2O
17): (2)FSP ILM CORD and q H2O = (2)FSP ILM CORD sill q H2O
18): (2)FSP ILM CORD sill q H2O = (2)FSP ILM CORD LIQtc sill q H2O
19): (2)FSP ILM CORD LIQtc sill q H2O = FSP ILM CORD LIQtc sill q H2O
20): FSP ILM CORD LIQtc sill q H2O = FSP ILM CORD LIQtc sill H2O
21): FSP ILM CORD LIQtc sill = ILM CORD LIQtc sill
22): ILM CORD LIQtc sill = ILM CORD LIQtc
23): (2)FSP ILM BIO and q H2O = (2)FSP ILM BIO sill q H2O
24): (2)FSP ILM BIO sill q H2O = (2)FSP ILM BIO CORD sill q H2O
25): (2)FSP ILM BIO CORD sill q H2O = (2)FSP ILM CORD sill q H2O
26): (2)FSP ILM CORD LIQtc sill q H2O = (2)FSP ILM CORD LIQtc sill q

27): (2)FSP ILM CORD LIQtc sill q = FSP ILM CORD LIQtc sill q
28): FSP ILM CORD LIQtc sill q = FSP ILM CORD LIQtc sill
29): (2)FSP ILM PHNG BIO sill q = (2)FSP ILM PHNG BIO and q
30): (2)FSP ILM PHNG BIO sill q = (2)FSP ILM PHNG BIO sill q H2O
31): (2)FSP ILM PHNG BIO sill q H2O = (2)FSP ILM BIO sill q H2O
32): (2)FSP ILM BIO sill q H2O = (2)FSP ILM BIO LIQtc sill q H2O
33): (2)FSP ILM BIO LIQtc sill q H2O = (2)FSP ILM BIO LIQtc sill q
34): (2)FSP ILM BIO LIQtc sill q = (2)FSP ILM BIO CORD LIQtc sill q
35): (2)FSP ILM BIO CORD LIQtc sill q = (2)FSP ILM CORD LIQtc sill q
36): ILM CORD LIQtc ru = ILM CORD LIQtc
37): (2)FSP ILM PHNG BIO ky q = (2)FSP ILM PHNG BIO sill q
38): (2)FSP ILM BIO LIQtc sill q = FSP ILM BIO LIQtc sill q
39): FSP ILM BIO LIQtc sill q = FSP ILM BIO CORD LIQtc sill q
40): FSP ILM BIO CORD LIQtc sill q = FSP ILM CORD LIQtc sill q
41): (2)FSP ILM PHNG BIO sill q = (2)FSP ILM PHNG BIO LIQtc sill q
42): (2)FSP ILM PHNG BIO LIQtc sill q = (2)FSP ILM BIO LIQtc sill q
43): ILM CORD LIQtc sill ru = ILM CORD LIQtc sill
44): FSP ILM PHNG BIO ky zo q = (2)FSP ILM PHNG BIO ky zo q
45): (2)FSP ILM PHNG BIO ky zo q = (2)FSP ILM PHNG BIO ky q
46): (2)FSP ILM PHNG BIO LIQtc sill q = FSP ILM BIO LIQtc sill q
47): FSP ILM BIO CORD LIQtc sill q = FSP ILM GARNET BIO CORD LIQtc sill q
48): FSP ILM GARNET BIO CORD LIQtc sill q = FSP ILM GARNET CORD LIQtc sill q
49): FSP ILM GARNET CORD LIQtc sill q = FSP ILM CORD LIQtc sill q
50): FSP ILM GARNET PHNG BIO ky zo q = FSP ILM PHNG BIO ky zo q
51): (2)FSP ILM PHNG BIO LIQtc sill q = FSP ILM PHNG BIO LIQtc sill q
52): FSP ILM PHNG BIO LIQtc sill q = FSP ILM BIO LIQtc sill q
53): FSP ILM BIO LIQtc sill q = FSP ILM GARNET BIO LIQtc sill q
54): FSP ILM GARNET BIO LIQtc sill q = FSP ILM GARNET BIO CORD LIQtc sill q
55): FSP ILM GARNET BIO LIQtc sill q = FSP ILM GARNET BIO CORD LIQtc sill q
56): FSP ILM GARNET BIO LIQtc sill q = FSP ILM GARNET BIO CORD LIQtc sill q
57): FSP ILM GARNET CORD LIQtc sill q = FSP ILM GARNET CORD LIQtc sill
58): FSP ILM GARNET CORD LIQtc sill = FSP ILM CORD LIQtc sill
59): CORD LIQtc sill ru = ILM CORD LIQtc sill ru
60): FSP ILM GARNET PHNG BIO ky zo q = (2)FSP ILM GARNET PHNG BIO ky zo q
61): (2)FSP ILM GARNET PHNG BIO ky zo q = (2)FSP ILM GARNET PHNG BIO ky q
62): (2)FSP ILM GARNET PHNG BIO ky q = (2)FSP ILM PHNG BIO ky q
63): FSP ILM GARNET BIO LIQtc sill q = FSP ILM GARNET BIO LIQtc sill q ru
64): FSP ILM GARNET BIO LIQtc sill q ru = FSP ILM GARNET BIO LIQtc sill ru
65): FSP ILM GARNET LIQtc sill ru = FSP ILM GARNET BIO LIQtc sill ru
66): FSP ILM GARNET LIQtc sill ru = ILM GARNET LIQtc sill ru
67): ILM GARNET LIQtc sill ru = GARNET LIQtc sill ru
68): GARNET LIQtc sill ru = LIQtc sill ru
69): FSP ILM GARNET PHNG BIO ky q = FSP ILM GARNET PHNG BIO ky zo q
70): FSP ILM GARNET BIO LIQtc sill q ru = FSP ILM GARNET LIQtc sill q ru
71): FSP ILM GARNET LIQtc sill q ru = FSP ILM GARNET LIQtc sill ru
72): (2)FSP ILM GARNET PHNG BIO ky q = (2)FSP ILM GARNET PHNG BIO LIQtc ky q
73): (2)FSP ILM GARNET PHNG BIO LIQtc ky q = FSP ILM GARNET PHNG BIO LIQtc ky q
74): FSP ILM GARNET PHNG BIO LIQtc ky q = FSP ILM PHNG BIO LIQtc ky q
75): FSP ILM PHNG BIO LIQtc ky q = FSP ILM BIO LIQtc ky q
76): FSP ILM BIO LIQtc ky q = FSP ILM BIO LIQtc sill q
77): FSP ILM GARNET LIQtc sill q ru = FSP GARNET LIQtc sill q ru
78): FSP GARNET LIQtc sill q ru = GARNET LIQtc sill q ru
79): GARNET LIQtc sill q ru = GARNET LIQtc sill ru
80): (2)FSP ILM PHNG BIO ky q = (2)FSP ILM PHNG BIO and q
81): (2)FSP ILM PHNG BIO LIQtc sill q = (2)FSP ILM PHNG BIO sill q H2O
82): ILM GARNET CORD LIQtc sill ru = ILM CORD LIQtc sill ru
83): ILM GARNET LIQtc sill ru = ILM GARNET CORD LIQtc sill ru
84): ILM GARNET LIQtc sill ru = ILM GARNET LIQtc sill q ru
85): GARNET LIQtc sill q ru = ILM GARNET LIQtc sill q ru
86): ILM CORD LIQtc ru = ILM CORD LIQtc sill ru
87): LIQtc sill ru = CORD LIQtc sill ru
88): (2)FSP ILM PHNG BIO CORD and q = (2)FSP ILM PHNG BIO CORD and q H2O
89): FSP ILM CORD LIQtc sill q H2O = FSP ILM CORD LIQtc sill q
90): FSP ILM GARNET BIO CORD LIQtc sill q = FSP ILM GARNET BIO CORD LIQtc sill
91): FSP ILM GARNET BIO CORD LIQtc sill = FSP ILM GARNET CORD LIQtc sill
92): FSP ILM GARNET CORD LIQtc sill = ILM GARNET CORD LIQtc sill
93): ILM GARNET CORD LIQtc sill = ILM CORD LIQtc sill
94): FSP ILM GARNET BIO CORD LIQtc sill = FSP ILM GARNET BIO LIQtc sill q
95): (2)FSP ILM PHNG BIO LIQtc sill q = (2)FSP ILM BIO LIQtc sill q H2O
96): (2)FSP ILM PHNG BIO ky q = (2)FSP ILM PHNG BIO LIQtc ky q
97): (2)FSP ILM PHNG BIO LIQtc ky q = FSP ILM PHNG BIO LIQtc ky q
98): FSP ILM BIO CORD LIQtc sill q = FSP ILM GARNET CORD LIQtc sill q
99): GARNET CORD LIQtc sill ru = ILM GARNET CORD LIQtc sill ru
100): GARNET CORD LIQtc sill ru = GARNET LIQtc sill ru
101): (2)FSP ILM BIO CORD sill q H2O = (2)FSP ILM BIO CORD and q H2O

102): (2)FSP ILM BIO CORD sill q H2O = (2)FSP ILM BIO CORD LIQtc sill q H2O
103): (2)FSP ILM BIO CORD LIQtc sill q H2O = (2)FSP ILM BIO CORD LIQtc sill q
104): (2)FSP ILM BIO CORD LIQtc sill q = FSP ILM BIO CORD LIQtc sill q
105): FSP ILM GARNET BIO LIQtc sill ru = ILM GARNET LIQtc sill ru
106): ILM GARNET CORD LIQtc sill = ILM GARNET BIO CORD LIQtc sill
107): ILM GARNET BIO CORD LIQtc sill ru = ILM GARNET BIO CORD LIQtc sill
108): ILM GARNET BIO LIQtc sill ru = ILM GARNET BIO CORD LIQtc sill ru
109): ILM GARNET BIO LIQtc sill ru = ILM GARNET LIQtc sill ru
110): (2)FSP ILM PHNG BIO ky zo q = (2)FSP ILM GARNET PHNG BIO ky zo q
111): FSP ILM GARNET BIO LIQtc sill q = FSP ILM GARNET CORD LIQtc sill q
112): FSP ILM GARNET BIO CORD LIQtc sill q = FSP ILM GARNET CORD LIQtc sill q
113): GARNET CORD LIQtc sill ru = CORD LIQtc sill ru
114): (2)FSP ILM CORD LIQtc and q H2O = (2)FSP ILM CORD LIQtc sill q H2O
115): FSP ILM PHNG BIO LIQtc ky q = FSP ILM PHNG BIO LIQtc sill q
116): FSP ILM GARNET BIO CORD LIQtc sill q = FSP ILM GARNET BIO CORD LIQtc sill
117): FSP ILM GARNET BIO CORD LIQtc sill = FSP ILM GARNET BIO LIQtc sill q
118): (2)FSP ILM PHNG BIO LIQtc ky q = (2)FSP ILM GARNET PHNG BIO LIQtc ky q
119): FSP ILM GARNET BIO LIQtc sill q = FSP ILM GARNET BIO LIQtc sill
120): FSP ILM GARNET BIO LIQtc sill = FSP ILM GARNET BIO CORD LIQtc sill
121): FSP ILM GARNET BIO LIQtc sill ru = FSP ILM GARNET BIO CORD LIQtc sill
122): FSP ILM GARNET BIO LIQtc sill ru = ILM GARNET BIO LIQtc sill ru
123): ILM GARNET BIO LIQtc sill ru = FSP ILM GARNET BIO CORD LIQtc sill
124): (2)FSP ILM PHNG BIO and q = (2)FSP ILM PHNG BIO CORD and q H2O
125): (2)FSP ILM BIO CORD LIQtc sill q H2O = (2)FSP ILM CORD LIQtc sill q H2O
126): (2)FSP ILM BIO LIQtc sill q H2O = (2)FSP ILM BIO CORD LIQtc sill q H2O
127): (2)FSP ILM PHNG BIO LIQtc ky q = (2)FSP ILM PHNG BIO LIQtc sill q
128): ILM GARNET CORD LIQtc sill ru = ILM GARNET CORD LIQtc sill
129): FSP ILM BIO CORD LIQtc sill q = FSP ILM GARNET CORD LIQtc sill q
130): FSP ILM BIO CORD LIQtc sill q = FSP ILM GARNET CORD LIQtc sill q
131): FSP ILM GARNET BIO CORD LIQtc sill q = FSP ILM GARNET CORD LIQtc sill q
132): FSP ILM BIO CORD LIQtc sill q = FSP ILM GARNET BIO CORD LIQtc sill q
133): FSP ILM GARNET BIO LIQtc sill q = FSP ILM GARNET CORD LIQtc sill q
134): FSP ILM GARNET BIO CORD LIQtc sill q = FSP ILM GARNET CORD LIQtc sill q
135): FSP ILM GARNET BIO LIQtc sill q = FSP ILM GARNET BIO CORD LIQtc sill q
136): FSP ILM GARNET BIO LIQtc sill q = FSP ILM GARNET BIO LIQtc sill ru
137): FSP ILM GARNET BIO LIQtc sill = FSP ILM GARNET BIO LIQtc sill ru
138): FSP ILM GARNET LIQtc sill q ru = ILM GARNET LIQtc sill q ru
139): ILM GARNET BIO CORD LIQtc sill = FSP ILM GARNET BIO CORD LIQtc sill
140): (2)FSP ILM PHNG BIO and q H2O = (2)FSP ILM BIO CORD and q H2O
141): (2)FSP ILM PHNG BIO and q H2O = (2)FSP ILM PHNG BIO CORD and q H2O
142): FSP ILM CORD LIQtc sill q H2O = FSP ILM CORD LIQtc and q H2O
143): (2)FSP ILM PHNG BIO ky q = (2)FSP ILM PHNG BIO LIQtc sill q
144): FSP ILM BIO LIQtc sill q = FSP ILM BIO CORD LIQtc sill q
145): FSP ILM BIO CORD LIQtc sill q = FSP ILM GARNET BIO CORD LIQtc sill q
146): FSP ILM BIO LIQtc sill q = FSP ILM GARNET BIO CORD LIQtc sill q
147): (2)FSP ILM PHNG BIO LIQtc ky q = FSP ILM PHNG BIO LIQtc sill q
148): ILM GARNET CORD LIQtc sill ru = ILM GARNET BIO CORD LIQtc sill ru
149): ILM GARNET BIO CORD LIQtc sill ru = FSP ILM GARNET BIO CORD LIQtc sill
150): FSP ILM CORD LIQtc sill q = FSP ILM CORD LIQtc sill H2O
151): (2)FSP ILM PHNG BIO and q H2O = (2)FSP ILM PHNG BIO sill q H2O
152): (2)FSP ILM BIO CORD sill q H2O = (2)FSP ILM CORD LIQtc sill q H2O
153): (2)FSP ILM BIO CORD LIQtc sill q = FSP ILM CORD LIQtc sill q
154): FSP ILM GARNET CORD LIQtc sill q = FSP ILM CORD LIQtc sill
155): FSP ILM GARNET PHNG BIO ky zo q = (2)FSP ILM PHNG BIO ky zo q
156): (2)FSP ILM GARNET PHNG BIO ky zo q = (2)FSP ILM PHNG BIO ky q
157): FSP ILM GARNET BIO CORD LIQtc sill q = FSP ILM BIO LIQtc sill q
158): GARNET CORD LIQtc sill ru = ILM CORD LIQtc sill ru
159): FSP ILM GARNET BIO CORD LIQtc sill ru = FSP ILM GARNET BIO CORD LIQtc sill
160): FSP ILM GARNET BIO LIQtc sill ru = FSP ILM GARNET BIO CORD LIQtc sill ru
161): FSP ILM GARNET BIO CORD LIQtc sill q = FSP ILM GARNET CORD LIQtc sill q
162): FSP ILM BIO CORD LIQtc sill q = FSP ILM GARNET BIO CORD LIQtc sill q

## B.4. Sample UAS

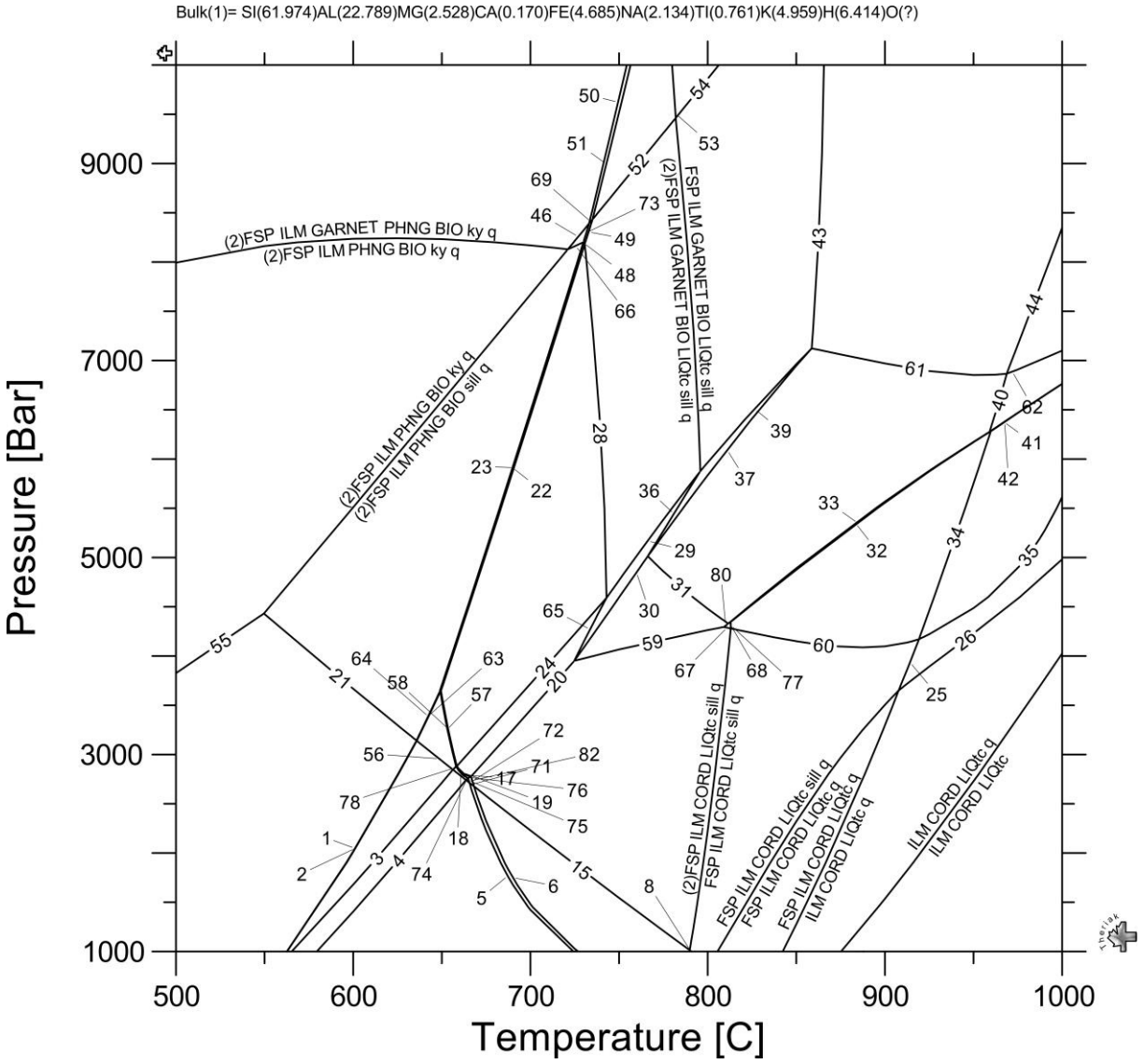


1): (2)FSP ILM PHNG BIO and q = (2)FSP ILM PHNG BIO and q H2O
2): (2)FSP ILM PHNG BIO and q H2O = (2)FSP ILM BIO and q H2O
3): (2)FSP ILM BIO and q H2O = (2)FSP ILM BIO CORD and q H2O
4): (2)FSP ILM BIO CORD and q H2O = (2)FSP ILM CORD and q H2O
5): (2)FSP ILM CORD and q H2O = (2)FSP ILM CORD LIQtc and q H2O
6): (2)FSP ILM CORD LIQtc and q H2O = (2)FSP ILM CORD LIQtc and q
7): (2)FSP ILM CORD LIQtc and q = FSP ILM CORD LIQtc and q
8): FSP ILM CORD LIQtc and q = FSP ILM CORD LIQtc sill q
9): FSP ILM CORD LIQtc sill q = FSP ILM CORD LIQtc q
10): FSP ILM CORD LIQtc q = ILM CORD LIQtc q
11): ILM CORD LIQtc q = ILM CORD LIQtc
12): ILM CORD LIQtc = ClAMP CORD LIQtc sill q ru
13): ILM CORD LIQtc = ILM ClAMP CORD LIQtc
14): ILM CORD LIQtc = ILM ClAMP LIQtc sill q ru
15): (2)FSP ILM CORD LIQtc sill q = (2)FSP ILM CORD LIQtc and q
16): (2)FSP ILM CORD LIQtc sill q = FSP ILM CORD LIQtc sill q
17): (2)FSP ILM BIO CORD and q H2O = (2)FSP ILM BIO CORD sill q H2O
18): (2)FSP ILM BIO CORD LIQtc sill q H2O = (2)FSP ILM BIO CORD sill q H2O
19): (2)FSP ILM BIO CORD LIQtc sill q = (2)FSP ILM BIO CORD LIQtc sill q H2O
20): (2)FSP ILM BIO CORD LIQtc sill q = (2)FSP ILM CORD LIQtc sill q
21): (2)FSP ILM PHNG BIO sill q = (2)FSP ILM PHNG BIO and q
22): (2)FSP ILM PHNG BIO sill q = (2)FSP ILM PHNG BIO LIQtc sill q
23): (2)FSP ILM PHNG BIO LIQtc sill q = (2)FSP ILM BIO LIQtc sill q
24): (2)FSP ILM BIO LIQtc sill q = (2)FSP ILM BIO CORD LIQtc sill q
25): FSP ILM CORD LIQtc sill q = ILM CORD LIQtc sill q
26): ILM CORD LIQtc sill q = ILM CORD LIQtc q

27): (2)FSP ILM PHNG BIO ky q = (2)FSP ILM PHNG BIO sill q
28): (2)FSP ILM BIO LIQtc sill q = (2)FSP ILM GARNET BIO LIQtc sill q
29): (2)FSP ILM GARNET BIO LIQtc sill q = (2)FSP ILM GARNET BIO CORD LIQtc sill q
30): (2)FSP ILM GARNET BIO CORD LIQtc sill q = (2)FSP ILM GARNET CORD LIQtc sill q
31): (2)FSP ILM GARNET CORD LIQtc sill q = FSP ILM GARNET CORD LIQtc sill q
32): FSP ILM GARNET CORD LIQtc sill q = FSP ILM GARNET CORD SPIN LIQtc sill q
33): FSP ILM GARNET CORD SPIN LIQtc sill q = FSP ILM CORD SPIN LIQtc sill q
34): FSP ILM CORD SPIN LIQtc sill q = ILM CORD SPIN LIQtc sill q
35): ILM CORD SPIN LIQtc sill q = ILM CORD LIQtc sill q
36): (2)FSP ILM GARNET BIO CORD LIQtc sill q = FSP ILM GARNET BIO CORD LIQtc sill q
37): FSP ILM GARNET BIO CORD LIQtc sill q = FSP ILM GARNET CORD LIQtc sill q
38): (2)FSP ILM GARNET BIO LIQtc sill q = FSP ILM GARNET BIO LIQtc sill q
39): FSP ILM GARNET BIO LIQtc sill q = FSP ILM GARNET BIO CORD LIQtc sill q
40): FSP ILM GARNET CORD LIQtc sill q = ILM GARNET CORD LIQtc sill q
41): ILM GARNET CORD LIQtc sill q = ILM GARNET CORD SPIN LIQtc sill q
42): ILM GARNET CORD SPIN LIQtc sill q = ILM CORD SPIN LIQtc sill q
43): FSP ILM GARNET BIO LIQtc sill q = FSP ILM GARNET LIQtc sill q
44): FSP ILM GARNET LIQtc sill q = ILM GARNET LIQtc sill q
45): (2)FSP ILM GARNET PHNG BIO ky q = (2)FSP ILM PHNG BIO ky q
46): (2)FSP ILM GARNET PHNG BIO ky q = (2)FSP ILM GARNET PHNG BIO sill q
47): (2)FSP ILM GARNET PHNG BIO sill q = (2)FSP ILM PHNG BIO LIQtc sill q
48): (2)FSP ILM GARNET PHNG BIO LIQtc sill q = (2)FSP ILM PHNG BIO LIQtc sill q
49): (2)FSP ILM GARNET PHNG BIO LIQtc sill q = (2)FSP ILM GARNET BIO LIQtc sill q
50): (2)FSP ILM GARNET PHNG BIO ky q = (2)FSP ILM GARNET PHNG BIO LIQtc ky q
51): (2)FSP ILM GARNET PHNG BIO LIQtc ky q = (2)FSP ILM GARNET BIO LIQtc ky q
52): (2)FSP ILM GARNET BIO LIQtc ky q = (2)FSP ILM GARNET BIO LIQtc sill q
53): (2)FSP ILM GARNET BIO LIQtc ky q = FSP ILM GARNET BIO LIQtc ky q
54): FSP ILM GARNET BIO LIQtc ky q = FSP ILM GARNET BIO LIQtc sill q
55): (2)FSP ILM PHNG BIO ky q = (2)FSP ILM PHNG BIO and q
56): (2)FSP ILM BIO sill q H2O = (2)FSP ILM BIO and q H2O
57): (2)FSP ILM BIO LIQtc sill q H2O = (2)FSP ILM BIO sill q H2O
58): (2)FSP ILM BIO LIQtc sill q H2O = (2)FSP ILM BIO LIQtc sill q
59): (2)FSP ILM GARNET CORD LIQtc sill q = (2)FSP ILM CORD LIQtc sill q
60): FSP ILM CORD SPIN LIQtc sill q = FSP ILM CORD LIQtc sill q
61): FSP ILM GARNET LIQtc sill q = FSP ILM GARNET CORD LIQtc sill q
62): ILM GARNET LIQtc sill q = ILM GARNET CORD LIQtc sill q
63): (2)FSP ILM PHNG BIO sill q = (2)FSP ILM PHNG BIO sill q H2O
64): (2)FSP ILM PHNG BIO sill q H2O = (2)FSP ILM BIO sill q H2O
65): (2)FSP ILM BIO CORD LIQtc sill q = (2)FSP ILM GARNET BIO CORD LIQtc sill q
66): (2)FSP ILM PHNG BIO sill q = (2)FSP ILM GARNET PHNG BIO sill q
67): (2)FSP ILM CORD SPIN LIQtc sill q = (2)FSP ILM CORD LIQtc sill q
68): (2)FSP ILM CORD SPIN LIQtc sill q = FSP ILM GARNET CORD SPIN LIQtc sill q
69): (2)FSP ILM GARNET PHNG BIO LIQtc ky q = (2)FSP ILM GARNET PHNG BIO LIQtc sill q
70): (2)FSP ILM BIO sill q H2O = (2)FSP ILM BIO CORD and q H2O
71): (2)FSP ILM CORD LIQtc sill q H2O = (2)FSP ILM CORD LIQtc and q H2O
72): (2)FSP ILM CORD LIQtc sill q H2O = (2)FSP ILM CORD LIQtc sill q
73): (2)FSP ILM GARNET PHNG BIO sill q = (2)FSP ILM GARNET PHNG BIO LIQtc sill q
74): (2)FSP ILM BIO CORD sill q H2O = (2)FSP ILM CORD sill q H2O
75): (2)FSP ILM CORD sill q H2O = (2)FSP ILM CORD LIQtc sill q H2O
76): (2)FSP ILM BIO CORD LIQtc sill q H2O = (2)FSP ILM CORD LIQtc sill q H2O
77): (2)FSP ILM CORD SPIN LIQtc sill q = FSP ILM CORD SPIN LIQtc sill q
78): (2)FSP ILM BIO sill q H2O = (2)FSP ILM BIO CORD sill q H2O
79): (2)FSP ILM PHNG BIO LIQtc sill q = (2)FSP ILM BIO LIQtc sill q H2O
80): (2)FSP ILM GARNET CORD LIQtc sill q = (2)FSP ILM CORD SPIN LIQtc sill q
81): ILM GARNET CORD SPIN LIQtc sill q = FSP ILM GARNET CORD SPIN LIQtc sill q
82): (2)FSP ILM CORD and q H2O = (2)FSP ILM CORD sill q H2O
83): (2)FSP ILM CORD LIQtc and q = FSP ILM CORD LIQtc sill q
84): (2)FSP ILM BIO CORD LIQtc sill q = (2)FSP ILM CORD LIQtc sill q H2O
85): (2)FSP ILM GARNET PHNG BIO ky q = (2)FSP ILM PHNG BIO sill q
86): (2)FSP ILM GARNET BIO CORD LIQtc sill q = FSP ILM GARNET CORD LIQtc sill q
87): FSP ILM GARNET CORD LIQtc sill q = (2)FSP ILM CORD SPIN LIQtc sill q
88): FSP ILM GARNET BIO LIQtc sill q = FSP ILM GARNET CORD LIQtc sill q

## B.5. Sample APS after melt loss (melt vol%)

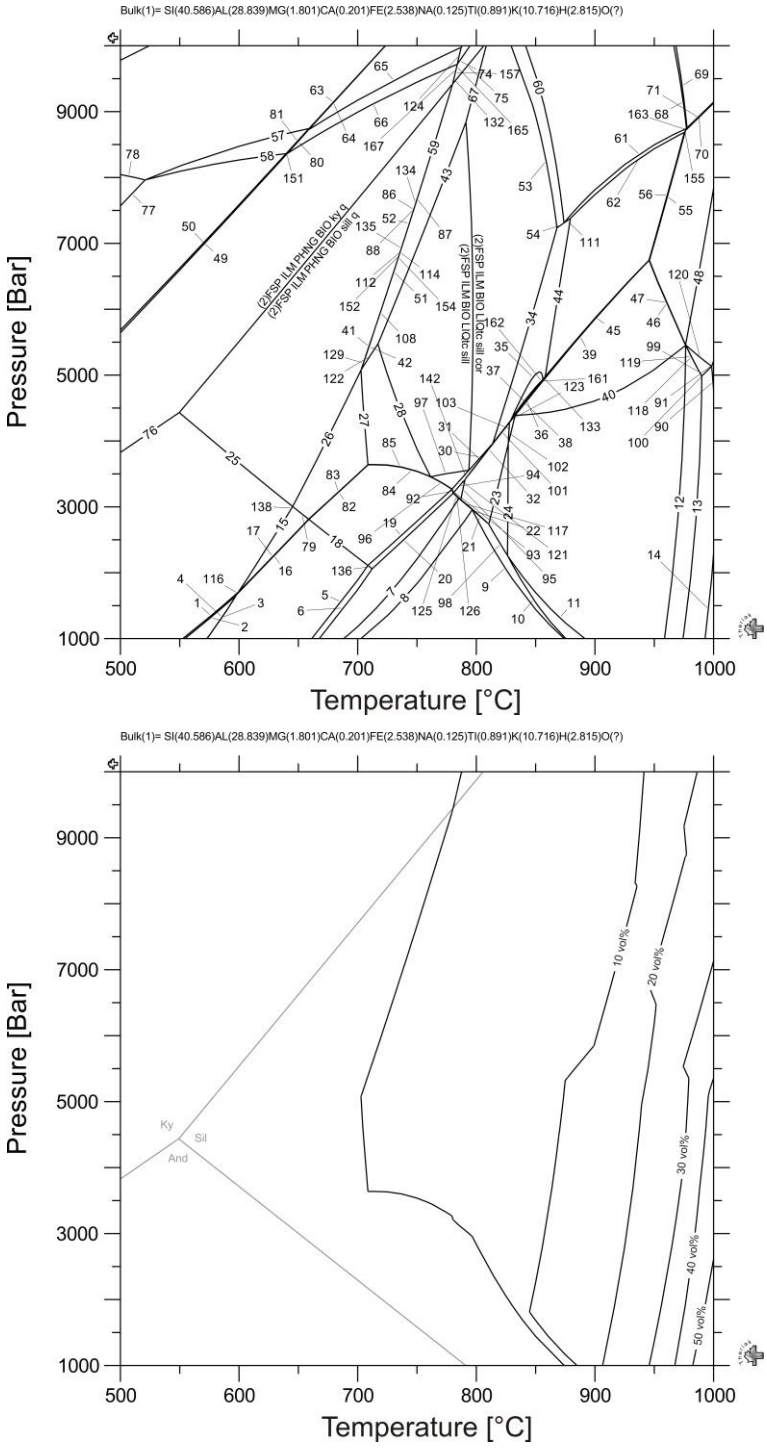


1): (2)FSP ILM PHNG BIO and q = (2)FSP ILM PHNG BIO CORD and q
2): (2)FSP ILM PHNG BIO CORD and q = (2)FSP ILM PHNG BIO CORD and
3): (2)FSP ILM PHNG BIO CORD and = (2)FSP ILM PHNG BIO CORD and H2O
4): (2)FSP ILM PHNG BIO CORD and H2O = (2)FSP ILM BIO CORD and H2O
5): (2)FSP ILM BIO CORD and H2O = (2)FSP ILM BIO CORD and cor H2O
6): (2)FSP ILM BIO CORD and cor H2O = (2)FSP ILM BIO CORD cor H2O
7): (2)FSP ILM BIO CORD cor H2O = (2)FSP ILM BIO CORD SPIN cor H2O
8): (2)FSP ILM BIO CORD SPIN cor H2O = (2)FSP ILM CORD SPIN cor H2O
9): (2)FSP ILM CORD SPIN cor H2O = (2)FSP ILM CORD SPIN LIQtc cor H2O
10): (2)FSP ILM CORD SPIN LIQtc cor H2O = FSP ILM CORD SPIN LIQtc cor H2O
11): FSP ILM CORD SPIN LIQtc cor H2O = FSP ILM CORD SPIN LIQtc cor
12): FSP ILM CORD SPIN LIQtc cor = FSP ILM CORD SPIN LIQtc ru cor
13): FSP ILM CORD SPIN LIQtc ru cor = FSP CORD SPIN LIQtc ru cor
14): FSP CORD SPIN LIQtc ru cor = FSP SPIN LIQtc ru cor

15): (2)FSP ILM PHNG BIO and q = (2)FSP ILM BIO and q H2O
16): (2)FSP ILM BIO and q H2O = (2)FSP ILM BIO CORD and q H2O
17): (2)FSP ILM BIO CORD and q H2O = (2)FSP ILM BIO CORD and H2O
18): (2)FSP ILM BIO CORD sill H2O = (2)FSP ILM BIO CORD and H2O
19): (2)FSP ILM BIO CORD sill H2O = (2)FSP ILM BIO CORD sill cor H2O
20): (2)FSP ILM BIO CORD sill cor H2O = (2)FSP ILM BIO CORD cor H2O
21): (2)FSP ILM BIO CORD SPIN LIQtc cor H2O = (2)FSP ILM CORD SPIN LIQtc cor H2O
22): (2)FSP ILM BIO CORD SPIN LIQtc cor = (2)FSP ILM BIO CORD SPIN LIQtc cor H2O
23): (2)FSP ILM BIO CORD SPIN LIQtc cor = (2)FSP ILM CORD SPIN LIQtc cor
24): (2)FSP ILM CORD SPIN LIQtc cor = FSP ILM CORD SPIN LIQtc cor
25): (2)FSP ILM PHNG BIO and q = (2)FSP ILM PHNG BIO sill q
26): (2)FSP ILM PHNG BIO sill q = (2)FSP ILM BIO sill q H2O
27): (2)FSP ILM BIO sill q H2O = (2)FSP ILM BIO LIQtc sill H2O
28): (2)FSP ILM BIO LIQtc sill H2O = (2)FSP ILM BIO LIQtc sill
29): (2)FSP ILM BIO LIQtc sill = (2)FSP ILM BIO LIQtc sill cor
30): (2)FSP ILM BIO LIQtc sill cor = (2)FSP ILM BIO CORD LIQtc sill cor
31): (2)FSP ILM BIO CORD LIQtc sill cor = (2)FSP ILM BIO CORD SPIN LIQtc sill cor
32): (2)FSP ILM BIO CORD SPIN LIQtc sill cor = (2)FSP ILM BIO CORD SPIN LIQtc cor
33): (2)FSP ILM PHNG BIO ky q = (2)FSP ILM PHNG BIO sill q
34): (2)FSP ILM BIO LIQtc sill cor = (2)FSP ILM BIO SPIN LIQtc sill cor
35): (2)FSP ILM BIO SPIN LIQtc sill cor = (2)FSP ILM BIO SPIN LIQtc sill
36): (2)FSP ILM BIO SPIN LIQtc sill = (2)FSP ILM BIO CORD SPIN LIQtc sill
37): (2)FSP ILM BIO CORD SPIN LIQtc sill = (2)FSP ILM BIO CORD SPIN LIQtc sill cor
38): (2)FSP ILM BIO CORD SPIN LIQtc sill cor = FSP ILM BIO CORD SPIN LIQtc sill cor
39): FSP ILM BIO CORD SPIN LIQtc sill cor = FSP ILM CORD SPIN LIQtc sill cor
40): FSP ILM CORD SPIN LIQtc sill cor = FSP ILM CORD SPIN LIQtc cor
41): (2)FSP ILM PHNG BIO sill q = (2)FSP ILM PHNG BIO LIQtc sill q
42): (2)FSP ILM PHNG BIO LIQtc sill q = (2)FSP ILM PHNG BIO LIQtc sill
43): (2)FSP ILM PHNG BIO LIQtc sill = (2)FSP ILM BIO LIQtc sill
44): (2)FSP ILM BIO SPIN LIQtc sill cor = FSP ILM BIO SPIN LIQtc sill cor
45): FSP ILM BIO SPIN LIQtc sill cor = FSP ILM BIO CORD SPIN LIQtc sill cor
46): FSP ILM CORD SPIN LIQtc sill cor = FSP ILM CORD SPIN LIQtc sill ru cor
47): FSP ILM CORD SPIN LIQtc sill ru cor = FSP ILM SPIN LIQtc sill ru cor
48): FSP ILM SPIN LIQtc sill ru cor = FSP SPIN LIQtc sill ru cor
49): FSP ILM PHNG BIO ky zo q = (2)FSP ILM PHNG BIO ky zo q
50): (2)FSP ILM PHNG BIO ky zo q = (2)FSP ILM PHNG BIO ky q
51): (2)FSP ILM PHNG BIO sill q = (2)FSP ILM PHNG BIO LIQtc sill
52): (2)FSP ILM PHNG BIO sill q = (2)FSP ILM PHNG BIO LIQtc sill
53): (2)FSP ILM GARNET BIO LIQtc sill cor = (2)FSP ILM BIO LIQtc sill cor
54): (2)FSP ILM GARNET BIO LIQtc sill cor = (2)FSP ILM BIO SPIN LIQtc sill cor
55): FSP ILM BIO SPIN LIQtc sill cor = FSP ILM BIO SPIN LIQtc sill ru cor
56): FSP ILM BIO SPIN LIQtc sill ru cor = FSP ILM SPIN LIQtc sill ru cor
57): FSP ILM GARNET PHNG BIO ky zo = FSP ILM GARNET PHNG BIO ky zo q
58): FSP ILM GARNET PHNG BIO ky zo q = FSP ILM PHNG BIO ky zo q
59): (2)FSP ILM PHNG BIO sill q = (2)FSP ILM PHNG BIO LIQtc sill
60): (2)FSP ILM GARNET BIO LIQtc sill cor = FSP ILM GARNET BIO LIQtc sill cor
61): FSP ILM GARNET BIO LIQtc sill cor = FSP ILM GARNET BIO SPIN LIQtc sill cor
62): FSP ILM GARNET BIO SPIN LIQtc sill cor = FSP ILM BIO SPIN LIQtc sill cor
63): FSP ILM GARNET PHNG BIO ky zo = (2)FSP ILM GARNET PHNG BIO ky zo
64): (2)FSP ILM GARNET PHNG BIO ky zo = (2)FSP ILM GARNET PHNG BIO ky
65): (2)FSP ILM GARNET PHNG BIO ky = (2)FSP ILM GARNET PHNG BIO ky q
66): (2)FSP ILM GARNET PHNG BIO ky q = (2)FSP ILM PHNG BIO ky q
67): (2)FSP ILM PHNG BIO LIQtc sill = (2)FSP ILM BIO LIQtc sill cor
68): FSP ILM GARNET BIO LIQtc sill cor = FSP ILM GARNET BIO LIQtc sill ru cor
69): FSP ILM GARNET BIO LIQtc sill ru cor = FSP ILM GARNET LIQtc sill ru cor
70): FSP ILM GARNET LIQtc sill ru cor = FSP ILM GARNET SPIN LIQtc sill ru cor
71): FSP ILM GARNET SPIN LIQtc sill ru cor = FSP ILM SPIN LIQtc sill ru cor
72): FSP ILM GARNET PHNG BIO ky = FSP ILM GARNET PHNG BIO ky zo
73): (2)FSP ILM GARNET PHNG BIO ky = (2)FSP ILM GARNET PHNG BIO LIQtc ky
74): (2)FSP ILM GARNET PHNG BIO LIQtc ky = (2)FSP ILM PHNG BIO LIQtc ky
75): (2)FSP ILM PHNG BIO LIQtc ky = (2)FSP ILM PHNG BIO LIQtc sill
76): (2)FSP ILM PHNG BIO ky q = (2)FSP ILM PHNG BIO and q
77): FSP ILM PHNG BIO ky zo = FSP ILM PHNG BIO ky zo q
78): FSP ILM GARNET PHNG BIO ky zo = FSP ILM PHNG BIO ky zo
79): (2)FSP ILM BIO sill q H2O = (2)FSP ILM BIO and q H2O
80): (2)FSP ILM GARNET PHNG BIO ky q = (2)FSP ILM GARNET PHNG BIO ky zo q
81): FSP ILM GARNET PHNG BIO ky zo q = (2)FSP ILM GARNET PHNG BIO ky zo q
82): (2)FSP ILM BIO CORD sill H2O = (2)FSP ILM BIO CORD sill q H2O
83): (2)FSP ILM BIO CORD sill q H2O = (2)FSP ILM BIO sill q H2O
84): (2)FSP ILM BIO CORD LIQtc sill H2O = (2)FSP ILM BIO CORD sill H2O
85): (2)FSP ILM BIO LIQtc sill H2O = (2)FSP ILM BIO CORD LIQtc sill H2O
86): (2)FSP ILM PHNG BIO LIQtc sill q = (2)FSP ILM PHNG BIO LIQtc sill
87): (2)FSP ILM PHNG BIO LIQtc sill q = (2)FSP ILM PHNG BIO LIQtc sill
88): (2)FSP ILM PHNG BIO sill q = (2)FSP ILM PHNG BIO LIQtc sill q
89): (2)FSP ILM PHNG BIO sill q = (2)FSP ILM PHNG BIO LIQtc sill q

90): FSP SPIN LIQtc ru cor = FSP CORD SPIN LIQtc ru cor
91): FSP SPIN LIQtc sill ru cor = FSP SPIN LIQtc ru cor
92): (2)FSP ILM BIO CORD LIQtc sill cor H2O = (2)FSP ILM BIO CORD sill cor H2O
93): (2)FSP ILM BIO CORD LIQtc sill cor H2O = (2)FSP ILM BIO CORD LIQtc sill cor
94): (2)FSP ILM BIO CORD LIQtc sill cor = (2)FSP ILM BIO CORD LIQtc cor
95): (2)FSP ILM BIO CORD LIQtc cor = (2)FSP ILM BIO CORD SPIN LIQtc cor
96): (2)FSP ILM BIO CORD LIQtc sill = (2)FSP ILM BIO CORD LIQtc sill H2O
97): (2)FSP ILM BIO LIQtc sill = (2)FSP ILM BIO CORD LIQtc sill
98): (2)FSP ILM CORD SPIN LIQtc cor H2O = (2)FSP ILM CORD SPIN LIQtc cor
99): FSP CORD SPIN LIQtc sill ru cor = FSP ILM CORD SPIN LIQtc ru cor
100): FSP CORD SPIN LIQtc sill ru cor = FSP CORD SPIN LIQtc ru cor
101): (2)FSP ILM BIO SPIN LIQtc sill cor = (2)FSP ILM BIO CORD SPIN LIQtc sill cor
102): (2)FSP ILM BIO CORD SPIN LIQtc cor = FSP ILM BIO CORD SPIN LIQtc cor
103): FSP ILM BIO CORD SPIN LIQtc cor = FSP ILM CORD SPIN LIQtc cor
104): (2)FSP ILM PHNG BIO ky q = (2)FSP ILM PHNG BIO LIQtc ky q
105): (2)FSP ILM PHNG BIO ky q = (2)FSP ILM PHNG BIO LIQtc ky q
106): (2)FSP ILM PHNG BIO LIQtc ky q = (2)FSP ILM PHNG BIO LIQtc ky
107): (2)FSP ILM PHNG BIO LIQtc ky q = (2)FSP ILM PHNG BIO LIQtc ky
108): (2)FSP ILM PHNG BIO sill q = (2)FSP ILM PHNG BIO LIQtc sill
109): (2)FSP ILM PHNG BIO LIQtc sill q = (2)FSP ILM PHNG BIO LIQtc sill
110): (2)FSP ILM PHNG BIO sill q = (2)FSP ILM PHNG BIO LIQtc sill q
111): (2)FSP ILM BIO SPIN LIQtc sill cor = FSP ILM GARNET BIO SPIN LIQtc sill cor
112): (2)FSP ILM PHNG BIO sill q = (2)FSP ILM PHNG BIO LIQtc sill q
113): (2)FSP ILM PHNG BIO sill q = (2)FSP ILM PHNG BIO LIQtc sill q
114): (2)FSP ILM PHNG BIO LIQtc sill q = (2)FSP ILM PHNG BIO LIQtc sill
115): (2)FSP ILM PHNG BIO LIQtc sill q = (2)FSP ILM PHNG BIO LIQtc sill
116): (2)FSP ILM PHNG BIO CORD and q = (2)FSP ILM BIO CORD and q H2O
117): (2)FSP ILM BIO CORD SPIN LIQtc cor H2O = (2)FSP ILM BIO CORD SPIN cor H2O
118): FSP ILM CORD SPIN LIQtc ru cor = FSP ILM CORD SPIN LIQtc sill ru cor
119): FSP ILM CORD SPIN LIQtc sill ru cor = FSP CORD SPIN LIQtc sill ru cor
120): FSP SPIN LIQtc sill ru cor = FSP CORD SPIN LIQtc sill ru cor
121): (2)FSP ILM BIO CORD LIQtc sill = (2)FSP ILM BIO CORD LIQtc sill cor
122): (2)FSP ILM PHNG BIO LIQtc sill = (2)FSP ILM BIO LIQtc sill H2O
123): FSP ILM BIO CORD SPIN LIQtc sill cor = FSP ILM BIO CORD SPIN LIQtc cor
124): (2)FSP ILM GARNET PHNG BIO ky q = (2)FSP ILM GARNET PHNG BIO LIQtc ky
125): (2)FSP ILM BIO CORD LIQtc cor H2O = (2)FSP ILM BIO CORD cor H2O
126): (2)FSP ILM BIO CORD LIQtc cor H2O = (2)FSP ILM BIO CORD LIQtc cor
127): (2)FSP ILM PHNG BIO and q H2O = (2)FSP ILM BIO and q H2O
128): (2)FSP ILM PHNG BIO and q = (2)FSP ILM PHNG BIO and q H2O
129): (2)FSP ILM PHNG BIO sill q = (2)FSP ILM PHNG BIO LIQtc sill
130): (2)FSP ILM PHNG BIO ky q = (2)FSP ILM PHNG BIO LIQtc ky q
131): (2)FSP ILM PHNG BIO LIQtc ky q = (2)FSP ILM PHNG BIO LIQtc ky
132): (2)FSP ILM PHNG BIO LIQtc ky = (2)FSP ILM PHNG BIO ky q
133): (2)FSP ILM BIO SPIN LIQtc sill cor = FSP ILM BIO CORD SPIN LIQtc sill cor
134): (2)FSP ILM PHNG BIO sill q = (2)FSP ILM PHNG BIO LIQtc sill
135): (2)FSP ILM PHNG BIO sill q = (2)FSP ILM PHNG BIO LIQtc sill
136): (2)FSP ILM BIO CORD sill cor H2O = (2)FSP ILM BIO CORD and cor H2O
137): (2)FSP ILM BIO CORD SPIN LIQtc cor = (2)FSP ILM CORD SPIN LIQtc cor H2O
138): (2)FSP ILM PHNG BIO and q = (2)FSP ILM BIO and q H2O
139): (2)FSP ILM PHNG BIO LIQtc sill q = (2)FSP ILM PHNG BIO LIQtc sill
140): (2)FSP ILM PHNG BIO sill q = (2)FSP ILM PHNG BIO LIQtc sill q
141): (2)FSP ILM PHNG BIO sill q = (2)FSP ILM PHNG BIO LIQtc sill q
142): (2)FSP ILM BIO CORD LIQtc sill cor = (2)FSP ILM BIO CORD SPIN LIQtc cor
143): (2)FSP ILM BIO SPIN LIQtc sill = (2)FSP ILM BIO CORD SPIN LIQtc sill cor
144): (2)FSP ILM BIO CORD SPIN LIQtc sill cor = FSP ILM BIO CORD SPIN LIQtc cor
145): (2)FSP ILM PHNG BIO sill q = (2)FSP ILM PHNG BIO LIQtc sill q
146): (2)FSP ILM PHNG BIO sill q = (2)FSP ILM PHNG BIO LIQtc sill q
147): (2)FSP ILM PHNG BIO LIQtc sill q = (2)FSP ILM PHNG BIO LIQtc sill
148): (2)FSP ILM PHNG BIO LIQtc sill q = (2)FSP ILM PHNG BIO LIQtc sill
149): (2)FSP ILM BIO CORD SPIN LIQtc sill = FSP ILM BIO CORD SPIN LIQtc sill cor
150): (2)FSP ILM BIO CORD SPIN LIQtc sill = FSP ILM BIO CORD SPIN LIQtc sill cor
151): (2)FSP ILM GARNET PHNG BIO ky zo q = (2)FSP ILM PHNG BIO ky zo q
152): (2)FSP ILM PHNG BIO sill q = (2)FSP ILM PHNG BIO LIQtc sill
153): (2)FSP ILM PHNG BIO LIQtc sill q = (2)FSP ILM PHNG BIO LIQtc sill
154): (2)FSP ILM PHNG BIO sill q = (2)FSP ILM PHNG BIO LIQtc sill q
155): FSP ILM GARNET BIO SPIN LIQtc sill cor = FSP ILM BIO SPIN LIQtc sill ru cor
156): (2)FSP ILM GARNET PHNG BIO ky q = (2)FSP ILM PHNG BIO LIQtc ky
157): (2)FSP ILM PHNG BIO LIQtc ky = (2)FSP ILM PHNG BIO ky q
158): (2)FSP ILM BIO CORD SPIN LIQtc cor H2O = (2)FSP ILM BIO CORD LIQtc cor H2O
159): (2)FSP ILM PHNG BIO LIQtc sill q = (2)FSP ILM BIO LIQtc sill H2O
160): (2)FSP ILM PHNG BIO sill q = (2)FSP ILM PHNG BIO LIQtc sill
161): (2)FSP ILM BIO CORD SPIN LIQtc sill = (2)FSP ILM BIO CORD SPIN LIQtc sill cor
162): (2)FSP ILM BIO CORD SPIN LIQtc sill cor = FSP ILM BIO CORD SPIN LIQtc sill cor
163): FSP ILM GARNET BIO SPIN LIQtc sill cor = FSP ILM GARNET SPIN LIQtc sill ru cor
164): (2)FSP ILM GARNET PHNG BIO ky zo q = (2)FSP ILM GARNET PHNG BIO ky zo

165): (2)FSP ILM PHNG BIO LIQtc ky = (2)FSP ILM PHNG BIO ky q
166): FSP CORD SPIN LIQtc sill ru cor = FSP SPIN LIQtc ru cor
167): (2)FSP ILM PHNG BIO LIQtc ky = (2)FSP ILM PHNG BIO ky q
168): (2)FSP ILM PHNG BIO LIQtc ky q = (2)FSP ILM PHNG BIO LIQtc ky
169): (2)FSP ILM PHNG BIO ky q = (2)FSP ILM PHNG BIO LIQtc ky q
170): (2)FSP ILM PHNG BIO CORD and q = (2)FSP ILM PHNG BIO CORD and H2O
171): (2)FSP ILM BIO CORD and H2O = (2)FSP ILM BIO CORD sill cor H2O
172): (2)FSP ILM BIO CORD sill cor H2O = (2)FSP ILM BIO CORD LIQtc cor H2O
173): (2)FSP ILM BIO CORD LIQtc cor = (2)FSP ILM BIO CORD SPIN LIQtc cor H2O
174): (2)FSP ILM BIO sill q H2O = (2)FSP ILM BIO LIQtc sill q H2O
175): (2)FSP ILM BIO LIQtc sill q H2O = (2)FSP ILM BIO LIQtc sill H2O
176): (2)FSP ILM PHNG BIO LIQtc ky = (2)FSP ILM PHNG BIO ky q
177): (2)FSP ILM BIO CORD SPIN LIQtc sill = FSP ILM BIO CORD SPIN LIQtc sill cor
178): FSP ILM GARNET PHNG BIO ky zo = FSP ILM PHNG BIO ky zo q
179): FSP ILM GARNET BIO LIQtc sill ru cor = FSP ILM GARNET SPIN LIQtc sill ru cor
180): (2)FSP ILM PHNG BIO LIQtc ky = (2)FSP ILM PHNG BIO ky q
181): (2)FSP ILM PHNG BIO LIQtc ky q = (2)FSP ILM PHNG BIO LIQtc ky
182): (2)FSP ILM PHNG BIO ky q = (2)FSP ILM PHNG BIO LIQtc ky q
183): (2)FSP ILM PHNG BIO sill q = (2)FSP ILM PHNG BIO LIQtc sill
184): (2)FSP ILM PHNG BIO LIQtc sill q = (2)FSP ILM PHNG BIO LIQtc sill
185): (2)FSP ILM PHNG BIO sill q = (2)FSP ILM PHNG BIO LIQtc sill q
186): (2)FSP ILM PHNG BIO sill q = (2)FSP ILM PHNG BIO LIQtc sill
187): (2)FSP ILM PHNG BIO sill q = (2)FSP ILM PHNG BIO LIQtc sill
188): (2)FSP ILM BIO CORD SPIN LIQtc sill = FSP ILM BIO CORD SPIN LIQtc sill cor
189): (2)FSP ILM BIO CORD SPIN LIQtc sill cor = FSP ILM BIO CORD SPIN LIQtc sill cor
190): (2)FSP ILM BIO CORD SPIN LIQtc sill = (2)FSP ILM BIO CORD SPIN LIQtc sill cor
191): (2)FSP ILM BIO CORD SPIN LIQtc sill = (2)FSP ILM BIO CORD SPIN LIQtc sill cor
192): (2)FSP ILM BIO CORD SPIN LIQtc sill cor = FSP ILM BIO CORD SPIN LIQtc sill cor

# Appendix C: Whole rock geochemical data

Table C.1. Chemistry of the high temperature (HTM) and low temperature (LTM) migmatites and of the two modeled samples.

| | HTM-L | HTM-CR | HTM-FR | LTM-L | LTM-M | LTM-R | UAS[c] | APS[d] |
|---|---|---|---|---|---|---|---|---|
| $SiO_2$ (wt%) | 55.0 | 49.6 | 50.2 | 88.4 | 66.5 | 52.4 | 62.5 | 48.8 |
| $TiO_2$ | 0.817 | 1.97 | 1.91 | 0.055 | 0.869 | 1.58 | 1.02 | 1.07 |
| $Al_2O_3$ | 20.4 | 18.0 | 17.6 | 7.40 | 14.7 | 18.6 | 19.5 | 28.4 |
| $Fe_2O_3$ | 4.33 | 10.1 | 9.93 | 0.45 | 6.45 | 11.9 | 6.28 | 4.62 |
| MnO | 0.040 | 0.114 | 0.146 | bdl | 0.076 | 0.136 | 0.03 | 0.01 |
| MgO | 1.98 | 6.02 | 6.31 | 0.13 | 2.08 | 4.03 | 1.71 | 1.33 |
| CaO | 5.71 | 5.66 | 7.35 | 0.52 | 0.90 | 0.49 | 0.16 | 0.10 |
| $Na_2O$ | 5.59 | 1.58 | 0.85 | 2.10 | 3.67 | 1.78 | 1.11 | 0.10 |
| $K_2O$ | 2.68 | 3.16 | 2.11 | 0.33 | 2.68 | 5.08 | 3.92 | 10.71 |
| $P_2O_5$ | 1.81 | 0.497 | 0.493 | 0.051 | 0.100 | 0.113 | 0.11 | 0.06 |
| $H_2O$ | 0.98 | 2.06 | 1.91 | 0.50 | 1.52 | 3.01 | – | – |
| $CO_2$ | 0.08 | 0.24 | 0.34 | 0.05 | 0.06 | 0.07 | – | – |
| LOI | – | – | – | – | – | – | 3.32 | 4.87 |
| Total | 99.5 | 98.9 | 99.1 | 99.9 | 99.6 | 99.3 | 99.1 | 100.1 |
| Li (ppm) | 42 | 67 | 48 | 22 | 130 | 248 | – | – |
| Be | 0.7 | 2.0 | 2.5 | 3.5 | 4.4 | 6.5 | – | – |
| Sc | 7.4 | 25.0 | 25.9 | 0.8 | 11.9 | 23.7 | 15 | 17 |
| V[b] | 54 | 168 | 175 | 10 | 81 | 142 | 105 | 151 |
| Cr[b] | 39 | 215 | 211 | 14 | 81 | 153 | 95 | 113 |
| Co | 11 | 28 | 32 | 1.3 | 13 | 23 | 13 | 10 |
| Ni[b] | 21 | 52 | 60 | 3[a] | 35 | 64 | 33 | 22 |
| Cu | 11 | 16 | 14 | 2.6 | 5.1 | 9.1 | | |
| Zn[b] | 97 | 162 | 109 | bdl | 138 | 268 | 104 | 62 |
| Ga[b] | 28 | 20 | 19 | 8[a] | 23 | 36 | 26 | 38 |
| Rb | 193 | 252 | 164 | 25 | 306 | 565 | 179 | 551 |
| Sr | 402 | 423 | 510 | 80 | 136 | 68 | 117 | 16 |
| Y[b] | 98 | 31 | 29 | bdl | 27 | 74 | – | – |
| Zr[b] | 327 | 348 | 308 | 11 | 413 | 726 | 254 | 213 |
| Nb[b] | 18 | 22 | 14 | 1.3[a] | 19 | 39 | 21 | 32 |
| Mo | 0.2 | 0.9 | 1.0 | 0.2 | 0.2 | 0.3 | 0.45 | 0.20 |
| Cd | 0.18 | 0.10 | 0.12 | 0.04 | 0.06 | 0.03 | – | – |
| Sn | 2.5 | 1.4 | 1.8 | 2.0 | 7.3 | 13 | 4.4 | 8.2 |
| Sb | 0.03 | 0.02 | 0.02 | 0.03 | 0.04 | 0.04 | 4.8 | 3.0 |
| Cs | 3.7 | 5.0 | 3.3 | 1.9 | 34.4 | 59.7 | 11.2 | 29 |
| Ba[b] | 319 | 731 | 661 | 52 | 283 | 473 | 605 | 1166 |
| La | 44 | 31 | 34 | 1.0[a] | 39 | 97 | 58 | 17.8 |
| Ce | 118 | 67 | 74 | 1.2[a] | 61 | 188 | 114 | 49 |
| Pr | 16 | 8.2 | 9.1 | 0.20[a] | 8.6 | 23 | 13 | 5.56 |
| Nd | 70 | 35 | 38 | 0.72[a] | 32 | 87 | 47.4 | 20.9 |
| Sm | 16 | 6.7 | 7.3 | 0.13[a] | 5.7 | 17 | 9.34 | 4.16 |
| Eu | 1.9 | 1.5 | 1.8 | 0.32[a] | 0.83 | 1.2 | 1.77 | 0.89 |
| Gd | 14 | 5.9 | 6.2 | 0.10[a] | 4.6 | 14 | 7.58 | 3.56 |
| Tb | 2.6 | 0.87 | 0.94 | 0.01[a] | 0.69 | 2.1 | 1.1 | 0.51 |
| Dy | 16 | 4.7 | 5.1 | 0.08[a] | 3.4 | 12 | 6.5 | 2.89 |
| Ho | 2.8 | 0.84 | 0.94 | 0.01[a] | 0.69 | 2.3 | 1.2 | 0.59 |
| Er | 7.8 | 2.5 | 2.8 | 0.04[a] | 1.9 | 6.5 | 3.5 | 1.74 |
| Tm | 1.1 | 0.34 | 0.4 | 0.01[a] | 0.26 | 1 | 0.52 | 0.27 |
| Yb | 6.3 | 2.2 | 2.5 | 0.05[a] | 2.0 | 6.3 | 3.41 | 1.9 |
| Lu | 0.83 | 0.31 | 0.36 | 0.01[a] | 0.31 | 0.95 | 0.55 | 0.31 |
| W | 0.4 | 0.3 | 0.3 | 0.5 | 1.4 | 2.9 | – | – |
| Tl | 0.92 | 1.3 | 0.86 | 0.11 | 1.7 | 3.1 | 0.9 | 2.6 |
| Pb | 27.2 | 7.2 | 6.5 | 9.0 | 16.9 | 10.5 | 16.5 | 1.86 |
| Bi | 0.67 | 0.20 | 0.14 | 0.33 | 0.15 | 0.51 | – | – |
| Th | 1.9 | 4.6 | 2.9 | 0.4 | 17 | 38 | 3.68 | 6 |
| U | 7.5 | 1.5 | 1.1 | 0.5 | 5.3 | 15 | 16.1 | 2.8 |

Notes: Unless otherwise specified, major elements were measured with XRF, trace elements with ICP-MS, and REE with ICP-AES.
[a] Measured with ICP-MS.
[b] Measured with XRF.
[c] Sample 5284 in Romer and Hahne 2010.
[d] Sample GLHL-543 in Romer and Hahne 2010.
bdl = Below detection limit.

# Verdankung

Mein besonderer Dank gilt meinem Doktorvater, Rolf L. Romer. Mit seiner inspirierenden und stimulierenden Art sowie seinem uneingeschränkten Rückhalt hat er entscheidend zum Gelingen dieser Arbeit beigetragen. Er hatte stets ein offenes Ohr für fachliche und persönliche Anliegen und hat mich konsequent unterstützt. Diese prägende und lehrreiche Zeit wird mir stets in guter Erinnerung bleiben.

Ganz herzlich bedanke ich mich bei Bettina Hübner, Johannes Glodny, Wang Dan und Marie Lefebvre. Es war stets eine Freude sich mit euch auszutauschen und mit euch zusammen zu arbeiten.

Angelina, dir gebührt mein ganz besonderer Dank. Deine Unterstützung, deine Geduld und dein Rückhalt während der letzten Jahre können gar nicht genug gewürdigt werden.

Für ihre fortwährende Unterstützung bedanke mich herzlich bei meiner Familie, insbesondere bei meiner Mutter und meinem Bruder.

Uwe, Max, Phil und Alex, es war mir eine besondere Freude, die vergangenen Jahre mit euch zu verbringen.

Des Weiteren möchte ich all jenen danken, die direkt oder indirekt zu dieser Arbeit beigetragen haben und nicht namentlich erwähnt wurden.

# Erklärung

Hiermit versichere ich, dass die vorliegende Dissertationsschrift von mir selbständig verfasst wurde und keine anderen als die angegebenen Quellen und Hilfsmittel verwendet wurden.

Des Weiteren versichere ich, dass diese Arbeit an keiner anderen Hochschule eingereicht worden ist.

Potsdam, 28.01.2019

Mathias Wolf